Nickel and osmium isotope and trace element geochemistry of organic-rich sedimentary rocks: The first investigation of Ni isotope systematics in marine sediments

PORTER, SARAH,JULIE

Nickel and osmium isotope and trace element geochemistry of organic-rich sedimentary rocks: The first investigation of Ni isotope systematics in marine sediments

Sarah J. Porter

A thesis submitted in partial fulfilment of the requirements for the degree of Doctor of Philosophy at Durham University

Department of Earth Sciences, Durham University

2012

Abstract

Understanding the chemical composition of organic-rich marine sediments has the potential to: 1) allow evaluation of variations in ocean chemistry, enabling assessment of changes in global processes throughout geological time; and 2) provide an increased temporal and spatial understanding of petroleum systems. Herein two geologically distinct organic-rich sedimentary formations are explored utilising trace elements, and rhenium-osmium (Re-Os) and nickel (Ni) isotope systematics. Additionally, this thesis is the first study to investigate the behaviour of Ni isotope systematics in organic-rich marine sediments.

Osmium isotope profiling across the Sinemurian-Pliensbachian boundary GSSP indicates that there was a significant contribution of unradiogenic Os to the oceans at this time. Seawater $^{187}Os/^{188}Os_{(i)}$ values range from ~0.20 – 0.48, becoming increasingly unradiogenic up-section. This progressive change in ocean chemistry is coincident with flooding of the Hispanic Corridor, formed during rifting of the Pangean supercontinent and creation of the Central Atlantic Ocean, evident from sudden levels of faunal exchange between the eastern Pacific and western Tethyan oceans. The Os isotope signal here reflects the onset of hydrothermal activity associated with formation of the Hispanic Corridor.

New Ni stable isotope data presented herein for the Sinemurian-Pliensbachian (S-P) GSSP and the Devonian-Mississippian Exshaw Formation, demonstrates that organic-rich marine sediments are characterised by $\delta^{60}Ni$ values that are distinct to those of extraterrestrial and abiotic terrestrial samples. Further, the level of Ni isotope fractionation in organic-rich sediments (ranging from ~1.32 ‰ in the S-P sediments, and ~2.04 ‰ in the Exshaw Formation) is far greater than that seen in the other sample suites (ranges of ~0.17 – 0.37 ‰; Cameron *et al.,* 2009). Although there are limited datasets available for comparison at present, the ranges of $\delta^{60}Ni$ values for the S-P GSSP and Exshaw Formation are similar (0.28 ± 0.05 to 1.60 ±0.05 ‰ and 0.46 ± 0.04 to 2.50 ± 0.04 ‰, respectively), suggesting that such variation in Ni isotope fractionation may be characteristic of organic-rich sediments. This may be due to complexities that are ubiquitous to the sediment-seawater depositional environment. In addition, trace element ratios utilised to establish depositional paleoredox conditions demonstrate that redox did not exert control on the level of Ni isotope fractionation observed in these sediments. The study herein also demonstrates that thermal maturation of the Exshaw Formation has a negligible effect on Ni isotope systematics in mature source rocks, strongly suggesting that Ni isotopes may have the potential to be developed as an oil-source correlation tool.

Declaration

I declare that this thesis, which I submit for the degree of Doctor of Philosophy at Durham University, is my own work and not substantially the same as any which has previously been submitted at this or any other university.

Sarah J. Porter

Durham University

March 2012

Acknowledgements

Well, it may have taken three and a half years but it's finally written! It's certainly been an experience and as you'd expect at times it's been fairly hard-going, but the good times have far outweighed the bad. It wasn't until I started thinking about who to thank that I realised just how many people have contributed, both to the project and to making PhD life, for the most part, pretty awesome. To you all, there's no way I could've done this without you.

Firstly, many thanks to my supervisor, Dave Selby, for his guidance, support and encouragement throughout. Having a good supervisor is the key to a positive PhD experience, and I think I've been pretty lucky in that sense. I've learnt a lot from Dave in the lab and through discussion, and he has always been willing to discuss my thoughts and ideas for the project. I'm also grateful that he took me on having already been my supervisor for 2 years whilst I was an undergraduate! Thanks for everything Dave, it's been a pleasure (and a laugh) working with you, and I look forward to collaborating in the future.

Thanks also to my second and third supervisors, Geoff Nowell and Christ Ottley, for their time and guidance in the lab. I'd like to thank Jon Davidson too, for the laughs and the banter (maybe not so much for the foul smells in the car), and for letting me go on the USA trip 2 years in a row.

A huge thank you to Vyllinniskii Cameron at Bristol University for obtaining Ni isotope data for my samples. Completion of this thesis would not have been possible if you had not agreed to help me out at the last minute. I am extremely grateful to you, and hope that there can be further collaboration in the future.

My funding came from NERC, without which this project would not have been possible. Two months of funding also came from the Japan Society for the Promotion of Science (JSPS) for a Summer Research Fellowship at JAMSTEC (Japan Agency for Marine-Earth Science and Technology) in 2010, enabling me to conduct lab work that contributed to this PhD. Many thanks to Katz Suzuki, Ryoko Senda and Akira Ishikawa for welcoming me to JAMSTEC and for their assistance in the labs. Through the JSPS I was lucky enough to experience a homestay in Japan with Namiko Obata and her lovely family. Thank you for your wonderful hospitality and for looking after me! Thanks also to the other JSPS ladies, Alana, Adele, Maddy and Elnaz, for all the fun we had travelling around Japan together.

Thank you to the rest of the lab group: Viv, Ali, Jo, Alex, Alan and Chris.

To all my friends from school, Alison, Kate H., Emily and Sophie; from university, Jess, Liane, Amy, Jayne, Amanda; and those that were in Durham for part of the PhD, Katie, Jen and Ali, THANK YOU for keeping me sane, for the fun times, for the unending encouragement and support, for letting me crash at your houses (I would undoubtedly have gone crazy if I hadn't been able to escape the Durham bubble and visit you!), for the phone chats, for the nights out, and the many, many laughs.

I firmly believe that a place is what you make of it, but above all, the level to which you like and enjoy the place is dictated by the people you meet and spend time with there. In that regard, I really couldn't have asked for anything more. When I looked forward to coming to work, I'll be the first to admit that it wasn't to sit down and write my thesis, it was to see the people that have made my time in Durham over the last three and a half years what it has been: FUN!!! Izzy, Claire, Jenna, Iona, Harriet, Dave A., Ben Franklin, Viv, Kathy, Amy, Simon, Leo, Dave D., Amelie and Pete, I couldn't have gotten through this without your friendship. There have been so many good times, including: a 3 month trip to Japan for lab work, a trip to Peru and Bolivia including the Inca Trail and Machu Picchu (thank you Claire for having an awesome fieldwork location – AMAZING holiday), Alton Towers (Izzy I will never forget you screaming at me, it'll always make me laugh), trips to the beach at Seaham for BBQs, movie nights, drinking, a joint Big Fat Gypsy Wedding birthday party with Izzy (spot the photos in the collage), slack-lining, trips to the Lake District and Scotland, takeaway evenings, gatherings for watching terrible yet highly addictive tv series, Pandemic board game marathons (Dave A. and Izzy, you know what I mean…), many nights out, Go Ape (sorry for screaming at you Ben), demonstrating on field trips to the USA (when I say demonstrating, I mostly mean laughing and pratting around with Amelie, Jon Davidson, Dave Selby and James Baldini), meals out and meals in, wine tasting, birthday cake baking sessions, Christmas parties, dead celebrities Halloween party, some more drinking, cinema trips (one of my favourites so far has been whilst sitting between Iona and Dave A. during "Woman in Black"), climbing, bouldering, and conferences in Prague and Davos.....to name a few! Thank you all for being such great friends. It really has been a lot of fun, and I will miss you immensely. Claire, thanks for being an awesome travel buddy. South America was incredible, and I hope we can make Everest basecamp happen in the not too distant future! Finally, a big and very special thank you to Yeo (Izzy), for everything, for always being there, for the AMAZING food, and for making me laugh

a ridiculous amount! Thank you for being such a special friend - Durham would not have been the same without you.

Finally, to my incredibly supportive and wonderful family, I'm so grateful for your love, inspiration, support and encouragement. Mum and Dad, you've always been there for me and have been so supportive. I love you and I hope I've made you proud. Thanks for all that you've done, and especially recently, for spell-checking chapter drafts for me. I'm extremely grateful for that, and understand how boring and, to quote Dad, "headache-inducing" it must have been for you! To my grandparents, Nan Dot, Nan Dorrie and Grandad Jim, thank you for always being proud of me. I love you and miss you all.

The photo collage at the back of this thesis is there to say a big thank you to all of you that have contributed so much. I know it sounds a bit melodramatic, but I genuinely couldn't have done this without you. Thank you ☺

Table of Contents

List of Figures

Chapter 2: Opening of a trans-Pangean marine corridor during the Early Jurassic: Insights from Osmium isotopes across the Sinemurian-Pliensbachian boundary GSSP, Robin Hood's Bay, UK

Chapter 3: Developing a new geochemical analytical protocol for the separation of nickel from organic-rich sedimentary matrices, Durham University, UK

Chapter 4: Geochemical characterisation of the Sinemurian-Pliensbachian GSSP: Application of Ni isotopes to organic-rich sediments

List of Tables

1 *Introduction*

1.1 Thesis rationale

Organic-rich sediments (total organic carbon or TOC ≥ 0.5 wt. %) are a key, widespread component in the global sedimentary record. In some instances they have significant economic potential, either through hosting syn- or post-depositional ore-grade mineralisation or by generating hydrocarbons. The latter constitutes a vital precursor to, and essential component in, the formation of petroleum systems. Numerous studies have focused on understanding the distribution, structure and composition of organic-rich sediments in these settings (eg. Alexander *et al.,* 1981; Alberdi and Lafargue, 1993; Alberdi-Genolet and Tocco, 1999; Selby and Creaser, 2005*a*; Selby *et al.,* 2005; Finlay *et al.,* 2011), with a view to enhancing stratigraphic and chemical (isotopic and elemental) correlations, essential for prospecting and exploration (eg. Curiale, 2008), and to better understand depositional processes.

It has also been recognised that organic-rich sediments can be utilised for geochronology, allowing their application to multiple geological investigations. The rhenium-osmium (Re-Os) geochronometer, together with biostratigraphy, has enabled the use of organic-rich sediments for geological timescale calibration studies (eg. the Devonian-Mississippian boundary in the Exshaw Formation; Selby and Creaser, 2005*b*; the Sinemurian-Pliensbachian boundary; Gradstein *et al.,* 2004; this study, Chapter 2).

Rhenium-osmium geochronology is based upon the beta decay of ^{187}Re to ^{187}Os, with a half life of ~45 Ga (eg. Lindner *et al.,* 1989). In order to determine a depositional Re-Os age for a given suite or organic-rich samples, an isochron must be constructed by plotting $^{187}Re/^{188}Os$ vs. $^{187}Os/^{188}Os$. These ratios will positively correlate, assuming that Re-Os systematics have remained undisturbed and that the $^{187}Os/^{188}Os$ composition of the samples at the time of deposition is constant. As such, an isochron age can be calculated using the following equation:

$$\left(\frac{^{187}Os}{^{188}Os}\right)_{(present)} = \left(\frac{^{187}Os}{^{188}Os}\right)_{(initial)} + \left(\frac{^{187}Re}{^{188}Os}\left(e^{\lambda t}-1\right)\right)$$

The ^{187}Re decay constant is represented by λ ($1.666 \times 10^{-11} a^{-1}$; Smoliar *et al.,* 1996) and t is the age.

Additionally, utilisation of this chronometer permits the determination of the osmium isotope composition ($^{187}Os/^{188}Os$) of the sediments at the time of deposition, which is inferred to represent the composition of seawater synchronous with sediment deposition. Osmium isotope profiling of organic-rich sedimentary successions is useful for chemostratigraphic correlation of global stratigraphy (eg. Kuroda *et al.,* 2010) and also to evaluate the chemical composition of the water column and the evolution of seawater chemistry throughout geological time (Ravizza *et al.,* 1996; Levasseur *et al.,* 1999; Cohen *et al.,* 1999; Peucker-Ehrenbrink and Ravizza, 2000; this thesis Chapter 2). This in turn provides valuable insight into changes in global environments, including fluctuations in climatic conditions, as well as allowing identification of the causal factors that induced these variations (eg. Esser and Turekian, 1993; Levasseur *et al.,* 1998; Cohen *et al.,* 1999; Ravizza and Peucker-Ehrenbrink, 2003; Cohen and Coe, 2007; Selby *et al.,* 2009). Further, the ability to constrain absolute depositional ages of organic-rich sediments has permitted the evaluation of basin-basin and cratonic correlations, essential to research of paleocontinental reconstruction (eg. Rooney *et al.,* 2010).

The Re-Os geochronometer has also been applied to organic-rich hydrocarbon source rocks to investigate the behaviour of isotope systematics (eg. Creaser *et al.,* 2002) and to enable increased temporal understanding of petroleum systems (eg. Selby and Creaser, 2005*a*). Further, application of this chronometer has allowed precise dating of hydrocarbon

deposits, thus providing insight into hydrocarbon migration, whilst also allowing the possibility of oil to source correlation (eg. Selby and Creaser, 2005*a*; Selby *et al.,* 2005; Finlay *et al.,* 2011). Such factors are of significant value to petroleum exploration (Curiale, 2008).

Organic-rich sediments can contain abundant faunal assemblages, of significance to biostratigraphical investigations. As well as being extremely valuable for geological timescale calibration, based on first occurrences and extinctions of species and genera (eg. as applicable to the Sinemurian-Pliensbachian boundary, Robin Hood's Bay, UK; Hesselbo *et al.,* 2000; Gradstein *et al.,* 2004; Meister *et al.,* 2006), biostratigraphic analysis can yield substantial insight into the conditions of paleodepositional environments, allowing us to better understand the formation of organic-rich sediments. Further, examination of fauna hosted by these sediments has proven to be essential for paleogeographic reconstruction (eg. Smith and Tipper, 1986; Smith *et al.,* 1990; Boomer and Ballant, 1996; Cameron, 2006, 2007).

In addition, understanding the chemical composition of organic-rich marine sediments has the potential to provide vital information regarding Earth systems, and can be utilised as a valuable forensic tool to evaluate changes in global processes throughout geological time. Through thorough geochemical investigation, changes in the composition of sediment influxes and variations in global depositional environments can be recognised, and the subsequent implications identified. As such, the research presented herein focuses on the geochemical examination of organic-rich sediments, focusing on the following themes:

1. **Changes in global seawater composition:** Organic-rich marine sediments record changes in the balance of inputs to the global oceans (Jones *et al.,* 1994; Cohen *et al.,* 1999; Peucker-Ehrenbrink and Ravizza, 2000; Jones and Jenkyns, 2001; Pálfy *et al.,* 2001). By utilising powerful isotopic tracers such as osmium, strontium and carbon, we are able to identify the environmental factors that may have caused these temporal changes. As such

it is possible to distinguish significant input from continental weathering, meteorite impact and mantle-derived fluxes throughout geological time (Ravizza *et al.,* 1996; Levasseur *et al.,* 1999; Cohen *et al.,* 1999; Peucker-Ehrenbrink and Ravizza, 2000; Ravizza and Peucker-Ehrenbrink, 2003).

2. **Variations in bottom-water redox conditions:** The distribution of specific trace elements in marine sediments, such as V, Cr, Ni, Co, Mo, U and Th (eg. Lewan and Maynard, 1982; Hatch and Leventhal, 1992; Calvert and Pedersen, 1993; Jones and Manning, 1994; Schovsbo, 2001; Algeo and Maynard, 2004; Rimmer, 2004), some isotopic ratios, such as $^{98}Mo/^{95}Mo$ (eg. Barling *et al.,* 2001; McManus *et al.,* 2002; Siebert *et al.,* 2003; Anbar, 2004; Arnold *et al.,* 2004; Anbar and Gordon, 2008; Pearce *et al.,* 2008) and the relationships of these variables with TOC (eg. Mo/TOC; Algeo and Lyons, 2006), allows evaluation of the redox conditions of the bottom waters at the time of sediment deposition. This provides valuable insight into the formation of organic-rich sediments (eg. Pederson and Calvert, 1990), paleoceanographic and paleogeographic variations, and fluctuations in the geochemical balance of these elements within the oceans (eg. Calvert and Pedersen, 1993; Rimmer, 2004; Piper and Calvert, 2009).

3. **Oil to source correlation studies:** Understanding the chemical composition of petroleum source rocks provides critical information regarding the temporal and spatial controls on hydrocarbon formation (eg. Curiale, 2008). Further, the identification of chemical similarities between the source rocks and their associated oils allows significant potential for oil-source correlation studies that are crucial to petroleum exploration (Alexander *et al.,* 1981; Ellrich *et al.,* 1985; Scotchman *et al.,* 1998; Alberdi-Genolet and Tocco, 1999; Selby and Creaser, 2005*a*; Selby *et al.,* 2005; Onyema and Manilla, 2010; Finlay *et al.,*

2011). Such studies yield details of petroleum migration pathways and in turn provide knowledge of the structural morphology of the petroleum system under investigation (eg. Piggott and Lines, 1992; Curiale, 2008).

This thesis aims to further investigate the chemical and isotopic structure of organic-rich sediments, with a view to providing insight into:

1. Changes in global seawater chemistry in the Early Jurassic, using osmium (Os) isotopes, and the implications of such changes for paleogeographic reconstruction.
2. The redox conditions at the time of sediment deposition (using select trace elements), and the effects of redox on the chemistry (metal uptake and Ni isotope composition) and organic content of the sediments.
3. The application of nickel (Ni) isotopes to organic-rich marine sediments and the ability of utilising them to provide meaningful information when used to create a stratigraphic isotope profile.
4. The Ni isotope composition of source rocks (Exshaw Formation shales).
5. The effect of thermal maturation on the Ni isotope and trace element composition of the source rocks.
6. Whether or not any potential exists to develop Ni isotopes as a valuable oil-source correlation tool.

The research in this thesis is presented as paper format, with each chapter representing a complete study. The following sections in this introductory chapter outline the scientific focus for each subsequent chapter within this thesis.

1.2 Chapter 2: Opening of a trans-Pangean marine corridor during the Early Jurassic: Insights from osmium isotopes across the Sinemurian-Pliensbachian GSSP, Robin Hood's Bay, UK.

This chapter focuses on the Sinemurian-Pliensbachian GSSP, Robin Hood's Bay, UK. Until now, the geochemical focus of this section had been limited to strontium isotopes ($^{87}Sr/^{86}Sr$; Jones *et al.,* 1994; Hesselbo *et al.,* 2000), and oxygen and carbon isotope data from belemnites ($\delta^{18}O$ and $\delta^{13}C$; Hesselbo *et al.,* 2000). This chapter applies Os isotope stratigraphy to this boundary section, with a view to understanding seawater chemistry and paleogeographic reconstruction during the Early Jurassic. All rhenium (Re) and Os analysis were conducted by the author through the Japan Society for the Promotion of Science (JSPS) Summer Fellowship Program (summer 2010) at the Japan Agency for Marine-Earth Science and Technology (JAMSTEC), Yokosuka, Japan, with the assistance of Dr Katsuhiko Suzuki and Dr Ryoko Senda. This chapter was written by the author, with Drs David Selby, Darren Gröcke and Paul Smith providing editorial comments and suggestions.

1.3 Chapter 3: Developing a new geochemical analytical protocol for the separation of nickel from organic-rich sedimentary matrices, Durham University, UK.

This chapter describes the progress made in developing a novel geochemical technique for the separation of Ni from organic-rich sedimentary matrices at Durham University. A detailed evaluation of previously published analytical protocols and background to Ni isotope work is also presented. Analytical work was carried out by the author, with guidance from Drs David Selby and Geoff Nowell. This chapter was written by the author, with Dr Geoff Nowell and Dr David Selby providing editorial comments and suggestions.

1.4 Chapter 4: Geochemical characterisation of the Sinemurian-Pliensbachian GSSP: The first application of Ni isotopes to organic-rich sediments.

This chapter, in addition to Chapter 2, provides new geochemical data for the Sinemurian-Pliensbachian boundary, Robin Hood's Bay, UK. This research presents trace element, total organic carbon (TOC) and Ni isotope data for a vertical section spanning this boundary. This study is the first to analyse Ni isotopes in organic-rich sediments and to apply Ni isotopes to stratigraphic isotopic profiling. The trace element data herein is used to explore the paleoredox conditions at the time of sediment deposition, and a critical evaluation of the suitability and reliability of these redox proxies is also presented. In addition, this study attempts to determine the controls on metal uptake into these sediments, and whether relationships exist between trace element and TOC content. Sample preparation, trace element and TOC analyses were conducted by the author at Durham University, UK, with assistance from Drs David Selby, Darren Gröcke and Chris Ottley, and laboratory technician Joanne Peterkin. Nickel isotope work was conducted by Dr Vyllinniskii Cameron at the University of Bristol, UK. This chapter was written by the author, with Dr David Selby providing editorial comments and suggestions.

1.5 Chapter 5: Understanding the effects of thermal maturation on source rock geochemistry: Can Ni isotopes be used as an oil-source correlation tool?

This chapter documents the first study that applies Ni isotopes to hydrocarbon-generating source rocks. This investigation attempts to determine whether thermal maturation of source rocks has any effect on their Ni isotope composition, with a view to

assessing the potential for Ni isotopes to be used as an oil-source correlation tool. Additionally, trace element abundances, redox ratios and TOC concentrations were established, in order to evaluate the behaviour of metallo-organic complexes in organic-rich sediments. Sample preparation, trace element and TOC analyses were conducted by the author at Durham University, UK, with assistance from Drs David Selby, Darren Gröcke and Chris Ottley, together with laboratory assistant Joanne Peterkin. All Ni isotope analyses were conducted by Dr Vyllinniskii Cameron at the University of Bristol, UK. This chapter was written by the author, with editorial suggestions from Dr David Selby.

1.6 Chapter 6: Conclusions and Future work

This final chapter draws together and summarises the work detailed in the main research chapters of this thesis. In addition, it provides an outline of future work that could be conducted to further develop the research presented herein.

1.7 References

Alberdi-Genolet, M., and Tocco, R., 1999, Trace metals and organic geochemistry of the Machiques Member (Aptian-Albian) and La Luna Formation (Cenomanian-Campanian), Venezuela: Chemical Geology, v. 160, no. 1-2, p. 19-38.

Alberdi, M., and Lafargue, E., 1993, Vertical variations of organic matter content in Guayuta Group (upper Cretaceous), Interior Mountain Belt, Eastern Venezuela: Organic Geochemistry, v. 20, no. 4, p. 425-436.

Alexander, R., Kagi, R. I., and Woodhouse, G. W., 1981, Geochemical correlation of Windalia oil and extracts of Winning Group (Cretaceous) potential source rocks, Barrow Sub-basin, Western Australia: American Association of Petroleum Geologists Bulletin, v. 65, p. 235-250.

Algeo, T. J., and Lyons, T. W., 2006, Mo–total organic carbon covariation in modern anoxic marine environments: Implications for analysis of paleoredox and paleohydrographic conditions: Paleoceanography, v. 21, no. 1, p. PA1016.

Algeo, T. J., and Maynard, J. B., 2004, Trace-element behavior and redox facies in core shales of Upper Pennsylvanian Kansas-type cyclothems: Chemical Geology, v. 206, no. 3-4, p. 289-318.

Anbar, A. D., 2004, Molybdenum Stable Isotopes: Observations, Interpretations and Directions: Reviews in Mineralogy and Geochemistry, v. 55, no. 1, p. 429-454.

Anbar, A. D., and Gordon, G. W., 2008, Redox renaissance: Geology, v. 36, p. 271-272.

Arnold, G. L., Anbar, A. D., Barling, J., and Lyons, T. W., 2004, Molybdenum Isotope Evidence for Widespread Anoxia in Mid-Proterozoic Oceans: Science, v. 304, no. 5667, p. 87-90.

Barling, J., Arnold, G. L., and Anbar, A. D., 2001, Natural mass-dependent variations in the isotopic composition of molybdenum: Earth and Planetary Science Letters, v. 193, no. 3–4, p. 447-457.

Boomer, I., and Ballent, S., 1996, Early-Middle Jurassic ostracod migration between the northern and southern hemispheres: Further evidence for a proto Atlantic-Central America connection: Palaeogeography, Palaeoclimatology, Palaeoecology, v. 121, no. 1–2, p. 53-64.

Calvert, S. E., and Pedersen, T. F., 1993, Geochemistry of Recent oxic and anoxic marine sediments: Implications for the geological record: Marine Geology, v. 113, no. 1-2, p. 67-88.

Carmen, A., 2006, Northern and Southern Hemispheres ostracod palaeobiogeography during the Early Jurassic: Possible migration routes: Palaeogeography, Palaeoclimatology, Palaeoecology, v. 233, no. 1–2, p. 63-95.

Carmen, A., 2007, Pliensbachian–Toarcian ostracod biogeography in NW Europe: Evidence for water mass structure evolution: Palaeogeography, Palaeoclimatology, Palaeoecology, v. 251, no. 3–4, p. 398-421.

Cohen, A. S., Coe, A. L., Bartlett, J. M., and Hawkesworth, C. J., 1999, Precise Re-Os ages of organic-rich mudrocks and the Os isotope composition of Jurassic seawater: Earth and Planetary Science Letters, v. 167, no. 3-4, p. 159-173.

Cohen, A. S., and Coe, A. L., 2007, The impact of the Central Atlantic Magmatic Province on climate and on the Sr- and Os-isotope evolution of seawater: Palaeogeography, Palaeoclimatology, Palaeoecology, v. 244, no. 1-4, p. 374-390.

Creaser, R. A., Sannigrahi, P., Chacko, T., and Selby, D., 2002, Further evaluation of the Re-Os geochronometer in organic-rich sedimentary rocks: a test of hydrocarbon maturation effects in the Exshaw Formation, Western Canada Sedimentary Basin: Geochimica et Cosmochimica Acta, v. 66, no. 19, p. 3441-3452.

Curiale, J. A., 2008, Oil-source rock correlations - Limitations and recommendations: Organic Geochemistry, v. 39, no. 8, p. 1150-1161.

Ellrich, J., Hirner, A., and Stärk, H., 1985, Distribution of trace elements in crude oils from southern Germany: Chemical Geology, v. 48, no. 1-4, p. 313-323.

Esser, B. K., and Turekian, K. K., 1993, The osmium isotopic composition of the continental crust: Geochimica et Cosmochimica Acta, v. 57, no. 13, p. 3093-3104.

Finlay, A. J., Selby, D., and Osborne, M. J., 2011, Re-Os geochronology and fingerprinting of United Kingdom Atlantic margin oil: Temporal implications for regional petroleum systems: Geology, v. 39, no. 5, p. 475-478.

Gradstein, F. M., Ogg, J. G., Smith, A. G., Bleeker, W., and Lourens, L. J., 2004, A new Geologic Time Scale, with special reference to Precambrian and Neogene: Episodes, v. 27, no. 2, p. 83-100.

Hatch, J. R., and Leventhal, J. S., 1992, Relationship between inferred redox potential of the depositional environment and geochemistry of the Upper Pennsylvanian (Missourian) Stark Shale Member of the Dennis Limestone, Wabaunsee County, Kansas, U.S.A: Chemical Geology, v. 99, no. 1-3, p. 65-82.

Hesselbo, S. P., Meister, C., and Grocke, D. R., 2000, A potential global stratotype for the Sinemurian-Pliensbachian boundary (Lower Jurassic), Robin Hood's Bay, UK: ammonite faunas and isotope stratigraphy: Geological Magazine, v. 137, no. 6, p. 601-607.

Jones, B., and Manning, D. A. C., 1994, Comparison of geochemical indices used for the interpretation of palaeoredox conditions in ancient mudstones: Chemical Geology, v. 111, no. 1-4, p. 111-129.

Jones, C. E., and Jenkyns, H. C., 2001, Seawater strontium isotopes, oceanic anoxic events, and seafloor hydrothermal activity in the Jurassic and Cretaceous: American Journal of Science, v. 301, p. 112-149.

Jones, C. E., Jenkyns, H. C., and Hesselbo, S. P., 1994, Strontium isotopes in Early Jurassic seawater: Geochimica et Cosmochimica Acta, v. 58, no. 4, p. 1285-1301.

Kuroda, J., Hori, R. S., Suzuki, K., Gröcke, D. R., and Ohkouchi, N., 2010, Marine osmium isotope record across the Triassic-Jurassic boundary from a Pacific pelagic site: Geology, v. 38, no. 12, p. 1095-1098.

Levasseur, S., Birck, J.-L., and Allègre, C. J., 1998, Direct Measurement of Femtomoles of Osmium and the $^{187}Os/^{186}Os$ Ratio in Seawater: Science, v. 282, no. 5387, p. 272-274.

Levasseur, S., Birck, J. L., and Allègre, C. J., 1999, The osmium riverine flux and the oceanic mass balance of osmium: Earth and Planetary Science Letters, v. 174, no. 1-2, p. 7-23.

Lewan, M. D., and Maynard, J. B., 1982, Factors controlling enrichment of vanadium and nickel in the bitumen of organic sedimentary rocks: Geochimica et Cosmochimica Acta, v. 46, no. 12, p. 2547-2560.

Lindner, M., Leich, D. A., Russ G. P., Bazan, J. M., and Borg, R. J., 1989, Direct determination of the half-life of ^{187}Re: Geochimica et Cosmochimica Acta, v. 53, no. 7, p. 1597-1606.

McManus, J., Nägler, T. F., Siebert, C., Wheat, C. G., and Hammond, D. E., 2002, Oceanic molybdenum isotope fractionation: Diagenesis and hydrothermal ridge-flank alteration: Geochem. Geophys. Geosyst., v. 3, no. 12, p. 1078.

Meister, C., Aberhan, M., Blau, J., Dommergues, J.-L., Feist-Burkhardt, S., Hailwood, E. A., Hart, M., Hesselbo, S. P., Hounslow, M. W., Hylton, M., Morton, N., Page, K., and Price, G. D., 2006, The Global Boundary Stratotype Section and Point (GSSP) for the base of the Pliensbachian Stage (Lower Jurassic), Wine Haven, Yorkshire, UK: Episodes, v. 29, no. 2, p. 93-114.

Onyema, M. O., and Manilla, P. N., 2010, Light Hydrocarbon Correlation of Niger Delta Crude Oils: Journal of American Science, v. 6, no. 6, p. 82-88.

Pálfy, J., Demény, A., Haas, J., Hetényi, M., Orchard, M. J., and Veto, I., 2001, Carbon isotope anomaly and other geochemical changes at the Triassic-Jurassic boundary from a marine section in Hungary: Geology, v. 29, no. 11, p. 1047-1050.

Pearce, C. R., Cohen, A. S., Coe, A. L., and Burton, K. W., 2008, Molybdenum isotope evidence for global ocean anoxia coupled with perturbations to the carbon cycle during the Early Jurassic: Geology, v. 36, no. 3, p. 231-234.

Pedersen, T. F., and Calvert, S. E., 1990, Anoxia vs. Productivity: What Controls the Formation of Organic-Carbon-Rich Sediments and Sedimentary Rocks?: American Association of Petroleum Geologists Bulletin, v. 74, no. 4, p. 454-466.

Peucker-Ehrenbrink, B., and Ravizza, G., 2000, The marine osmium isotope record: Terra Nova, v. 12, no. 5, p. 205-219.

Piggott, N., and Lines, M. D., 1992, A case study of migration from the West Canada Basin, *in* England, W. A., and Fleet, A. J., eds., Petroleum Migration, Volume 59, Geological Society Special Publication, p. 207-225.

Piper, D. Z., and Calvert, S. E., 2009, A marine biogeochemical perspective on black shale deposition: Earth-Science Reviews, v. 95, no. 1–2, p. 63-96.

Ravizza, G., Martin, C. E., German, C. R., and Thompson, G., 1996, Os isotopes as tracers in seafloor hydrothermal systems: metalliferous deposits from the TAG hydrothermal area, 26°N Mid-Atlantic Ridge: Earth and Planetary Science Letters, v. 138, no. 1-4, p. 105-119.

Ravizza, G., and Peucker-Ehrenbrink, B., 2003, Chemostratigraphic Evidence of Deccan Volcanism from the Marine Osmium Isotope Record: Science, v. 302, p. 1392-1395.

Rimmer, S. M., 2004, Geochemical paleoredox indicators in Devonian-Mississippian black shales, Central Appalachian Basin (USA): Chemical Geology, v. 206, no. 3-4, p. 373-391.

Rooney, A. D., Selby, D., Houzay, J.-P., and Renne, P. R., 2010, Re-Os geochronology of a Mesoproterozoic sedimentary succession, Taoudeni basin, Mauritania: Implications for basin-wide correlations and Re-Os organic-rich sediments systematics: Earth and Planetary Science Letters, v. 289, no. 3-4, p. 486-496.

Schovsbo, N. H., 2001, Why barren intervals? A taphonomic case study of the Scandinavian Alum Shale and its faunas: Lethaia, v. 34, no. 4, p. 271-285.

Scotchman, I. C., Griffith, C. E., Holmes, A. J., and Jones, D. M., 1998, The Jurassic petroleum system north and west of Britain: a geochemical oil-source correlation study: Organic Geochemistry, v. 29, no. 1–3, p. 671-700.

Selby, D., and Creaser, R. A., 2005a, Direct Radiometric Dating of Hydrocarbon Deposits Using Rhenium-Osmium Isotopes: Science, v. 308, p. 1293.

Selby, D., and Creaser, R. A., 2005b, Direct radiometric dating of the Devonian-Mississippian time-scale boundary using the Re-Os black shale geochronometer: Geology, v. 33, p. 545-548.

Selby, D., Creaser, R. A., Dewing, K., and Fowler, M., 2005, Evaluation of bitumen as a ^{187}Re–^{187}Os geochronometer for hydrocarbon maturation and migration: A test case from the Polaris MVT deposit, Canada: Earth and Planetary Science Letters, v. 235, no. 1–2, p. 1-15.

Selby, D., Mutterlose, J., and Condon, D. J., 2009, U-Pb and Re-Os geochronology of the Aptian/Albian and Cenomanian/Turonian stage boundaries: Implications for timescale calibration, osmium isotope seawater composition and Re-Os systematics in organic-rich sediments: Chemical Geology, v. 265, no. 3-4, p. 394-409.

Siebert, C., Nägler, T. F., von Blanckenburg, F., and Kramers, J. D., 2003, Molybdenum isotope records as a potential new proxy for paleoceanography: Earth and Planetary Science Letters, v. 211, no. 1-2, p. 159-171.

Smith, P. L., and Tipper, H. W., 1986, Plate Tectonics and Paleobiogeography: Early Jurassic (Pliensbachian) Endemism and Diversity: PALAIOS, v. 1, no. 4, p. 399-412.

Smith, P. L., Westermann, G. E. G., Stanley, G. D., Jr., Yancey, T. E., and Newton, C. R., 1990, Paleobiogeography of the Ancient Pacific: Science, v. 249, no. 4969, p. 680-683.

Smoliar, M. I., Walker, R. J., and Morgan, J. W., 1996, Re-Os isotope constraints on the age of Group IIA, IIIA, IVA, and IVB iron meteorites: Science, v. 271, p. 1099-1102.

2 *Opening of a trans-Pangean marine corridor during the Early Jurassic: Insights from Osmium isotopes across the Sinemurian-Pliensbachian boundary GSSP, Robin Hood's Bay, UK.*

2.1 Introduction

Marine sedimentary rocks hold the key to understanding past chemical changes to the oceans. Analysis of hydrogenous rhenium (Re) and osmium (Os) in organic-rich sediments allows detailed evaluation of seawater chemistry at the time of sediment deposition. The Os isotope system ($^{187}Os/^{188}Os$) is a particularly powerful tool for tracing temporal changes in the balance of global inputs to the oceans (Ravizza *et al.,* 1996; Levasseur *et al.,* 1999; Cohen *et al.,* 1999; Peucker-Ehrenbrink and Ravizza, 2000), and as such it permits the evaluation of fluctuations in seawater chemistry throughout geological time. Specifically, significant input from meteorite impact, continental weathering and mantle-derived fluxes can be identified and distinguished.

The present-day seawater Os isotope composition may be relatively uniform ($^{187}Os/^{188}Os$ ratio of ~1.06; Levasseur *et al.,* 1998; Peucker-Ehrenbrink and Ravizza, 2000) but it has varied significantly throughout geological time. The short seawater residence time of Os of ~10-40 Ka (Sharma *et al.,* 1997; Oxburgh, 1998; Levasseur *et al.,* 1998; Peucker-Ehrenbrink and Ravizza, 2000), longer than the mixing time of the oceans (~2 – 4 Ka; Palmer *et al.,* 1988), allows the Os isotope composition to respond rapidly to any alterations in the composition and flux of these inputs (Oxburgh, 1998; Cohen *et al.,* 1999). This has been successfully exploited by past studies, where Os has been used as a chemostratigraphic marker of significant volcanic events (eg. Cohen *et al.,* 1999; Ravizza and Peucker-Ehrenbrink, 2003).

Until now, isotope stratigraphy of the Sinemurian-Pliensbachian boundary Global Stratotype Section and Point (GSSP) at Robin Hood's Bay has been limited to $^{87}Sr/^{86}Sr$ (Jones *et al.*, 1994; Hesselbo *et al.,* 2000), $\delta^{18}O$ and $\delta^{13}C$ data (Hesselbo *et al.,* 2000) from belemnites. Herein we compile these datasets with Re-Os data to provide new Os isotope characterisation of the Sinemurian-Pliensbachian GSSP. The longer seawater residence time of Sr (~2.4 Ma;

Jones and Jenkyns, 2001) relative to Os, slows the response of Sr ratios to changes in the balances of inputs to the oceans (eg. Cohen and Coe, 2002). Therefore, using Os isotopes provides improved resolution for changes in seawater chemistry across this boundary section. Combined with data from previous studies, this work has two significant outcomes by providing: (1) an increased geochemical understanding of an important GSSP, thereby also enhancing understanding of Lower Jurassic stratigraphy in the UK; and (2) a detailed $^{187}Os/^{188}Os$ profile for contemporaneous Jurassic seawater allowing insight into the contributions of the various global inputs into the oceans at this time, in turn yielding an understanding of ocean connectivity during the Early Jurassic. The timing of development of oceanic seaways during Pangean separation is currently poorly constrained, with estimates that include both the Hettangian and Sinemurian. The Hispanic Corridor, an initially epicontinental but later fully oceanic seaway, connected the western Tethyan and eastern Pacific oceans along the Central Atlantic rift zone (Smith and Tipper, 1986; Smith *et al.,* 1990; Riccardi, 1991; Hallam and Wignall, 1997; Aberhan, 2001). Formed through separation of the Pangean supercontinent, this proto-Atlantic seaway resulted from one of the most significant paleogeographic reorganisations in Earth's history (Smith *et al.,* 1990). Initially developing over rifting continental crust (Smith *et al.,* 1994), this marine corridor signified the tectonic transition from rifting to drifting prior to the formation of the Atlantic Ocean (Smith *et al.,* 1990). In addition to the profound impact on ocean circulation and the equatorial distribution of marine organisms at this time, the marine corridor acted as a filter during its early stages, preferentially allowing passage of on-shore benthic species whilst acting as an effective barrier for off-shore species (eg. Hallam and Wignall, 1997; Smith *et al.,* 1994; Aberhan, 2001). However, without direct sedimentological or geophysical evidence, determining the timing for the establishment of the corridor using biogeography has been the subject of continuous debate. As such, the timing of seaway formation is currently imprecise and is suggested to

have occurred sometime during the ~25 myr duration of the Early Jurassic (eg. Damborenea, 2000; Aberhan, 2001).

The $^{187}Os/^{188}Os_{(i)}$ values from the Sinemurian-Pliensbachian GSSP, Robin Hood's Bay, UK, provide evidence for significant low-temperature hydrothermal activity in the oceans during this time. Herein we demonstrate that this hydrothermal activity was likely to be associated with continental fragmentation during the break-up of Pangea. The combination of biogeography, faunal exchange patterns and the new Os data from this time, suggest that connectivity between the Eastern Pacific and Tethyan oceans may have initiated during the Latest Sinemurian, associated with the formation of the Hispanic Corridor. Therefore, this study may better constrain the timing of establishment of the Hispanic Corridor, previously limited to poorly defined biogeography.

2.2 Geology of the Sinemurian-Pliensbachian boundary GSSP

Our study focuses on the marine sediments at the Sinemurian-Pliensbachian Global Boundary Stratotype Section and Point (GSSP) at Wine Haven, ~3 km S-SE of Robin Hood's Bay, Yorkshire, UK (Grid ref. NZ9762 0230 eg. Hesselbo *et al.,* 2000; Meister *et al.,* 2006; Fig. 2.1). This Early Jurassic boundary occurs in the Pyritous Shales of the Redcar Mudstone Formation within the Lias Group (Powell, 1984). It has been the subject of scientific interest for many years, with the earliest reference to the site being by Young and Bird (1822). Exposure at Robin Hood's Bay is optimal, with lower beds exposed by a series of wave-cut platforms (Fig. 2.2a – b). The succession here is also well known for its complete ammonite assemblages (eg. Tate and Blake, 1876; Dommergues and Meister, 1992). From such well-preserved ammonite biostratigraphy, the base of the Pliensbachian Stage can be unambiguously located at the

bottom of the Taylori Subzone of the Jamesoni Zone, marked by the first occurrence of species of the genus *Apoderoceras* (Dean *et al.,* 1961; Hesselbo *et al.,* 2000; Gradstein *et al.,* 2004; Meister *et al.,* 2006).

The age for the base of the Pliensbachian has been defined by the Geological Time Scale (GTS) 2004 as 189.6 ± 1.5 Ma (Gradstein *et al.,* 2004), derived from cycle-scaled linear Sr trends and ammonite occurrences (above; also includes the lowest occurrence of *Bifericeras donovani*; Gradstein *et al.,* 2004). Herein, this age for the Sinemurian-Pliensbachian boundary is used.

The Sinemurian-Pliensbachian boundary is placed very close to the base of Bed 73 (bed classification from Hesselbo and Jenkyns, 1995), ~6 cm above the midline of nodules forming the upper margin of Bed 72 in the Wine Haven section (Hesselbo *et al.,* 2000; Fig. 2.2c).

An epicontinental sea, positioned to the west of the deep Tethyan basin (Dera *et al.,* 2009) covered most of Northern Europe, including Britain, during the Mesozoic (Sellwood and Jenkyns, 1975; Fig. 2.3). Lithological evidence for sea level rise, combined with sedimentological evidence (Smith *et al.,* 1994), indicates that the epicontinental sea of this time was not landlocked but free to circulate with the Tethyan ocean. The open ocean Os isotope composition across the boundary interval should therefore be echoed in the sampled sediments. Analysis of hydrogenous Re and Os from these samples instils certainty that the calculated initial Os isotope composition ($^{187}Os/^{188}Os_{(i)}$) reflects that of contemporaneous seawater.

Over a ~10 m interval, the lithology of the Wine Haven succession gradually progresses from pale siliceous mudrocks with intermittent coarser sand beds in the Upper Sinemurian (Aplanatum Subzone), to finer, much darker clay-rich shales ~1.5 m above the boundary in the Lower Pliensbachian (Taylori Subzone; Meister *et al.,* 2006; Hesselbo and Jenkyns, 1995, 1998; this study). These facies changes indicate an overall relative increase in sea level of at least

regional, but possibly global extent (Hallam, 1981; Sellwood, 1972; Hesselbo and Jenkyns 1995, 1998; Hesselbo *et al.,* 2000; Meister *et al.,* 2006).

Nodular beds of concretionary siderite (~10 cm in thickness) of both laterally continuous (Beds 70 and 72) and semi-continuous extent (Bed 74 and within Bed 71) are present throughout the Wine Haven section (Fig. 2.2b – c; Sellwood, 1972; Meister *et al.,* 2006; this study). The origin of these nodules is uncertain, although they are suggested to represent non- or slow depositional phases based on their unique association with fauna found in life-position (Sellwood, 1972).

The sedimentation rate across the Sinemurian-Pliensbachian boundary has not previously been quantified, and has therefore been approximated here by taking ~64 Ma as the duration for the Jurassic period (Gradstein *et al.,* 2004) and using mean thicknesses of ammonite zonal subdivisions estimated by Hallam and Sellwood (1976). This provides a combined thickness for the Sinemurian and Pliensbachian of ~278 m, ~23 % of the total for the Jurassic. By disregarding the uncertain effects of compaction (Hallam and Sellwood, 1976), a steady sedimentation rate during this interval has been calculated at ~1m/54 Ka, in turn suggesting that the interval sampled by this study (~6 m) spans ~320 Ka.

Although the $^{87}Sr/^{86}Sr$ profile (Hesselbo *et al.,* 2000) shows a systematic decrease up-section (~0.707487 to 0.707395 over a 10 m interval), a lack of any abrupt changes in the $^{87}Sr/^{86}Sr$ ratio indicates that sedimentation was continuous (Jones *et al.,* 1994; Hesselbo *et al.,* 2000; Meister *et al.,* 2006). At the boundary level, a drop in $^{87}Sr/^{86}Sr$ value from ~0.707433 to 0.707418 (Hesselbo *et al.,* 2000) could possibly reflect minor slowing or hiatus in sediment deposition (Hesselbo *et al.,* 2000; Meister *et al.,* 2006). However, replicate analyses of belemnites from 1 – 4 cm above the boundary give an average $^{87}Sr/^{86}Sr$ value of 0.707422 ± 0.000012, well within uncertainty of the ratio recorded for the boundary (0.707425 ± 0.000004) (Hesselbo *et al.,* 2000), suggesting a slowing rather than break in deposition

(Hesselbo *et al.,* 2000; Meister *et al.,* 2006). Further evidence for continuous deposition is supported by a lack of lithological unconformities (Meister *et al.,* 2006; this study).

2.3 Sampling and analytical protocol

2.3.1 Sampling

A set of 32 samples (SP7-09 to SP39-09) was collected from the Pyritous Shales Member of the Redcar Mudstone Formation, along a 6 m vertical section bracketing the Sinemurian-Pliensbachian boundary (sample SP22-09) at Robin Hood's Bay (Fig. 2.4). Sampling occurred at a consistent interval of ~20 cm for 3 m above and 3 m below the boundary from Beds 69 – 75 except within Bed 72, where a smaller sampling interval of ~15 cm was used (Fig. 2.4). Based on our approximation above for the duration of sedimentation across this section, sampling at ~20 cm intervals allowed us to capture an estimated resolution of ~11 Ka per sample.

In preparation for geochemical analyses, the samples were cut and polished to expose fresh surfaces, and were then powdered in a Zr disc.

2.3.2 Rhenium-osmium analysis

Rhenium and osmium analyses of Robin Hood's Bay whole-rock powders were conducted at the Japan Agency for Marine-Earth Science and Technology (JAMSTEC) as part of the JSPS Summer Fellowship Program 2010, following the CrO_3-H_2SO_4 procedure outlined by (Selby and Creaser, 2003). This digestion technique minimises removal of Re and Os from the nonhydrogenous (detrital) component of the sample, allowing analysis and evaluation of the hydrogenous fraction (Selby and Creaser, 2003). Sample powders of known quantities (500 mg

for samples with >50 ppb Re or 1g for samples with <50 ppb Re) were digested with a measured amount of ^{185}Re and ^{190}Os spike solution, in 8 ml of CrO_3-H_2SO_4 solution in Carius tubes at 240^{o}C for 48 hrs. After cooling, Os was removed and purified from the solution by solvent extraction and micro-distillation.

Following Os removal, the remaining solution was prepared for anion exchange chromatography to purify the Re fraction. To reduce Cr^{6+} to Cr^{3+}, necessary to avoid complications during chromatography (Selby and Creaser, 2003), 1 ml of the remaining solution was removed and reduced drop by drop (due to the violent exothermic reaction) using 3 ml of ethanol (gradual addition of ethanol to the sample solution is advised to avoid loss of sample during the reduction reaction). Once reduced, the solution was evaporated to dryness on a hotplate at ~80^{o}C.

The dried Re fraction was taken up in a 10 ml 0.5 N HCl loading solution, before being purified by a two-stage HCl - HNO_3 anion chromatography procedure. The purified Re and Os was loaded onto Ni and Pt filaments, respectively, and the Re and Os isotope ratios were measured using NTIMS (Creaser *et al.,* 1991; Völkening *et al.,* 1991) using Faraday collectors and the SEM, respectively. The initial Os isotope composition ($^{187}Os/^{188}Os_{(i)}$) was calculated using an independently assumed sample age of ~189.6 Ma (Gradstein *et al.,* 2004) and $\lambda\ ^{187}Re = 1.666 \times 10^{-11}\ a^{-1}$ (Smoliar *et al.,* 1996). During this study total procedural blanks were 14.1 ± 0.2 pg and 3.56 ± 0.52 pg (1σ S.D., n = 2) for Re and Os, respectively, with an average $^{187}Os/^{188}Os$ value of 0.19 ± 0.005 (n = 2). Uncertainties presented in Table 2.1 include full error propagation of uncertainties in Re and Os mass spectrometer measurements, blank abundances and isotopic compositions, spike calibrations and reproducibility of standard Re and Os isotopic values.

2.4 Results

2.4.1 Rhenium and osmium abundance

All Re-Os abundance and isotope data for the Sinemurian-Pliensbachian boundary is presented in Table 2.1. The Re and Os abundances define a large range of values, from ~1.5 – 117 and ~0.12 – 1.9 ppb, respectively (Table 2.1). These values are much greater than those of average continental crust: 0.39 ppb (Re) and 0.05 ppb (Os) (Sun *et al.,* 2003 and references therein). Both Re and Os abundances show an overall increase up-section that become more pronounced following the Sinemurian-Pliensbachian boundary.

2.4.2 Re-Os geochronology

In order to conduct Re-Os geochronology, the targeted samples should fulfil three criteria. Each sample must possess a similar initial Os isotope composition ($^{187}Os/^{188}Os_{(i)}$) together with variable $^{187}Re/^{188}Os$ ratios, and have experienced no disturbance to the isotope system since the time of formation (Cohen *et al*., 1999). The Robin Hood's Bay section shows no evidence of post-depositional disturbance, eg. no veining is evident and the section is thermally immature. Additionally, similar Jurassic sections have been utilised for Re-Os geochronology (Cohen *et al*., 1999).

For the Robin Hood's Bay section, the $^{187}Re/^{188}Os$ and present-day $^{187}Os/^{188}Os$ ratios vary from ~25 – 443 and ~0.3 – 1.6, respectively (Table 2.1; Fig. 2.5). Both $^{187}Re/^{188}Os$ and $^{187}Os/^{188}Os$ ratios decrease between 2.8 to 0.9 m below the Sinemurian-Pliensbachian boundary ($^{187}Re/^{188}Os$, ~195 – 20; $^{187}Os/^{188}Os$, ~1 – 0.3; Fig. 2.5), before systematically increasing across the boundary into the lowermost Pliensbachian. Although all of the $^{187}Re/^{188}Os$ and $^{187}Os/^{188}Os$ ratios are positively correlated (R^2 = 0.95), the Re-Os data yield a model 3 age of 179 ± 16 Ma (2σ, n = 32, MSWD = 473; Fig. 2.6a). Although within uncertainty

of the calculated age for the Sinemurian-Pliensbachian boundary (189.6 ± 1.5 Ma; Gradstein *et al.,* 2004), the uncertainty is large (~9 %) and is accompanied by an extremely large MSWD, indicating significant scatter of the data about the isochron that relates to more than analytical uncertainties. We suggest that this scatter relates to the sample set possessing variable initial $^{187}Os/^{188}Os$ values (Fig. 2.6b). The calculated initial $^{187}Os/^{188}Os$ ($^{187}Os/^{188}Os_{(i)}$ at 189.6 Ma; Gradstein *et al.,* 2004) values for this Sinemurian-Pliensbachian section are variable, but consistently unradiogenic for all samples, ranging from ~0.20 – 0.48 (Fig. 2.5). Overall, with exceptions at 1.1 m below the boundary and at the boundary itself (sample SP22-09, $^{187}Os/^{188}Os_{(i)}$ = ~0.48 and SP17-09 = ~0.44, respectively; Fig. 2.5; 2.6b), the $^{187}Os/^{188}Os_{(i)}$ values become progressively less radiogenic up-section (Fig. 2.5).

If we consider samples with similar $^{187}Os/^{188}Os_{(i)}$ values (~0.20 – 0.30) regression of the Re-Os data produces a model 3 age of 183.4 ± 3.3 Ma (2σ, n = 17, MSWD = 20; Fig. 2.6c). This age is outside of uncertainty of that given by Gradstein *et al.* (2004). Regression of Re-Os data for the top four organic-rich samples in the stratigraphic section (SP34-09, SP35-09, SP36-09 and SP37-09) provides a model 1 age of 194 ± 4.8 Ma (2σ, n = 4, MSWD = 0.04; Fig. 2.6d). These samples are ideally suited to Re-Os geochronology because they possess extremely similar initial $^{187}Os/^{188}Os$ compositions (~0.20 – 0.22) and variable $^{187}Re/^{188}Os$ ratios (~268 – 443). As such, the model age is within uncertainty of that given by Gradstein *et al.* (2004). Although the Robin Hood's Bay section is not ideally suited for Re-Os geochronology, the positive correlation of $^{187}Re/^{188}Os$ with $^{187}Os/^{188}Os$ that yields dates in agreement with the Geological Time Scale 2004 (Gradstein *et al*., 2004), suggests that the Re-Os systematics have not been disturbed and that the calculated initial $^{187}Os/^{188}Os$ values can be used to discuss Early Jurassic ocean chemistry.

2.5 Discussion

The Jurassic was a dynamic period that witnessed major geological events of Earth's history; notably the full-scale tectonic plate reorganisation associated with the break-up of Pangea. Ocean chemistry was therefore subject to fluctuations as the balance of inputs changed, and as such the seawater Os isotope composition was highly variable. In order to look critically at the data herein and to determine the potential source of the Os isotope signal observed across the Sinemurian-Pliensbachian boundary, there needs to be an understanding of the background seawater Os isotope composition at this time. However, currently no studies conclusively document background seawater Os for the Early Jurassic. The first estimation of stable, steady-state $^{187}Os/^{188}Os$ values for the Sinemurian is given as ~ 0.47 (Kuroda *et al.,* 2010). The sampled section (Triassic-Jurassic chert succession from Kurusu, Japan; Kuroda *et al.,* 2010) was positioned to the east of the separating supercontinent, in an intra-ocean setting. The recorded Os isotope composition would therefore not have been directly affected by nearby continental flux, and would have been a good representation of open ocean chemistry at this time. For this investigation, we will assume that this value represents the best estimation of background seawater Os isotope composition at the Sinemurian-Pliensbachian transition.

2.5.1 Origin of the Sinemurian-Pliensbachian seawater Os isotope composition

The Os data from Robin Hood's Bay shows that the calculated seawater initial $^{187}Os/^{188}Os$ value becomes progressively more unradiogenic from the latest Sinemurian into the Pliensbachian. Although there is some fluctuation, this trend to unradiogenic values can be broadly separated into three groups, with average $^{187}Os/^{188}Os_{(i)}$ values of ~0.38, 0.28 and 0.21 (Fig. 2.5). These results indicate that there was a marked and progressive increase of

unradiogenic Os input into the global ocean during the transition from the Sinemurian to the Pliensbachian.

A peak towards a relatively radiogenic $^{187}Os/^{188}Os_{(i)}$ value of 0.48 is coincident with the boundary (Fig. 2.5). This is also matched by an increase in the $^{187}Re/^{188}Os$ ratio (from ~31 to 100) and a decrease in ^{192}Os (from ~208 to 102 ppb). Assuming a background seawater Os isotope composition of ~0.47 (Kuroda *et al.,* 2010), this peak may reflect a period of hiatus in the input of unradiogenic Os to the oceans.

The Os isotope composition ($^{187}Os/^{188}Os$) of seawater can be directly controlled by three major inputs: (1) radiogenic input from weathering of continental crust; (2) unradiogenic contribution from meteorites; (3) an unradiogenic signal from igneous and hydrothermal activity (eg. Peucker-Ehrenbrink and Ravizza, 2000). The effects that these inputs can have on the Os isotope composition of seawater are discussed below. In addition, they are compared to the observed $^{187}Os/^{188}Os_{(i)}$ signal across the Sinemurian-Pliensbachian boundary in order to evaluate its origin.

2.5.1.1 Why is the signal not induced by continental weathering?

The gradual trend towards unradiogenic Os isotope values observed in this study indicates that continental weathering is unlikely to be the cause of the Os isotopic signal shown over the Sinemurian-Pliensbachian boundary. Belemnite oxygen stable isotope data displays a marked increase of ~1 ‰ over 10 m across the boundary (Hesselbo *et al.,* 2000; Fig. 2.5). This 1 ‰ increase is equivalent to a substantial temperature decrease of ~5^{o}C (Hesselbo *et al.,* 2000; Meister *et al.,* 2006). Such considerable lowering of temperature, coupled with evidence for low mean land relief and absence of ice sheets during the Early Jurassic (Golonka *et al.,* 1994), would favour reduced rates of continental weathering.

The Os isotope signal resulting from continental weathering is also significantly more radiogenic ($^{187}Os/^{188}Os$ = ~1.4*;* Peucker-Ehrenbrink and Jahn, 2001) than that observed in this study. This indicates that the seawater Os isotope composition was dominated by an unradiogenic source that outweighed the input of radiogenic Os from continental weathering. It is extremely difficult to constrain the exact continental $^{187}Os/^{188}Os$ input to the oceans during the Early Jurassic. However, following Cohen *et al.* (1999), we can attempt to quantify the approximate contribution of crustal Os into the ocean. Assuming an average $^{187}Os/^{188}Os$ value of ~1.4 for weathering of ancient continental crust (Peucker-Ehrenbrink and Jahn, 2001), and a $^{187}Os/^{188}Os$ value of ~0.13 for an unradiogenic mantle-derived source (Allegre and Luck, 1980; Esser and Turekian, 1993; Sharma *et al.,* 1997; Levasseur *et al.,* 1998), an input of crustal-sourced Os of just 5 – 22 % is required to obtain seawater $^{187}Os/^{188}Os$ ratios of ~0.44 – 0.20, respectively. In contrast, the present-day radiogenic contribution to the oceans from the continental crust is between ~ 70 and 80 % (Peucker-Ehrenbrink, 1996; Sharma *et al.* 1997). Given the geographical location of Robin Hood's Bay in close-proximity to continental landmasses (Fig. 2.3 and 2.7), and the absence of ice sheets, there would almost certainly be radiogenic continental input regardless of land-relief and climate. Further, although challenging to quantify, the epicontinental setting would mean increased sensitivity to continental input. There is no evidence for the weathering of unradiogenic lithologies, e.g., mafic and ultramafic units, thus the decrease in seawater $^{187}Os/^{188}Os$ composition during the earliest Pliensbachian indicates that input of Os into the ocean at this time was dominated by an unradiogenic source, not accounted for by the continental weathering flux.

2.5.1.2 Why is the unradiogenic Os not from an extraterrestrial source?

Extraterrestrial and mantle-derived influxes are the dominant unradiogenic sources of Os to the global oceans. The calculated $^{187}Os/^{188}Os_{(i)}$ values of these sources (~0.13) are

indistinguishable (Allegre and Luck, 1980; Esser and Turekian, 1993; Sharma *et al.,* 1997; Levasseur *et al.,* 1998). It is therefore necessary to examine the structure of the Os isotope profiles from each source to determine which was responsible for the unradiogenic Os signal across the Sinemurian-Pliensbachian boundary.

Although the extraterrestrial flux to Earth during the Jurassic is poorly constrained, the possibility of meteorite impact at the Sinemurian-Pliensbachian boundary does not reconcile the gradual decline in $^{187}Os/^{188}Os$ ratios. Following an impact, the Os isotope system should recover quickly due to the relatively short seawater residence time of Os (Peucker-Ehrenbrink and Ravizza, 2000). Further, studies of the Os isotope excursion due to meteorite impact across the K-T boundary (Ravizza and Peucker-Ehrenbrink, 2003), show relatively rapid recovery of the Os isotope system to a steady state following impact ($^{187}Os/^{188}Os$ value increases from ~0.16 to 0.40 in a maximum of ~200 Ka; Pegram and Turekian, 1999; Peucker-Ehrenbrink and Ravizza, 2000; Ravizza and Peucker-Ehrenbrink, 2003). Therefore, although impacts have been documented ~5 – 20 Ma prior to the Triassic – Jurassic boundary (Hallam and Wignall, 1997), the unradiogenic Os signal from the Sinemurian into the Pliensbachian is unlikely to be meteoritic in origin.

2.5.1.3 Unradiogenic Os from a mantle-derived source

The unradiogenic $^{187}Os/^{188}Os_{(i)}$ values are therefore most likely to be mantle-derived. Unlike the other potential sources of oceanic Os discussed above, increased input from a mantle source at the time of the Sinemurian-Pliensbachian boundary can explain the observed isotope profiles.

Rifting of the Pangean Supercontinent began during the latest Triassic (Marzoli *et al.,* 1999; Hames *et al.,* 2000). The initial stages of continental break-up were focused along the 6000 km lineament that would eventually form the continental margins of the Central North

Atlantic Ocean (Hames *et al.,* 2000). Consequently there is evidence for substantial magmatism during the Late Triassic – Early Jurassic (Marzoli *et al.,* 1999; Hames *et al.,* 2000), defined by extensive continental basalts in North America, Europe, Africa and South America (Wilson, 1997; Marzoli *et al.,* 1999). This formed what is termed as the Central Atlantic Magmatic Province (CAMP). The scale of the CAMP has been postulated to exceed that of the Karoo-Ferrar, the Deccan Traps and the Siberian continental flood basalt provinces (Hames *et al.,* 2000), with a total areal extent and volume of at least 7 x 10^6 Km^2 and 2 x 10^6 km^3, respectively (Marzoli *et al.,* 1999; Hames *et al.,* 2000).

High-precision $^{40}Ar/^{39}Ar$ geochronology of the oldest CAMP volcanic rocks indicates that emplacement occurred during the transition from the Late Triassic to Early Jurassic (ca. 200 Ma) with a brief duration of ~ <2 Ma (Marzoli *et al.,* 1999; Hames *et al.,* 2000). A volcanic event of this magnitude, considering both its sizeable magmatic and hydrothermal outputs, would have had a considerable impact on ocean chemistry regardless of its exceptionally brief duration (Ravizza and Peucker-Ehrenbrink, 2003). This has been documented by several Os isotope studies of seawater at the Triassic-Jurassic boundary and during the Hettangian (Cohen *et al.,* 1999; Cohen and Coe, 2002; Cohen, 2004). Prior to and immediately following the Triassic-Jurassic boundary, there was a significant unradiogenic contribution of Os to the oceans that persisted into the Hettangian (Cohen *et al.,* 1999; Cohen and Coe, 2002; Cohen, 2004). This has been attributed to seawater interaction and alteration of recently emplaced CAMP lavas, together with enhanced hydrothermal activity (Cohen *et al.,* 1999; Cohen and Coe, 2002; Cohen, 2004). High chemical weathering rates of juvenile basalts (Louvat and Allègre, 1997) characteristically promote relatively rapid release of unradiogenic Os, which can be seen in the Triassic-Jurassic and Hettangian sample suites (Cohen *et al.,* 1999; Cohen and Coe, 2002; Cohen, 2004). The seawater Os isotopic composition then becomes increasingly unradiogenic across the Sinemurian-Pliensbachian boundary ($^{187}Os/^{188}Os$ ratios of ~0.20). Using

estimates for Early Jurassic stage durations from Gradstein *et al.* (2004), this boundary occurred ~ 10 Ma after the Triassic-Jurassic boundary and at least ~8 Ma after emplacement of CAMP. Further, the total duration of weathering of CAMP basalts is estimated at ~3.5 Ma (Cohen and Coe, 2007), producing a seawater $^{187}Os/^{188}Os$ value of ~0.30. It is therefore difficult to reconcile the observed Sinemurian-Pliensbachian seawater Os isotope composition with the CAMP emplacement event (ca. 200 Ma) or weathering of the continental flood basalts, given a date for the Sinemurian-Pliensbachian stage boundary of 189.6 ± 1.5 Ma (Gradstein *et al.,* 2004).

However, when considering paleogeographic and biogeographic evidence, it is possible to determine a mantle-derived origin for the unradiogenic seawater Os isotope composition that does not rely on emplacement of CAMP lavas. Hydrothermal activity would have been prevalent in this tectonic setting, and low temperature hydrothermal fluids have a characteristically unradiogenic Os isotope composition of ~0.12 (Cohen *et al.,* 1999; Sharma *et al.,* 2000). The possibility of a hydrothermally-induced Os isotope signal at the Sinemurian-Pliensbachian boundary is discussed below, together with the implications of this on Early Jurassic paleogeography.

2.5.2 Osmium isotope evidence for oceanic connectivity via the 'Hispanic Corridor' during the Early Pliensbachian

The separation of Pangea and onset of a global sea level rise established a number of epeiric seaways, including the Hispanic Corridor (Aberhan, 2001). This initially epicontinental, but later fully oceanic seaway was established along the Central Atlantic rift zone between the areas of North America, South America and Africa (Smith and Tipper, 1986), eventually connecting the western Tethyan and eastern Pacific oceans (eg. Smith and Tipper, 1986; Smith *et al.,* 1990; Riccardi, 1991; Aberhan, 2001; Fig. 2.7). No connectivity existed between these

oceans during the Hettangian or Sinemurian, providing an effective barrier to oceanic circulation and thus to faunal exchange (eg. Smith and Tipper, 1986; Riccardi, 1991; Aberhan, 2001). Further, biogeographic and sedimentological evidence indicates that a fully marine corridor did not develop before the Middle Jurassic (Aberhan, 2001). However, substantial evidence for sudden low levels of faunal exchange between the eastern Pacific and western Tethyan oceans exists in the earliest Pliensbachian (Damborenea and Manceñido, 1979; Smith and Tipper, 1986; Smith *et al.,* 1990), suggesting that the Hispanic Corridor was established as a shallow but continuous seaway by the beginning of this stage. Schootbrugge *et al.* (2005) also suggest that short bursts in the diversification of dinoflagellates during the latest Sinemurian are consistent with the opening of this seaway. The decline of seawater $^{187}Os/^{188}Os$ ratios and the rise in sea level evident across the Sinemurian-Pliensbachian boundary section at Robin Hood's Bay, are therefore coincident with the onset of flooding of the Hispanic Corridor. Further, this study suggests that the isotopic signals observed at the boundary reflect increasing hydrothermal activity associated with the opening of the Hispanic Corridor.

The Hispanic Corridor developed across rifting continental crust (Smith *et al.,* 1994), with significant crustal stretching and attenuation occurring before creation of the oceanic strait (Hallam and Wignall, 1997). Growing evidence also indicates that substantial off-axis hydrothermal venting may occur in cooler crustal regions away from the immediate rift zone, driven by exothermic reactions between seawater and mantle-derived rocks (Kelley *et al.,* 2001). This is evident at the Mid-Atlantic and Juan de Fuca ridges, respectively (Kelley *et al.*, 2001; Sharma *et al.*, 2000),. Off-axis fluids are typically cool (~40 – 75^{o}C) with high Os concentrations (~500 femtomol/kg) and unradiogenic $^{187}Os/^{188}Os$ ratios of ~0.12 (Sharma *et al.,* 2000). Seawater-rock interaction via fissures and deeply-penetrating faults associated with rifting would have ensued following the initial flooding event, driving extensive low-temperature hydrothermal fluid circulation (eg. Kelley *et al.,* 2001). This would have therefore

promoted an increase in the release of unradiogenic Os into the seawater (Sharma *et al.,* 2000) across the Sinemurian-Pliensbachian transition.

However, whilst the formation of the Hispanic Corridor would have certainly contributed to the global ocean Os isotope signal, it is also important to consider that additional widespread tectonism associated with Pangean rifting may have had an effect on ocean chemistry during this time. Whilst the Os isotope tool can be used to identify the 3 predominant sources of Os (mantle, meteorite and continental), it alone cannot be used to differentiate between multiple examples of the same source (a number of global spreading centres, for example). Additional geological and geochemical tools must therefore be used in conjunction with Os isotopes to attempt to achieve this.

Herein, the data combined from biostratigraphical, sedimentological (sea-level studies) and geochemical investigations (Os isotopes; this study), demonstrate that opening of the Hispanic Corridor is likely to have had an effect on seawater chemistry at this time, by providing a significant contribution of unradiogenic Os to the ocean. However, a limitation of the current dataset is that a contribution of unradiogenic Os from additional sources associated with Pangean separation cannot be ruled out.

2.6 Conclusions

The Sinemurian-Pliensbachian boundary GSSP at Robin Hood's Bay, UK, has the potential to provide a significantly increased understanding of seawater chemistry during the Early Jurassic. Further, understanding changes in ocean chemistry during this time has the potential to yield valuable insight into ocean connectivity during Pangean separation.

Seawater during the Sinemurian-Pliensbachian transition became dominated by an unradiogenic $^{187}Os/^{188}Os$ signal that is not resolvable by influxes from continental weathering or meteorite impact. The break-up of Pangea was of fundamental importance to this observed isotopic trend, and a mantle-derived source favours the constructed Os isotope profile.

The Triassic-Jurassic boundary marks the onset of volcanism in the Central Atlantic Magmatic Province, directly associated with Pangean fragmentation. Following this there is strong taxonomic evidence for sudden, albeit restricted levels, of faunal exchange between the western Tethyan and eastern Pacific oceans in the latest Sinemurian and the start of the Pliensbachian, via the Hispanic Corridor (defining the rift zone between North America, South America and Africa). The initial flooding event of this trans-Pangean corridor therefore occurred close to the stage boundary. Seawater inundation would have initiated seawater interaction with, and circulation into, deep crustal fissures associated with rifting in this region, thus driving extensive low-temperature hydrothermal activity. Such low-temperature hydrothermal fluids are characterised by unradiogenic $^{187}Os/^{188}Os$ ratios of ~0.12 (Sharma *et al.,* 2000; Kelley *et al.,* 2001).

The global separation of Pangea during this time initiated a number of rift zones in addition to the Hispanic Corridor. Whilst evidence from biogeography and Os isotopes (this study) suggest that formation of the Hispanic Corridor contributed significantly to the $^{187}Os/^{188}Os$ trend observed across the Sinemurian-Pliensbachian boundary, the contribution of unradiogenic Os from other regions in close proximity to Robin Hood's Bay at this time (eg., Tethys), cannot be ruled out.

2.7 References

Aberhan, M., 2001, Bivalve palaeobiogeography and the Hispanic Corridor: time of opening and effectiveness of a proto-Atlantic seaway: Palaeogeography, Palaeoclimatology, Palaeoecology, v. 165, p. 375-394.

Allègre, C.J., and Luck, J.-M., 1980, Osmium isotopes as petrogenetic and geological tracers: Earth and Planetary Science Letters, v. 48, p. 148-154.

Cohen, A.S., 2004, The rhenium-osmium isotope system: applications to geochronological and palaeoenvironmental problems: Journal of the Geological Society, v. 161, p. 729-734.

Cohen, A.S., and Coe, A.L., 2002, New geochemical evidence for the onset of volcanism in the central Atlantic magmatic province and environmental change at the Triassic-Jurassic boundary: Geology, v. 30, p. 267-270.

Cohen, A.S., and Coe, A.L., 2007, The impact of the Central Atlantic Magmatic Province on climate and on the Sr- and Os-isotope evolution of seawater: Palaeogeography, Palaeoclimatology, Palaeoecology, v. 244, p. 374-390.

Cohen, A.S., Coe, A.L., Bartlett, J.M., and Hawkesworth, C.J., 1999, Precise Re-Os ages of organic-rich mudrocks and the Os isotope composition of Jurassic seawater: Earth and Planetary Science Letters, v. 167, p. 159-173.

Creaser, R.A., Papanastassiou, D.A., and Wasserburg, G.J., 1991, Negative thermal ion mass spectrometry of osmium, rhenium and iridium: Geochimica et Cosmochimica Acta, v. 55, p. 397-401.

Damborenea, S.E., 2000, Hispanic Corridor: It's evolution and biogeography of bivalve molluscs, *in* Hall, R., and Smith, P.L., eds., Advances in Jurassic Research 2000. Proceedings of the Fifth International Symposium on the Jurassic System, Trans Tech, Switzerland, Volume 6, GeoResearch Forum, p. 369-380.

Damborenea, S.E., and Manceñido, M.O., 1979, On the palaeogeographical distribution of the pectinid genus weyla (bivalvia, lower jurassic): Palaeogeography, Palaeoclimatology, Palaeoecology, v. 27, p. 85-102.

Dean, W.T., Donovan, D.T., and Howarth, M.K., 1961, The Liassic ammonite Zones and Subzones of the North West European Province: Bulletin of the Natural History Museum, v. 4, p. 435-505.

Dera, G., Pucéat, E., Pellenard, P., Neige, P., Delsate, D., Joachimski, M.M., Reisberg, L., and Martinez, M., 2009, Water mass exchange and variations in seawater temperature in the NW Tethys during the Early Jurassic: Evidence from neodymium and oxygen isotopes of fish teeth and belemnites: Earth and Planetary Science Letters, v. 286, p. 198-207.

Dommergues, J.-L., and Meister, C., 1992, Late Sinemurian and Early Carixian ammonites in Europe with cladistic analysis of sutural characteristics: Neues Jahrbuch fur Geologie and Palaontologie Abhandlungen, v. 185, p. 211-237.

Esser, B.K., and Turekian, K.K., 1993, The osmium isotopic composition of the continental crust: Geochimica et Cosmochimica Acta, v. 57, p. 3093-3104.

Golonka, J., Ross, M.I., and Scotese, C.R., 1994, Phanerozoic paleogeographic and paleoclimatic modeling maps, *in* Embry, A.F., Beauchamp, B., and Glass, D.J., eds., Pangaea: Global environments and resources. Canadian Society of Petroleum Geologists Memoir, Volume 17, p. 1-47.

Gradstein, F.M., Ogg, J.G., Smith, A.G., Bleeker, W., and Lourens, L.J., 2004, A new Geologic Time Scale, with special reference to Precambrian and Neogene: Episodes, v. 27, p. 83-100.

Hallam, A., and Sellwood, B.W., 1976, Middle Mesozoic Sedimentation in Relation to Tectonics in the British Area: The Journal of Geology, v. 84, p. 301-321.

Hallam, A., and Wignall, P.B., 1997, Mass Extinctions and Their Aftermath, Oxford Univ. Press, Oxford.

Hames, W.E., Renne, P.R., and Ruppel, C., 2000, New evidence for geologically instantaneous emplacement of earliest Jurassic Central Atlantic Magamtic Province basalts on the North American margin: Geology, v. 28.

Hesselbo, S.P., and Jenkyns, H.C., 1995, A comparison of the Hettangian to Bajocian successions of Dorset and Yorkshire, *in* Taylor, P.D., ed., Field Geology of the British Jurassic, The Geological Society, p. 105-150.

Hesselbo, S.P., and Jenkyns, H.C., 1998, British Lower Jurassic Sequence Stratigraphy, *in* De Graciansky, P.C., Hardenbol, J., Jacquin, T., and Vail, P.R., eds., Mesozoic and Cenozoic Sequence Stratigraphy of European Basins, Volume 60, Special Publication Society for Sedimentology (SEPM), p. 561-581.

Hesselbo, S.P., Meister, C., and Grocke, D.R., 2000, A potential global stratotype for the Sinemurian-Pliensbachian boundary (Lower Jurassic), Robin Hood's Bay, UK: ammonite faunas and isotope stratigraphy: Geological Magazine, v. 137, p. 601-607.

Jones, C.E., and Jenkyns, H.C., 2001, Seawater strontium isotopes, oceanic anoxic events, and seafloor hydrothermal activity in the Jurassic and Cretaceous: American Journal of Science, v. 301, p. 112-149.

Jones, C.E., Jenkyns, H.C., and Hesselbo, S.P., 1994, Strontium isotopes in Early Jurassic seawater: Geochimica et Cosmochimica Acta, v. 58, p. 1285-1301.

Kelley, D.S., Karson, J.A., Blackman, D.K., Fruh-Green, G.L., Butterfield, D.A., Lilley, M.D., Olson, E.J., Schrenk, M.O., Roe, K.K., Lebon, G.T., Rivizzigno, P., and Party, A.-S., 2001, An off-axis hydrothermal vent field near the Mid-Atlantic Ridge at 30^{o}N: Nature, v. 412, p. 145-149.

Kuroda, J., Hori, R.S., Suzuki, K., Gröcke, D.R., and Ohkouchi, N., 2010, Marine osmium isotope record across the Triassic-Jurassic boundary from a Pacific pelagic site: Geology, v. 38, p. 1095-1098.

Levasseur, S., Birck, J.-L., and Allègre, C.J., 1998, Direct Measurement of Femtomoles of Osmium and the ^{187}Os/^{186}Os Ratio in Seawater: Science, v. 282, p. 272-274.

Levasseur, S., Birck, J.L., and Allègre, C.J., 1999, The osmium riverine flux and the oceanic mass balance of osmium: Earth and Planetary Science Letters, v. 174, p. 7-23.

Louvat, P., and Allègre, C.J., 1997, Present denudation rates on the island of Réunion determined by river geochemistry: Basalt weathering and mass budget between chemical and mechanical erosions: Geochimica et Cosmochimica Acta, v. 61, p. 3645-3669.

Ludwig, K. R., 1980, Calculation of uncertainties of U-Pb isotope data: Earth and Planetary Science Letters, v. 46, no. 2, p. 212-220.

Marzoli, A., Renne, P.R., Piccirillo, E.M., Ernesto, M., Bellieni, G., and De Min, A., 1999, Extensive 200-Million-Year-Old Continental Flood Basalts of the Central Atlantic Magmatic Province: Science, v. 284, p. 616-618

Meister, C., Aberhan, M., Blau, J., Dommergues, J.-L., Feist-Burkhardt, S., Hailwood, E.A., Hart, M., Hesselbo, S.P., Hounslow, M.W., Hylton, M., Morton, N., Page, K., and Price, G.D., 2006, The Global Boundary Stratotype Section and Point (GSSP) for the base of the

Pliensbachian Stage (Lower Jurassic), Wine Haven, Yorkshire, UK: Episodes, v. 29, p. 93-114.

Oxburgh, R., 1998, Variations in the osmium isotope composition of sea water over the past 200,000 years: Earth and Planetary Science Letters, v. 159, p. 183-191.

Palmer, M.R., Falkner, K.K., Turekian, K.K., and Calvert, S.E., 1988, Sources of osmium isotopes in manganese nodules: Geochimica et Cosmochimica Acta, v. 52, p. 1197-1202.

Pegram, W. J., and Turekian, K. K., 1999, The osmium isotopic composition change of Cenozoic sea water as inferred from a deep-sea core corrected for meteoritic contributions: Geochimica et Cosmochimica Acta, v. 63, no. 23–24, p. 4053-4058.

Peucker-Ehrenbrink, B., and Jahn, B., 2001, Rhenium-osmium isotope systematics and platinum group element concentrations: Loess and the upper continental crust: Geochemistry Geophysics Geosystems, v. 2, no. 10, p. 1061-1083.

Peucker-Ehrenbrink, B., and Ravizza, G., 2000, The marine osmium isotope record: Terra Nova, v. 12, p. 205-219.

Powell, J.H., 1984, Lithostratigraphical nomenclature of the Lias Group in the Yorkshire Basin: Proceedings of the Yorkshire Geological Society, v. 45, p. 51-57.

Ravizza, G., Martin, C.E., German, C.R., and Thompson, G., 1996, Os isotopes as tracers in seafloor hydrothermal systems: metalliferous deposits from the TAG hydrothermal area, 26°N Mid-Atlantic Ridge: Earth and Planetary Science Letters, v. 138, p. 105-119.

Ravizza, G., and Peucker-Ehrenbrink, B., 2003, Chemostratigraphic Evidence of Deccan Volcanism from the Marine Osmium Isotope Record: Science, v. 302, p. 1392-1395.

Riccardi, A.C., 1991, Jurassic and cretaceous marine connections between the Southeast Pacific and Tethys: Palaeogeography, Palaeoclimatology, Palaeoecology, v. 87, p. 155-189.

Schootbrugge, B., Bailey, T.R., Rosenthal, Y., Katz, M.E., Wright, J.D., Miller, K.G., Feist-Burkhardt, S., and Falkowski, P.G., 2005, Early Jurassic climate change and the radiation of organic-walled phytoplankton in the Tethys Ocean: Paleobiology, v. 31, p. 73-97.

Selby, D., and Creaser, R.A., 2003, Re-Os geochronology of organic rich sediments: an evaluation of organic matter analysis methods: Chemical Geology, v. 200, p. 225-240.

Sellwood, B.W., and Jenkyns, H.C., 1975, Basins and swells and the evolution of an epeiric sea (Pliensbachian-Bajocian of Great Britain): Journal of the Geological Society, v. 131, p. 373-388.

Sellwood, W., 1972, Regional environmental changes across a Lower Jurassic stage-boundary in Britain: Palaeontology, v. 15, p. 125-157.

Sharma, M., Papanastassiou, D.A., and Wasserburg, G.J., 1997, The concentration and isotopic composition of osmium in the oceans: Geochimica et Cosmochimica Acta, v. 61, p. 3287-3299.

Sharma, M., Wasserburg, G.J., Hofmann, A.W., and Butterfield, D.A., 2000, Osmium isotopes in hydrothermal fluids from the Juan de Fuca Ridge: Earth and Planetary Science Letters, v. 179, p. 139-152.

Smith, A.G., Smith, D.G., and Funnell, B.M., 1994, Atlas of Mesozoic and Cenozoic Coastlines, Cambridge University Press.

Smith, P.L., and Tipper, H.W., 1986, Plate Tectonics and Paleobiogeography: Early Jurassic (Pliensbachian) Endemism and Diversity: PALAIOS, v. 1, p. 399-412.

Smith, P.L., Westermann, G.E.G., Stanley, G.D., Jr., Yancey, T.E., and Newton, C.R., 1990, Paleobiogeography of the Ancient Pacific: Science, v. 249, p. 680-683.

Smoliar, M.I., Walker, R.J., and Morgan, J.W., 1996, Re-Os Ages of Group IIA, IIIA, IVA, and IVB Iron Meteorites: Science, v. 23, p. 1099-1102.

Sun, W., Bennett, V. C., Eggins, S. M., Kamenetsky, V. S., and Arculus, R. J., 2003, Enhanced mantle-to-crust rhenium transfer in undegassed arc magmas: Nature, v. 422, no. 6929, p. 294-297.

Tate, R., and Blake, J.F., 1876, The Yorkshire Lias: J. van Voorst, London.

Völkening, J., Walczyk, T., and G. Heumann, K., 1991, Osmium isotope ratio determinations by negative thermal ionization mass spectrometry: International Journal of Mass Spectrometry and Ion Processes, v. 105, p. 147-159.

Wilson, M., 1997, Thermal evolution of the Central Atlantic passive margins: continental break-up above a Mesozoic super-plume: Journal of the Geological Society, v. 154, p. 491-495.

Young, G.M., and Bird, J., 1822, A geological survey of the Yorkshire Coast:describing the strata and fossils occurring between the Humber and the Tees, from the German Ocean to the Plain of York. Whitby, p. 366.

www.scotese.com (Figure 2.7: Pangean reconstruction in the Early Jurassic)

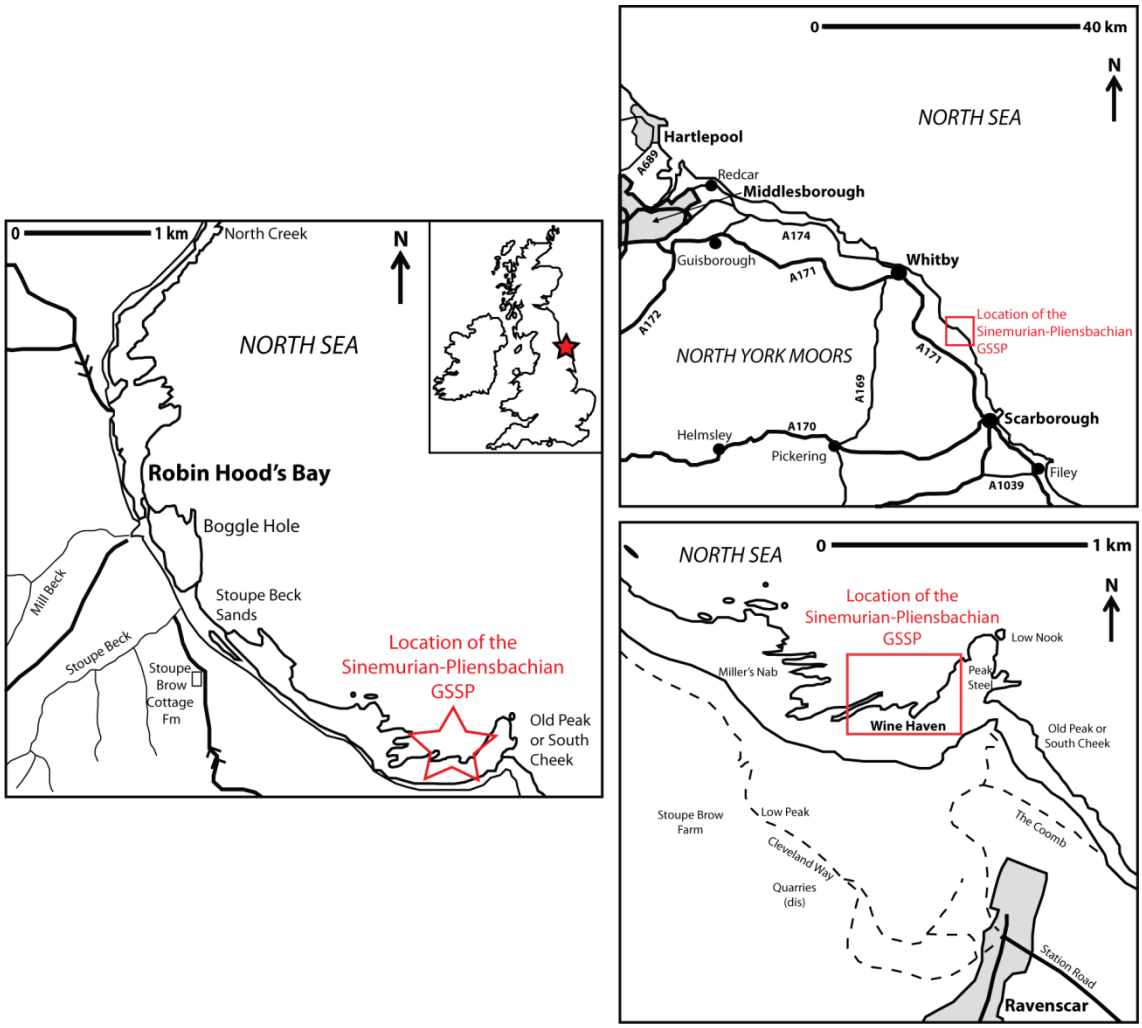

Figure 2.1: Maps of the UK (inset) and Robin Hood's Bay, showing the location of the Sinemurian-Pliensbachian boundary GSSP sampling site at Wine Haven.

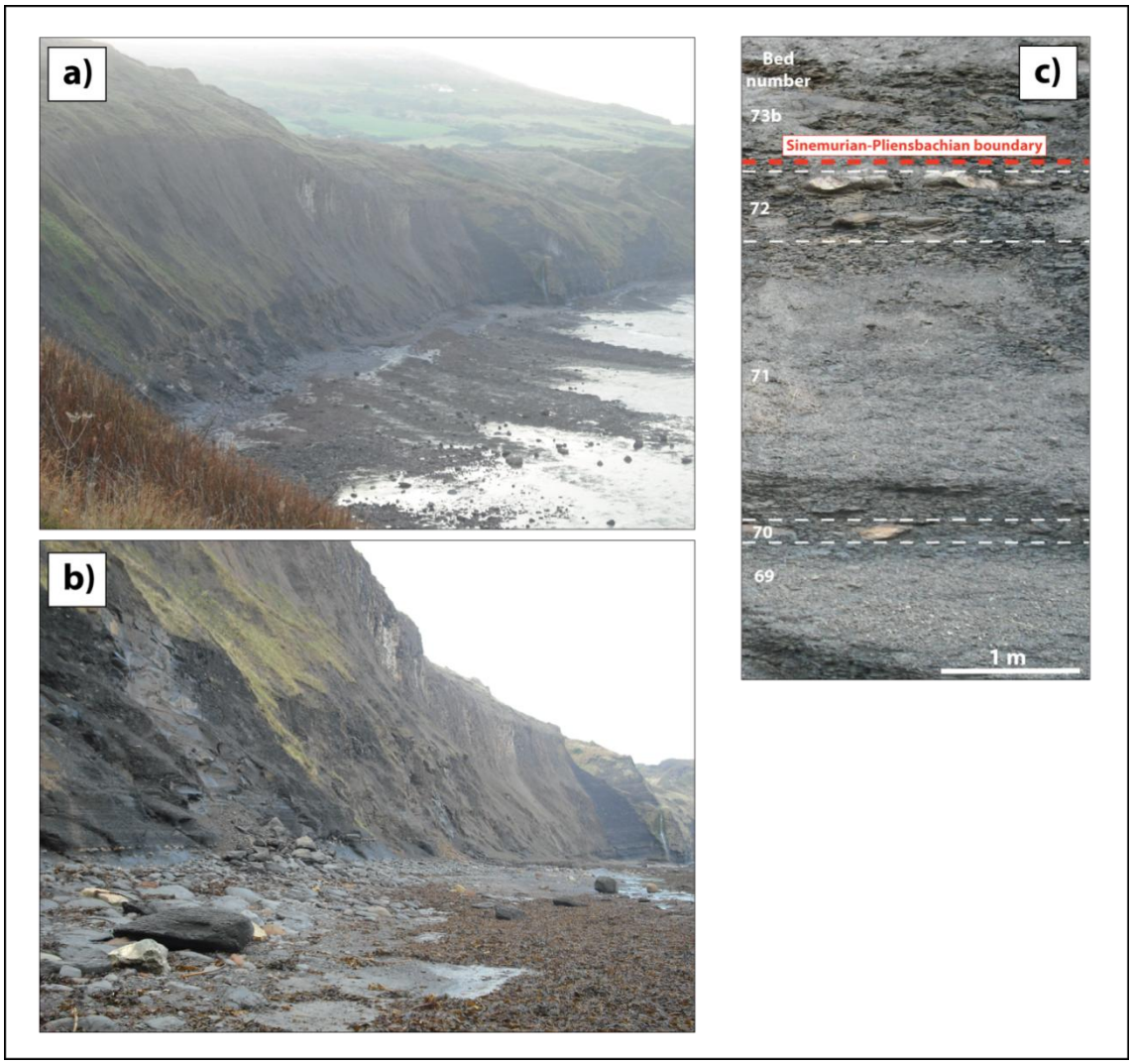

Figure 2.2: Photographs of Robin Hood's Bay: a) the Sinemurian-Pliensbachian boundary GSSP sampling site at Wine Haven from cliffs to the south (looking NNW); b) mudstone cliffs with wave-cut platforms at the base and laterally continuous nodular beds (looking NNW); c) the Sinemurian-Pliensbachian boundary (looking W).

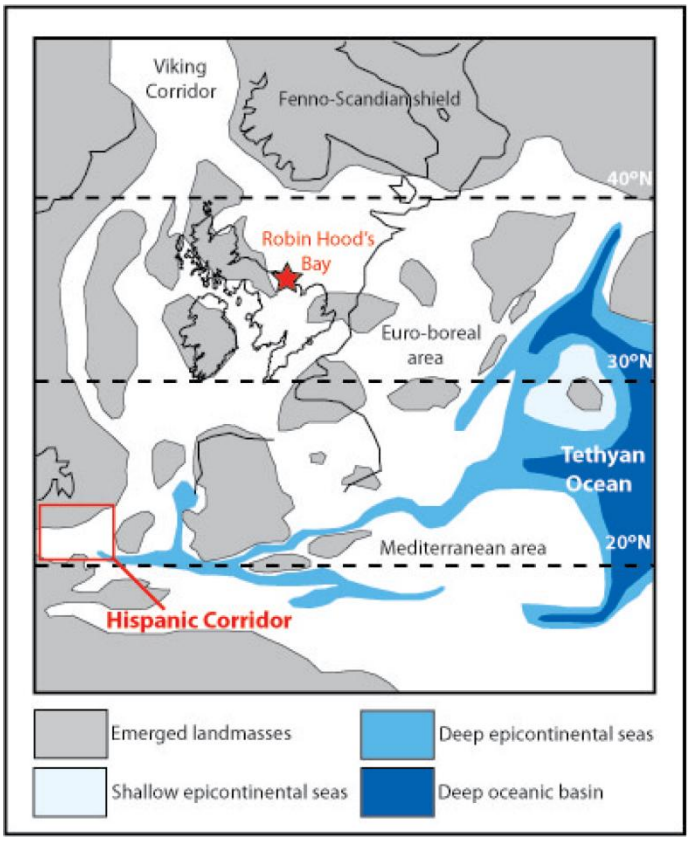

Figure 2.3: Map showing the European epicontinental sea and the geographical relationship between the Hispanic Corridor, Tethyan Ocean and Robin Hood's Bay. Modified after Dera *et al.* (2009).

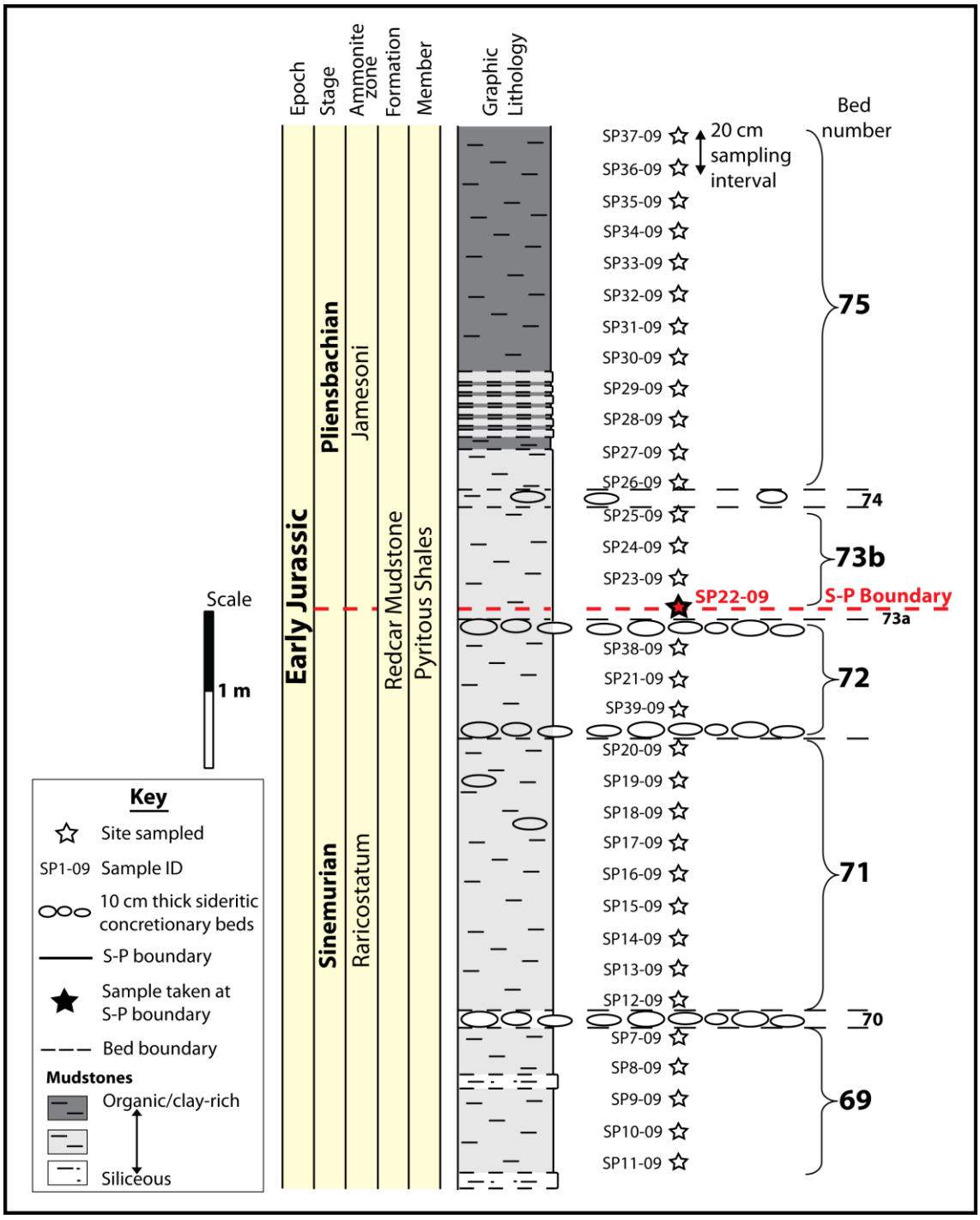

Figure 2.4: Graphic log showing the Sinemurian-Pliensbachian boundary GSSP and the relative locations of the samples analysed in this study. Bed number classification taken from Hesselbo and Jenkyns (1995).

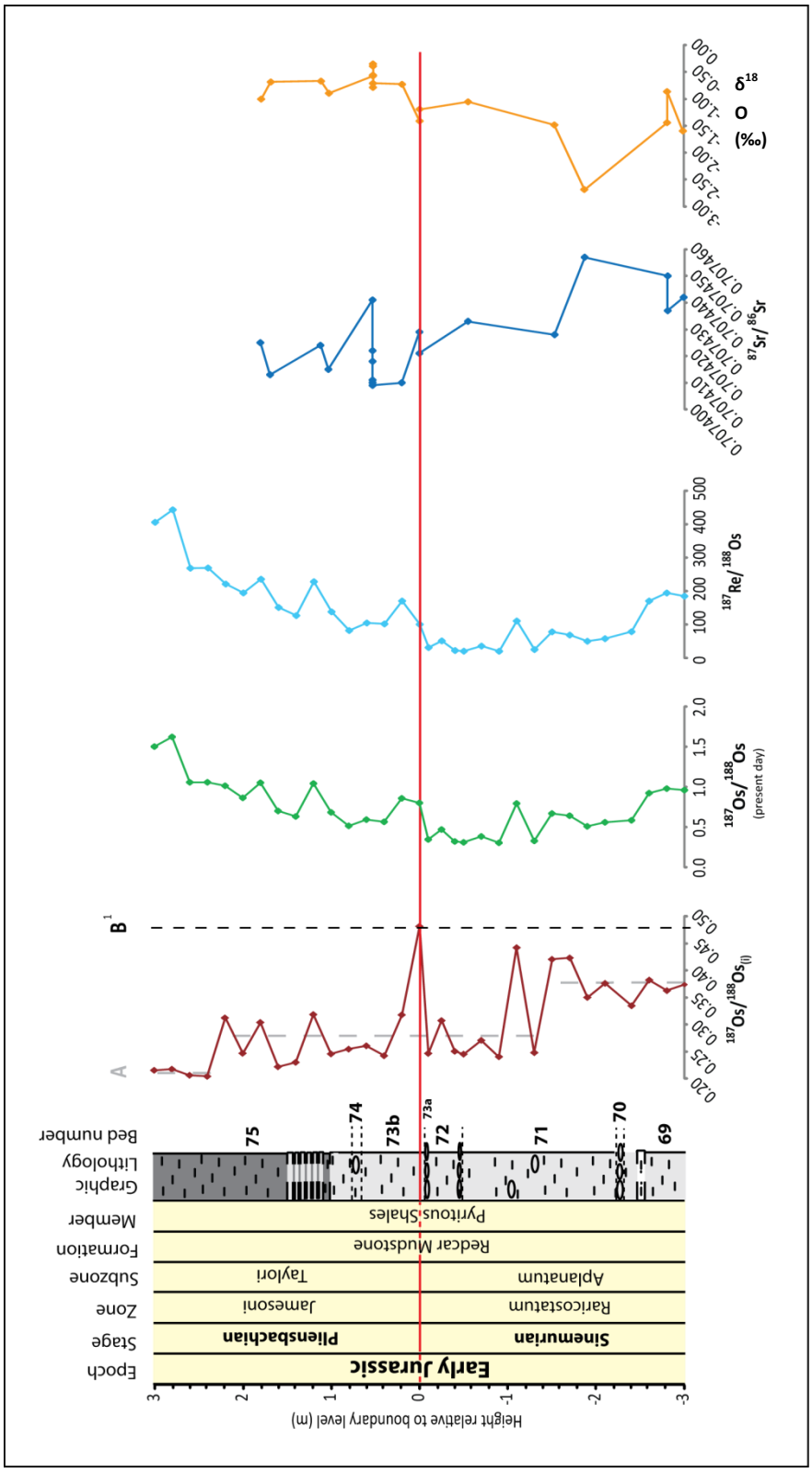

Figure 2.5: Re-Os isotope stratigraphy across the Sinemurian-Pliensbachian boundary GSSP, UK. Strontium isotope data ($^{87}Sr/^{86}Sr$) from Jones *et al.* (1994) and Hesselbo *et al.* (2000), and $\delta^{18}O$ data from Hesselbo *et al.* (2000). Grey dashed line, A, reflects the three groups of $^{187}Os/^{188}Os_{(i)}$ values for seawater across the Sinemurian-Pliensbachian boundary (~0.38, 0.28 and 0.21). Black dashed line, B^1, represents the first estimation of stable steady-state $^{187}Os/^{188}Os$ values for Early Jurassic seawater (~0.47; Kuroda *et al.*, 2010). Bed number classification taken from Hesselbo and Jenkyns (1995).

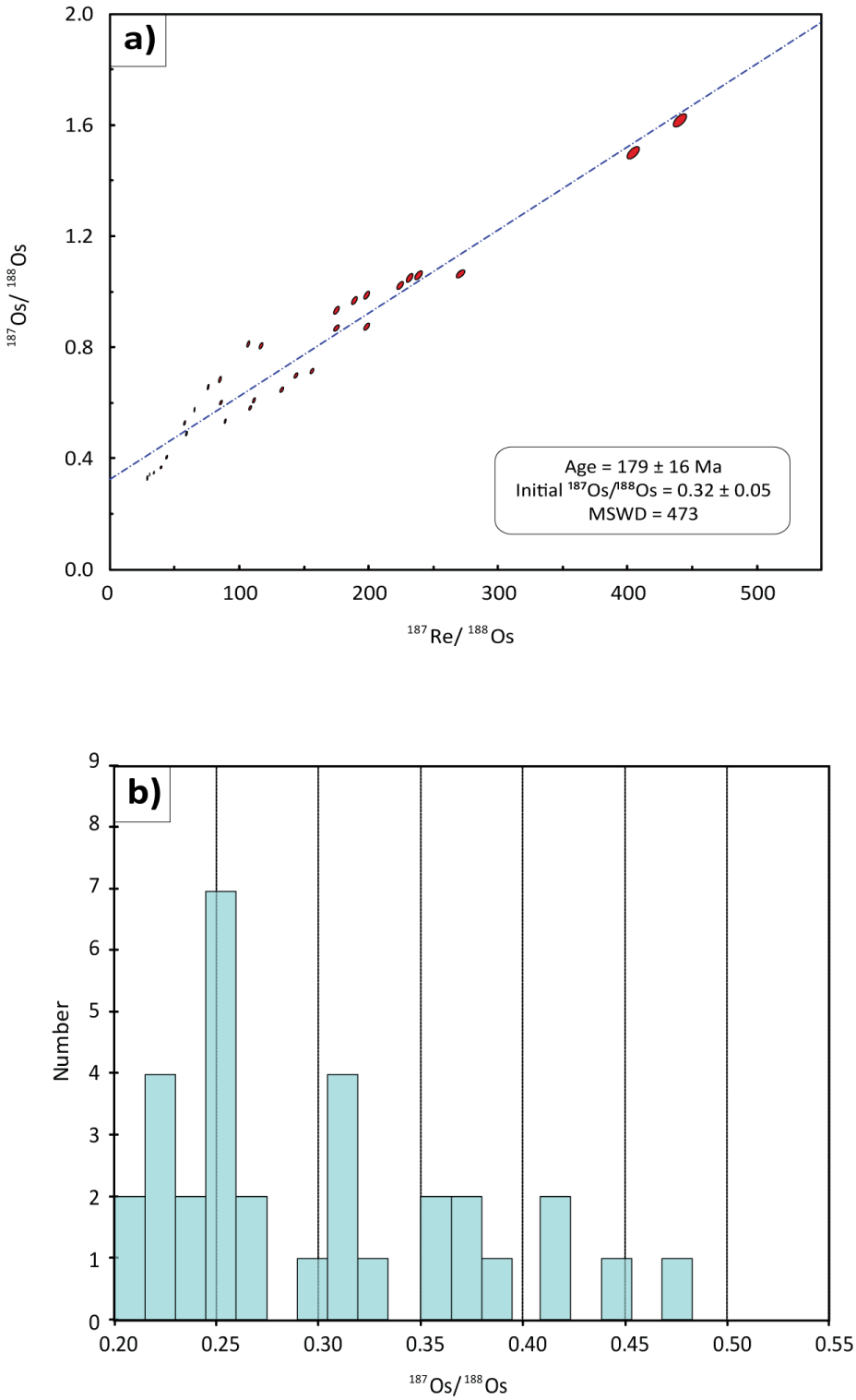

Figure 2.6: a) Re-Os isochron for all Robin Hood's Bay samples (n = 32); b) Histogram showing the variability of the initial $^{187}Os/^{188}Os$ ratio in the Robin Hood's Bay sediments.

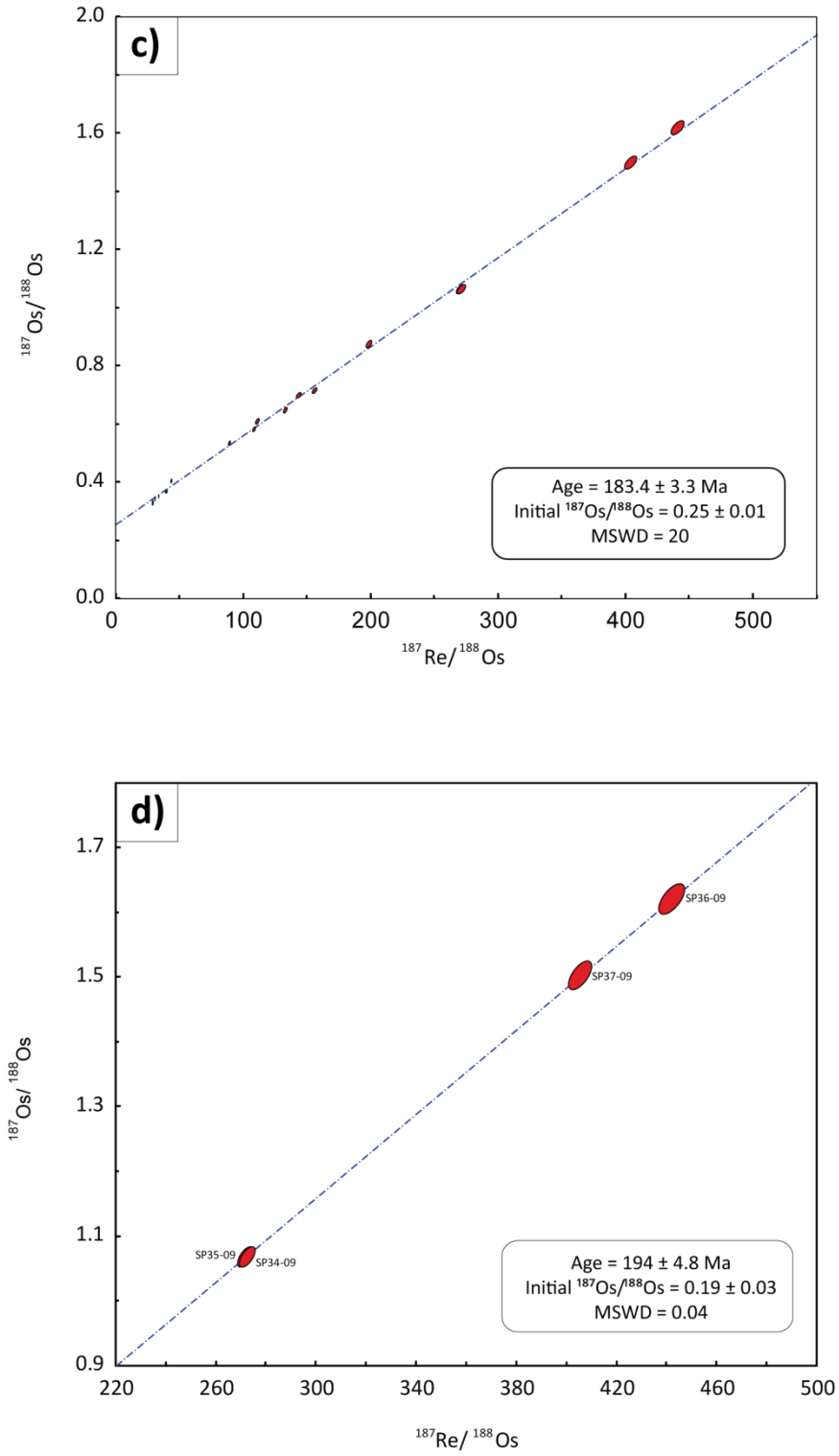

Figure 2.6: (cont.) Re-Os isochron diagrams for: c) All Robin Hood's Bay samples with initial $^{187}Os/^{188}Os$ ratios between ~0.20 – 0.30 (n = 17); d) The four samples at the top of the studied Robin Hood's Bay section that contain variable $^{187}Re/^{188}Os$ ratios (~268 – 443) and similar initial $^{187}Os/^{188}Os$ ratios (~0.20 – 0.22).

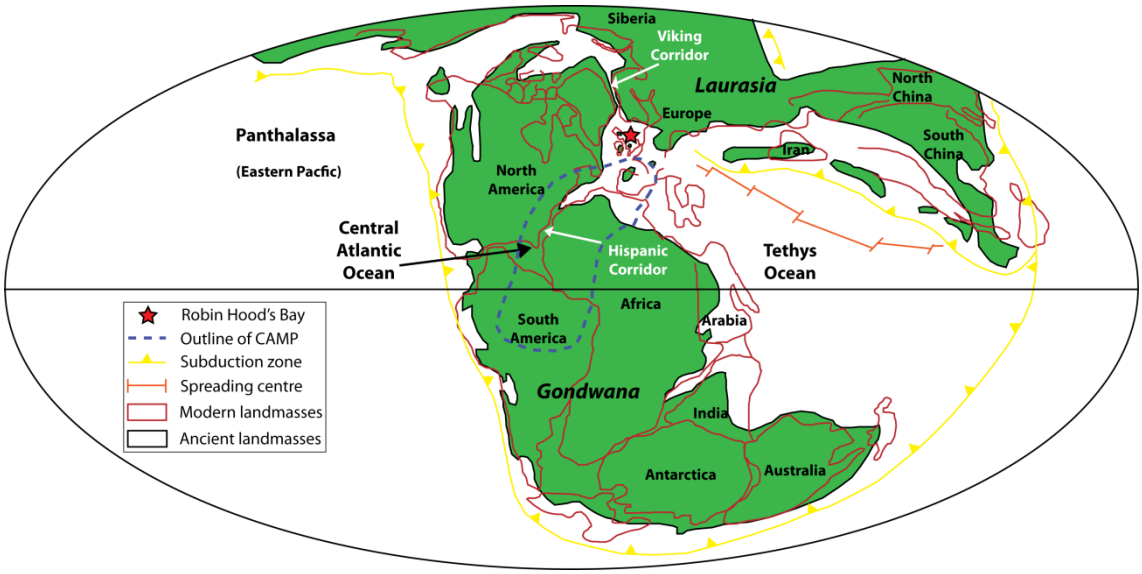

Figure 2.7: Global reconstruction of Pangea in the Early Jurassic. Map shows the relative locations of the Central Atlantic Magmatic Province (CAMP), the Hispanic Corridor, the Tethyan and Pacific oceans and Robin Hood's Bay. Modified after *www.scotese.com*.

Table 2.1: Re and Os isotope data for the Sinemurian-Pliensbachian boundary GSSP, UK.

Sample	Distance from S-P boundary (m)	Bed number	Re (ppb)	Os (ppt)	^{192}Os (ppt)	^{187}Re/^{188}Os	^{187}Os/^{188}Os	Rho [a]	^{187}Os/^{188}Os$_{(i)}$ [b]
SP37-09	3.0	75	88.40 ± 0.39	1237.56 ± 8.93	433.22	405.93 ± 3.96	1.502 ± 0.0184	0.630	0.22
SP36-09	2.8	75	117.36 ± 0.52	1524.48 ± 11.26	526.64	443.32 ± 4.32	1.623 ± 0.0199	0.630	0.22
SP35-09	2.6	75	62.97 ± 0.28	1266.69 ± 8.25	466.35	268.63 ± 2.62	1.058 ± 0.0130	0.629	0.21
SP34-09	2.4	75	62.45 ± 0.28	1253.15 ± 8.16	461.36	269.28 ± 2.63	1.058 ± 0.0130	0.629	0.20
SP33-09	2.2	75	78.38 ± 0.35	1903.42 ± 12.26	704.34	221.37 ± 2.16	1.014 ± 0.0125	0.630	0.31
SP32-09	2.0	75	19.44 ± 0.09	527.43 ± 3.24	198.66	194.69 ± 1.90	0.864 ± 0.0106	0.630	0.25
SP31-09	1.8	75	58.51 ± 0.26	1339.44 ± 8.71	493.48	235.86 ± 2.30	1.052 ± 0.0129	0.629	0.30
SP30-09	1.6	75	25.86 ± 0.12	885.97 ± 5.15	340.30	151.16 ± 1.47	0.701 ± 0.0086	0.628	0.22
SP29-09	1.4	75	20.62 ± 0.09	833.96 ± 4.73	323.00	127.03 ± 1.24	0.633 ± 0.0078	0.629	0.23
SP28-09	1.2	75	75.81 ± 0.34	1790.13 ± 11.60	660.20	228.44 ± 2.23	1.043 ± 0.0128	0.628	0.32
SP27-09	1.0	75	17.02 ± 0.08	636.65 ± 3.68	245.05	138.20 ± 1.35	0.684 ± 0.0084	0.629	0.25
SP26-09	0.8	75	6.71 ± 0.03	412.56 ± 2.23	162.12	82.29 ± 0.81	0.515 ± 0.0063	0.628	0.25
SP25-09	0.6	73b	10.69 ± 0.05	520.99 ± 2.91	202.77	104.85 ± 1.02	0.593 ± 0.0073	0.629	0.26
SP24-09	0.4	73b	11.15 ± 0.05	556.50 ± 3.07	217.32	102.05 ± 1.00	0.566 ± 0.0070	0.629	0.24
SP23-09	0.2	73b	10.65 ± 0.05	329.82 ± 2.03	124.31	170.51 ± 1.67	0.858 ± 0.0106	0.631	0.32
SP22-09	0.0	S-P boundary	5.19 ± 0.02	270.47 ± 1.64	102.65	100.56 ± 0.99	0.801 ± 0.0099	0.629	0.48
SP38-09	-0.1	72	3.28 ± 0.04	518.25 ± 2.57	208.02	31.38 ± 0.44	0.346 ± 0.0043	0.436	0.25
SP21-09	-0.3	72	2.81 ± 0.01	275.83 ± 1.46	109.00	51.30 ± 0.52	0.470 ± 0.0058	0.616	0.31
SP39-09	-0.4	72	2.19 ± 0.01	484.32 ± 2.37	195.01	22.32 ± 0.23	0.321 ± 0.0040	0.606	0.25
SP20-09	-0.5	71	1.68 ± 0.01	403.24 ± 1.96	162.59	20.58 ± 0.21	0.310 ± 0.0038	0.590	0.25
SP19-09	-0.7	71	2.08 ± 0.01	289.80 ± 1.47	115.77	35.73 ± 0.37	0.384 ± 0.0047	0.605	0.27
SP18-09	-0.9	71	1.79 ± 0.01	436.18 ± 2.11	176.00	20.27 ± 0.21	0.305 ± 0.0037	0.595	0.24
SP17-09	-1.1	71	2.27 ± 0.01	107.09 ± 0.66	40.68	110.84 ± 1.17	0.794 ± 0.0101	0.629	0.44
SP16-09	-1.3	71	2.09 ± 0.01	407.07 ± 2.00	163.76	25.33 ± 0.26	0.328 ± 0.0040	0.601	0.25
SP15-09	-1.5	71	1.98 ± 0.01	130.77 ± 0.77	50.43	78.30 ± 0.82	0.669 ± 0.0084	0.615	0.42
SP14-09	-1.7	71	1.58 ± 0.01	118.28 ± 0.69	45.76	68.82 ± 0.75	0.642 ± 0.0081	0.595	0.42
SP13-09	-1.9	71	1.87 ± 0.01	188.64 ± 1.03	74.18	50.21 ± 0.52	0.509 ± 0.0063	0.603	0.35
SP12-09	-2.1	71	2.03 ± 0.01	179.00 ± 1.00	69.96	57.81 ± 0.60	0.560 ± 0.0070	0.609	0.38
SP8-09	-2.3	69	2.97 ± 0.01	192.49 ± 1.08	74.99	78.84 ± 0.80	0.585 ± 0.0073	0.622	0.33
SP9-09	-2.6	69	5.26 ± 0.02	164.12 ± 1.04	61.38	170.52 ± 1.71	0.923 ± 0.0115	0.636	0.38
SP10-09	-2.8	69	5.43 ± 0.02	149.32 ± 0.97	55.48	194.57 ± 1.95	0.980 ± 0.0122	0.638	0.36
SP11-09	-3.0	69	5.29 ± 0.02	152.90 ± 0.98	56.94	184.94 ± 1.86	0.960 ± 0.0120	0.637	0.37

Results presented to 2σ level of uncertainty.

[a] Rho is the associated error correlation (Ludwig, 1980)

[b] The initial ^{187}Os/^{188}Os isotope ratio calculated at 189.6 Ma

Ages calculated using the $\lambda\,^{187}Re = 1.666 \times 10^{-11}\ yr^{-1}$

3 *Developing a new geochemical analytical protocol for the separation of nickel from organic-rich sedimentary matrices, Durham University, UK.*

3.1 Introduction

The transition metals and their stable isotope systems have attracted increasing scientific interest in studies of both geological and biological processes. Nickel, a first row transition metal, has five stable isotopes, ^{58}Ni, ^{60}Ni, ^{61}Ni, ^{62}Ni and ^{64}Ni, with abundances of 68.0769 %, 26.2231 %, 1.1399 %, 3.6345 % and 0.9256 %, respectively (Gramlich *et al.,* 1989). Nickel is incorporated in both sulphide and silicate minerals within the Earth's crust, and its presence in most geological reservoirs has recently been used to evaluate the potential of Ni as a geological tracer (eg. Cameron *et al.,* 2011).

Previous Ni isotope fractionation studies have focused predominantly on extraterrestrial materials such as chondrites and iron meteorites. Discovery of isotopic anomalies in meteorites has been fundamental in contributing to our understanding of the isotopic composition of the early Solar System (eg. Birck and Lugmair, 1988). Further, due to improvement in mass spectrometry techniques, stable isotope systems such as Ni are able to provide a new perspective on nebular and planetary processes (Moynier *et al.,* 2007). Meteoritic Ni is present as a result of equilibrium processes and as such is highly dependent on parameters such as temperature, density and neutron enrichment (Morand and Allegre, 1983). Nickel isotope fractionation can occur during processes such as diffusion or evaporation (Davis and Brownlee, 1993; Herzog *et al.,* 1994; Engrand *et al.,* 2005), and thus quantifying this fractionation has significant potential to provide key information regarding early events and processes in the Solar System (eg. Quitté and Oberli, 2006).

Investigations have also focused on radiogenic ^{60}Ni anomalies in the quest for evidence of the extinct parent radionuclide ^{60}Fe (eg. Kohman and Robison, 1980; Morand and Allegre, 1983; Shimamura and Lugmair, 1983; Birck and Lugmair, 1988; Shukolyukov and Lugmair, 1993; Tachibana and Huss, 2003; Mostefaoui *et al.,* 2004; Quitté *et al.,* 2006; Moynier *et al.,*

2007). The ^{60}Fe-^{60}Ni chronometer is of particular interest as it could be used to precisely date planetary accretion and evolution (Quitté and Oberli, 2006). However, so far ^{60}Ni anomalies have remained elusive (eg. Birck, 2004), indicating that ^{60}Fe was either not present in measureable proportions or most of this nuclide decayed away during Solar System formation (Moynier *et al.,* 2007) due to its short half-life (~1.49 Myr; Kutschera, 1984).

Nickel also plays a significant role as a bioessential trace metal (eg. Frausto da Silva and Williams, 2001; Cameron *et al.,* 2007; 2009), being a key component in enzymes necessary for methanogenesis in predominantly prokaryotic microorganisms (Cameron *et al.,* 2007) that evolved in a much different Archean environment (Bapteste *et al.,* 2005; Frausto da Silva and Williams, 2001; Tice and Lowe, 2006). As such, the potential for Ni stable isotopes to identify primitive methanogenesis and ancient metabolisms that existed on the early Earth before the appearance of oxygen (Frausto da Silva and Williams, 2001) has recently been recognised (Cameron *et al.,* 2007; 2009; 2011). Nickel stable isotopes are therefore becoming an increasingly powerful biological tool for studies of early life on Earth (Cameron *et al.,* 2009; 2011).

In addition to studies of cosmochemistry and biochemistry, analyses of organic-rich materials such as petroleum source rocks and crude oils (eg. Lewan and Maynard, 1982; Lewan, 1984, Dewaker *et al.,* 2000), have demonstrated that Ni isotopes also have significant potential to be a powerful geological tracer in these environments. Currently, only one study exists that explores Ni isotope fractionation to evaluate the potential use of Ni isotopes as an oil-source correlation tool (Dewaker *et al.,* 2000). Previous investigations had focused on Ni distribution rather than isotopic analysis for correlation purposes (eg. Ellrich *et al.,* 1985; Manning *et al.,* 1991; Alberdi and Lafargue, 1993; Lopez *et al.,* 1995).

No studies exist that have documented Ni isotope analysis of organic-rich materials, partly due to the lack of a well-established analytical protocol for the separation and

purification of Ni from such a geological sample matrix. Whilst studies do document separation of Ni from other geological matrices (eg. Victor, 1986), there is a need for both improvement to yield consistency and for increased precision (eg. Chen *et al.,* 2009). Difficulties in removing and destroying the organic components can have a profound impact during mass spectrometry as discussed by Chen *et al.* (2009). It is therefore critical, especially when dealing with organic-rich samples, to develop a separation method that eliminates this problem. In addition, it is only in recent studies (eg. Chen and Papanastossiou, 2006; Tanimizu and Hirata, 2006; Cameron *et al.,* 2009; Gall *et al.,*2012) that high precision measurements of mass-dependent Ni isotope variations have been obtained, enabled by the use of a multi-collector inductively coupled mass spectrometer (MC-ICPMS).

This paper outlines our progress in developing a new procedure for the separation of Ni from organic-rich sample matrices. We also discuss our progress in being able to conduct isotopic analyses of Ni isotope variations by MC-ICPMS at NCEIT, Durham University, UK.

3.2 Scientific background: Ni in organic-rich sediments

Early investigations noted enriched concentrations of Ni in organic-rich materials, including crude oils (eg. Hodgson, 1954; Bonham, 1956; Witherspoon and Nagashima, 1957; Ball and Wenger, 1960), asphalts (Erickson *et al.,* 1954) and black shales (Krauskopf, 1955; Turekian and Wedepohl, 1961; Vine and Tourtelot, 1970). Nickel in organic-rich sediments is most likely to occur in tetrapyrrole complexes (Lewan and Maynard, 1982). Tetrapyrroles are metallo-organic complexes with four pyrrole-nitrogen atoms (organic N) bound to the central Ni atom. Tetrapyrroles have a strong affinity for both Ni and V (eg. Lewan, 1984; Lewan and Maynard, 1982) and as such vanadyl and nickelous cations are, almost exclusively, the only

metals found in naturally occurring tetrapyrrole complexes (Hodgson *et al.,* 1968; Filby, 1975). This affinity is partly attributed to the small ionic radii of the metals in these cations giving them a physical advantage over the other cations (Lewan and Maynard, 1982).

In organic-rich sediments tetrapyrrole complexes are likely to originate from chlorophyll (predominant in plants; Mg) and heme (most significant in animals; Fe) pigments found in living materials (Hodgson *et al.,* 1960; Blumer and Snyder, 1967; Yen, 1975). However, although Shiobara and Taguchi (1975) report heme pigments from some sediments, chlorophyll pigment is the most common precursor to tetrapyrrole complexes (Corwin, 1959) due to its wider distribution and greater abundance in the biosphere. Metallation of the tetrapyrrole complexes (ie, conversion of the chlorophyll pigment via replacement of Mg by Ni) occurs during burial of the unconsolidated sediments (Orr *et al.,* 1958; Baker and Smith, 1973; Yen, 1975; Lewan, 1984) prior to lithification (eg. Lewan and Maynard, 1982), indicated primarily by the absence of metallo-organic complexes of Ni in recent surface sediments (Louda and Baker, 1981).

These metallo-organic complexes have a high thermal stability (Hodgson and Baker, 1957) and are resistant to microbial degradation and weathering (Davis and Gibbs, 1975), ensuring that they will remain intact during lithification (Lewan, 1984; Lewan and Maynard, 1982) and will not cleave under diagenetic conditions (Constantinides *et al.,* 1959; Lewan, 1984; Lewan and Maynard, 1982). Further, their high thermal stability suggests that the generation, migration and entrapment of crude oil are unlikely to affect the metallo-organic bonds (Lewan, 1984).

There are two predominant sources of Ni that supply organic-rich sediments: Ni that is endemic to the living material from which the organic accumulation is derived (Manskaya and Drozdova, 1968; Yen, 1975), and dissolved Ni in the interstitial sediment pore-waters with which the organic matter is deposited (Lewan and Maynard, 1982). Endemic Ni concentrations,

whilst variable for different types of organisms (Martin and Knauer, 1973), will generally not exceed levels of ~45 ppm (eg. Lewan and Maynard, 1982). Therefore, organic-rich sediments that contain enriched concentrations of Ni (> 45 ppm) require an additional source (Lewan and Maynard, 1982). For a closed sediment system, one that no longer has access to the overlying water column, Ni is limited to concentrations within the order of the 10's of ppb level (Lewan and Maynard, 1982) and therefore is not able to provide enriched concentrations of Ni to the sediments. However, an open sediment system enables the overlying water column to supply Ni to the accumulating sediment, replacing the Ni that is removed from the interstitial pore-waters by metallation of tetrapyrroles (Lewan and Maynard, 1982). This is therefore a more effective source (Lewan, 1984; Lewan and Maynard, 1982) and will remain effective if the open sediment system persists, and if sedimentation rates do not increase (Lewan and Maynard, 1982).

An additional factor controlling the amount of Ni in organic-rich sedimentary rocks relates to the preservation of the tetrapyrrole complexes (Lewan, 1984; Lewan and Maynard, 1982). The degree of preservation is directly controlled by both the source of the organic matter and the water column conditions (Lewan and Maynard, 1982). Tetrapyrroles, and the organic matter accompanying them, are preferentially preserved under anaerobic conditions during sediment accumulation (Zobell, 1946; Brongersma-Sanders, 1951; Gorhan and Sanger, 1967; Koyama and Tomino, 1967; Drozdova and Gorskiy, 1972; Drozdova, 1975; Didyk *et al.,* 1978; Lewan and Maynard, 1982). Therefore, organic matter that has settled through an aerobic water column or has had prolonged exposure to aerobic conditions, for example at the sediment-water interface, will have a low tetrapyrrole content and is unlikely to be enriched in Ni (Lewan and Maynard, 1982). In contrast, enrichment in Ni (due to the higher tetrapyrrole content of the organic matter) will occur where the organic matter has been rapidly buried

under anaerobic conditions, or where it has interacted with anaerobic waters (Lewan and Maynard, 1982).

In natural samples Ni is predominantly present as Ni^{2+}, although it can occupy a range of oxidation states (0 to 4+). This indicates that Ni is unresponsive to changes in redox reactions. However, in organic-rich sediments, where the stability of the metallo-organic complexes is reliant on the redox conditions during deposition, redox can directly influence the degree of enrichment of Ni in the sediments (eg. Lewan, 1984; Lewan and Maynard, 1982).

3.3 Scientific background: Ni separation

The ability to separate metals from geological samples by cation exchange chromatography was first recognised by a number of early studies (eg. Strelow, 1960; Mann and Swanson, 1961; Fritz and Pierzyk, 1961; Wilkins and Smith, 1961; Fritz and Rettig, 1962; Korkisch and Ahluwalia, 1966; Peterson *et al.,* 1969; Wahlgren *et al.,* 1970; Strelow *et al.,* 1971; Morand and Allegre, 1983; Victor, 1986). Briefly, chromatography in geochemistry is a technique used for separating elemental components of a sample by taking advantage of the different adsorption rates and distribution coefficients of these components. In chromatography, the distribution coefficient refers to the ratio of the concentration of the solute in the stationary phase to that in the mobile phase.

In order to separate Ni from other elements, these workers utilised a liquid-liquid separation technique involving hydrochloric acid (HCl) and an organic solvent (acetone) media combined with dimethylglyoxime (DMG) [$(CH_3CHNO)_2$], a Ni complex-forming agent. This procedure has formed the basis for more recent developments of ion exchange separation

procedures for Ni (eg. Chen and Papanastossiou, 2006; Quitté and Oberli, 2006; Tanimizu and Hirata, 2006).

The affinity of Ni for DMG was utilised by workers in the early stages of Ni separation experiments (eg. Wahlgren *et al.,* 1970; Morand and Allegre, 1983; Victor, 1986). The use of DMG enables effective separation of Ni from metal ions which are co-adsorbed with Ni in the acetone:HCl eluants in previous stages of the exchange process (Wahlgren *et al.,* 1970). As such, DMG has become a key component in the Ni extraction procedure.

Studies of the distribution coefficients for the partitioning of metals and the cation exchange behaviour of elements in HCl-acetone and HCl-ethanol media (Strelow, 1960; Mann and Swanson, 1961; Pierzyk, 1961; Strelow *et al.,* 1971), demonstrate that acetone provides conditions favourable for separations at considerably lower HCl concentrations due to promotion of chloride complex formation (Strelow *et al.,* 1971). It is critical for the metal ions (other than Ni) to form chloro-complexes as these are held less strongly to the resin (Fritz and Rettig, 1962) than the Ni-DMG complex, allowing elution from the column and in turn purification of the Ni fraction.

Acetone is critical to enhancing the differences in distribution coefficients of many metal ions (Fritz and Rettig, 1962); the basis for separation procedures. In addition, Strelow *et al.* (1971) state that cation exchange separation of Ni^{2+}, the only oxidation state of Ni present in natural samples, is exceptionally difficult using HCl-ethanol solutions. The low viscosities of HCl-acetone mixtures also benefit flow rates (Strelow *et al.,* 1971).

The concentrations of acetone and HCl have considerable influence on the distribution coefficients for Ni^{2+}, emphasising the importance of acid concentration with regard to complexation (Fritz and Rettig, 1962; Strelow *et al.,* 1971; Victor, 1986). With increased percentage of acetone at low concentrations (0.5 N) of HCl, the distribution coefficients of many metal ions, with the exception of Ni^{2+}, drop considerably (Fritz and Rettig, 1962);

attributed to the other elements readily forming chloro-complexes (Fritz and Rettig, 1962; Victor, 1986).

Following thorough analysis and determination of distribution coefficients by these early studies, Victor (1986) developed a Ni separation procedure that relies on the formation of chloro-complex ions using 0.5 N HCl/93 % acetone solutions. Nickel is then eluted using a 0.5 N HCl/95 % acetone solution containing DMG. This forms the basis of the cation exchange procedure discussed in this paper.

3.4 Nickel separation from organic-rich sample matrices at Durham University, UK

3.4.1 Standards

3.4.1.1 National Institute of Standards and Technology, Standard Reference Material 986 (NIST 986 SRM)

Absolute values obtained for the isotopic abundance ratios of NIST 986 SRM (by Thermal Ionisation Mass Spectrometry) are defined by Gramlich *et al.* (1989) as: $^{58}Ni/^{60}Ni$ = 2.596061 ± 0.000728; $^{61}Ni/^{60}Ni$ = 0.043469 ± 0.000015; $^{62}Ni/^{60}Ni$ = 0.138600 ± 0.000045; and $^{64}Ni/^{60}Ni$ = 0.035295 ± 0.000024 (2σ uncertainties). These in turn yield absolute atomic abundances of: ^{58}Ni = 68.076886 ± 0.005919; ^{60}Ni = 26.223146 ± 0.005144; ^{61}Ni = 1.139894 ± 0.000433; ^{62}Ni = 3.634528 ± 0.001142; and ^{64}Ni = 0.925546 ± 0.000599 (Gramlich *et al.,* 1989).

This synthetic standard was calibrated and gravimetrically prepared from chemically and isotopically pure Ni metal at the Northern Centre for Elemental and Isotopic Tracing (NCEIT) Durham University, UK.

3.4.1.2 USGS SDO-1 SRM

U. S. Geological Survey reference sample SDO-1 is a brownish-black, brittle shale collected from the Huron Member of the Late Devonian Ohio Shale, western Rowan County, Kentucky (Kane *et al.,* 1990). It is organic-rich with abundant microfossils and contains flattened pyrite nodules (Kane *et al.,* 1990), in addition to being relatively radioactive (2 to 4 times background level; Provo *et al.,* 1978).

3.4.2 Analytical protocol

In order to use nickel (Ni) as a geological tracer, it is critical to have the ability to fully isolate Ni from geological materials. Successful separation of Ni from organic-rich samples must involve optimal recovery (yield) and the removal of both elemental and organic interferences. A successful analytical technique should:

1. Reduce the potential for interference during mass spectrometry, by removing elemental interferences and organic components.
2. Isolate and purify Ni (with >90 % recovery) from a variety of geological sample matrices.
3. Permit detection of low per mil variations (≥0.5 ‰) in Ni isotopes within samples, which is critical for the development of Ni as a geological tracer.
4. Produce blanks that are insignificant or/and reliably correctable.

3.4.2.1 Sample preparation and digestion

Sample powders (~100 mg) are loaded into a Carius Tube with a reverse aqua-regia solution (4 ml HNO_3 + 2 ml HCl), digesting in an oven at ~220 ^{o}C for ~48 hrs. This digestion technique ensures complete breakdown of the organic component of the sample (Cohen *et al.,* 1999; Selby and Creaser, 2003), therefore allowing the complete liberation of Ni from the organics.

Once cooled and prior to column chromatography, the solution is transferred to 15 ml centrifuge tubes and centrifuged for ~3 minutes removing the silicate fraction and any non-organic particulates that did not readily dissolve in the digestion stage. The supernatant solution is then transferred to 10 ml teflon vials and evaporated to near dryness at ~80 ^{o}C for ~48 hrs. In preparation for column chemistry (based upon HCl solutions), 3 ml 6N HCl is added to the sample and evaporated to dryness at ~80 ^{o}C, before 200 µl 9 N HCl is added to re-dissolve the Ni.

3.4.2.2 Nickel separation using column chromatography

To ensure separation and purification of Ni, the analytical protocol involves a two-stage column procedure, outlined below.

Stage 1: The first-stage column procedure is outlined in Figure 3.1. It consists of a disposable column made from a 1 ml graduated pipette with a quartz wool frit, filled to the base of the pipette reservoir with 1 ml AG-1-X (*anion*) resin. Iron, specifically ^{58}Fe, represents the most significant isobaric interference on ^{58}Ni during mass spectrometry. Due to the high Fe content of organic-rich sediments, usually in the weight percent level (> 10,000 ppm) (eg. Turekian and Wedepohl, 1961) and the fact that it is not possible to resolve ^{58}Fe from ^{58}Ni during mass spectrometry, it is critical that the chemistry eliminates the potential for this interference or reduces it to a level that allows algebraic correction using ^{57}Fe as a monitor. For this reason, a rapid anion exchange chromatography procedure using 9 N HCl elutions (modified from Strelow, 1980 and Herzog *pers. comms.*) is utilised as the first stage in our two-stage Ni purification and separation protocol.

Stage 2: The second-stage column procedure is detailed in Figure 3.2. It consists of a disposable column made from a 2 ml fine-tipped pipette with a quartz wool frit, and filled to the base of the pipette reservoir with AG50W-X4 (*cation*) resin. This column is designed to separate and purify the Ni fraction from the sample (modified from Victor, 1986).

Removal of residual organic components: It is critical to fully destroy any organic components originating from the column procedure (eg. from the acetone, DMG, column resin) prior to mass spectrometry, to reduce the potential for molecular interferences. In particular, acetone has the tendency to polymerize in acid solution, forming non-volatile organic matter (Strelow *et al.,* 1971). Following stage 2 step 17, the sample does not evaporate to complete dryness and instead forms a dark brown "sludge" that smells distinctly of DMG, a clear indication of the presence of organic residues in the Ni separate. To fully destroy these remaining organics, 1 ml 16 N HNO_3 is added to the sample, which is placed back on the hotplate (closed-cap) overnight at ~120 ^{o}C. Following this, the sample is evaporated to dryness (at ~100 ^{o}C) before the addition of 0.5 ml 30 % H_2O_2 (placed back on the hot plate, closed-cap, for 30 mins at ~140 ^{o}C). The sample is then evaporated to dryness at ~90 ^{o}C.

In preparation for mass spectrometry, 1 ml 3 % HNO_3 is added to the dried sample. To ensure that all of the sample is taken up into solution, it is placed on the hotplate (closed-cap) for 30 mins at ~50 ^{o}C. Finally, the sample is transferred to a micro-centrifuge and centrifuged for 3 mins to remove any particulates that may cause complications during analysis.

3.4.2.3 Column calibration using NIST 986 SRM

The column calibration plot for NIST 986 SRM after processing through the full column procedure (collection from the stage 2 column following prior collection from the stage 1 column) is presented in Figure 3.3. Also shown are the percentage yields of Ni at each stage of

the Ni elution phase (steps 10 – 17). The total yield of Ni from NIST 986 SRM for the full procedure is ~ 90 %. Of this 90 %, the greatest proportion of Ni is eluted from the column during steps 11 and 12 (~32 and 60 %, respectively). Following this, the elution peak drops dramatically to ~3 % yield at step 13.

As mentioned previously, the elements that present the greatest interferences on Ni are Fe and Zn (^{58}Fe on ^{58}Ni and ^{64}Zn on ^{64}Ni), and it is therefore critical that we are able to successfully isolate Ni from these elements. As our isotope measurement procedure involves doping with an internal Cu reference solution, isolation of Ni from Cu is also required. Figure 3.4 shows a calibration plot, as above, but also including Fe, Zn and Cu. A significant contribution of Cu is observed at the start of the Ni elution peak (45,000 cps; step 10) and continues to elute, although to a lesser degree (<10,000 cps) throughout steps 11 – 17 (Ni collection steps; Fig. 3.4). Similarly, the largest contribution of Zn is seen at step 10 (~7000 cps; Fig. 3.4), followed by elution intensities of <2000 cps between steps 11 – 17. The majority of Fe is eluted from the sample during the early stages of the first column procedure. Following this, there are two small Fe peaks during Ni collection on the second-stage column (steps 11 and 15, <5000 cps; Fig. 3.4).

3.4.2.4 Column calibration using USGS SDO-1 SRM

Although column calibrations based on NIST 986 SRM were instructive it is nevertheless a clean matrix and perhaps not entirely indicative of the behaviour of a complex rock matrix on the columns. For this reason calibrations were also based on the USGS SDO-1 SRM and are presented in Figure 3.5. The calibrations were conducted on separate days, although each calibration used ~100 mg of USGS SDO-1 powder.

It is immediately apparent that the maximum intensity in counts per second (cps) for the Ni elution peaks for the two replicate calibrations were different at ~$2.7*10^7$ and ~$1.4*10^6$

cps on plots a) and b), respectively (Fig. 3.5). Initially this indicates inconsistency between the Ni yields obtained during each calibration. There are several potential explanations for this, including:

1. Sample heterogeneity
2. Inconsistent yield from sample dissolution
3. Variations in instrument sensitivity
4. Inconsistent yield induced by the column chemistry, either during column 1 or column 2

USGS SDO-1 SRM is understood to be homogenous so Ni heterogeneity in the order of a factor of 20 is regarded as unlikely. Although the same weight of sample powder (~100 mg) was used for both calibrations and as such sample dissolution should be reproducible, the addition of only 200 µl of loading solution prior to the stage 1 column (Fig. 3.1) might induce inconsistent recovery if not all of the Ni is taken back up into solution. As the analyses were conducted on different days, instrument sensitivity could have contributed to the different intensities observed at the maximum Ni peaks. However, this does not account for the variations observed between the two peak shapes (Fig. 3.5). Specifically, there are inconsistencies between step 10 on the upward limb of the elution peaks, and step 12 on the downward limb of the elution peaks (Fig. 3.5). At step 10, the first stage of Ni elution, the amount of Ni eluted from the column in plot a) is equivalent to ~25 % (~$7.0*10^6$ cps) of the maximum peak (~$2.7*10^7$ cps; Fig. 3.5). However, this percentage at step 10 is far lower on plot b) and is ~5 % (~$8.0*10^4$ cps) of the maximum peak of ~$1.4*10^6$ cps. Similarly, at step 12, the Ni elution intensity is equivalent to ~60 % of the maximum peak on plot a), but is much lower, at ~14 %, on plot b) (Fig. 3.5).

The variations in proportionality between the individual Ni elutions across the entire elution peak indicate that there are inconsistencies in Ni yield from USGS SDO-1 SRM. Further,

this demonstrates that significant variation in yield for a sample matrix more complex than that of NIST 986 SRM, is induced by the column chemistry. This has also been demonstrated by other workers, who note that differences in the Ni to matrix ratio of samples can induce significant variation in the final yields of Ni from the separation procedure (Cameron *et al.,* 2009; Gall *et al.,* 2012).

3.5 Nickel stable isotope analysis at Durham University, UK

3.5.1 Mass spectrometry

Ni isotopes are measured in solution-mode on the Neptune MC-ICPMS at Durham University using a static collection routine and medium resolution (MR>7000) to avoid polyatomic interferences. The potential interference from ^{58}Fe on ^{58}Ni is corrected for algebraically using ^{57}Fe as the monitor. Samples (in this case NIST 986 SRM that has been run through the columns) and standards are doped with an internal Cu reference solution to allow correction of Ni mass bias using the ^{63}Cu/^{65}Cu ratio and an exponential law. The value of the ^{63}Cu/^{65}Cu ratio is determined daily relative to the certified NIST 986 ^{62}Ni/^{60}Ni ratio of 0.1386.

3.5.2 Analysis of pure NIST 986 SRM

Preliminary measurements of ^{58}Ni/^{62}Ni on pure NIST 986 SRM deviate by ~0.06 ‰ from the certified NIST 986 SRM value (Gramlich *et al*., 1989), and show excellent reproducibility (± 118 ppm, 2SD; n=20). Our preliminary data are more accurate than that reported by Tanimizu and Hirata (2006; 2.5 ‰ offset from accepted value). The good reproducibility of our data on NIST 986 SRM suggests that we should be able to resolve and

quantify Ni isotope variations in samples in the low per mil range (≥ 0.5 ‰), which is essential for the development of Ni a geological tracer.

The next step is to analyse NIST 986 SRM that has been processed through our column procedure (detailed above; Figs. 3.1 and 3.2) to ensure that no Ni fractionation is induced by the column chemistry. This includes analysis of the entire Ni collection for each separate column, as well as incremental elutions collected at each step of the Ni collection phase (ie. collection following each addition of acid during Ni elution). Whilst there should not be any measured Ni fractionation if the entire Ni elution is collected, attempting to collect the whole elution peak (including the tails of the peak) will result in collection of tails from other elemental peaks. This may promote interferences during mass spectrometry. As such, the total column collections analysed in section 3.5.3.1 collect Ni from the main body of the Ni elution peak (Fig. 3.3).

3.5.3 Analysis of NIST 986 SRM processed through column chemistry

3.5.3.1 Analysis of total column collections

Initial measurements of $^{58}Ni/^{60}Ni$ on 5 pure and 5 Fe-doped NIST 986 SRM (run at the start of the analytical session to show instrument performance) show good reproducibility (± 125 ppm; 2 SD; n = 20; Fig. 3.6) and reproducibility per atomic mass unit (amu) for $^{58}Ni/^{60}Ni$ and $^{61}Ni/^{60}Ni$ on pure and Fe-doped NIST 986 SRM is approximately similar (60 and 75 ppm, respectively; Fig. 3.6). The slightly improved reproducibility on $^{58}Ni/^{60}Ni$ is expected, as these are the most abundant isotopes and beam intensity is therefore greater.

Some shift is observed in $^{58}Ni/^{60}Ni$ and $^{61}Ni/^{60}Ni$ ratios for NIST 986 SRM processed through the column procedure (stage 2 and the full procedure; Fig. 3.6), although, with the exception of the $^{61}Ni/^{60}Ni$ ratio on run number 12, all are within error of the average for the

non-processed NIST 986 SRMs analysed in that session. Standards run through the column chemistry may have a slightly more complex matrix than pure NIST 986 SRM due to possible incomplete breakdown of organic components, which may account for some of the variation.

There is an observed increase in the degree of Ni and Cu instrumental mass bias throughout the analytical session with several notable jumps (Fig. 3.7a). These jumps in mass bias are seen to correspond with changes in the analyte matrix (Fig. 3.7b); for example, with the addition of Fe to pure NIST 986 SRM (runs 6 – 10; shift of 0.000260 units; Fig. 3.7b) followed by analysis of NIST 986 SRM run through the stage 2 column (runs 11 – 14; shift of 0.000365 units). Pure and column-processed NIST 986 SRMs are doped with Cu, to the same Cu/Ni ratio, immediately prior to mass spectrometry such that, for Cu at least, if mass bias was constant the $^{63}Cu/^{65}Cu$ ratio should be consistent for both pure and column-treated NIST 986 SRM. In other words, by doping after column processing we can eliminate column-induced fractionation as the cause for the drift in measured $^{63}Cu/^{65}Cu$. The variations seen in the measured Ni and Cu ratios are therefore most likely to reflect a gradual change in degree of instrumental mass bias throughout this particular analytical session. This is further supported by a lack of correlation between the measured $^{63}Cu/^{65}Cu$ ratio and Cu beam intensity (Fig. 3.9).

There are two important observations that can be drawn from Figures 3.7a and 3.7b. Figure 3.7a demonstrates that it is *possible* to induce sudden, albeit slight, changes in mass bias behaviour by subtle changes to the matrix, for example adding Fe or processing the sample through columns which may add other matrix. This is most likely to occur on days where there is a greater shift in mass bias throughout the analytical session (see section 3.5.3.2 and Fig. 3.11, where no systematic jump in mass bias is observed with Fe doping). If the mass bias behaviour for Ni and Cu are the same, the difference in measured $^{58}Ni/^{60}Ni$ and $^{63}Cu/^{65}Cu$ should remain constant despite the change in degree of mass bias, which Figure 3.7b

clearly shows was not the case during this analytical session. These observations highlight the drawbacks of using Cu-doping to correct for mass bias during stable Ni isotope analysis.

Despite these observations, the $^{58}Ni/^{60}Ni$ and $^{61}Ni/^{60}Ni$ ratios for replicate total collections of NIST 986 SRM processed through the stage 2 column and the full column procedure (stages 1 and 2) indicate that, if fractionation does occur during column chemistry, it is not resolvable with the current analytical protocol when the entire Ni elution is collected. The next step is to determine whether isotopic fractionation of Ni occurs during Ni elution, by analysing incremental steps of the Ni collection phase.

3.5.3.2 Analysis of incremental column collections

Analysis of incremental collections of Ni off the columns is important to ascertain whether Ni is fractionated during the early and/or late stage of the elution and therefore whether incomplete recovery of Ni will result in column-induced fractionation. Such an effect has been clearly illustrated for Sr on Eichrom Sr resin by Charlier *et al* (*in press*). One obvious difficulty with such measurements is the fact the amount of Ni recovered at the very start and end of the elution is small and therefore the precision, and accuracy, of the measurements are compromised simply by the lack of analyte. Analysis of the incremental fractions were carried out during a separate analytical session during which measurements of $^{58}Ni/^{60}Ni$ and $^{61}Ni/^{60}Ni$ on pure and Fe-doped NIST 986 SRM show excellent reproducibility (± 60 and ± 34 ppm, respectively; 2 SD; n = 18; Fig. 3.10).

A summary of the run numbers and their associated elution steps from the two columns is presented in Table 3.1. Unlike the total collections of NIST 986 SRM from the columns, the incremental elutions of NIST 986 SRM collected from the stage 1 and stage 2 columns (individually) show significant variation from the pure standards (Fig. 3.10). These include run numbers 13, 18 and 19, which correspond to the final elution of stage 1 Ni

collection, and the second and fourth steps of collection from the stage 2 column, respectively. Further, these show substantial deviations on $^{58}Ni/^{60}Ni$ from pure NIST 986 SRM, of ~0.3, 2.0 and 33.9 ‰, respectively.

There is little variation in mass bias behaviour at the start of the analytical session even with the addition of Fe to the pure NIST 986 SRM, as illustrated by the measured $^{58}Ni/^{60}Ni$ and $^{63}Cu/^{65}Cu$ ratios (Fig. 3.11), although a systematic drift in mass bias between the pure and Fe-doped NIST 986 SRM standards can be seen towards the end of the session. This illustrates that when the Neptune is stable, mass bias is less sensitive to additions of other matrices. For the initial elutions of NIST 986 SRM from the stage 1 column (run numbers 9 – 11), there is also no obvious change in the absolute degree of mass bias relative to the pure and Fe-doped NIST 986 SRM at the start of the session (Fig. 3.11). However, significant variation in the difference between the measured $^{58}Ni/^{60}Ni$ and $^{63}Cu/^{65}Cu$ ratios is observed for the final steps of stage 1 collection (run numbers 12 and 13) and the second and fourth steps of stage 2 collection (run numbers 18 and 19; Fig. 3.11). As alteration of the analyte matrix initially had no effect on the mass bias behaviour (Fig. 3.11), these variations may at least partially reflect the effects of column-induced isotope fractionation.

Figure 3.12 shows the mass bias corrected $^{63}Cu/^{65}Cu$ ratio (using $^{62}Ni/^{60}Ni$) for the analytical period. As discussed previously, no Cu fractionation should be measured as samples and standards were doped following chemical separation and prior to mass spectrometry. The substantial uncertainty on run number 19 can be partially attributed to the exceptionally low Ni beam intensity for this sample (^{60}Ni = ~0.1 volts), due to its position on the tail end of the Ni elution peak. Although there is no clear overall relationship between measured $^{63}Cu/^{65}Cu$ and Ni beam intensity (Fig. 3.13) the *measured* $^{63}Cu/^{65}Cu$ value for run number 19 (~2.141) does not vary significantly from that of the pure and Fe-doped NIST 986 SRM standards (not processed through columns). This suggests that the relatively high $^{63}Cu/^{65}Cu$ ratio after

correction for mass bias using the $^{62}Ni/^{60}Ni$ ratio (Fig. 3.12) reflects the fractionated nature of the Ni in that column fraction rather than odd Cu or mass bias behaviour. It is clear that there is a significant contribution of Fe from the stage 2 column (steps 11 and 13; Fig. 3.15). This was not previously observed on the calibration plot in Figure 3.4, possibly due to the analyses being conducted during different and separate sessions and limitations of lower resolution analysis used for the calibrations. When the measured $^{63}Cu/^{65}Cu$ and $^{58}Ni/^{60}Ni$ ratios are plotted against one another, two outliers are apparent (Fig. 3.16). These correspond to the two analytes that contain the greatest proportion of Fe (run numbers 18 and 19; ^{57}Fe = 0.034384 and 0.032642 volts, respectively). Similarly, these samples also have exceptionally low, and therefore less reliable, Ni beam intensities (^{60}Ni = 5.918210 and 0.128580, respectively). As mentioned previously, the correction for Fe is done algebraically using ^{57}Fe. However, the unfavourable Ni to Fe ratio in these samples does not allow for effective correction of Fe. As such, these samples (run numbers 18 and 19) are positioned below the scale shown on the mass bias corrected $^{58}Ni/^{60}Ni$ plot shown in Figure 3.10a (see arrow on figure), due to over-correcting using ^{57}Fe. Whilst the mass bias corrected $^{61}Ni/^{60}Ni$ ratio is not affected by the Fe correction, the large error present on run number 19 (Fig. 3.10b) reflects the limitations in accuracy and precision resulting from small Ni beam intensity. This emphasises the importance of fully isolating Ni from Fe, as well as the necessity of eliminating the effects of column-induced isotope fractionation.

Analysis of the incremental elution of the Ni collection indicates that, despite much greater uncertainties during the analysis attributed to very low beam intensity, Ni fractionation does occur during collection of the stage 2 column, when collecting the tails of the elution peak, and possibly during the final phase of collection of the stage 1 column.

3.6 Conclusions

Although column-induced Ni isotope fractionation for NIST 986 SRM is not resolvable when the entire Ni elution is collected, it is clear from analysis of the incremental column collections that Ni fractionation does occur during the final stages of collection. Further, using the current analytical technique at Durham, detailed in this chapter, chemical separation of Ni from more complex, organic-rich matrices, such as that of USGS SDO-1 SRM, provides incomplete and inconsistent Ni yields, and we therefore directly capture the effect of column-induced fractionation. Given the variability and inconsistency of yields using a standard that is of a similar matrix to the organic-rich samples that this method was originally intended for, our approach needs to be re-evaluated in order to account for this fractionation.

As stated previously, our technique currently involves doping pure standards and standards processed through the columns (samples) with an internal Cu reference solution prior to mass spectrometry, in order to correct for mass discrimination. There are 2 alternative methods that can be used to achieve this, and all 3 methods are outlined briefly below:

1. *Doping with another element*. This involves doping the sample with an aliquot of an element of similar mass to the element of interest (eg. Maréchal *et al.,* 1999; Archer and Vance, 2004). This technique requires that the mass bias behaviour of the analyte and dopant elements is similar (eg. Archer and Vance, 2004).
2. *Standard-sample bracketing (SSB)*. The isotope ratio of the analyte element is measured in standard solutions run between the samples (eg. Beard *et al.,* 2003; Bermin *et al.,* 2006; Peel *et al.,* 2008). This is potentially the simplest method of performing mass discrimination corrections in MC-ICPMS data (eg. Beard *et al.,* 2003; Bermin *et al.,* 2006), although this approach is potentially compromised by

differences in the matrices of pure standards and real samples (Bermin *et al.,* 2006), as it requires that the mass bias behaviour of the standards and samples is the same (Archer and Vance, 2004).

3. *Double-spiking*. This utilises the addition of a tracer of the analyte element with known 'exotic' isotopic composition (eg. Dodson, 1963; Johnson and Beard, 1999; Thirlwall, 2002; Cameron *et al.,* 2009; Gall *et al.,* 2012). This approach can be used for any element that has a minimum of four naturally occurring isotopes. There are a number of advantages to using the double-spike technique. Firstly, there are no issues arising from differences in the behaviour of samples and standards (SSB), or samples and dopants. Secondly, if added to the sample prior to chemical separation, difficulties arising from potential column-induced fractionation resulting from incomplete and inconsistent yields, are removed (eg. Johnson and Beard, 1999; Cameron *et al.,* 2009; Gall *et al.,* 2012). However, the double-spike technique cannot solve potential problems relating to polyatomic interferences during mass spectrometry and therefore a clean separation procedure that results in a pure Ni separate is still necessary.

Recent studies investigating the chemical separation of Ni and analysis of Ni isotopes in varying geological matrices, have advocated use of the double spike approach (eg. Cameron *et al.,* 2009; Gall *et al.,* 2012), particularly as it eliminates problems regarding fractionation induced by chemical separation. From our work at Durham, it is clear that this approach is necessary in order to successfully analyse the Ni isotope composition of organic-rich sample matrices using our chemical separation procedure.

However, calibration of the spike is time consuming and data reduction using this technique is algebraically extremely complex. Therefore, due to time constraints, although this

is undoubtedly the next step for Ni isotope analysis at Durham, we were unable to implement this during the duration of the PhD research presented herein.

3.7 References

Alberdi, M., and Lafargue, E., 1993, Vertical variations of organic matter content in Guayuta Group (upper Cretaceous), Interior Mountain Belt, Eastern Venezuela: Organic Geochemistry, v. 20, p. 425-436.

Archer, C., and Vance, D., 2004, Mass discrimination correction in multiple-collector plasma source mass spectrometry: an example using Cu and Zn isotopes: Journal of Analytical Atomic Spectrometry, v. 19, no. 5.

Baker, E.W., and Smith, G.D., 1973, Pleitocene changes in chlorophyll pigments, *in* Tissot, B., and Bienner, F., eds., Advances in Organic Geochemistry, Editions Technip, Paris, p. 649-660.

Ball, J.S., and Wenger, W.J., 1960, Metal content of twenty-four petroleums: Journal of Chemical and Engineering Data, v. 5, p. 553-557.

Bapteste, E., Brochier, C., and Boucher, Y., 2005, Higher-level classification of the Archaea: Evolution of methanogenesis and methanogens: Archaea, v. 1, p. 353-363.

Beard, B. L., Johnson, C. M., Skulan, J. L., Nealson, K. H., Cox, L., and Sun, H., 2003, Application of Fe isotopes to tracing the geochemical and biological cycling of Fe: Chemical Geology, v. 195, no. 1–4, p. 87-117.

Bermin, J., Vance, D., Archer, C., and Statham, P. J., 2006, The determination of the isotopic composition of Cu and Zn in seawater: Chemical Geology, v. 226, no. 3–4, p. 280-297.

Birck, J.L., 2004, An overview of isotopic anomalies in extraterrestrial materials and their nucleosynthetic heritage, *in* Johnson, C.M., Beard, B.L., and Albarède, F., eds., Geochemistry of Non-Traditional Stable Isotopes, Volume 55, Mineralogical Society of America, Washington, p. 26-63.

Birck, J.L., and Lugmair, G.W., 1988, Nickel and chromium isotopes in Allende inclusions: Earth and Planetary Science Letters, v. 90, p. 131-143.

Blumer, M., and Snyder, W.D., 1967, Porphyrins of high molecular weight in a Triassic oil shale: Evidence by gel permeation chromatography: Chemical Geology, v. 2, p. 35-45.

Bonham, L.C., 1956, Geochemical investigation of crude oils: American Association of Petroleum Geologists Bulletin, v. 40, p. 897-908.

Brongersma-Sanders, M., 1951, On conditions favoring the preservation of chlorophyll in marine sediments: Proceedings of the 3rd World Petroleum Congress, Hague, v. Sec. 1, p. 401-411.

Cameron, V., Vance, D., Archer, C., and House, C.H., 2007, Nickel stable isotopes as biogeochemical tracers, Goldschmidt Conference Abstracts, p. A141.

Cameron, V., Vance, D., Archer, C., and House, C.H., 2009, A biomarker based on the stable isotopes of nickel: Proceedings of the National Academy of Sciences, v. 106, p. 10944-10948.

Cameron, V., Vance, D., and Poulton, S., 2011, Nickel isotopes, BIFs and the Archean oceans, Goldschmidt Conference Abstracts, Mineralogical Magazine, p. 615.

Charlier, B. L. A., Nowell, G. M., Parkinson, I. J., Kelley, S. P., Pearson, D. G., and Burton, K. W., *in press*, High-Temperature Stable Strontium Isotope (δ^{88}Sr) Fractionation in Terrestrial and Extraterrestrial Materials: Earth and Planetary Science Letters.

Chen, J.H., and Papanastassiou, D.A., 2006, Nickel Isotope Investigation by MC-ICP-MS and PTIMS, 37th Annual Lunar and Planetary Science Conference: League City, Texas.

Chen, J.H., Papanastassiou, D.A., and Wasserburg, G.J., 2009, A search for nickel isotopic anomalies in iron meteorites and chondrites: Geochimica et Cosmochimica Acta, v. 73, p. 1461-1471.

Cohen, A.S., Coe, A.L., Bartlett, J.M., and Hawkesworth, C.J., 1999, Precise Re-Os ages of organic-rich mudrocks and the Os isotope composition of Jurassic seawater: Earth and Planetary Science Letters, v. 167, p. 159-173.

Constantinides, G., Arich, G., and Lomi, C., 1959, Detection and behaviour of porphyrin aggregates in petroleum residues and bitumens: Proceedings of the 5th World Petroleum Congress, v. Section V, p. 131-142.

Cook, D.L., Wadhwa, M., Clayton, R., Dauphas, N., Janney, P.E., and Davis, A.M., 2007, Mass-dependent fractionation of nickel isotopes in meteoritic metal: Meteoritics and Planetary Science, v. 42, p. 2067-2077.

Corwin, A.H., 1959, Petroporphyrins: Proceedings of the 5th World Petroleum Congress, v. Section 5, p. 120-129.

Davis, A.M., and Brownlee, D.E., 1993, Iron and nickel isotopic mass fractionation in deep-sea spherules Lunar and Planetary Science, v. 24, p. 373-374.

Davis, S.J., and Gibbs, C.F., 1975, The effects of weathering on a crude oil residue exposed at sea: Water Research, v. 9, p. 275-285.

Dewaker, K.N., Chandra, K., Arunachalam, J., and Karunasagar, D., 2000, Isotopic fractionation of Ni60/Ni61 in kerogen and bitumen samples: Current Science, v. 79, p. 1720-1723.

Didyk, B.M., Simoneit, B.R.T., Brassell, S.C., and Eglinton, G., 1978, Organic geochemical indicators of paleoenvironmental conditions of sedimentation: Nature, v. 272, p. 216-222.

Dodson, M.H., 1970, Simplified equations for double-spiked isotopic analyses: Geochimica et Cosmochimica Acta, v. 34, no. 11, p. 1241-1244.

Drozdova, T.V., 1975, Geochemical conditions for the preservation of amino acids and porphyrin structures in sediments, *in* Tugarinov, A., ed., Recent Contributions to Geochemistry and Analytical Chemistry, John Wiley & Sons, Inc., p. 523-529.

Drozdova, T.V., and Gorskiy, Y.N., 1972, Conditions of preservation of chlorophyll, pheophytin and humic matter in Black Sea sediments: Geochemistry International, v. 9, p. 208-218.

Ellrich, J., Hirner, A., and Stärk, H., 1985, Distribution of trace elements in crude oils from southern Germany: Chemical Geology, v. 48, p. 313-323.

Engrand, C., McKeegan, K.D., Leshin, L.A., Herzog, G.F., Schnabel, C., Nyquist, L.E., and Brownlee, D.E., 2005, Isotopic compositions of oxygen, iron, chromium, and nickel in cosmic spherules: Toward a better comprehension of atmospheric entry heating effects: Geochimica et Cosmochimica Acta, v. 69, p. 5365-5385.

Erickson, R.L., Myers, A.T., and Horr, C.A., 1954, Association of uranium and other metals with crude oil, asphalt, and petroliferous rocks: American Association of Petroleum Geologists Bulletin, v. 38, p. 2200-2218.

Filby, R.H., 1975, The nature of metals in petroleum, *in* Yen, ed., The Role of Trace Elements in Petroleum, Ann Arbor Science Publishers, p. 31-58.

Frausto da Silva, J.J.R., and Williams, R.J.P., 2001, The Biological Chemistry of the Elements: The Inorganic Chemistry of Life, Oxford University Press, Oxford, p. 436-449.

Fritz, J.S., 1962, Separation of Metals by Cation Exchange in Acetone-Water-Hydrochloric Acid: Analytical Chemistry, v. 34, p. 1562-1566.

Fritz, J.S., and Pietrzyk, D.J., Non-aqueous solvents in anion-exchange separations: Talanta, v. 8, p. 143-162.

Gall, L., Williams, H., Siebert, C., and Halliday, A., 2012, Determination of mass-dependent variations in nickel isotope compositions using double spiking and MC-ICPMS: Journal of Analytical Atomic Spectrometry, v. 27, no. 1, p. 137-145.

Gorhan, E., and Sanger, J., 1967, Plant pigments in woodland soils: Ecology, v. 48, p. 306-308.

Gramlich, J.W., Machlan, L.A., Barnes, I.L., and Paulsen, P.J., 1989, Absolute Isotopic Abundance Ratios and Atomic Weight of a Reference Sample of Nickel: Journal of Research of the National Institute of Standards and Technology, v. 94, p. 347-356.

Herzog, G.F., hall, G.S., and Brownlee, D.E., 1994, Mass fractionation of nickel isotopes in metallic cosmic spheres: Geochimica et Cosmochimica Acta, v. 58, p. 5319-5323.

Hodgson, G.W., 1954, Vanadium, nickel, and iron trace metals in crude oils of Western Canada: American Association of Petroleum Geologists Bulletin, v. 38, p. 2537-2554.

Hodgson, G.W., and Baker, B.L., 1957, Vanadium, nickel, and porphyrins in thermal geochemistry of petroleum: American Association of Petroleum Geologists Bulletin, v. 41, p. 2416-2426.

Hodgson, G.W., Hitchon, B., Elofson, R.M., Baker, B.L., and Peake, E., 1960, Petroleum pigments from Recent fresh-water sediments: Geochimica et Cosmochimica Acta, v. 19, p. 272-288.

Hodgson, G.W., Hitchon, B., Taguchi, K., Baker, B.L., and Peake, E., 1968, Geochemistry of porphyrins, chlorins and polycyclic aromatics in soils, sediments and sedimentary rocks: Geochimica et Cosmochimica Acta, v. 32, p. 737-772.

Johnson, C. M., and Beard, B. L., 1999, Correction of instrumentally produced mass fractionation during isotopic analysis of fe by thermal ionization mass spectrometry: International Journal of Mass Spectrometry, v. 193, no. 1, p. 87-99.

Kane, J.S., Arbogast, B., and Leventhal, J., 1990, Characterization of Devonian Ohio Shale SDO-1 as a USGS Geochemical Reference Sample: Geostandards Newsletter, v. 14, p. 169-196.

Kohman, T.P., and Robison, M.S., 1980, Iron-60 as a possible heat source and chronometer in the early solar system: Lunar and Planetary Science, v. 11, p. 564-566.

Korkisch, J., and Ahluwalia, S.S., 1967, Cation-exchange behaviour of several elements in hydrochloric acid—organic solvent media: Talanta, v. 14, p. 155-170.

Koyama, T., and Tomino, T., 1967, Decomposition process of organic carbon and nitrogen in lake water: Geochemical Journal, v. 1, p. 109-124.

Krauskopf, K.B., 1955, Sedimentary deposits of rare metals, Economic Geology, Volume 50th Annual Volume, p. 1905-1955.

Kutschera, W., 1984, Half-life of ^{60}Fe: Nuclear Instruments and Methods, v. B5, p. 430-435.

Lewan, M.D., 1984, Factors controlling the proportionality of vanadium to nickel in crude oils: Geochimica et Cosmochimica Acta, v. 48, p. 2231-2238.

Lewan, M.D., and Maynard, J.B., 1982, Factors controlling enrichment of vanadium and nickel in the bitumen of organic sedimentary rocks: Geochimica et Cosmochimica Acta, v. 46, p. 2547-2560.

López, L., Lo Mónaco, S., Galarraga, F., Lira, A., and Cruz, C., 1995, VNi ratio in maltene and asphaltene fractions of crude oils from the west Venezuelan basin: correlation studies: Chemical Geology, v. 119, p. 255-262.

Louda, J.W., and W., B.E., 1981, Geochemistry of tetrapyrrole, carotenid, and perylene pigments in sediments from the San Miguel Gap (site 467) and Baja California Borderland (site 471), Deep Sea Drilling Project Leg 63, *in* Orlofsky, S., ed., Initial Reports of the Deep Sea Drilling Project-LXIII: Washington, U.S. Govt. Printing Office, p. 785-818.

Mann, C.K., and Swanson, C.L., 1961, Cation Exchange Elution of Metallic Chlorides by Hydrochloric Acid: Analytical Chemistry, v. 33.

Manning, L.K., Frost, C.D., and Branthaver, J.F., 1991, A neodymium isotopic study of crude oils and source rocks: potential applications for petroleum exploration: Chemical Geology, v. 91, p. 125-138.

Manskaya, S.M., and Drozdova, T.V., 1968, Geochemistry of Organic Subtances, Pergamon Press.

Maréchal, C. N., Télouk, P., and Albarède, F., 1999, Precise analysis of copper and zinc isotopic compositions by plasma-source mass spectrometry: Chemical Geology, v. 156, no. 1–4, p. 251-273.

Martin, J.H., and Knauer, G.A., 1973, The elemental composition of plankton: Geochimica et Cosmochimica Acta, v. 37, p. 1639-1653.

Morand, P., and Allègre, C.J., 1983, Nickel isotopic studies in meteorites: Earth and Planetary Science Letters, v. 63, p. 167-176.

Mostefaoui, S., Lugmair, G.W., Hoppe, P., and Goresy, A., 2004, Evidence for live ^{60}Fe in meteorites: New Astronomy Reviews, v. 48, p. 155-159.

Moynier, F., Blichert-Toft, J., Telouk, P., Luck, J.-M., and Albarède, F., 2007, Comparative stable isotope geochemistry of Ni, Cu, Zn, and Fe in chondrites and iron meteorites: Geochimica et Cosmochimica Acta, v. 71, p. 4365-4379.

Orr, W.L., Emery, K.O., and Grady, J.R., 1958, Preservation of chlorophyll derivatives in sediments off southern California: American Association of Petroleum Geologists Bulletin, v. 42, p. 925-962.

Peel, K., Weiss, D., Chapman, J., Arnold, T., and Coles, B., 2008, A simple combined sample-standard bracketing and inter-element correction procedure for accurate mass bias correction and precise Zn and Cu isotope ratio measurements: Journal of Analytical Atomic Spectrometry, v. 23, no. 1.

Peterson, S.F., Tera, F., and Morrison, G.H., 1969, Isotopic ion exchange separation of radioisotopes using an acetone-water-hydrochloric acid system: Journal of Radioanalytical Chemistry, v. 2, p. 115-125.

Pietrzky, D.J., 1961, Ph.D. thesis.

Provo, L.J., Kepferle, R.C., and Potter, P.E., 1978, Division of black Ohio Shale in eastern Kentucky: American Association of Petroleum Geologists Bulletin, v. 62, p. 1703-1713.

Quitté, G., Meier, M., Latkoczy, C., Halliday, A.N., and Günther, D., 2006, Nickel isotopes in iron meteorites–nucleosynthetic anomalies in sulphides with no effects in metals and no trace of ^{60}Fe: Earth and Planetary Science Letters, v. 242, p. 16-25.

Quitté, G., and Oberli, F., 2006, Quantitative extraction and high precision isotope measurements of nickel by MC-ICPMS: Journal of Analytical Atomic Spectrometry, v. 21, p. 1249-1255.

Selby, D., and Creaser, R.A., 2003, Re-Os geochronology of organic rich sediments: an evaluation of organic matter analysis methods: Chemical Geology, v. 200, p. 225-240.

Shimamura, T., and Lugmair, G.W., 1983, Ni isotopic compositions in Allende and other meteorites: Earth and Planetary Science Letters, v. 63, p. 177-188.

Shiobara, M., and Taguchi, K., 1975, Early diagenetic transformation of porphyrin compunds in some Japanese sediments, *in* Campos, R., and Goni, J., eds., Advances in Organic Geochemistry, Empressa Nacional Adaro De Investigaciones Mineras, p. 237-251.

Shukolyukov, A., and Lugmair, G.W., 1993, Live iron-60 in the early Solar System: Science, v. 259, p. 1138-1142.

Strelow, F.W.E., 1960, An Ion Exchange Selectivity Scale of Cations Based on Equilibrium Distribution Coefficients: Analytical Chemistry, v. 32, p. 1185-1188.

Strelow, F.W.E., 1980, Improved separation of iron from copper and other elements by anion-exchange chromatography on a 4% cross-linked resin with high concentrations of hydrochloric acid: Talanta, v. 27, p. 727-732.

Strelow, F.W.E., Victor, A.H., van Zyl, C.R., and Eloff, C., 1971, Distribution coefficients and cation exchange behaviour of elements in hydrochloric acid-acetone: Analytical Chemistry, v. 43, p. 870-876.

Tachibana, S., and Huss, G.R., 2003, The initial abundance of ^{60}Fe in the Solar System: Astrophysical Journal, v. 588, p. L41-L44.

Tanimizu, M., and Hirata, T., 2006, Determination of natural isotopic variation in nickel using inductively coupled plasma mass spectrometry: Journal of Analytical Atomic Spectrometry, v. 21, p. 1423-1426.

Tice, M.M., and Lowe, D.R., 2006, The origin of carbonaceous matter in pre-3.0 Ga greenstone terrains: A review and new evidence from the 3.42 Ga Buck Reef Chert: Earth-Science Reviews, v. 76, p. 259-300.

Thirlwall, M. F., 2002, Multicollector ICP-MS analysis of Pb isotopes using a 207pb-204pb double spike demonstrates up to 400 ppm/amu systematic errors in Tl-normalization: Chemical Geology, v. 184, no. 3–4, p. 255-279.

Turekian, K.K., and Hans Wedepohl, K., 1961, Distribution of the Elements in Some Major Units of the Earth's Crust: Geological Society of America Bulletin, v. 72, p. 175-192.

Victor, A.H., 1986, Separation of nickel from other elements by cation-exchange chromatography in dimethylglyoxime/hydrochloric acid/acetone media: Analytica Chimica Acta, v. 183, p. 155-161.

Vine, J.D., and Tourtelot, E.B., 1970, Geochemistry of black shale deposits - A summary report: Economic Geology, v. 65, p. 253-272.

Wahlgren, M., Orlandini, K.A., and Korkisch, J., 1970, Specific cation-exchange separation of nickel: Analytica Chimica Acta, v. 52, p. 551-553.

Wilkins, D.H., and Smith, G.E., Ethanol-water-hydrochloric acid eluents in anion-exchange separations: Talanta, v. 8, p. 138-142.

Witherspoon, P.A., and Nagashima, K., 1957, Use of trace metals to identify Illinois crude oils: Illinois State Geological Survey, Circular, v. 239, p. 15.

Yen, T.F., 1975, Chemical aspects of metals in native petroleum, The Role of Trace Metals in Petroleum, Ann Arborm Science Publishers Inc., p. 1-30.

Zobell, C.E., 1946, Marine Microbiology, Chronica Botanica Company.

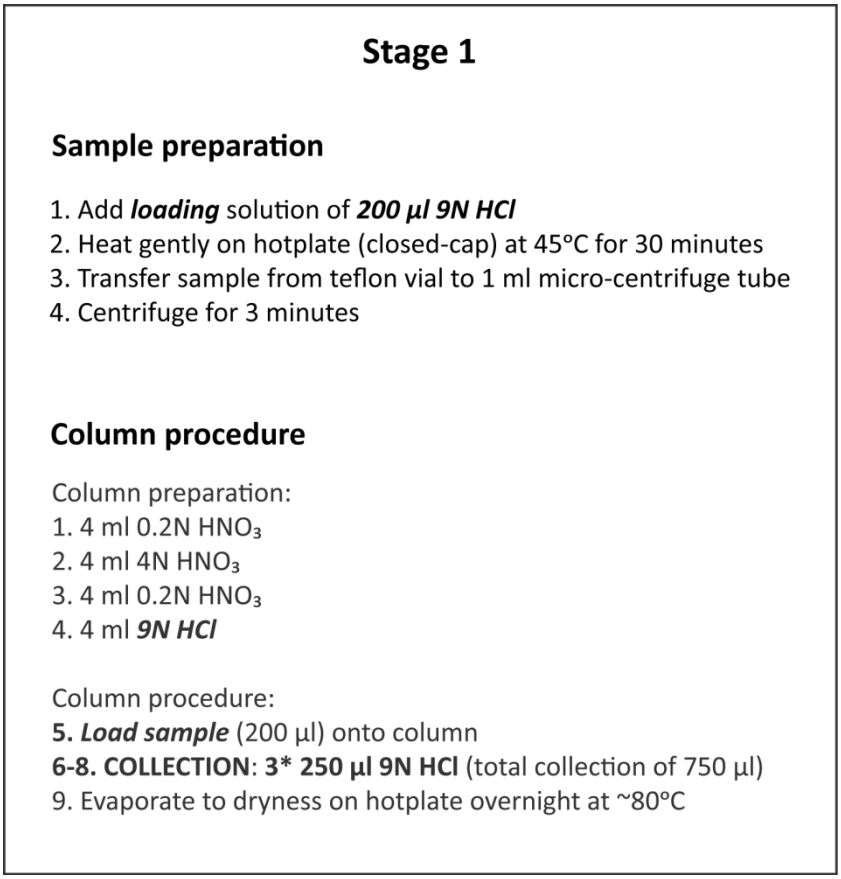

Figure 3.1: Outline of the stage 1 column procedure. This column is designed to remove a large proportion of the Fe from the sample.

Stage 2

Sample preparation

1. Dissolve sample (from Stage 1, step 7) in 100 µl 6N HCl
2. Evaporate to near dryness at ~70°C
3. Add ***loading*** solution of ***100 µl acetone:6N HCl (9:1)***

Column procedure

Column preparation:
1. 5 ml 6N HCl
2. 5 ml MQ (high-purity water)
3. 5 ml 6N HCl
4. 5 ml MQ

Column procedure:
5-6. 2* 5 ml acetone:6N HCl (9:1)
7. *Load sample*
8-9. 2* 1 ml acetone:6N HCl (9:1)
10. 6 ml acetone:6N HCl (9:1)
11-14. 4* 5 ml acetone:12N HCl (9.5:0.5)
15. 1 ml acetone:12N HCl (9.5:0.5) *+ dimethylglyoxime (DMG) (11mg/ml DMG)*
16-22. COLLECTION: 7* 1 ml acetone:12N HCl (9.5:0.5) + DMG (11mg/ml)
23. Evaporate to near dryness on hotplate overnight at ~80°C

Figure 3.2: Outline of the stage 2 column procedure. By utilising DMG, this column is designed to separate and purify Ni from the sample.

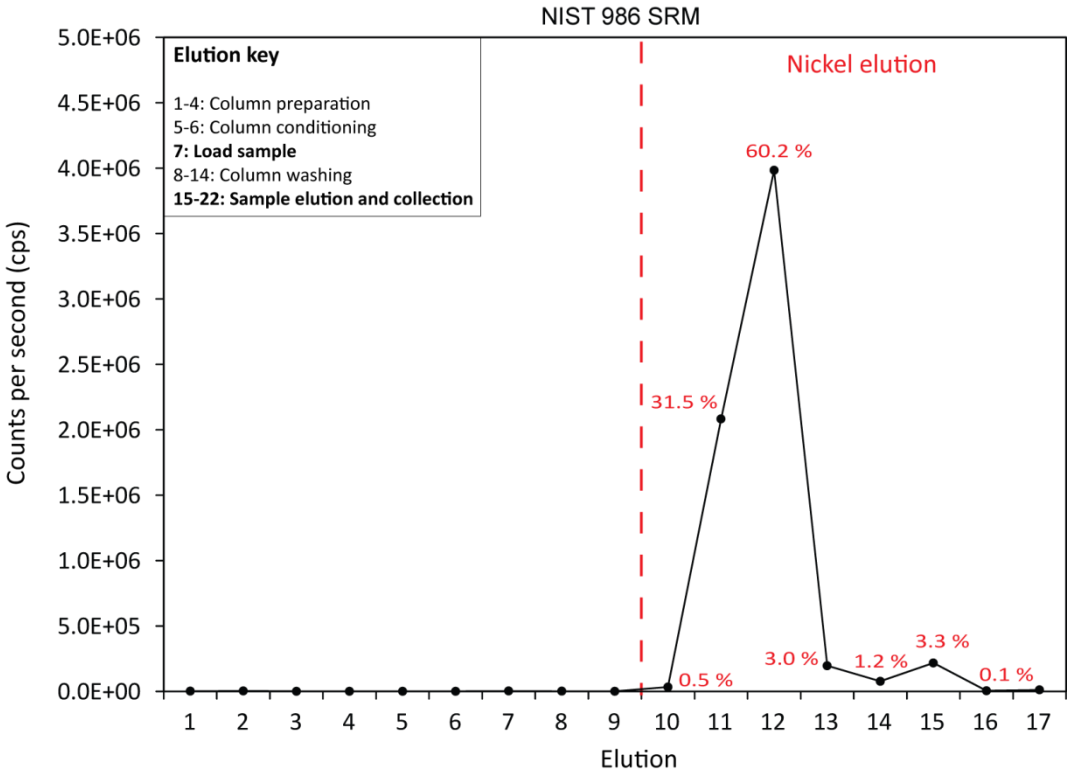

Figure 3.3: Nickel calibration plot for the full-stage column procedure using NIST 986 SRM. Plot shows elutions from the stage 2 column, following prior processing through the stage 1 column. Red dashed line marks the start of the Ni elution phase. Percentages presented in red correspond to the Ni yield. The unit 'Counts per second (cps)' corresponds to the measured counts of total Ni.

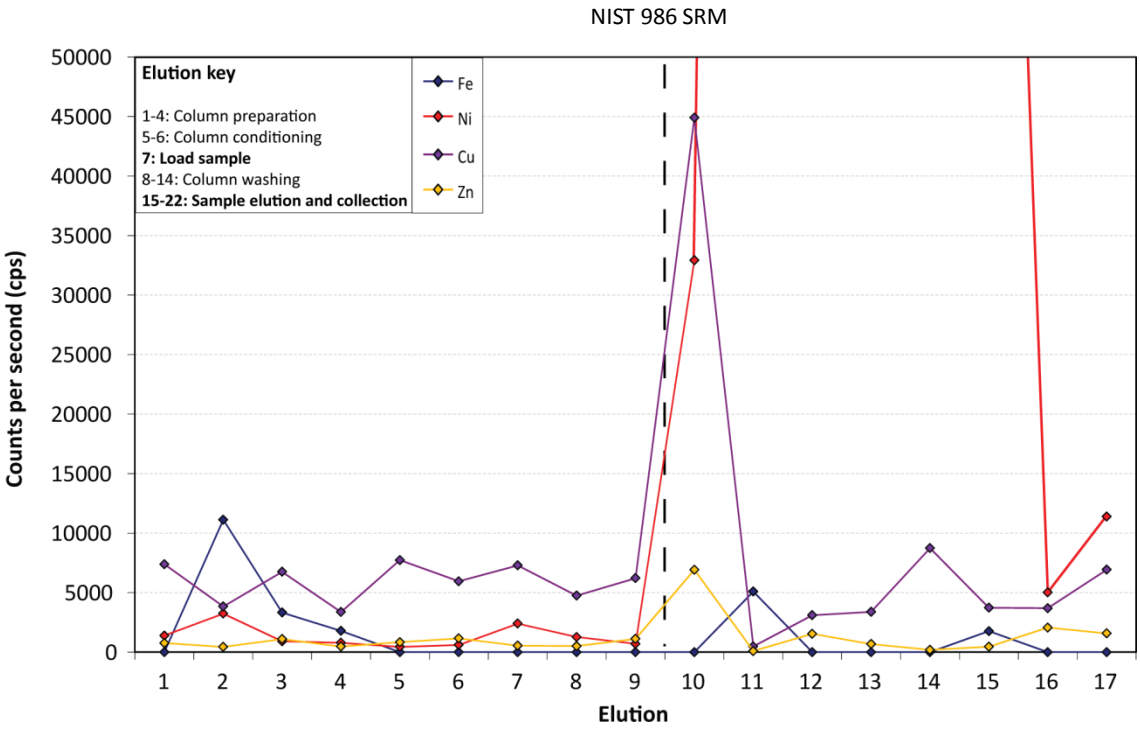

Figure 3.4: Calibration plot for the full-stage column procedure using NIST 986 SRM. Plot shows calibration lines for Fe (blue), Cu (purple) and Zn (yellow) in addition to Ni (red). Black dashed line marks the start of the Ni elution phase.

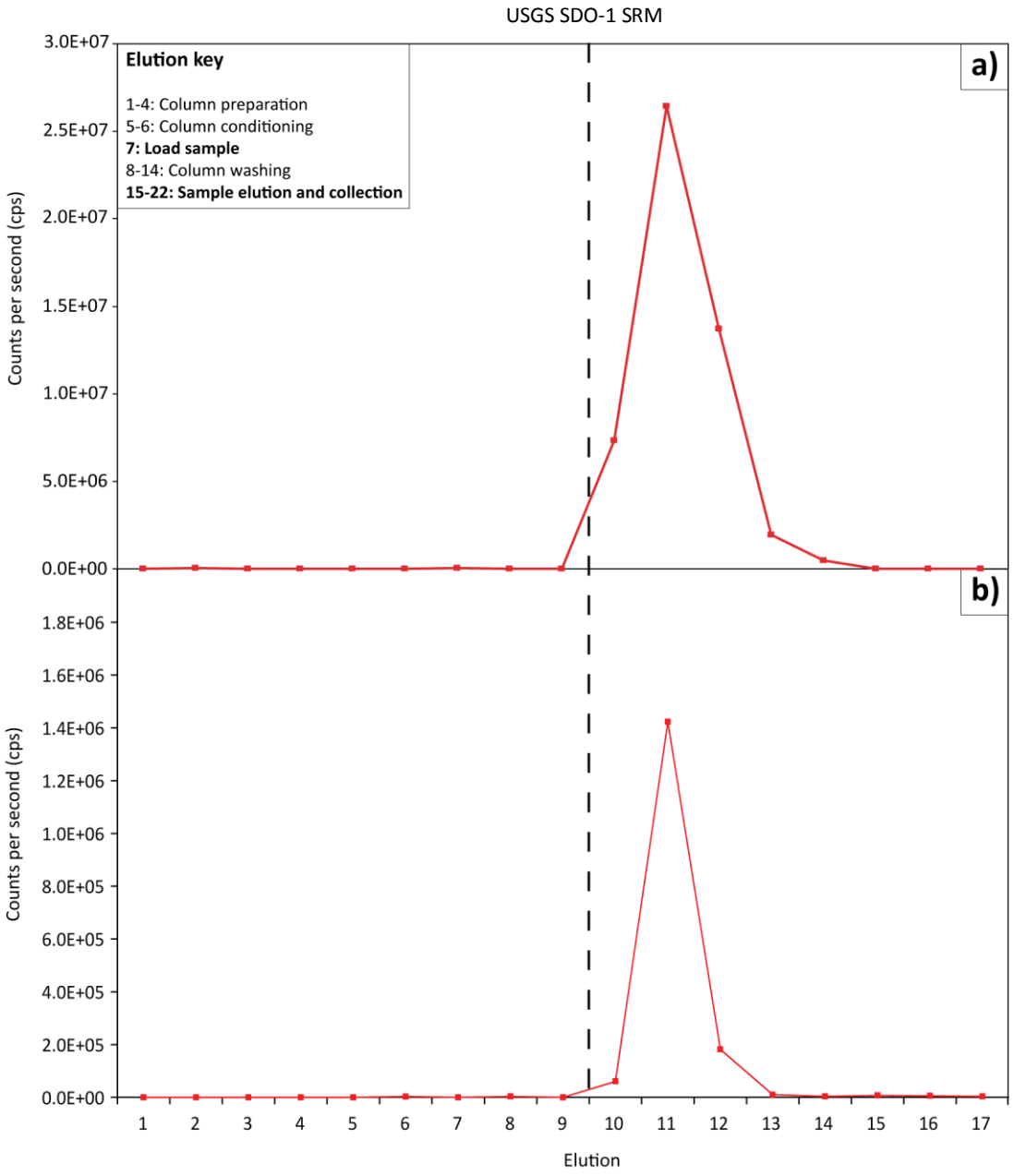

Figure 3.5: Nickel calibration plots for the full-stage column procedure using USGS SDO-1 SRM (shale standard). Plots a) and b) represent the same calibration process using near identical amounts of SDO-1 SRM powder (~100 mg) analysed on the same ICP-MS, but conducted during separate analytical sessions. Black dashed line marks the start of the Ni elution phase.

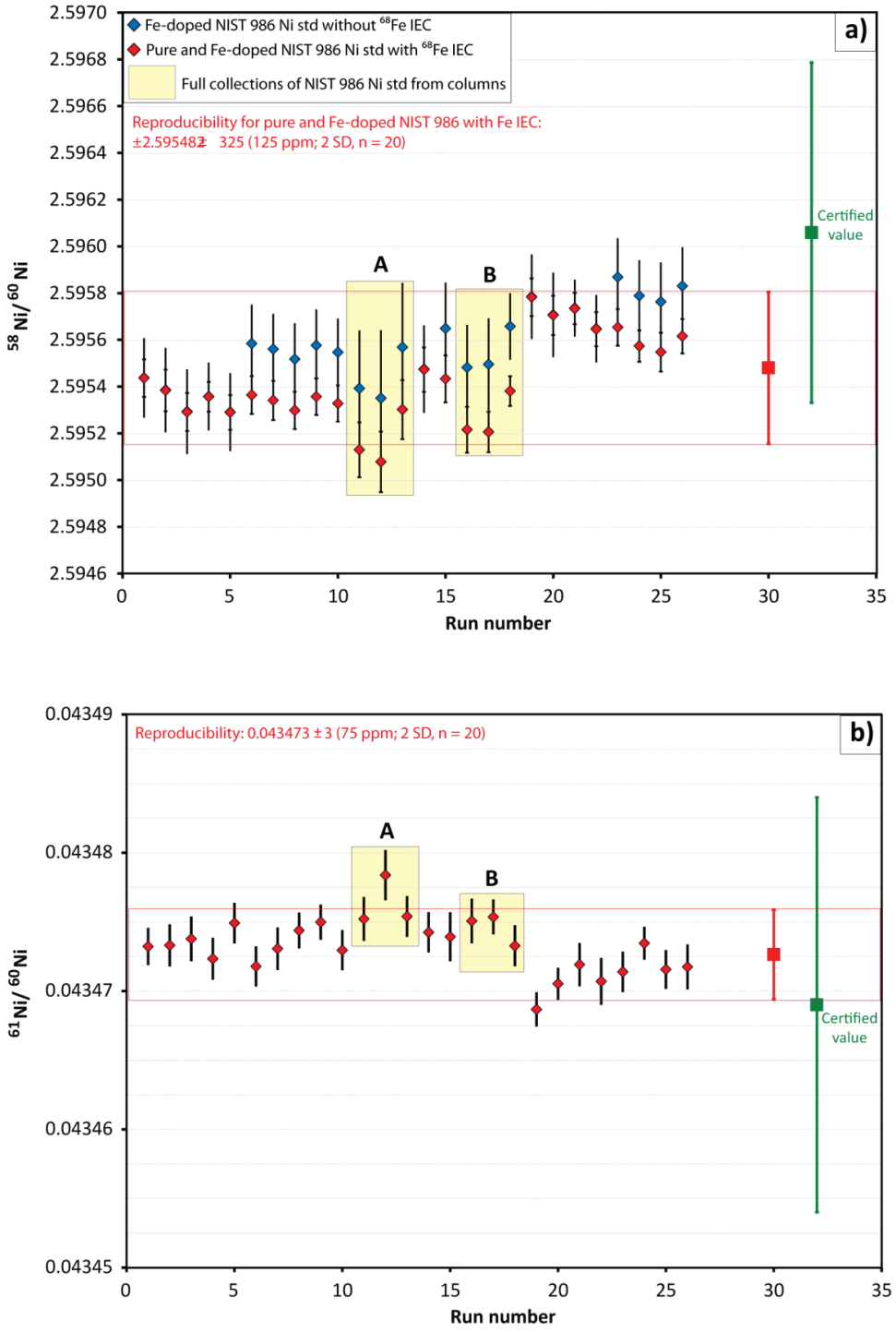

Figure 3.6: Plots of mass bias corrected $^{58}Ni/^{60}Ni$ (a) and $^{61}Ni/^{60}Ni$ (b) for pure and Fe-doped NIST 986 SRM run at the start and end of the analytical session to monitor instrument performance, as well as NIST 986 SRM processed through the column chemistry. Yellow boxes mark the standards run through the columns: Box A, 3 replicates of total Ni collection from the stage 2 column only; Box B, 3 replicates of total Ni collection from the full column procedure. The red lines indicate reproducibility for pure and Fe-doped NIST 986 SRM for the analytical session. The certified value for NIST 986 is from Gramlich *et al.* (1989).

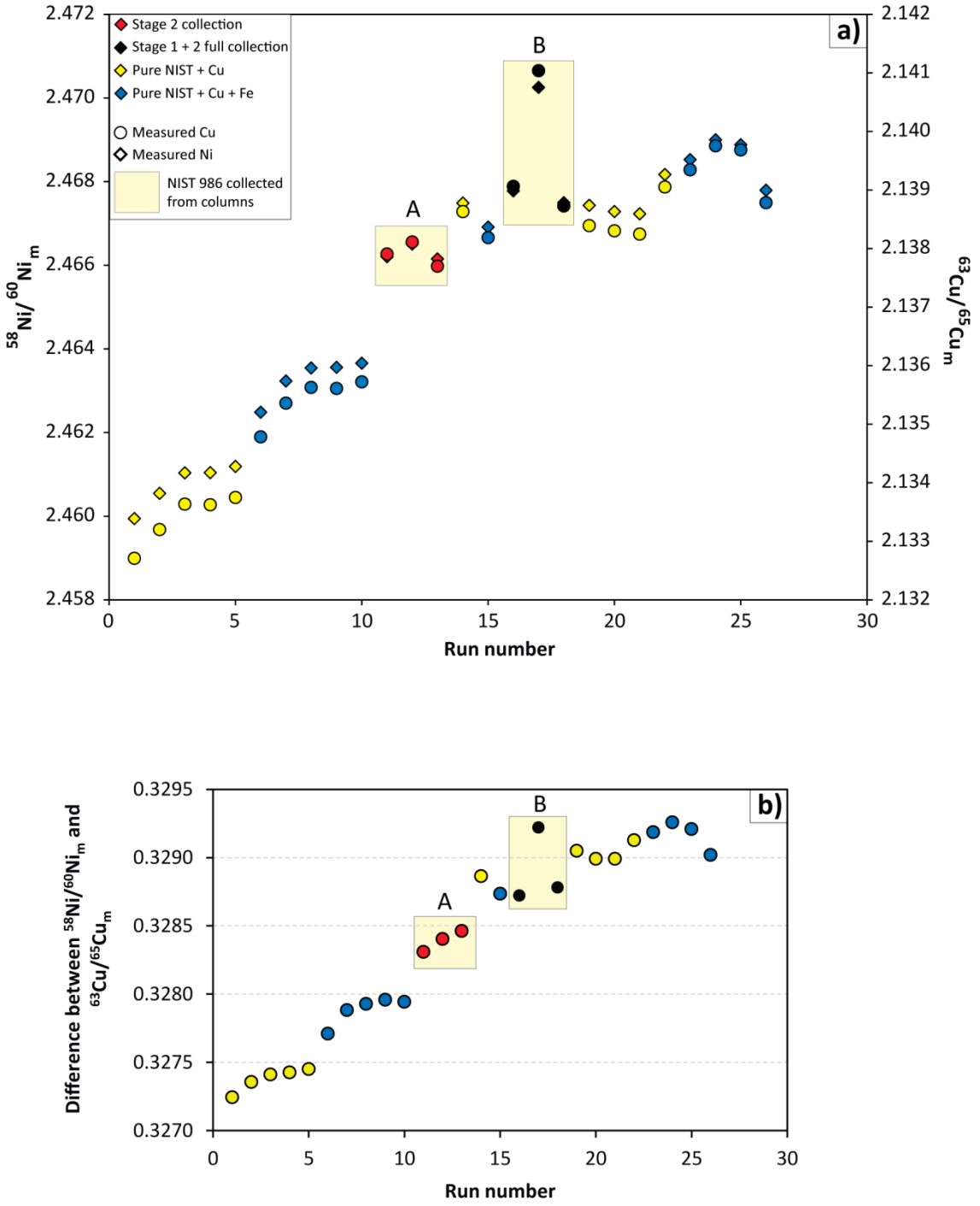

Figure 3.7: Plots of: a) measured $^{58}Ni/^{60}Ni$ and $^{63}Cu/^{65}Cu$ ratios vs. run number; and b) the difference between the measured $^{58}Ni/^{60}Ni$ and $^{63}Cu/^{65}Cu$ ratios, indicating instrumental mass bias behaviour during the analytical session. The observed drift in measured ratios is indicative of drift in mass bias behaviour throughout the day. Yellow boxes mark the standards run through the columns: Box A, 3 replicates of total Ni collection from the stage 2 column only; Box B, 3 replicates of total Ni collection from the full column procedure.

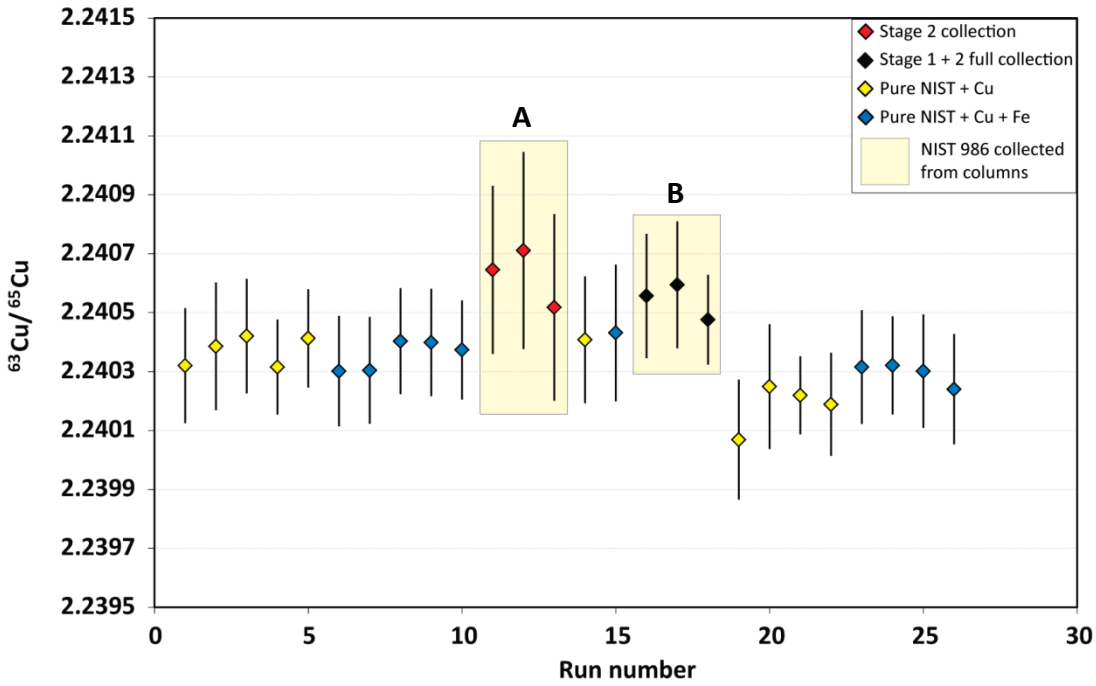

Figure 3.8: Plot of mass bias corrected $^{63}Cu/^{65}Cu$ (corrected using $^{62}Ni/^{60}Ni$) for pure and Fe-doped NIST 986 SRM (used to monitor instrument performance) and NIST 986 SRM subjected to column chemistry (stage 2 column and the full column procedure). Yellow boxes mark the standards run through the columns: Box A (red diamonds), 3 replicates of total Ni collection from the stage 2 column only; Box B (black diamonds), 3 replicates of total Ni collection from the full column procedure.

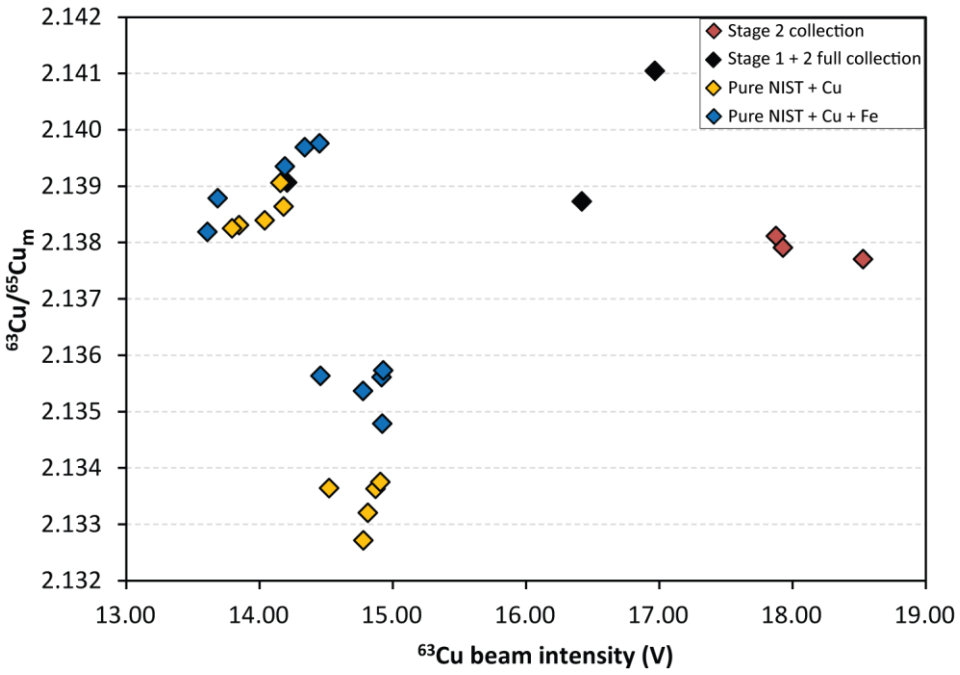

Figure 3.9: Measured $^{63}Cu/^{65}Cu$ vs. ^{63}Cu beam intensity (V) for pure and Fe-doped NIST 986 SRM (analysed to monitor instrument performance), and for full collections of NIST 986 SRM from the stage 2 column and the full-column procedure.

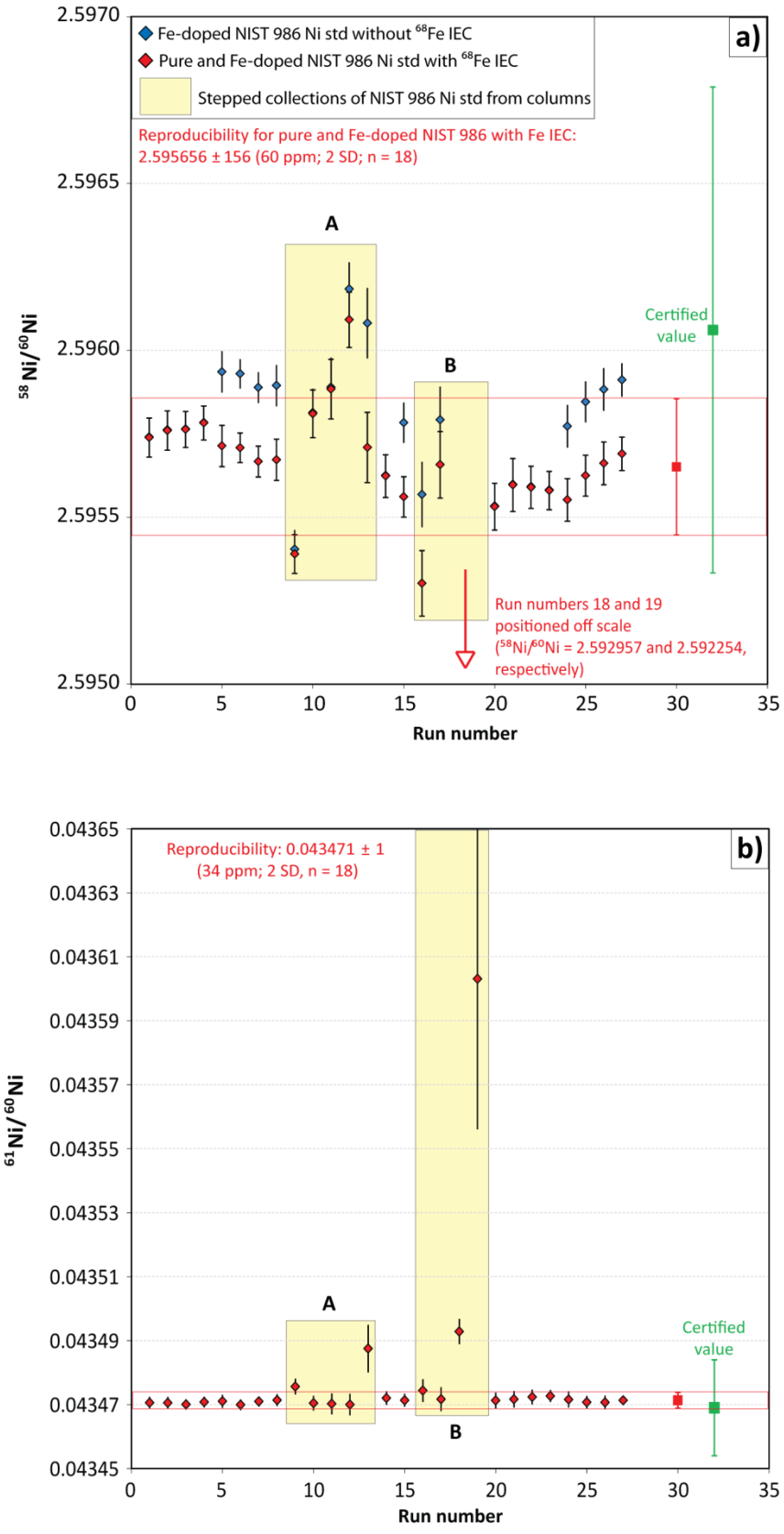

Figure 3.10: Plots of mass bias corrected $^{58}Ni/^{60}Ni$ (a) and $^{61}Ni/^{60}Ni$ (b) for pure and Fe-doped NIST 986 SRM, as well as NIST 986 SRM run through the column chemistry. Yellow boxes mark the standards run through the columns: Box A, incremental collections of Ni from the Ni elution phase of the stage 1 column; Box B, incremental collections of Ni from part of the Ni elution phase of the stage 2 column. The red lines indicate reproducibility for pure and Fe-doped NIST 986 SRM for the analytical session. The certified value for NIST 986 is from Gramlich *et al.* (1989).

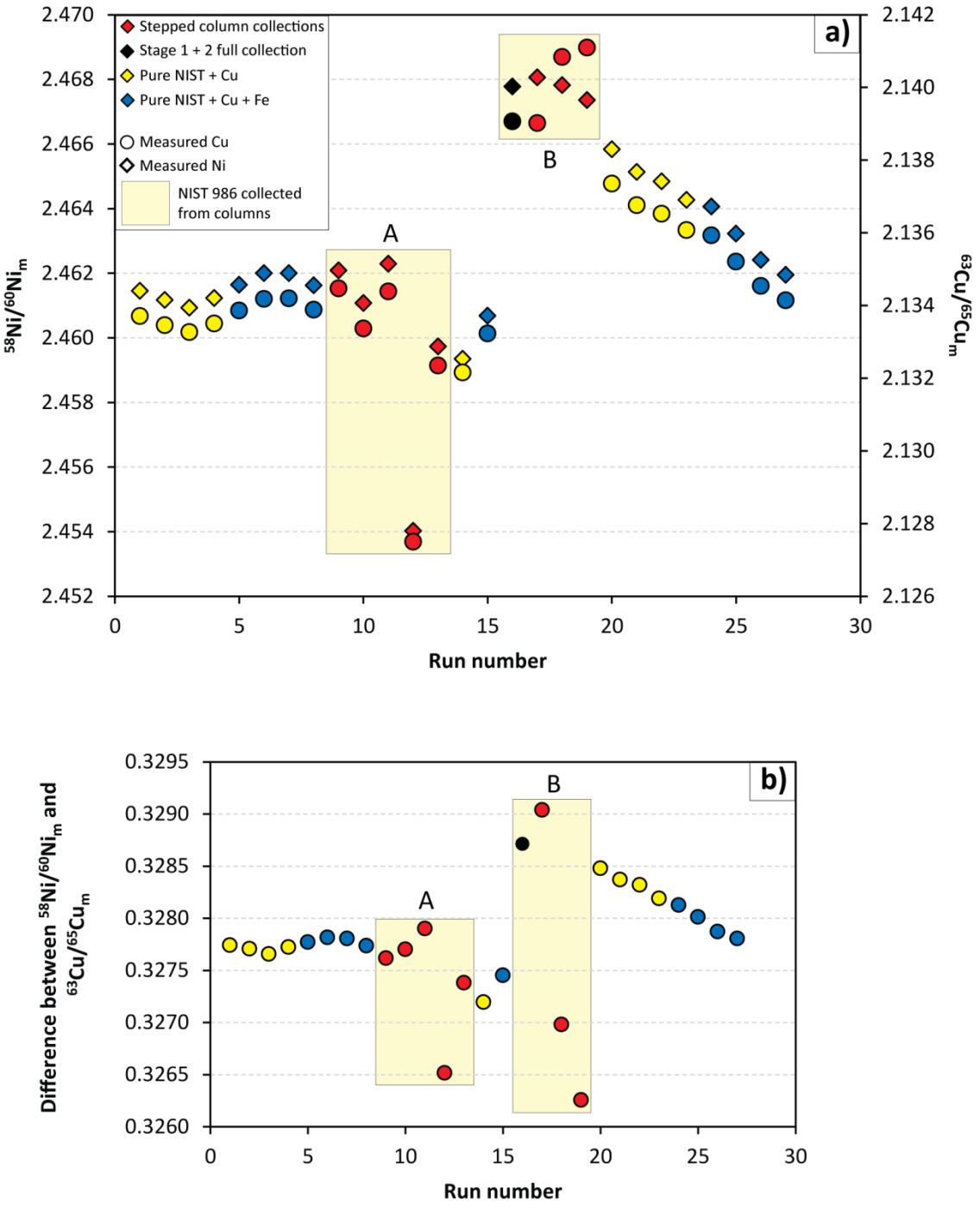

Figure 3.11: Plots of: a) measured $^{58}Ni/^{60}Ni$ and $^{63}Cu/^{65}Cu$ ratios vs. run number; and b) the difference between the measured $^{58}Ni/^{60}Ni$ and $^{63}Cu/^{65}Cu$ ratios, indicating instrumental mass bias behaviour during the analytical session. Yellow boxes mark the standards run through the columns: Box A, incremental collections of Ni from the Ni elution phase of the stage 1 column; Box B, incremental collections of Ni from part of the Ni elution phase of the stage 2 column.

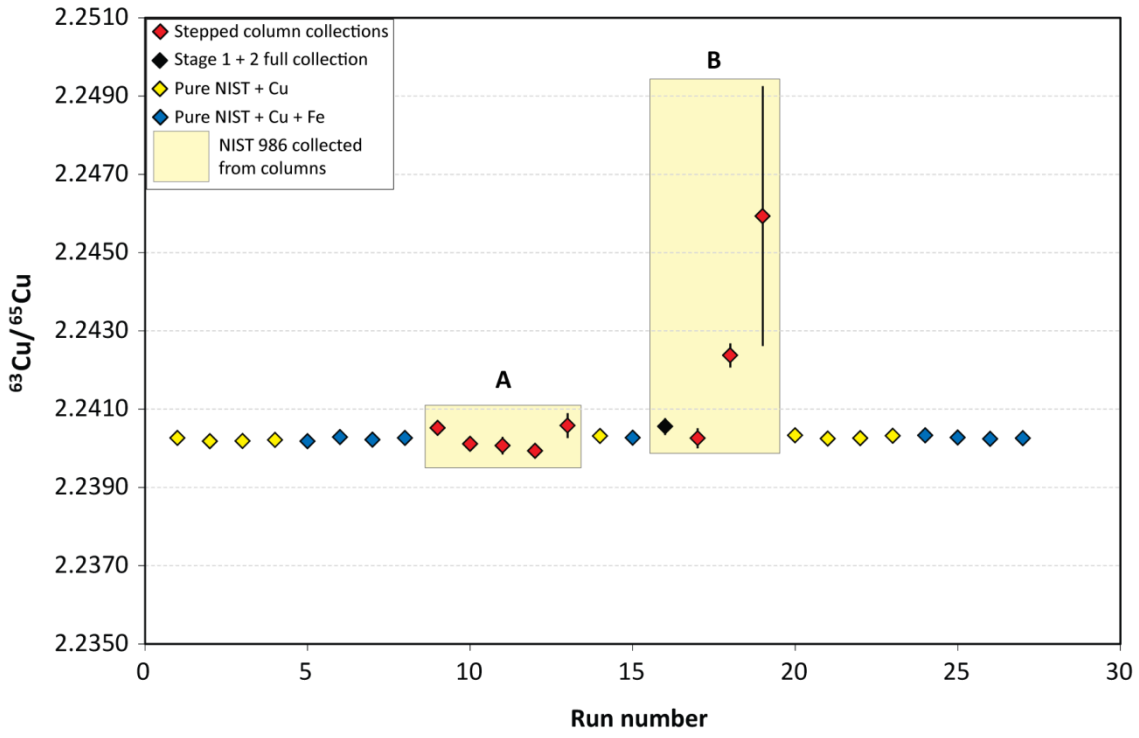

Figure 3.12: Plot of mass bias corrected $^{63}Cu/^{65}Cu$ (corrected using $^{62}Ni/^{60}Ni$) for pure and Fe-doped NIST 986 SRM (analysed to monitor instrument performance throughout the analytical session) and NIST 986 SRM subjected to column chemistry (stage 1 column and stage 2 column). Yellow boxes mark the standards run through the columns: Box A, incremental collections of Ni from the Ni elution phase of the stage 1 column; Box B, incremental collections of Ni from part of the Ni elution phase of the stage 2 column.

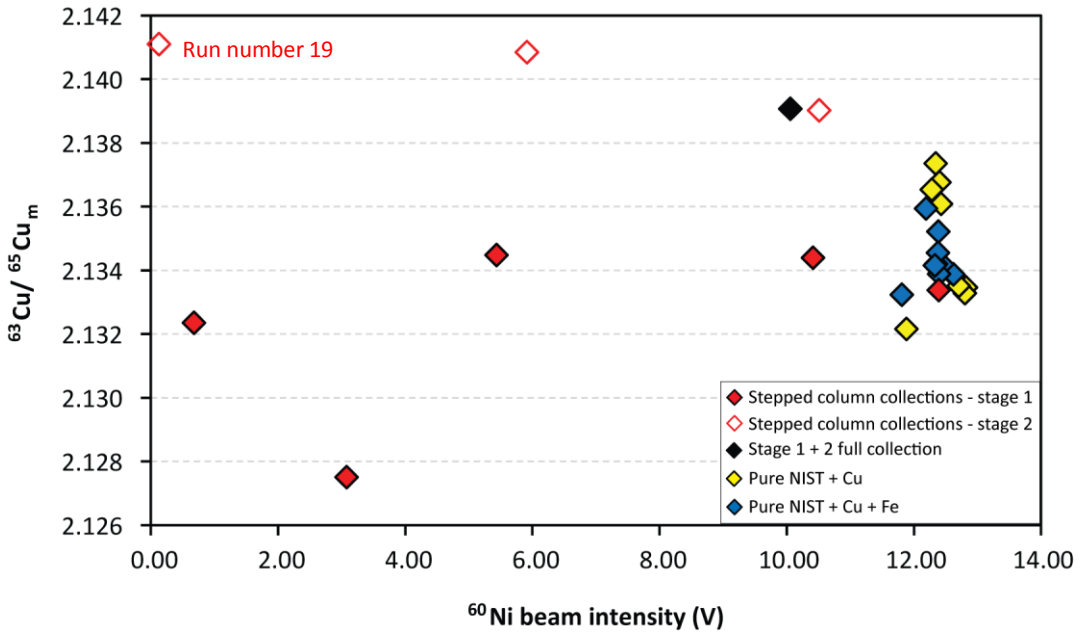

Figure 3.13: Plot showing the relationship between measured $^{63}Cu/^{65}Cu$ vs. ^{60}Ni beam intensity (V) for pure and Fe-doped NIST 986 SRM (measured to monitor instrument performance), and for incremental collections of NIST 986 SRM from the stage 1 (filled red diamonds) and stage 2 (hollow red diamonds) columns.

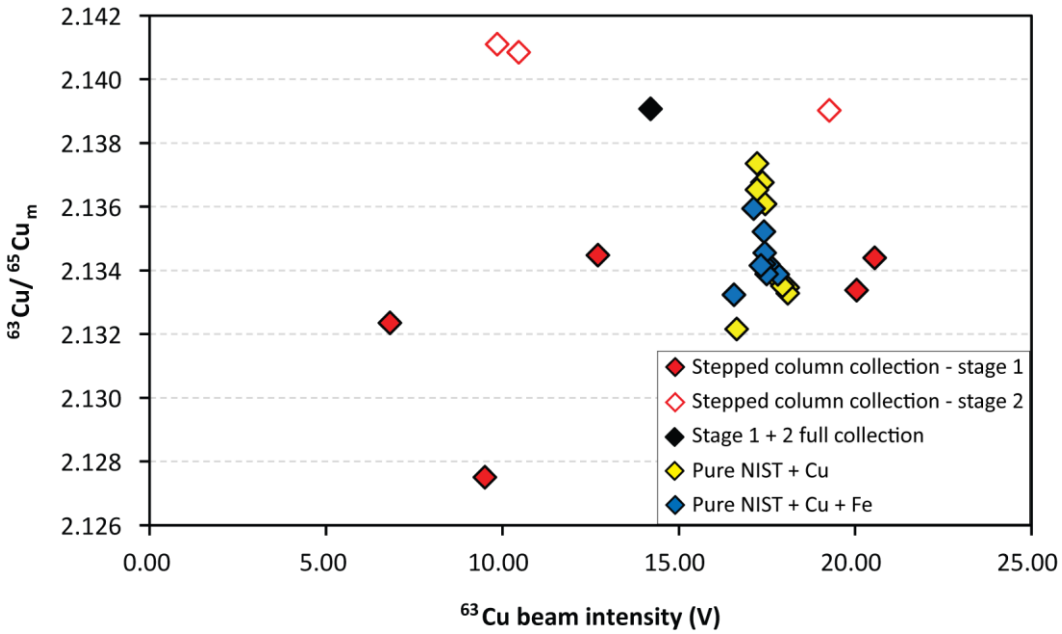

Figure 3.14: Measured $^{63}Cu/^{65}Cu$ vs. ^{63}Cu beam intensity (V) for pure and Fe-doped NIST 986 SRM, and for incremental collections of NIST 986 SRM from the stage 1 (filled red diamonds) and stage 2 (hollow red diamonds) columns.

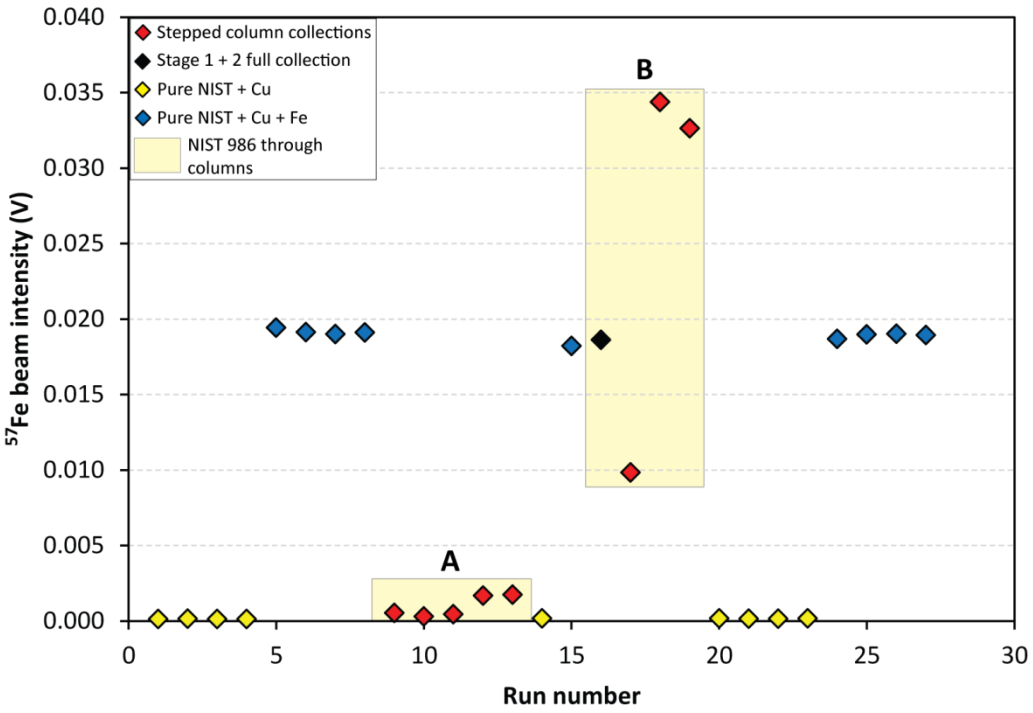

Figure 3.15: Plot of ^{57}Fe intensity (V) for pure and Fe-doped NIST 986 SRM, and incremental collections of NIST 986 SRM from the stage 1 (Box A) and stage 2 (Box B) columns.

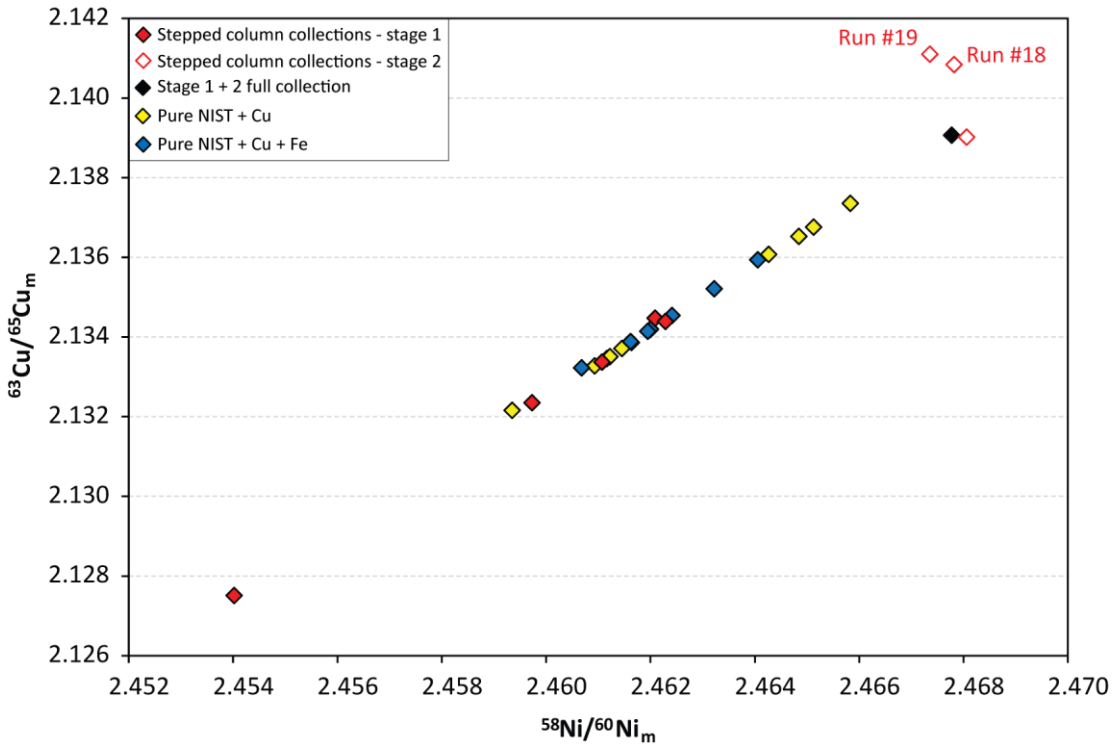

Figure 3.16: Plot showing the relationship between the measured $^{63}Cu/^{65}Cu$ vs. measured $^{58}Ni/^{60}Ni$ ratios for pure and Fe-doped NIST 986 SRM and NIST 986 SRM collected incrementally from the stage 1 (solid red diamonds) and stage 2 (hollow red diamonds) columns. For the meaning of the Run # notation, see text and Table 3.1.

Table 3.1: Table showing the run numbers and their corresponding positions on the Ni elution peaks for the stage 1 and stage 2 columns, and the proportion of the Ni elution peak analysed.

Run number	Total collection volume (ml)	Number of increments collection split into	Elution volume analysed (ml)	Position of elution on elution peak [1, 2]
Stage 1				
9			0.1	3 of 7
10			0.1	4 of 7
11	**0.75**	**7**	0.1	5 of 7
12			0.1	6 of 7
13			0.15	7 of 7
Stage 2				
17			1	3 of 8
18	**8**	**8**	1	2 of 8
19			1	4 of 8

[1] Refer to outline of stage 1 and 2 column procedures in figures 3.1 and 3.2, respectively

[2] For stage 2 refer to full procedure calibration plot for NIST 986 SRM in figure 3.3

4 *Geochemical characterisation of the Sinemurian-Pliensbachian GSSP: Application of Ni isotopes to organic-rich sediments*

4.1 Introduction

For several decades previous investigations of Ni isotopes have focused predominantly on characterising isotopic fractionation in extraterrestrial materials, with a view to enhancing our understanding of planetary processes and the isotopic composition of the early Solar System (eg. Kohman and Robison, 1980; Morand and Allegre, 1983; Shimamura and Lugmair, 1983; Birck and Lugmair, 1988; Herzog *et al.,* 1994; Xue *et al.,* 1995; Quitté *et al.,* 2006; Cook *et al.,* 2007; Moynier *et al.,* 2007; Chen *et al,.* 2009; outlined by this thesis, Chapter 3). In addition, the role of Ni as a bioessential trace metal (eg. Frausto da Silva and Williams, 2001; Cameron *et al.,* 2007; 2009) has led to the recognition that Ni isotopes have the potential to be utilised as a powerful biological tool for studies of early life on Earth (Cameron *et al.,* 2009; 2011).

However, as well as through cosmochemical and biochemical investigations, the potential of Ni to significantly enhance our understanding of organic-rich sedimentary environments and to provide a powerful geological tracer in the petroleum realm has been recognised, following pioneering work by Lewan and Maynard (1982) and Lewan (1984) (eg. Ellrich *et al.,* 1985; Manning *et al.,* 1991; Alberdi and Lafargue, 1993; López *et al.,*1995; as outlined in Chapter 3). Although these studies focused on the elemental distribution of Ni rather than isotopic fractionation, one study does exist that demonstrates the potential to use Ni isotopes as an oil-source correlation tool (Dewaker *et al.,* 2000).

Although there is enormous potential for Ni to be used as an oil-source correlation tool (Dewaker *et al.,* 2000), no previous study exists that characterises the behaviour of Ni isotopes in organic-rich sediments or indeed within a stratigraphic profile. This can be mostly attributed to the difficulty associated with separating Ni from such complex sample matrices (as discussed in Chapter 3). Before an oil-source correlation tool can be developed, it is crucial

that we have an understanding of the behaviour of Ni isotope systematics in such samples, and of how Ni isotope fractionation may vary stratigraphically. This is of paramount importance when trying to accurately evaluate any isotopic trends whilst attempting to conduct correlation studies.

Herein we present the first attempt at creating a Ni isotope stratigraphic profile for an organic-rich sedimentary succession. The marine section across the Sinemurian-Pliensbachian GSSP, Robin Hood's Bay, UK, is ideally suited to the present study, as it well understood biostratigraphically (Hesselbo *et al.,* 2000; Meister *et al.,* 2006) and has been previously characterised using other isotope stratigraphy techniques, including strontium isotopes ($^{87}Sr/^{86}Sr$; Jones *et al.,* 1994; Hesselbo *et al.,* 2000), oxygen ($\delta^{18}O$) and carbon isotopes ($\delta^{13}C$) (Hesselbo *et al.,* 2000), and Os isotopes (this thesis, Chapter 2). The section is also consistently thermally immature thereby eliminating any potential effects of thermal maturation on the Ni isotope signature.

To accurately assess and interpret any stratigraphic variation of Ni isotopes in the Robin Hood's Bay section, it is critical to determine whether any fluctuations in paleoredox conditions occur. Nickel only occupies one oxidation state in the natural environment (Ni^{4+}), suggesting that it is not redox sensitive. However, its preferential association with redox-sensitive metallo-organic complexes in organic-rich sediments (this thesis, Chapter 3) indicates that certainly within these sample matrices, redox conditions at the time of sediment deposition directly impact the degree of enrichment or depletion of Ni. No previous study applies Ni isotopes to an organic-rich sedimentary profile and as such, our understanding of the behaviour of Ni isotope systematics in this setting is limited. Herein, paleoredox conditions have been established for the Sinemurian-Pliensbachian GSSP section, Robin Hood's Bay, UK.

The distributions of certain trace elements in organic-rich marine sediments can allow us to determine the redox conditions at the time of sediment deposition (eg. Jones and

Manning, 1994; Hatch and Leventhal, 1992; Calvert and Pederson, 1993; Crusius *et al.,* 1996; Schovsbo, 2001; Rimmer, 2004). Being able to accurately evaluate such conditions is critical in enabling us to enhance our understanding of the environment in which organic-rich sediments were formed. Further, understanding the depositional paleoredox conditions can yield valuable insight into controls on the chemical composition of organic-rich sediments.

In this study we focus on utilising the trace elements that are well known for yielding accurate information about redox conditions at the time of sediment deposition. The V/Cr and Ni/Co ratios are recommended as the most consistent and reliable of the redox indices (eg. Jones and Manning, 1994; Rimmer, 2004), providing valid paleo-oxygenation information for the time of sediment deposition. A number of previous studies have successfully utilised V/Cr (eg. Ernst, 1970; Krecji-Graf, 1975; Dill, 1986; Rimmer, 2004; Selby *et al.,* 2009) and Ni/Co (Dypvik, 1984; Dill, 1986; Rimmer, 2004; Selby *et al.,* 2009) to accurately determine the redox conditions of the depositional environment. As such, these ratios will be employed by this study. The (Cu+Mo)/Zn ratio (Hallberg, 1976, 1982) conveys little information about paleoredox conditions (Jones and Manning, 1994), and therefore will not be considered by this study.

The V/(V+Ni) ratio is also interpreted by some workers to provide a measure of relative redox potential (eg. Lewan and Maynard, 1982; Hatch and Leventhal, 1992; Schovsbo, 2001). Development of this ratio as a redox index by Hatch and Leventhal (1992) resulted from preliminary work by Lewan and Maynard (1982), who determined that the wide range of V/(V+Ni) values that they observed in petroleum source rocks and oils was primarily controlled by redox potential. However, this ratio has also been found to yield apparent redox information that is inconsistent with the V/Cr and Ni/Co ratios (eg. Rimmer, 2004; Selby *et al.,* 2009). As a result, Rimmer (2004) suggests that the strict thresholds for the different redox parameters, and particularly those developed for specific geological formations (eg. V/(V+Ni)

developed by Hatch and Leventhal (1992) for the Pennsylvanian Stark Shale Member), should be used cautiously. In this study we will therefore also evaluate the suitability of the V/(V+Ni) index when applied to Robin Hood's Bay sediments.

4.2 Geological setting

This chapter focuses on the same marine sediments from the Sinemurian-Pliensbachian GSSP, Robin Hood's Bay, as Chapter 2 (Fig. 4.1). The geological setting of this section is detailed previously in Chapter 2.

The Sinemurian-Pliensbachian boundary, established from the succession's complete and well preserved ammonite assemblages (Spath, 1923; Dean *et al.,* 1961; Hesselbo *et al.,* 2000; Meister *et al.,* 2006), occurs in the Pyritous Shales of the Redcar Mudstone Formation within the Lias Group (Powell, 1984). At this point in the Early Jurassic Robin Hood's Bay was positioned on the margins of a shallow epicontinental sea (eg. Dera *et al.,* 2009) that covered most of Northern Europe, including Britain, during the Mesozoic (Sellwood and Jenkyns, 1975). The facies changes across the boundary, from pale siliceous to finer, more organic-rich mudstones, indicate an overall relative increase in sea level of at least regional extent (eg. Hesselbo *et al.,* 2000; Meister *et al.,* 2006).

4.3 Sampling

The same set of 32 samples (SP7-09 to SP39-09) from the Sinemurian-Pliensbachian boundary at Robin Hood's Bay analysed in Chapter 2 (Fig. 4.2), were also used in this study. Samples spanned a 6 m vertical section across the boundary and were taken from the Pyritous Shales Member of the Redcar Mudstone Formation. A sampling interval of ~20 cm was used consistently within Beds 69 – 75, except within Bed 72, where the sampling interval was ~15 cm.

4.4 Analytical protocol

Prior to geochemical analyses the samples were cut and polished before being powdered in a Zr disc mill.

4.4.1 Trace element abundance

Samples were prepared for trace element analysis at the Northern Centre for Isotopic and Elemental Tracing (NCIET) following the method of Ottley *et al.,* (2003). Sample powders (~100 mg) were digested in a 4:1 solution of 29 N HF (4 ml) and 16 N HNO_3 (1 ml) on a hotplate at ~150 ^{o}C for 48 hrs. Samples were then evaporated to near rather than total dryness, to avoid stabilisation of insoluble fluorides (Ottley *et al.,* 2003). Evaporation was followed by the addition of 1 ml 16 N HNO_3 and evaporation to near dryness. The previous stage was repeated before the addition of 2.5 ml 16 N HNO_3 and ~10 ml MQ (high purity water) to create a ~4 N HNO_3 solution. Sample beakers were capped and heated on the hotplate overnight at ~100 ^{o}C.

Once cooled, 1 ml of 1 ppm internal Re and Rh spike was added to the samples (to yield 20 ppb Re and Rh in the final analyte solution) before then being diluted up to 50 ml using MQ, yielding a ~0.5 N HNO_3 solution. The use of the Rh and Re internal spike improves data precision by compensating for calibration drift during analysis due to changes in the instrument's sensitivity, matrix suppression and dilution errors associated with sample preparation (as the sample-spike ratio is constant) (Ottley *et al.,* 2003). Prior to analysis, samples were diluted 10-fold by taking 1 ml from the 50 ml solution and diluting it to 10 ml using 0.5 N HNO_3. Samples were then analysed using the X-Series Inductively Coupled Plasma Mass Spectrometer (ICP-MS).

Replicate analyses of International Reference Materials (RMs) AGV-1, BHVO-1 and W-2 and synthetic standards solutions for Mo (10, 20 and 30 ppb solutions) were conducted for calibration per sample set.

4.4.2 Total Organic Carbon (TOC) and $\delta^{13}C_{org}$

Carbon stable-isotope measurements were performed at Durham University using a Costech Elemental Analyser (ECS 4010) coupled to a ThermoFinnigan Delta V Advantage. Carbon-isotope ratios are corrected for ^{17}O contribution and reported in standard delta (δ) notation in per mil (‰) relative to the Vienna PeeDee Belemnite scale. Data accuracy is monitored through routine analyses of in-house standards, which are stringently calibrated against international standards (e.g., USGS 40, USGS 24, IAEA 600, IAEA CH6): this provides a linear range in $\delta^{13}C$ between +2 ‰ and –47 ‰. Analytical uncertainty for $\delta^{13}C_{org}$ is typically ±0.1 ‰ for replicate analyses of the international standards and typically <0.2 ‰ on replicate sample analysis. Total organic carbon was obtained as part of the isotopic analysis using an internal standard (i.e., Glutamic Acid, 40.82 % C).

4.4.3 Rhenium and osmium

Rhenium and osmium analyses of Robin Hood's Bay whole-rock powders were conducted at the Japan Agency for Marine-Earth Science and Technology (JAMSTEC) as part of the JSPS Summer Fellowship Program 2010, following the CrO_3-H_2SO_4 procedure of Selby and Creaser (2003), outlined in detail in Chapter 2. Sample powders were digested in Carius tubes with a measured amount of ^{185}Re and ^{190}Os spike solution in 8 ml of CrO_3-H_2SO_4 solution at ~240 ^{o}C for 48 hrs. Once cooled, Os was removed by solvent extraction and microdistillation, and the remaining solution was prepared for Re purification by reducing Cr^{6+} to Cr^{3+} using ethanol. Once reduced, the sample solution was evaporated to dryness and the Re fraction was then purified using a two-stage anion exchange chromatography procedure. The purified Re and Os fractions were loaded onto Ni and Pt filaments, respectively, and the Re and Os isotope ratios were measured using the Triton NTIMS (Creaser *et al.,* 1991; Völkening *et al.,* 1991) using Faraday collectors (Re) and the SEM (Os) ($\lambda\ ^{187}Re = 1.666 \times 10^{-11}\ a^{-1}$; Smoliar *et al.,* 1996). Total procedural blanks were 14.1 ± 0.2 pg and 3.56 ± 0.52 pg (1σ S.D., n = 2) for Re and Os, respectively, with an average $^{187}Os/^{188}Os$ value of 0.19 ± 0.005 (n = 2). Uncertainties presented in Table 4.1 include full error propagation of uncertainties in Re and Os mass spectrometer measurements, blank abundances and isotopic compositions, spike calibrations and reproducibility of standard Re and Os isotopic values.

4.4.4 Nickel stable isotopes

All Ni isotope analyses were conducted at the University of Bristol, by Dr Vyllinniskii Cameron. Chemical separation and purification of Ni was achieved using a double-isotope dilution protocol (double-spike) coupled with a 2-stage ion exchange procedure outlined by Cameron *et al.,* (2009) and modified from Quitté and Oberli (2006). The double-spike protocol permits correction for instrumental mass discrimination (discussed in Chapter 3). The spike is

composed of a 1:1 mixture of ^{61}Ni and ^{62}Ni (Cameron *et al.,* 2009). Samples were first treated multiple times with concentrated HNO_3 (15.3 N) to destroy any organic components (Cameron *et al.,* 2009). Following this, samples were digested in closed beakers in a mixture of concentrated HNO_3 + HF (0.5 ml + 2 ml, respectively) at 140 ^{o}C for 48 hours.

Prior to the first-stage column, the sample was dissolved in 2 ml 1 N HCl before the addition of 0.4 ml ammonium citrate [$(NH_4)_2C_6H_6O_7$]. In preparation for loading onto the column, the pH of the sample was adjusted to 8 – 9 using NH_4OH (ammonium hydroxide). This stage of the procedure utilises teflon columns (made in-house) filled with Ni specific resin, which allows the complexation of Ni with DMG (previously discussed in Chapter 3). Matrix elements are eluted with the addition of 6 ml 2.8 N ammonium citrate and Ni is collected using 3 ml 3 N HNO_3 (Cameron *et al.,* 2009).

The second-stage column is designed to ensure complete removal of the major atomic interferences on Ni (Fe and Zn) (Cameron *et al.,* 2009) and utilises macroporous anion resin (AG MP-1 M; Bio-Rad). Removal of Fe and Zn using this resin is also outlined by Maréchal *et al.* (1999) and Archer and Vance (2004). Sample residues from the first column were treated several times with 0.3 ml HCl + H_2O_2 (hydrogen peroxide), before being loaded and eluted from the second column in 7 N HCl + H_2O_2 (Cameron *et al.,* 2009). Using HCl concentrations with normality >2 enables elution of Ni from the column, whilst Fe and Zn are retained on the resin (Cameron *et al.,* 2009). In preparation for mass spectrometry, the purified Ni fractions were evaporated to dryness, treated with 15.3 N HNO_3, evaporated, and finally dissolved in 2 % HNO_3. Typical procedural blanks were ≈2 ng (Cameron *et al.,* 2009).

All analyses were conducted using a ThermoFinnigan Neptune multi-collector (MC) ICPMS coupled to an Aridus desolvating nebuliser system (CETAC) fitted with a PFA nebuliser and spray chamber (CPI). All isotopes were measured simultaneously in static mode using a multiple Faraday collector array. Blank contributions generally accounted for <0.02 % (for ^{58}Ni)

of the ion beams, and the internal error on the $^{60}Ni/^{58}Ni$ ratio was 0.001 – 0.002 % (2 σ) (Cameron *et al.,* 2009). All Ni data are reported relative to NIST SRM 986, in the standard delta notation (see below) with all uncertainties reported to the 2 σ level.

$$\delta^{60}Ni = \left(\frac{^{60}Ni/^{58}Ni_{sample}}{^{60}Ni/^{58}Ni_{SRM986}} - 1 \right) \times 1000$$

4.5 Results

4.5.1 Trace elements

In this study only the trace elements necessary to accurately evaluate the redox conditions at the time of sediment deposition have been used. These are as follows: Ni, V, Cr and Co.

4.5.1.1 Abundance

The Ni, Co, V and Cr abundances for the Robin Hood's Bay organic-rich sediments are given in Table 4.2, and their respective profiles across the Sinemurian-Pliensbachian boundary are presented in Figure 4.3.

The minimum abundances for all four elements occur ~2.2 m above the Sinemurian-Pliensbachian boundary (sample SP33-09; Ni = ~18.4 ppm, Co = ~12.9 ppm, V = ~152.9 ppm and Cr = ~107.5 ppm). Similarly, the maximum abundances for V (~332.6 ppm) and Cr (~276.8 ppm) both occur at the Sinemurian-Pliensbachian boundary level (sample SP22-09). However, the maximum abundances for Ni (~190.5 ppm) and Co (~34.4 ppm) are slightly staggered, and

occur at ~1.4 m (sample SP29-09) and ~1.2 m (sample SP28-09) above the boundary, respectively.

All four element profiles (Fig. 4.3) show variation across the boundary section, and no discernible trend of increasing or decreasing abundance can be seen in any plot. However, it can be noted that the Ni and Co profiles are similar, as are those for V and Cr.

4.5.1.2 Enrichment

The enrichment factor (EF) defines the degree to which an element is enriched in a shale or an organic-rich sediment relative to a standard shale composition (eg. Calvert and Pederson, 1993). The hydrogenous fraction may be estimated by normalising the whole-rock trace element concentrations to an index of the detrital component (Al) (eg. Piper and Calvert, 2009). This approach has been advocated by a number of workers and has been used to determine trace element enrichments in both modern and ancient sediments (eg. Calvert and Pederson, 1993). The enrichment factor can be calculated as follows:

$$\mathbf{EF = (element/Al)_{sample}/(element/Al)_{shale}}$$

In this equation, the numerator includes the ratio for the shale under investigation, and the denominator defines the ratio for a "typical shale", using data from Wedepohl (1971).

The Al-normalised trace element values and enrichment factors for all 32 samples are presented in Table 4.3. The approximate order of trace element enrichment in the Robin Hood's Bay sediments (average value, n = 32) relative to average shale (Wedepohl, 1971) is as follows: V >Cr >Co>Ni (EF = 1.4, 1.2, 0.9 and 0.8, respectively; Tables 4.3 and 4.4, Fig. 4.4). All samples (n = 32) show enrichment in V and Cr relative to average shale (Fig. 4.4). However, although both Ni and Co are predominantly depleted (n = 22; 69 % of samples and n = 26; 81 %

of samples, respectively), both trace elements fluctuate from relative enrichment to depletion throughout the entire boundary section (Fig. 4.4).

4.5.1.3 Redox indices

The trace element ratios Ni/Co, V/Cr and V/(V+Ni) have been utilised by previous studies to evaluate paleoredox conditions at the time of deposition (eg. Hatch and Leventhal, 1992; Jones and Manning, 1994; Schovsbo, 2001). The published values of these indices and their corresponding redox conditions are summarised in Table 4.5.

The trace element ratios for the Robin Hood's Bay Sinemurian-Pliensbachian sediments and their inferred redox conditions are given in Table 4.2. The Ni/Co index indicates that oxic conditions were prevalent at the Sinemurian-Pliensbachian boundary (n = 29) with values of ~1.43 – 9.24 (Fig. 4.5a). Two samples, SP36-09 (Ni/Co = ~6.07) and SP11-09 (Ni/Co = ~5.19) suggest dysoxic conditions, and one sample, SP29-09 (Ni/Co = ~9.24; 1.4 m above the boundary) indicates suboxic to anoxic conditions (Fig. 4.5a). The V/Cr values range from ~1.13 – 2.30, also indicating predominantly oxic conditions (n = 29; Fig. 4.5b). Three samples, SP36-09 (~2.8 m above the boundary), SP34-09 (~2.4 m above) and SP13-09 (~1.9 m below the boundary), indicate dysoxic conditions with V/Cr values of ~2.18, 2.30 and 2.02, respectively (Fig. 4.5b).

Good agreement is observed between both the Ni/Co and V/Cr indices which show that 91 % of the samples were deposited under oxic conditions (Fig. 4.6a). However, there is significant disagreement between these ratios and the V/(V+Ni) index (Fig. 4.6b,c). Values for V/(V+Ni) range from ~0.51 – 0.89 and indicate that anoxic conditions prevailed across the Sinemurian-Pliensbachian boundary (n = 26; Fig. 4.5c). Further, six samples suggest that bottom-water circulation ceased and that conditions became euxinic intermittently between ~2.6 m above the boundary and ~1.9 m below it (Fig. 4.5c).

4.5.2 Total Organic Carbon (TOC) and $\delta^{13}C_{org}$

Measured TOC and $\delta^{13}C_{org}$ for the Robin Hood's Bay samples are shown in Table 4.2 and Figure 4.3. Total Organic Carbon is generally low, varying from ~0.53 – 2.46 wt. %. It shows only slight variation prior to the Sinemurian-Pliensbachian boundary (~0.57 – 0.86 wt. %; Fig. 4.3), but an overall gradual increase above the boundary (from ~0.58 – 2.46 wt. %; Fig. 4.3). The $\delta^{13}C_{org}$ values range from ~-25.3 - -28.9 ‰, progressively becoming isotopically lighter moving up-section and across the boundary (Fig. 4.3).

4.5.3 Rhenium and osmium

The measured rhenium and osmium abundances and isotopic compositions for the 32 samples taken across the Sinemurian-Pliensbachian boundary are summarised in Table 4.1 and Figure 4.7. Rhenium values range from ~1.5 – 117 ppb and in a similar manner to TOC, show relative consistency and little variation prior to the boundary (~1.6 – 5.3 ppb; n = 17; Fig. 4.7). However, in the earliest Pliensbachian a significant increase and variation in Re is observed (~6.7 – 117 ppb; n = 15; Fig. 4.7). Osmium values range from ~107 – 1790 ppt, and follow a similar pattern to Re both above and below the boundary (Fig. 4.7).

The $^{187}Re/^{188}Os$ and present-day $^{187}Os/^{188}Os$ ratios vary from ~25 – 443 and ~0.3 – 1.6, respectively. Both ratios decrease between ~2.8 to 0.9 m below the Sinemurian-Pliensbachian boundary ($^{187}Re/^{188}Os$, ~195 – 20; $^{187}Os/^{188}Os$, ~1 – 0.3) , before systematically increasing across the boundary into the lowermost Pliensbachian (Fig. 4.7).

4.5.4 Covariation plots

Covariation plots (Figs. 4.8 – 4.13) illustrate the relationships between trace element abundance (Ni, V, Cr and Co), Re and Os abundance, TOC and $\delta^{13}C_{org}$ across the Sinemurian-Pliensbachian boundary. The strongest positive correlation is observed between Re and TOC

(R^2 = 0.89; Fig. 4.8a). However, such a strong correlation is only present above the boundary (R^2 = 0.83; Fig. 4.8b) and no correlation exists between Re and TOC in samples of latest Sinemurian age (R^2 = 0.13; Fig. 4.8c). A noticeable negative correlation (R^2 = 0.77) is shown by Re vs. $\delta^{13}C_{org}$ (Fig. 4.9a). Similarly, the greatest correlation is exhibited above the boundary (R^2 = 0.71; Fig. 4.9b) and the weakest below (R^2 = 0.15; Fig. 4.9c).

Osmium has a strong positive correlation with TOC (R^2 = 0.80; Fig. 4.10a) and shows a similar trend to Re, with the strongest Os vs. TOC correlation occurring above the Sinemurian-Pliensbachian boundary (R^2 = 0.79; Fig. 4.10b), and the weakest correlation occurring below the boundary (R^2 = 0.34; Fig. 4.10c). Similarly, a noticeable trend is observed between $^{187}Re/^{188}Os$ vs. TOC (R^2 = 0.72; Fig. 4.11a), with the strongest relationship being present above the boundary (R^2 = 0.70; Fig. 4.11b).

No correlations exist between Ni vs. TOC or V vs. TOC, with R^2 values in both cases being significantly less than 0.1 (Fig. 4.12). Additionally, no trend is observed between Cr vs. TOC (R^2 = 0.18; Fig. 4.13a) or Co vs. TOC (R^2 = 0.04; Fig. 4.13b).

4.5.5 Nickel stable isotopes

New Ni stable isotope data for a select suite of the organic-rich sediments at Robin Hood's Bay is presented in Table 4.6. From the base of Bed 71 the sampling interval for Ni isotope analysis is ~40 cm (Fig. 4.14). A profile of $\delta^{60}Ni$ values for the section is shown alongside Ni concentration for comparison, together with TOC and $\delta^{13}C_{org}$ for correlation purposes, in Figure 4.14.

The Ni isotope composition ($\delta^{60}Ni$) of these samples is extremely variable, ranging from 0.28 ± 0.05 – 1.60 ± 0.05 ‰ (Fig. 4.14; Table 4.6). Two noticeable peaks in $\delta^{60}Ni$ values are observed 0.8 m above and 2.1 m below the Sinemurian-Pliensbachian boundary (1.26 ±

0.05 ‰ and 1.60 ± 0.05 ‰, respectively) that approximately correlate with the tops of beds 70 and 74.

The greatest range in δ^{60}Ni values occurs below the boundary (~1.32 ‰), compared to a range of ~0.97 ‰ above the boundary (Fig. 4.14). However, with the exception of the peak 2.1 m below the boundary, the structure of the δ^{60}Ni profile closely resembles that of the trace element profiles seen in Figure 4.3, with relatively consistent δ^{60}Ni values in the latest Sinemurian (0 to -1.7 m; ~0.21 ‰ variation) and a greater range in δ^{60}Ni values in the earliest Pliensbachian (~0.97 ‰). Further, an overall trend to heavier δ^{60}Ni values is observed up-stratigraphy (Fig. 4.14).

Crossplots of δ^{60}Ni vs. TOC, Ni, Re and Os are presented in Figure 4.15a-d. No trends are observed between δ^{60}Ni vs. TOC (Fig. 4.15a) or δ^{60}Ni vs. Ni (Fig. 4.15b) either above or below the Sinemurian-Pliensbachian boundary. However, if the outlying peak at 0.8 m is excluded (sample SP26-09), a positive correlation is exhibited between δ^{60}Ni and TOC above the boundary (R^2 = 0.74); in accord with trends previously noted between Re, Os and $^{187}Re/^{188}Os$ vs. TOC (Figs. 4.8, 4.10 and 4.11). No correlations are observed between δ^{60}Ni vs. Re or δ^{60}Ni vs. Os in either part of the section, with R^2 values ranging from 0 to 0.14 (Fig. 4.15c-d).

There is little to no correlation between δ^{60}Ni vs. V in samples either above or below the boundary (Fig. 4.16a). The samples exhibit a weak positive correlation between δ^{60}Ni vs. Co (R^2 = 0.48; Fig. 4.16c). However, no trend exists between δ^{60}Ni vs. Cr below the boundary (R^2 = 0.27; Fig. 4.16b), or between V, Cr, and Co vs. δ^{60}Ni above the boundary (R^2 = 0.04, 0.16 and 0.03, respectively).

Plots of δ^{60}Ni vs. Al-normalised trace element values (Ni, V, Cr and Co) are presented in Figure 4.17a-d. In a similar manner to the trace element concentrations discussed above, few correlations are observed in this dataset. Above the boundary, no relationship exists between

Ni, V or Co vs. δ^{60}Ni (with R^2 values ranging from 0 to 0.1; Fig. 4.17a,b,d) and only a very weak negative correlation is seen between δ^{60}Ni vs. Cr (R^2 = 0.34; Fig. 4.17c). Similarly, there are no distinct trends below the boundary for Ni, Cr or Co vs. TOC (R^2 values between 0.02 and 0.17) and only a weak positive correlation between V vs. δ^{60}Ni (R^2 = 0.42).

4.6 Discussion

4.6.1 Variations of Re, Os, TOC and $\delta^{13}C_{org}$ across the Sinemurian-Pliensbachian boundary

Peaks in Re, Os, TOC and $\delta^{13}C_{org}$ are observed ~1.2 m above the boundary (sample SP28-09; Fig. 4.7). This level lies ~0.2 m above the lithological transition from paler siliceous mudstones to darker, relatively organic-rich mudstones (SP27-09), marking a time of relative sea level rise (eg. Sellwood, 1971; Hesselbo and Jenkyns, 1995; Hesselbo *et al.,* 2000; Meister *et al.,* 2006; this study). At this transition there is a notable increase in Re, Os and TOC (~154 %, 54 % and 83 %, respectively). The pronounced peak ~0.2 m above this (SP28-09) displays more substantial increases for Re and Os (~345 % and 181 %, respectively), with a significantly smaller increase of TOC (~56 %). As a strong positive correlation is observed between Re and Os vs. TOC (R^2 = 0.89 and 0.80, respectively), it would be expected that an increase in TOC would be accompanied by a similar response in Re and Os. From 1 m above the boundary, Re, Os, TOC and $\delta^{13}C_{org}$ follow very similar profiles, with fluctuations correlating up-section. These fluctuations may partially reflect interbedding of the siliceous mudstone within the darker mudstone unit.

4.6.2 Correlation of Re and Os abundance with TOC and redox

The relationship between Re and Os abundance and TOC has been the subject of a number of studies (eg. Colodner *et al.,* 1993; Crusius *et al.,* 1996; Cohen *et al.,* 1999; Kendall *et al.,* 2004; Yamashita *et al.,* 2007; Selby *et al.,* 2009; Rooney *et al.,* 2010). Although a clear relationship between Re, Os and $^{187}Re/^{188}Os$ vs. TOC is observed for Early Jurassic samples in this study (Figs. 4.8, 4.10 and 4.11), Cohen *et al.* (1999) demonstrate that no such trend exists for other organic-rich samples (with higher TOC levels) from the Jurassic. Further, other workers have demonstrated that a direct link between TOC and Re and Os abundance is unlikely for all organic-rich sediments, as samples with low or high TOC content can have elevated Re/Os ratios and Re-Os abundances (eg. Kendall *et al.,*2004; Selby *et al.,* 2009; Rooney *et al.,* 2010). This indicates that the relationship between Re and Os with TOC is distinct for differing organic-rich sediments and further illustrates that sequestration by organic matter is not the sole control on Re and Os uptake.

Additional processes that control the uptake of Re and Os, assuming other physical factors remain stable, such as the salinity of the water column, depth of oxygen penetration into the sediment, and porosity, include the rate of sedimentation (Lewan and Maynard, 1982; Crusius and Thomson, 2000), recharge of Re and Os into the water column (Turgeon *et al.,* 2007) and post-depositional effects (Crusius and Thomson, 2000; Kendall *et al,.* 2004).

The redox conditions at the time of deposition have also been postulated to control Re and Os uptake into organic-rich sediments (Crusius *et al.,* 1996; Yamashita *et al.,* 2007), with several workers documenting uptake from seawater to organic-rich sediments in a suboxic-anoxic water column (Colodner *et al.,* 1993; Crusius *et al.,*1996; Morford and Emerson, 1999; Crusius and Thomson, 2000, 2003). Trace element data from the Sinemurian-Pliensbachian GSSP indicates that these sediments were deposited under predominantly oxic conditions (Figs. 4.5 and 4.6). Although the redox conditions remain constant throughout the section,

abundances of Re and Os are highly variable (~1.5 – 117 ppb and ~107 – 1903 ppt, respectively). If redox conditions are a primary control on the uptake of Re and Os, then little variation in Re and Os abundance would be expected in samples deposited under similar redox conditions. Further, the Robin Hood's Bay dataset presented in this study suggests that enrichment of Re and Os is not solely dependent on sediment deposition occurring under suboxic-anoxic conditions.

Rhenium-osmium data from previous studies show that organic-rich sediments deposited from a suboxic-anoxic water column will yield high $^{187}Re/^{188}Os$ values, ≥ 300 (Ravizza and Turekian, 1989; Cohen *et al.,* 1999; Selby and Creaser, 2003; Kendall *et al.,* 2004, 2006; Selby, 2007), and suggest that this ratio should show little variation when redox conditions remain constant if redox directly and primarily controls Re and Os. The $^{187}Re/^{188}Os$ values for the Sinemurian-Pliensbachian boundary, which was deposited under almost entirely oxic conditions, are significantly variable (~20 – 443 units; Fig. 4.7). In a similar manner to Re and Os enrichment, such variability in $^{187}Re/^{188}Os$ values would not be expected in samples deposited under consistent redox conditions if redox was the only direct control on the uptake of Re and Os (Selby *et al.,* 2009).

4.6.3 Evaluating Re-Os systematics as a proxy for distinguishing between marine and land-proximal depositional environments

To accurately interpret geochemical records for global seawater from organic-rich sediments, it is necessary to distinguish whether the sediments are from a fully marine or land-proximal (terrestrially-influenced) depositional environment (Baioumy *et al.,* 2011). Baioumy *et al.* (2011) show that a suite of fully marine organic-rich sediments from the Late Cretaceous contain high Re and Os concentrations and $^{187}Re/^{188}Os$ values, that correlate strongly with organic carbon (Fig. 4.18a-c). This suggests primary association of Re and Os with organic

matter in these samples (Baioumy *et al.,* 2011; Fig. 4.18). Conversely, their suite of Jurassic non-marine, land-proximal shales contain Re and Os concentrations similar to continental crust (~0.2 – 2 ppb and ~30 – 50 ppt, respectively; Esser and Turekian, 1993; Peucker-Ehrenbrink and Jahn, 2001) and generally do not show correlations of Re and Os with TOC (Baioumy *et al.,* 2011; Fig. 4.18). This is attributed to a preferential occurrence of Re and Os in the detrital fraction (Baioumy *et al.,* 2011).

The change in lithology across the Sinemurian-Pliensbachian boundary at Robin Hood's Bay reflects an overall sea-level rise (Sellwood, 1971; Hesselbo and Jenkyns, 1995; Hesselbo *et al.,* 2000; Meister *et al.,* 2006; this study), marking a progression from land-proximal siliceous shales to finer shales with a greater organic component. As this transition to a deeper marine depositional environment occurs, it is mirrored by significant increases in Re and Os abundance and the $^{187}Re/^{188}Os$ ratio (Fig. 4.7) to levels far greater than that of average continental crust, together with increased correlation of these factors with TOC. Plots of Re, Os and $^{187}Re/^{188}Os$ for marine and non-marine shales from Baioumy *et al.* (2011) and Robin Hood's Bay (Fig. 4.18) demonstrate that significant similarities in Re-Os isotope systematics exist between these two studies. This in turn suggests that these systematics may be used as a parameter to distinguish between marine and land-proximal organic-rich sediments at Robin Hood's Bay.

However, as with any proxy newly developed to yield information about the depositional environment, caution must be taken when utilising it as the sample suite originally used may not be representative of all organic-rich sediments. Further, variations in local and global factors and their influence on Re-Os systematics within organic-rich sediments have not been taken into account. Such variations that can be significant to the composition of organic-rich sediments include: changes in paleogeography and climate which affect oceanic

circulation and the level of contribution from the continental crust through time, the rate of sedimentation, and the type of organic matter present.

4.6.4 Evaluating the relationships between Ni and V abundance with TOC and redox

Unlike Re, no correlation exists between either Ni vs. TOC or V vs. TOC (R^2 = 0.02 and R^2 = 0.01, respectively; Fig. 4.12a,d). In addition, and again unlike Re vs. TOC, no trend is observed between these parameters either above or below the Sinemurian-Pliensbachian boundary (R^2 between ~ 0.01 and 0.38; Fig. 4.12b,c,e,f). This can be further visualised by comparing the stratigraphic profiles of Ni, V, Re and TOC in Figures 4.3 and 4.7. Whilst Re and TOC remain largely constant prior to the Sinemurian-Pliensbachian boundary, Ni and V show a greater degree of fluctuation. Similarly, Re and TOC trend towards higher concentrations in the earliest Pliensbachian, but V and Ni show no such increase and instead continue to fluctuate. Although there is no correlation between Ni and V with TOC, the greatest variation in the concentrations of these metals occurs when the stratigraphy changes from pale siliceous to darker mudrocks with greater TOC content (Fig. 4.3). These observations indicate that the abundance of Ni and V in the marine sediments across the Sinemurian-Pliensbachian boundary was not solely dependent on the concentration of organic matter in the water column at the time of deposition.

As discussed previously in Chapter 3, Ni and V in organic-rich sediments are typically bound in highly stable tetrapyrrole complexes (Lewan and Maynard, 1982; Lewan, 1984) and as a result of these strong bonds, the proportionality of these two metals should record the environmental conditions at the time of deposition (Lewan, 1984). These tetrapyrrole complexes are preferentially preserved under anoxic conditions (Lewan and Maynard, 1982). As such, organic matter that has been exposed to aerobic conditions should have a low tetrapyrrole content, resulting in low, largely endemic, concentrations of Ni and V (<10 ppm;

Lewan and Maynard, 1982). Conversely, elevated concentrations of Ni and V (~10 – 1000 ppm; Lewan and Maynard, 1982) in sediments are observed in those deposited under anoxic conditions (eg. Lewan and Maynard, 1982; Lewan, 1984; Shaw *et al.,* 1990; Emerson and Huested, 1991; Jones and Manning, 1994).

Despite being predominantly deposited in an oxic environment, the Robin Hood's Bay sediments contain elevated levels of V (~180 – 330 ppm; Table 4.2) and all samples are significantly more enriched in V relative to average shale (Fig. 4.4; Table 4.3). This suggests that V enrichment in the sediments here is not controlled by redox.

Although lower, the concentrations of Ni are also slightly elevated (~18 – 190 ppm). However, the majority of samples (n = 23, ~72 %) are depleted in Ni relative to average shale, with only nine being enriched (Fig. 4.4). Nickel enrichment in organic-rich sediments has been attributed to deposition in a suboxic-anoxic environment (eg. Lewan and Maynard, 1982; Lewan, 1984; Shaw *et al.,* 1990; Emerson and Huested, 1991; Jones and Manning, 1994). The relative depletion of Ni compared to average shale in the oxic sediments from Robin Hood's Bay is therefore consistent with these past observations.

At a glance, the constant variability of Ni abundance and enrichment across the Sinemurian-Pliensbachian section (Figs. 4.3 and 4.4) would suggest that redox has no effect on the concentration of Ni in the sediments. However, a closer look at the nine samples that are enriched in Ni relative to average shale disputes this (Fig. 4.19). The results provided by the trace element ratios V/Cr and Ni/Co indicate that this sedimentary succession was deposited under primarily oxic conditions, with intermittent periods that either approached or surpassed the oxic-dysoxic transition (Fig. 4.5). Of the nine samples that are enriched in Ni relative to average shale, ~67 % (n = 6; SP36-09, SP27-09, SP38-09, SP39-09, SP9-09, SP11-09) are representative of these intermittent periods (Fig. 4.19). Sample SP34-09, where both redox indices indicate redox conditions at or close to the oxic-dysoxic transition, has a $(Ni/Al)*10^4$

value of ~7.35, only 0.35 units lower than the average shale value of ~7.7. Additionally, the $(Ni/Al)*10^4$ value for sample SP29-09 (~17.2) shows the greatest level of Ni enrichment within this dataset, although there is significant disagreement between the two redox proxies for this sample. In summary, Figure 4.19 demonstrates that at Robin Hood's Bay, Ni enrichment is at least partially controlled by the depositional redox conditions.

With regard to organic matter accumulation, assuming the sediment composition has not been significantly altered by post-depositional and diagenetic changes (no field evidence for this), a strong correlation between the redox ratios and TOC should be observed if redox conditions were the only primary factor controlling this (Rimmer, 2004). However, this is not the case at Robin Hood's Bay (Fig. 4.20), suggesting that organic matter accumulation was influenced by conditions other than redox.

It is clear from this study that TOC content and redox conditions are not the sole controls on Ni and particularly V uptake in the Robin Hood's Bay sediments. Additional factors that may influence the metal contents of these sediments include type and classification of the organic matter, biogeochemical cycling of the elements in the ocean, partitioning of individual elements between solid and solution phases, as well as sediment accumulation rates (eg. Boyle *et al.,* 1976; 1977; 1981; Calvert and Pederson, 1993; Jones and Manning, 1994; Crusius *et al.,*1996; Rimmer, 2004).

The sedimentation rate throughout this section is postulated to be exceptionally slow (Chapter 2). As discussed previously in Chapter 3, interstitial pore waters in an open sediment system allow the overlying water body to provide a significant contribution of V and Ni to the sediments (Lewan and Maynard, 1982). This source is only effective if the sediment system remains open, and is most efficient when sedimentation rates are slowest (Lewan and Maynard, 1982). As such, the slow rates of sediment accumulation at Robin Hood's Bay may

have been a contributing factor to the elevated abundances of V and Ni seen in the sediments here.

4.6.5 Evaluating the suitability of V/(V+Ni) as a redox proxy: How applicable is it?

The Ni/Co and V/Cr redox indices are recommended by a number of workers as the most reliable of the paleo-environmental proxies (eg. Jones and Manning, 1994; Rimmer, 2004), and have been used by several studies to provide accurate and consistent evaluations of paleoredox conditions at the time of sediment deposition (eg. Rimmer, 2004; Selby *et al.,* 2009; this study). However, this study finds that there is significant disagreement between these indices and the V/(V+Ni) index (Fig. 4.6). For Robin Hood's Bay, the latter index suggests that the sediments were deposited in predominantly suboxic-anoxic bottom-waters, with intermittent euxinic periods. However, both the V/Cr and Ni/Co ratios indicate that the Robin Hood's Bay samples were deposited under largely oxic conditions (Fig. 4.5a,b). Such disparity between the redox indices is also noted by both Rimmer (2004) and Selby *et al.* (2009), who observe that the V/(V+Ni) index suggests suboxic-anoxic conditions for sediments otherwise indicated to have been deposited under oxic conditions by the V/Cr and Ni/Co ratios.

Preliminary work by Lewan and Maynard (1982) and Lewan (1984) suggested that redox potential was a dominant control on the wide range of V/(V+Ni) values observed in petroleum source rocks and oils. Following this, Hatch and Leventhal (1992) were the first to develop and utilise the V/(V+Ni) index as a measure of relative redox potential in organic-rich sediments. Their study focused on applying this index specifically to marine black shales in the Pennsylvanian Stark Shale Member of the Dennis Limestone, Wabaunsee County, Kansas, USA (Hatch and Leventhal, 1992). Therefore, the ranges they defined for the V/(V+Ni) ratio and the associated redox conditions (summarised in Table 4.5), are applicable to this specific geological basin and are sensitive to localised geochemical variations therein.

This can be observed by comparing aspects of the Robin Hood's Bay (herein) and Pennsylvanian Stark Shale Member (Hatch and Leventhal, 1992) datasets (Fig. 4.21). Hatch and Leventhal (1992) show that for the Stark Shale Member, with the exception of two outliers, low TOC values (<2.5 wt. %) correspond to V/(V+Ni) values <0.75, and samples containing greater TOC (>7.5 wt. %) have corresponding higher V/(V+Ni) values (0.75; Fig. 4.21). However, no such relationship is observed in the Robin Hood's Bay sediments (highlighted by the inset of Fig. 4.21), with samples containing low TOC (<2.5 wt. %) providing a range in V/(V+Ni) data from ~0.51 – 0.89. This immediately indicates that the two geological sites have differing geochemical frameworks. This may be due to differences in both geological age and stratigraphy, with the Stark Shale Member (Late Carboniferous) being a darker grey, non-sandy shale with higher TOC content (Hatch and Leventhal, 1992). As such, this comparison proves that the redox index V/(V+Ni), originally developed for a specific geological basin, may not be applicable to other geological sites, particularly those that possess differing geological and geochemical characteristics. Factors that may have a profound effect upon the applicability of such a threshold from one study to another include: differences in the influx of nutrients and trace elements, type and relative amounts of organic matter, and degrees of oceanic mixing (eg. Rimmer, 2004). In agreement with Rimmer (2004), this chapter therefore suggests that caution should be taken when applying redox indices established by other studies for specific geological sites.

4.6.6 Nickel isotope profiling across the Sinemurian-Pliensbachian boundary: what causes Ni isotope fractionation in marine sediments?

The Ni stable isotope data in Table 4.6 is the first to be obtained for a suite of organic-rich marine sediments. The vertical profile of Ni stable isotope data in Figure 4.14 indicates that significant Ni isotope fractionation occurs across the Sinemurian-Pliensbachian boundary

at Robin Hood's Bay (~1.32 ‰). Apart from two prominent peaks that coincide with the tops of beds 70 and 74, and taking the lower sample resolution of the Ni isotope profile into account, the δ^{60}Ni profile follows a similar trend to that of Ni concentration (Fig. 4.14). However, no correlation is observed between δ^{60}Ni and Ni abundance (Fig. 4.15), indicating that the level of Ni isotope fractionation in the marine sediments here is not controlled by the degree of Ni enrichment.

Similarly, no relationship exists between δ^{60}Ni and redox (Fig. 4.22), suggesting that the level of isotopic fractionation is not dictated by the paleoredox conditions at the time of sediment deposition. However, the samples used for Ni isotope analysis were deposited in predominantly oxic conditions (using the Ni/Co and V/Cr ratios; Fig. 4.5). The tetrapyrrole complexes known to hold the majority of the Ni in organic matter are poorly preserved under these conditions (Lewan and Maynard, 1982). As such, assuming break down of these complexes is heterogeneous, and that it does not result in the preferential loss of a particular isotope of Ni, this lack of preservation may partially account for the observed range in δ^{60}Ni values.

In a similar manner to Re, Os and ^{187}Re/^{188}Os, and disregarding data from SP26-09 and SP12-09, the most distinct positive correlation is observed between δ^{60}Ni and TOC in samples above the Sinemurian-Pliensbachian boundary (R^2 = 0.74; Fig. 4.15). This indicates that the degree of Ni isotope fractionation in these marine sediments (above the boundary) could at least partially be controlled by the TOC content. Further, this potential correlation suggests that increasing TOC content above the boundary may have resulted in the preferential uptake of ^{60}Ni into the sediments. However, the weaker correlation between TOC and δ^{60}Ni below the boundary suggests that for these samples, TOC had little control on Ni isotope fractionation. A preliminary hypothesis from this dataset could be that TOC concentration in marine sediments can partially control Ni isotope fractionation by promoting the preferential uptake of ^{60}Ni, but

only when TOC levels are above a certain threshold. In support of this, the outliers removed have low TOC contents of 0.5 wt. % (SP26-09) and 0.8 wt. % (SP12-09), and the majority of samples above the boundary have TOC > 1 wt. %. Further, a plot of TOC vs. δ^{60}Ni for the upper 5 samples with TOC concentrations >1 wt. %, yields an R^2 value of ~0.7.

Another possible cause of the degree of Ni isotope fractionation seen in the Robin Hood's Bay samples could be related to the lithology, and therefore the depositional environment. Unlike the Ni concentration profile, the δ^{60}Ni profile shows a similar level of fluctuation above and below the boundary level. However, it is difficult to determine whether this is due to a lack of correlation with Ni, or whether it is a relic of a lower sampling resolution.

Although the mudrocks become gradually less sand-silt rich and contain greater concentrations of clay and TOC up-section, the TOC content is low throughout (≤ 2 wt. %) and there is no drastic change in lithology. Further, the degree of Ni isotope fractionation seen in the suite of samples from Robin Hood's Bay is not distinct for either the sand-silt-rich or darker clay-rich sediments. This may suggest that the range of δ^{60}Ni values seen here is characteristic of these types of low TOC mudrocks. However, it is impossible to draw a definitive conclusion from this, as there is currently no other dataset for comparison.

4.6.7 Fractionation of nickel isotopes in marine organic-rich sediments vs. abiotic terrestrial and extraterrestrial samples

The marine organic-rich sediments at Robin Hood's Bay contain a substantial range in δ^{60}Ni values of ~1.32 ‰ (Fig. 4.14), indicating that significant Ni isotope fractionation occurs across the Sinemurian-Pliensbachian boundary. Figure 4.23 compares this fractionation with that of abiotic terrestrial and extraterrestrial samples from a study by Cameron *et al.* (2009), including meteorites (stone and iron), basalts and continental sediments (river and aeolian).

The δ^{60}Ni values defined by the meteorites, basalts and continental sediments are 0.19 ± 0.05 to 0.36 ± 0.04 ‰ (range of ~0.17 ‰), -0.03 ± 0.07 to 0.34 ± 0.08 ‰ (range of ~0.37 ‰), and -0.04 ± 0.02 to 0.23 ± 0.08 ‰ (range of ~0.27 ‰), respectively, with an overall average of 0.2 ‰ (Cameron *et al.,* 2009; Fig. 4.23). It is immediately obvious therefore, that Ni isotope fractionation occurs to a much greater degree in the marine sediments. However, despite the much greater degree of fractionation in these marine sediments, there is minimal overlap between their δ^{60}Ni values and those of the abiotic terrestrial and extraterrestrial samples (Fig. 4.23). As such, the marine sediments define a realm on the δ^{60}Ni plot that is mostly separate from these samples. This study is the first to apply Ni isotopes to marine sediments, and therefore there are no other similar datasets for comparison. However, Figure 4.23 may demonstrate that marine sediments contain a Ni isotopic signature that is distinct to that of meteorites, basalts and continental sediments.

The level of Ni isotope fractionation in marine sediments is certainly greater than that of the abiotic terrestrial and extraterrestrial samples. The reasons for this are currently poorly understood. However, there are a number of factors that can influence marine sediments that do not apply to abiotic terrestrial samples. Overall, with the exception of an outlier (discussed previously) there is a possible relationship between δ^{60}Ni and TOC (Fig. 4.15), suggesting that the organic matter in the sediments exerts some control on the Ni isotope composition, at least at Robin Hood's Bay. In addition, the type of organic matter may be a factor. Further, the preservation of the tetrapyrrole complexes holding the Ni could influence the degree of isotopic fractionation. The sediment-seawater system is extremely complex and it may be this complexity that causes the greater level of Ni isotope fractionation observed in marine sediments in comparison to the samples analysed by Cameron *et al.* (2009).

4.7 Conclusions

This investigation provides an increased understanding of the Sinemurian-Pliensbachian boundary GSSP at Robin Hood's Bay, UK, by presenting a geochemical dataset that builds upon one previously limited to TOC, oxygen, strontium and carbon isotopes.

Trace element data demonstrate that the sediments across the boundary were deposited under predominantly oxic conditions. Although there is good agreement between the Ni/Co and V/Cr proxies, disagreement between these and the V/(V+NI) ratio calls into question the applicability of V/(V+Ni) as a redox proxy.

The Al-normalised trace element values demonstrate that V and Cr are enriched in the Robin Hood's Bay sediments relative to average shale. Conversely, Ni and Co are depleted for most of the section. Whilst Ni enrichment may partly be controlled by redox conditions transitioning between oxic and dysoxic conditions, no such relationship exists for V enrichment. Similarly, TOC content does not exert control over Ni and V enrichment in these sediments. It is likely that factors in addition to TOC and redox, including the type of the organic matter, sediment accumulation rates, and biogeochemical cycling of the elements in the ocean, impacted the uptake of these metals into the sediments (eg. Boyle *et al.,* 1976; 1977; 1981; Calvert and Pederson, 1993; Jones and Manning, 1994; Crusius *et al.,*1996; Rimmer, 2004).

A clear relationship between Re, Os, $^{187}Re/^{188}Os$ and TOC is observed in the Pliensbachian sediments, but not below the boundary. This indicates that above the boundary TOC levels strongly influenced the uptake of Re and Os into the sediments. Additional factors that can control uptake of Re and Os, and that possibly prevailed below the boundary, include the rate of sedimentation (Lewan and Maynard, 1982; Crusius and Thomson, 2000), recharge

of Re and Os into the water column (Turgeon *et al.,* 2007) and post-depositional effects (Crusius and Thomson, 2000; Kendall *et al.,* 2004).

This is the first study to present Ni stable isotope data for marine organic-rich sediments. Nickel fractionation occurs to a far greater level in these marine sediments than in abiotic terrestrial and extraterrestrial samples analysed by Cameron *et al.* (2009). Further, the δ^{60}Ni values defined by the marine sediments are distinct to those of the samples presented by Cameron *et al.* (2009). With no other dataset available for comparison it is difficult to constrain whether the observed Ni isotope signature in these marine sediments is characteristic of low TOC mudrocks, or if Ni fractionation is instead controlled by depositional and chemical processes during accumulation.

In order to understand what causes Ni isotope fractionation in marine sediments it is important to consider whether fractionation occurs as a result of the preferential uptake of one or more isotopes into the sediment during deposition, or whether it relates to the loss of one or more isotopes during the break down of the tetrapyrrole complexes prior to lithification. Due to the lack of studies investigating Ni isotopes in marine sediments, this is currently poorly understood.

In the marine sediments herein there is a possible relationship between δ^{60}Ni and TOC when TOC levels are at their highest above the Sinemurian-Pliensbachian boundary (>1 wt. %). This implies that Ni isotope fractionation in these marine sediments may be partly controlled by the organic matter concentration in the sediment, but only when this concentration reaches and exceeds a necessary threshold.

No relationship exists between paleoredox conditions at the time of sediment deposition and Ni isotope fractionation. However, the tetrapyrrole complexes known to contain the Ni associated with the organic matter are poorly preserved under oxic conditions (Lewan and Maynard, 1982). It is possible that the δ^{60}Ni values may also reflect, at least in

part, the break-down of these complexes post-deposition and prior to lithification. In this case, the assumptions that break-down is heterogeneous and therefore does not result in the preferential loss of one particular Ni isotope, have to be made.

In the same way that the Ni concentration in organic-rich sediments may be influenced by factors such as the type and classification of organic matter in the sediment, sedimentation rate, recharge of Ni into the water column, preservation of tetrapyrrole complexes (Lewan and Maynard, 1982) and partitioning of Ni between solid and solution phases, these factors may also have a significant influence on the Ni isotope composition. As such and with limited datasets for comparison, it is not possible to deduce at this stage whether fractionation of Ni isotopes in these marine sediments occurred during sediment accumulation or prior to lithification, or indeed during both scenarios.

4.8 References

Alberdi, M., and Lafargue, E., 1993, Vertical variations of organic matter content in Guayuta Group (upper Cretaceous), Interior Mountain Belt, Eastern Venezuela: Organic Geochemistry, v. 20, no. 4, p. 425-436.

Archer, C., and Vance, D., 2004, Mass discrimination correction in multiple-collector plasma source mass spectrometry: an example using Cu and Zn isotopes: Journal of Analytical Atomic Spectrometry, v. 19, no. 5, p. 656-665.

Baioumy, H. M., Eglinton, L. B., and Peucker-Ehrenbrink, B., 2011, Rhenium–osmium isotope and platinum group element systematics of marine vs. non-marine organic-rich sediments and coals from Egypt: Chemical Geology, v. 285, no. 1–4, p. 70-81.

Birck, J. L., and Lugmair, G. W., 1988, Nickel and chromium isotopes in Allende inclusions: Earth and Planetary Science Letters, v. 90, no. 2, p. 131-143.

Boyle, E. A., Huested, S. S., and Jones, S. P., 1981, On the distribution of copper, nickel and cadmium in the surface waters of the North Atlantic and North Pacific Ocean: Journal of Geophysical Research, v. 86, p. 8048-8066.

Boyle, E. A., Sclater, F., and Edmond, J. M., 1976, On the marine geochemistry of cadmium: Nature, v. 263, p. 42-44.

Boyle, E. A., Sclater, F. R., and Edmond, J. M., 1977, The distribution of dissolved copper in the Pacific: Earth and Planetary Science Letters, v. 37, p. 38-54.

Calvert, S. E., and Pedersen, T. F., 1993, Geochemistry of Recent oxic and anoxic marine sediments: Implications for the geological record: Marine Geology, v. 113, no. 1-2, p. 67-88.

Cameron, V., Vance, D., Archer, C., and House, C. H., 2007, Nickel stable isotopes as biogeochemical tracers, Goldschmidt Conference Abstracts, p. A141.

Cameron, V., Vance, D., Archer, C., and House, C. H., 2009, A biomarker based on the stable isotopes of nickel: Proceedings of the National Academy of Sciences, v. 106, p. 10944-10948.

Cameron, V., Vance, D., and Poulton, S., 2011, Nickel isotopes, BIFs and the Archean oceans, Goldschmidt Conference Abstracts, Mineralogical Magazine, p. 615.

Chen, J. H., Papanastassiou, D. A., and Wasserburg, G. J., 2009, A search for nickel isotopic anomalies in iron meteorites and chondrites: Geochimica et Cosmochimica Acta, v. 73, no. 5, p. 1461-1471.

Cohen, A. S., Coe, A. L., Bartlett, J. M., and Hawkesworth, C. J., 1999, Precise Re-Os ages of organic-rich mudrocks and the Os isotope composition of Jurassic seawater: Earth and Planetary Science Letters, v. 167, no. 3-4, p. 159-173.

Colodner, D., Sachs, J., Ravizza, G., Turekian, K., Edmond, J., and Boyle, E., 1993, The geochemical cycle of rhenium: a reconnaissance: Earth and Planetary Science Letters, v. 117, no. 1-2, p. 205-221.

Cook, D. L., Wadhwa, M., Clayton, R., Dauphas, N., Janney, P. E., and Davis, A. M., 2007, Mass-dependent fractionation of nickel isotopes in meteoritic metal: Meteoritics and Planetary Science, v. 42, no. 12, p. 2067-2077.

Creaser, R. A., Papanastassiou, D. A., and Wasserburg, G. J., 1991, Negative thermal ion mass spectrometry of osmium, rhenium and iridium: Geochimica et Cosmochimica Acta, v. 55, no. 1, p. 397-401.

Crusius, J., Calvert, S., Pedersen, T., and Sage, D., 1996, Rhenium and molybdenum enrichments in sediments as indicators of oxic, suboxic and sulfidic conditions of deposition: Earth and Planetary Science Letters, v. 145, no. 1-4, p. 65-78.

Crusius, J., and Thomson, J., 2000, Comparative behavior of authigenic Re, U, and Mo during reoxidation and subsequent long-term burial in marine sediments: Geochimica et Cosmochimica Acta, v. 64, no. 13, p. 2233-2242.

Crusius, J., and Thomson, J., 2003, Mobility of authigenic rhenium, silver, and selenium during postdepositional oxidation in marine sediments: Geochimica et Cosmochimica Acta, v. 67, no. 2, p. 265-273.

Dean, W. T., Donovan, D. T., and Howarth, M. K., 1961, The Liassic ammonite Zones and Subzones of the North West European Province: Bulletin of the Natural History Museum, v. 4, p. 435-505.

Dera, G., Pucéat, E., Pellenard, P., Neige, P., Delsate, D., Joachimski, M. M., Reisberg, L., and Martinez, M., 2009, Water mass exchange and variations in seawater temperature in the NW Tethys during the Early Jurassic: Evidence from neodymium and oxygen isotopes of fish teeth and belemnites: Earth and Planetary Science Letters, v. 286, no. 1-2, p. 198-207.

Dewaker, K. N., Chandra, K., Arunachalam, J., and Karunasagar, D., 2000, Isotopic fractionation of Ni60/Ni61 in kerogen and bitumen samples: Current Science, v. 79, no. 12, p. 1720-1723.

Dill, H., 1986, Metallogenesis of early Paleozoic graptolite shales from the Graefenthal Horst (Northern Bavaria-Federal Republic of Germany): Econmic Geology, v. 81, p. 889-903.

Dypvik, H., 1984, Chemical compositions and depositional conditions of Upper Jurassic and Lower Cretaceous Yorkshire clays, England: Geological Magazine, v. 121, no. 5, p. 489-504.

Ellrich, J., Hirner, A., and Stärk, H., 1985, Distribution of trace elements in crude oils from southern Germany: Chemical Geology, v. 48, no. 1-4, p. 313-323.

Emerson, S. R., and Huested, S. S., 1991, Ocean anoxia and the concentrations of molybdenum and vanadium in seawater: Marine Chemistry, v. 34, no. 3-4, p. 177-196.

Ernst, T. W., 1970, Geochemical Facies Analysis, Elsevier, Amsterdam, p. 152.

Esser, B. K., and Turekian, K. K., 1993, The osmium isotopic composition of the continental crust: Geochimica et Cosmochimica Acta, v. 57, no. 13, p. 3093-3104.

Frausto da Silva, J. J. R., and Williams, R. J. P., 2001, The Biological Chemistry of the Elements: The Inorganic Chemistry of Life, Oxford University Press, Oxford, p. 436-449.

Hallberg, R. O., 1976, A geochemical method for investigation of paleoredox conditions in sediments: Ambio Special Report, v. 4, p. 139-147.

Hallberg, R. O., 1982, Diagenetic and environmental effects on heavy-metal distrubution on sediments: A hypothesis with an illustration from the Baltic Sea, *in* Fanning, K. A., and Manheim, F. T., eds., The Dynamic Environment of the Ocean Floor, Lexington Books, p. 305-316.

Hatch, J. R., and Leventhal, J. S., 1992, Relationship between inferred redox potential of the depositional environment and geochemistry of the Upper Pennsylvanian (Missourian) Stark Shale Member of the Dennis Limestone, Wabaunsee County, Kansas, U.S.A: Chemical Geology, v. 99, no. 1-3, p. 65-82.

Herzog, G. F., hall, G. S., and Brownlee, D. E., 1994, Mass fractionation of nickel isotopes in metallic cosmic spheres: Geochimica et Cosmochimica Acta, v. 58, no. 23, p. 5319-5323.

Hesselbo, S. P., and Jenkyns, H. C., 1995, A comparison of the Hettangian to Bajocian successions of Dorset and Yorkshire, *in* Taylor, P. D., ed., Field Geology of the British Jurassic, Geological Society, London, p. 105-150.

Hesselbo, S. P., Meister, C., and Grocke, D. R., 2000, A potential global stratotype for the Sinemurian-Pliensbachian boundary (Lower Jurassic), Robin Hood's Bay, UK: ammonite faunas and isotope stratigraphy: Geological Magazine, v. 137, no. 6, p. 601-607.

Jones, B., and Manning, D. A. C., 1994, Comparison of geochemical indices used for the interpretation of palaeoredox conditions in ancient mudstones: Chemical Geology, v. 111, no. 1-4, p. 111-129.

Jones, C. E., Jenkyns, H. C., and Hesselbo, S. P., 1994, Strontium isotopes in Early Jurassic seawater: Geochimica et Cosmochimica Acta, v. 58, no. 4, p. 1285-1301.

Kendall, B. S., Creaser, R. A., Ross, G. M., and Selby, D., 2004, Constraints on the timing of Marinoan "Snowball Earth" glaciation by ^{187}Re-^{187}Os dating of a Neoproterozoic post-glacial black shale in Western Canada: Earth and Planetary Science Letters, v. 222, p. 729-740.

Kohman, T. P., and Robison, M. S., 1980, Iron-60 as a possible heat source and chronometer in the early solar system: Lunar and Planetary Science, v. 11, p. 564-566.

Krecji-Graf, K., 1975, Geochemical facies of sediments: Soil Science, v. 119, p. 20-23.

Lewan, M. D., 1984, Factors controlling the proportionality of vanadium to nickel in crude oils: Geochimica et Cosmochimica Acta, v. 48, no. 11, p. 2231-2238.

Lewan, M. D., and Maynard, J. B., 1982, Factors controlling enrichment of vanadium and nickel in the bitumen of organic sedimentary rocks: Geochimica et Cosmochimica Acta, v. 46, no. 12, p. 2547-2560.

López, L., Lo Mónaco, S., Galarraga, F., Lira, A., and Cruz, C., 1995, VNi ratio in maltene and asphaltene fractions of crude oils from the west Venezuelan basin: correlation studies: Chemical Geology, v. 119, no. 1-4, p. 255-262.

Manning, L. K., Frost, C. D., and Branthaver, J. F., 1991, A neodymium isotopic study of crude oils and source rocks: potential applications for petroleum exploration: Chemical Geology, v. 91, no. 2, p. 125-138.

Maréchal, C. N., Télouk, P., and Albarède, F., 1999, Precise analysis of copper and zinc isotopic compositions by plasma-source mass spectrometry: Chemical Geology, v. 156, no. 1–4, p. 251-273.

Meister, C., Aberhan, M., Blau, J., Dommergues, J.-L., Feist-Burkhardt, S., Hailwood, E. A., Hart, M., Hesselbo, S. P., Hounslow, M. W., Hylton, M., Morton, N., Page, K., and Price, G. D., 2006, The Global Boundary Stratotype Section and Point (GSSP) for the base of the

Pliensbachian Stage (Lower Jurassic), Wine Haven, Yorkshire, UK: Episodes, v. 29, no. 2, p. 93-114.

Morand, P., and Allègre, C. J., 1983, Nickel isotopic studies in meteorites: Earth and Planetary Science Letters, v. 63, no. 2, p. 167-176.

Morford, J. L., and Emerson, S., 1999, The geochemistry of redox sensitive trace metals in sediments: Geochimica et Cosmochimica Acta, v. 63, no. 11-12, p. 1735-1750.

Moynier, F., Blichert-Toft, J., Telouk, P., Luck, J.-M., and Albarède, F., 2007, Comparative stable isotope geochemistry of Ni, Cu, Zn, and Fe in chondrites and iron meteorites: Geochimica et Cosmochimica Acta, v. 71, no. 17, p. 4365-4379.

Ottley, C. J., Pearson, D. G., and Irvine, G. J., 2003, A routine method for the dissolution of geological samples for the analysis of REE and trace elements via ICP-MS, *in* Holland, G., and Tanner, S. D., eds., Plasma source mass spectrometry: applications and emerging technologies, p. 221-230.

Peucker-Ehrenbrink, B., and Jahn, B., 2001, Rhenium-osmium isotope systematics and platinum group element concentrations: Loess and the upper continental crust: Geochemistry Geophysics Geosystems, v. 2, no. 10, p. 1061-1083.

Piper, D. Z., and Calvert, S. E., 2009, A marine biogeochemical perspective on black shale deposition: Earth-Science Reviews, v. 95, no. 1–2, p. 63-96.

Powell, J. H., 1984, Lithostratigraphical nomenclature of the Lias Group in the Yorkshire Basin: Proceedings of the Yorkshire Geological Society, v. 45, p. 51-57.

Quitté, G., Meier, M., Latkoczy, C., Halliday, A.N., and Günther, D., 2006, Nickel isotopes in iron meteorites–nucleosynthetic anomalies in sulphides with no effects in metals and no trace of ^{60}Fe: Earth and Planetary Science Letters, v. 242, p. 16-25.

Quitté, G., and Oberli, F., 2006, Quantitative extraction and high precision isotope measurements of nickel by MC-ICPMS: Journal of Analytical Atomic Spectrometry, v. 21, p. 1249-1255.

Ravizza, G., and Turekian, K. K., 1989, Application of the ^{187}Re-^{187}Os system to black shale geochronometry: Geochimica et Cosmochimica Acta, v. 53, no. 12, p. 3257-3262.

Rimmer, S. M., 2004, Geochemical paleoredox indicators in Devonian-Mississippian black shales, Central Appalachian Basin (USA): Chemical Geology, v. 206, no. 3-4, p. 373-391.

Rooney, A. D., Selby, D., Houzay, J.-P., and Renne, P. R., 2010, Re-Os geochronology of a Mesoproterozoic sedimentary succession, Taoudeni basin, Mauritania: Implications for

basin-wide correlations and Re-Os organic-rich sediments systematics: Earth and Planetary Science Letters, v. 289, no. 3-4, p. 486-496.

Schovsbo, N. H., 2001, Why barren intervals? A taphonomic case study of the Scandinavian Alum Shale and its faunas: Lethaia, v. 34, no. 4, p. 271-285.

Selby, D., 2007, Direct rhenium-osmium age of the Oxfordian-Kimmeridgian boundary, Staffin Bay, Isle of Skye, U.K., and the Late Jurassic time scale: Norwegian Journal of Geology, v. 87, p. 291-299.

Selby, D., and Creaser, R. A., 2003, Re-Os geochronology of organic rich sediments: an evaluation of organic matter analysis methods: Chemical Geology, v. 200, no. 3-4, p. 225-240.

Selby, D., Mutterlose, J., and Condon, D. J., 2009, U-Pb and Re-Os geochronology of the Aptian/Albian and Cenomanian/Turonian stage boundaries: Implications for timescale calibration, osmium isotope seawater composition and Re-Os systematics in organic-rich sediments: Chemical Geology, v. 265, no. 3-4, p. 394-409.

Sellwood, B. W., 1971, The genesis of some sideritic beds in the Yorkshire Lias: Journal of Sedimentary Petrology, v. 41, p. 854-858.

Sellwood, B. W., and Jenkyns, H. C., 1975, Basins and swells and the evolution of an epeiric sea (Pliensbachian-Bajocian of Great Britain): Journal of the Geological Society, v. 131, no. 4, p. 373-388.

Shaw, T. J., Gieskes, J. M., and Jahnke, R. A., 1990, Early diagenesis in differing depositional environments: The response of transition metals in pore water: Geochimica et Cosmochimica Acta, v. 54, no. 5, p. 1233-1246.

Shimamura, T., and Lugmair, G. W., 1983, Ni isotopic compositions in Allende and other meteorites: Earth and Planetary Science Letters, v. 63, no. 2, p. 177-188.

Smith, M. G., and Bustin, R. M., 2000, Late Devonian and Early Mississippian Bakken and Exshaw Black Shale Source Rocks, Western Canada Sedimentary Basin: A Sequence Stratigraphic Interpretation: AAPG Bulletin, v. 84, no. 7, p. 940-960.

Smoliar, M. I., Walker, R. J., and Morgan, J. W., 1996, Re-Os Ages of Group IIA, IIIA, IVA, and IVB Iron Meteorites: Science, v. 23, p. 1099-1102.

Spath, L. F., 1923, Correlation of the Ibex and Jamesoni Zones of the Lower Lias: Geological Magazine, v. 60, p. 6-11.

Turgeon, S. C., Creaser, R. A., and Algeo, T. J., 2007, Re-Os depositional ages and seawater Os estimates for the Frasnian-Famennian boundary: implications for weathering rates,

land plant evolution, and extinction mechanisms: Earth and Planetary Science Letters, v. 261, p. 649-661.

Völkening, J., Walczyk, T., and G. Heumann, K., 1991, Osmium isotope ratio determinations by negative thermal ionization mass spectrometry: International Journal of Mass Spectrometry and Ion Processes, v. 105, no. 2, p. 147-159.

Wedepohl, K. H., 1971, Environmental influences on the chemical composition of shales and clays: Physics and Chemistry of The Earth, v. 8, p. 305-333.

Xue, S., Herzog, G. F., Hall, G. S., Klein, J., Middleton, R., and Juenemann, D., 1995, Stable nickel isotopes and cosmogenic beryllium-10 and aluminum-26 in metallic spheroids from Meteor Crater, Arizona: Meteoritics, v. 30, p. 303-310.

Yamashita, Y., Takahashi, Y., Haba, H., Enomoto, S., and Shimizu, H., 2007, Comparison of reductive accumulation of Re and Os in seawater-sediment systems: Geochimica et Cosmochimica Acta, v. 71, no. 14, p. 3458-3475.

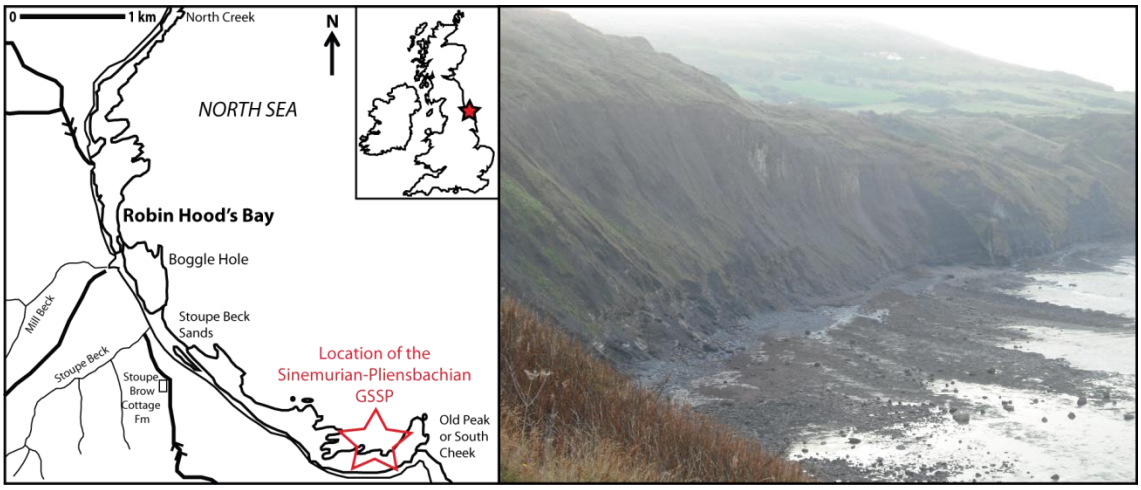

Figure 4.1: Map and photograph illustrating the location of the Sinemurian-Pliensbachian boundary GSSP at Robin Hood's Bay, UK.

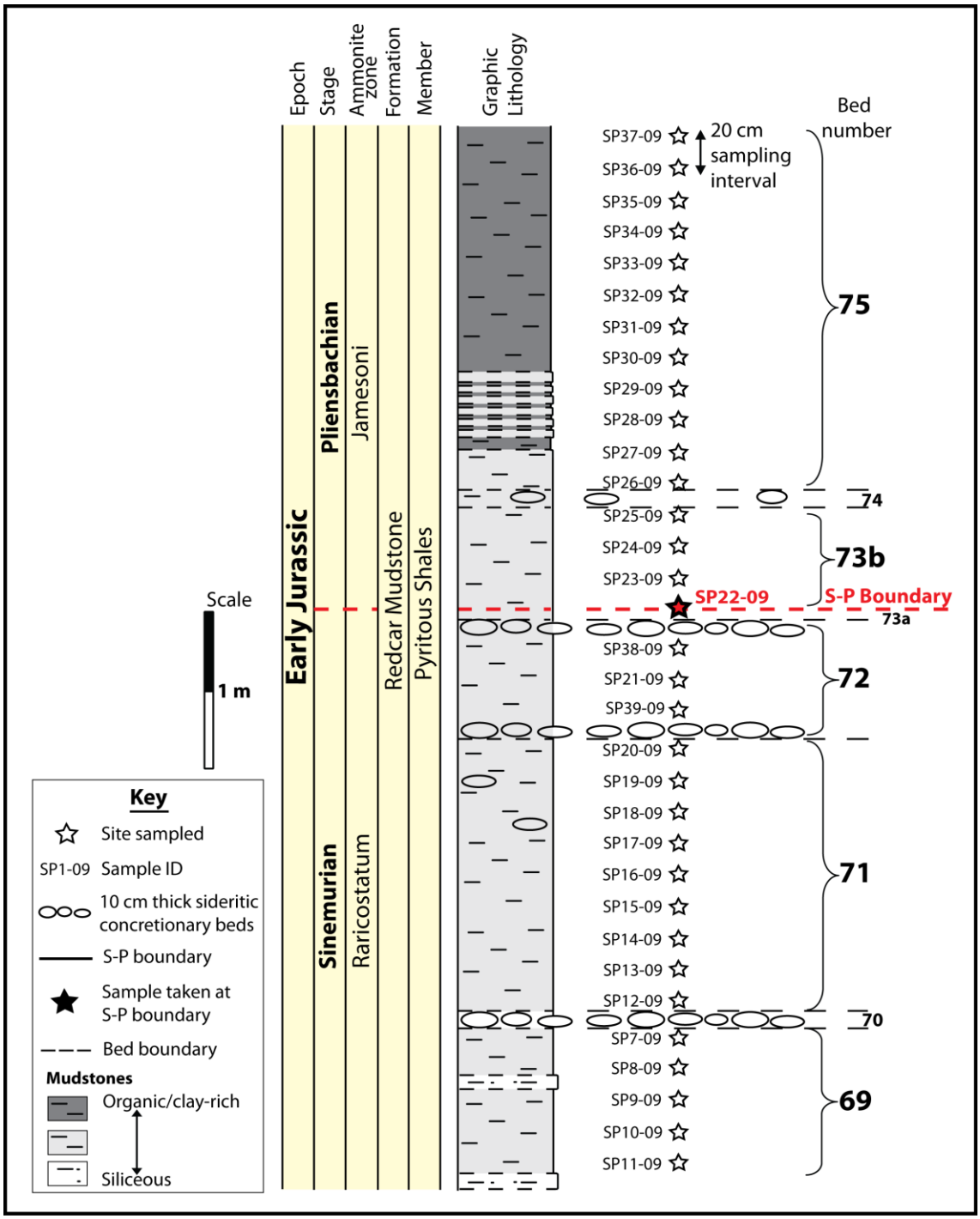

Figure 4.2: Graphic log showing the Sinemurian-Pliensbachian boundary GSSP and the relative locations of the samples analysed in this study. Bed number classification taken from Hesselbo and Jenkyns (1995).

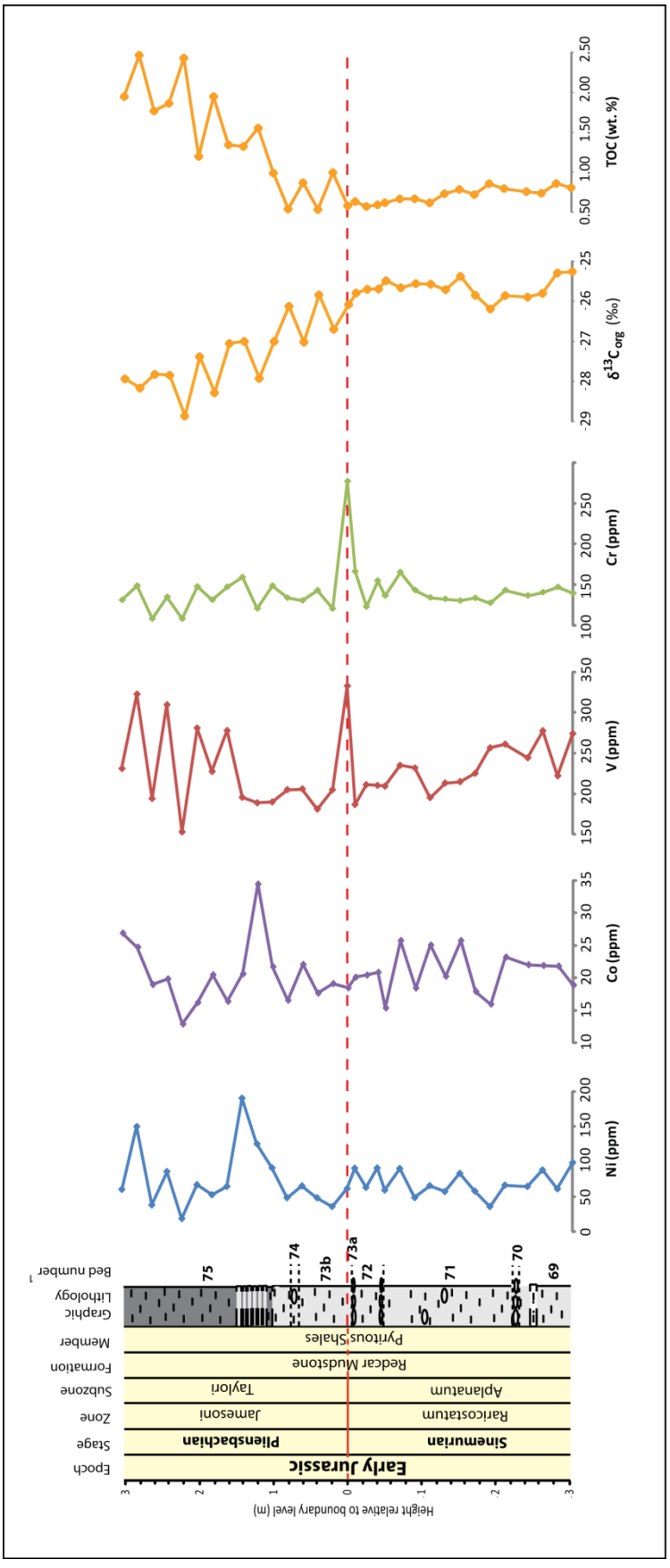

Figure 4.3: Trace element abundance, $\delta^{13}C_{org}$ and TOC profiles for the Robin Hood's Bay sediments, presented against a corresponding stratigraphic column and graphic log. Red dashed line indicates the position of the Sinemurian-Pliensbachian boundary. [1] Bed numbers are from Hesselbo and Jenkyns (1995).

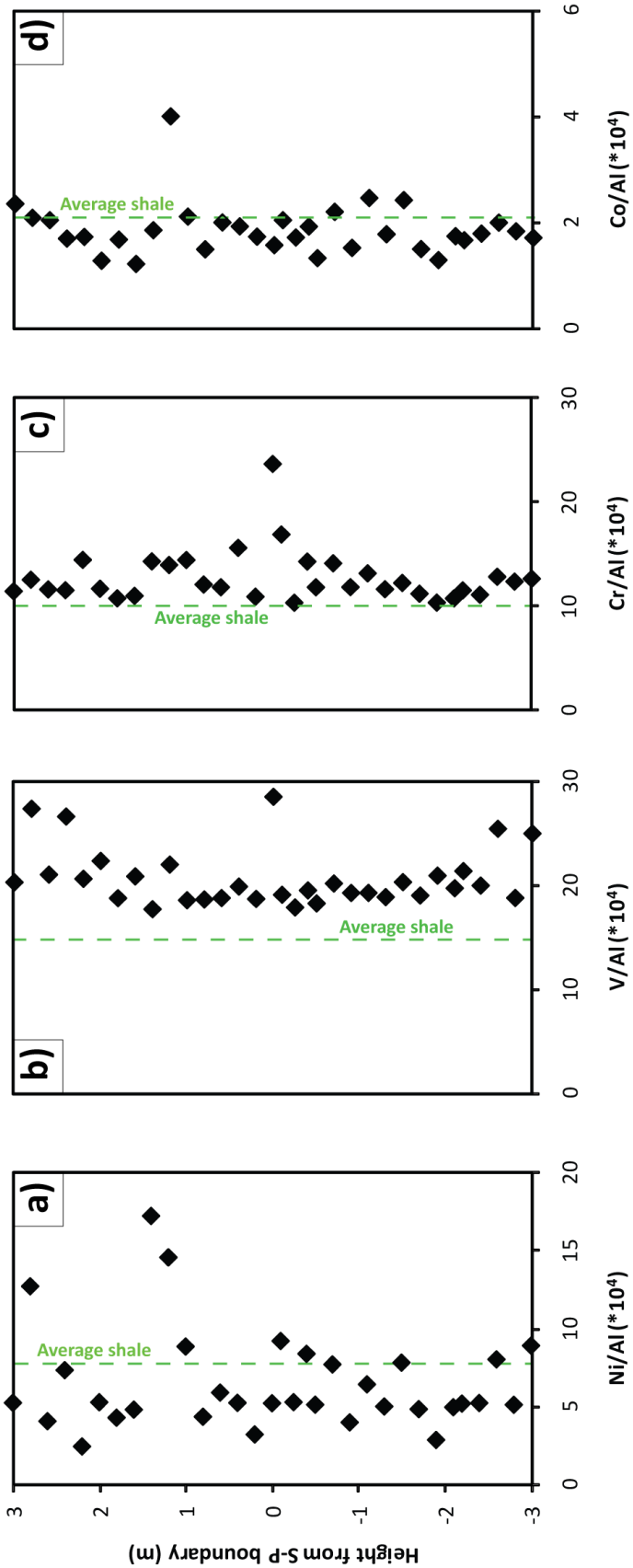

Figure 4.4: Section profiles showing the aluminium-normalised trace element values for the Robin Hood's Bay sediments, and their degree of enrichment relative to average shale values (green dashed line; from Wedepohl, 1971): a) Ni/Al; b) V/Al; c) Cr/Al; d) Co/Al.

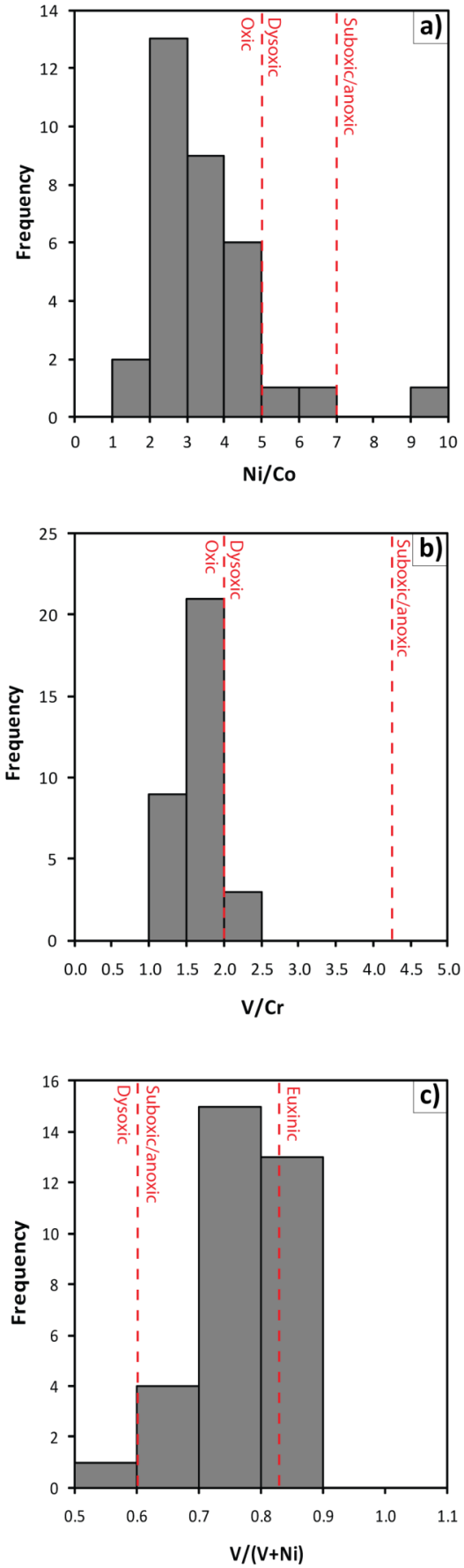

Figure 4.5: Histograms for the paleoredox proxies: a) Ni/Co; b) V/Cr; c) V/(V+Ni). Values defining the redox conditions for Ni/Co and V/Cr are from Jones and Manning (1994), and the ranges for V/(V+Ni) are taken from Hatch and Leventhal (1992). Red dashed line indicates the divisions between the different paleoredox environments.

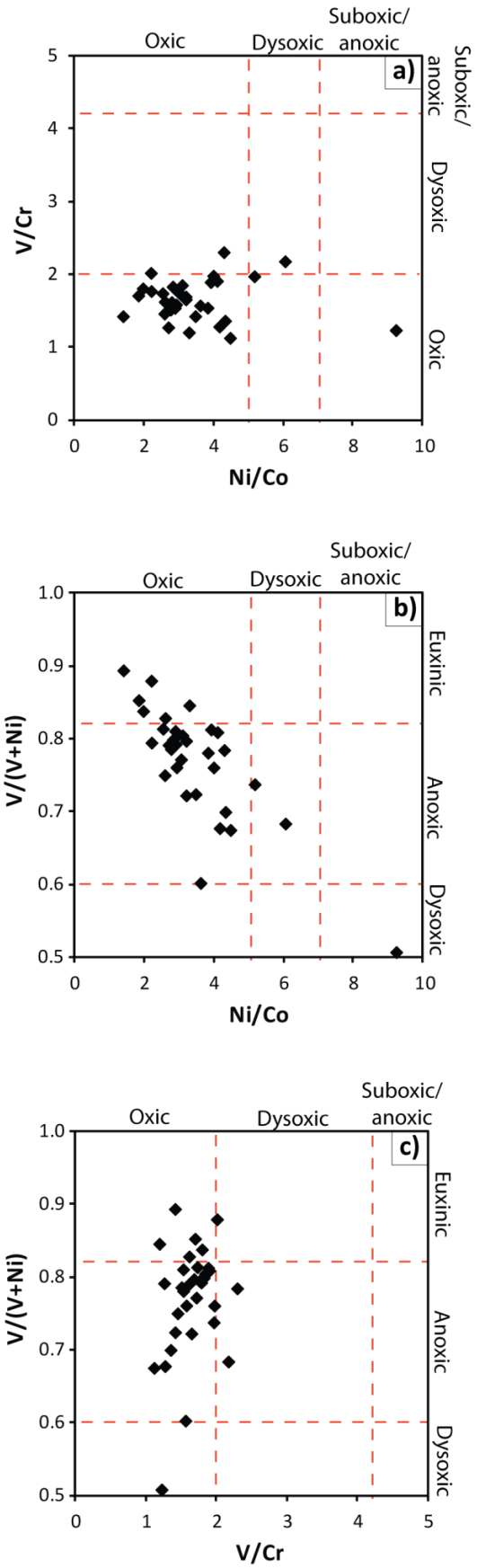

Figure 4.6: Crossplots illustrating the relationships between the trace element ratios used as redox proxies: a) V/Cr vs. Ni/Co; b) V/(V+Ni) vs. Ni/Co; and c) V/(V+Ni) vs. V/Cr. Ranges for Ni/Co and V/Cr are taken from Jones and Manning (1994), and those for V/(V+Ni) are from Hatch and Leventhal (1992). Red dashed line shows the division between the paleoredox conditions.

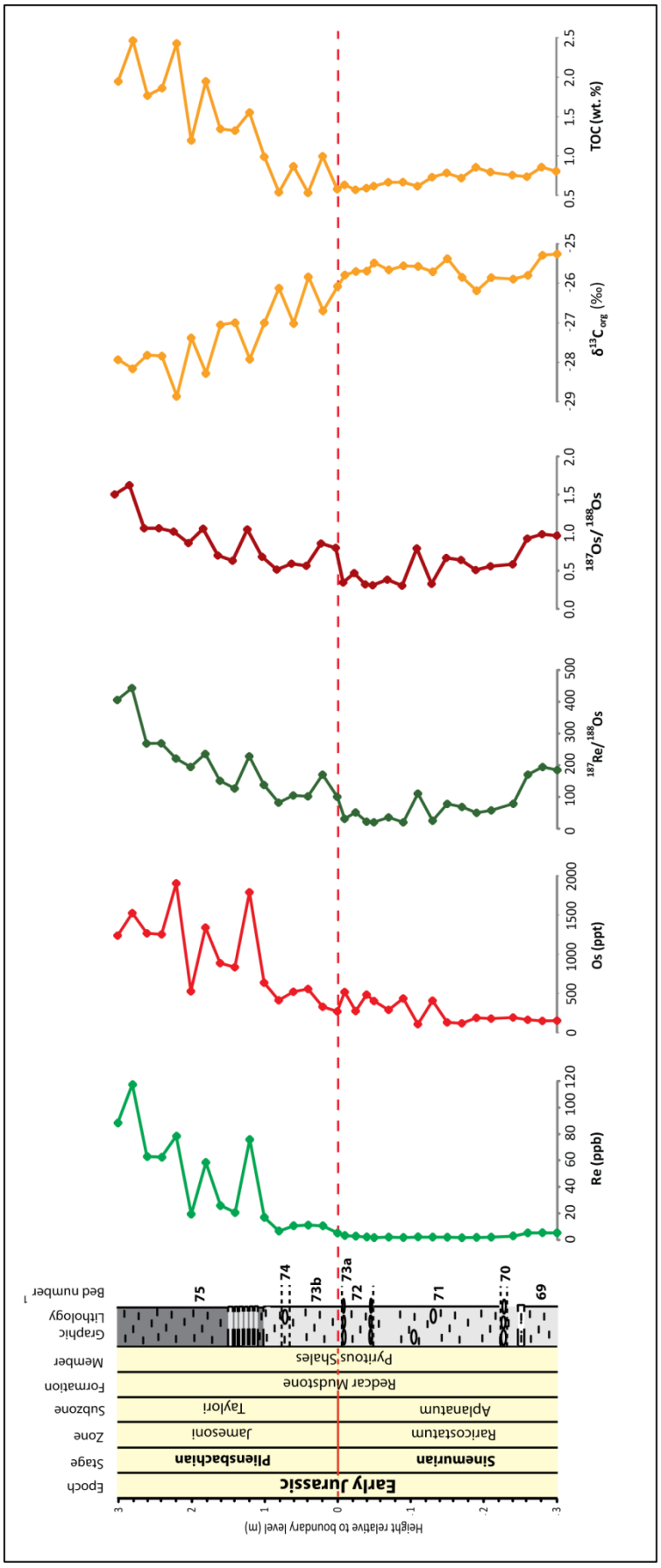

Figure 4.7: Re and Os abundance, $^{187}Re/^{188}Os$, present-day $^{187}Os/^{188}Os$, and TOC profiles for the Robin Hood's Bay sediments, presented against a corresponding stratigraphic column and graphic log. Red dashed line indicates the position of the Sinemurian-Pliensbachian boundary. [1] Bed numbers are from Hesselbo and Jenkyns (1995).

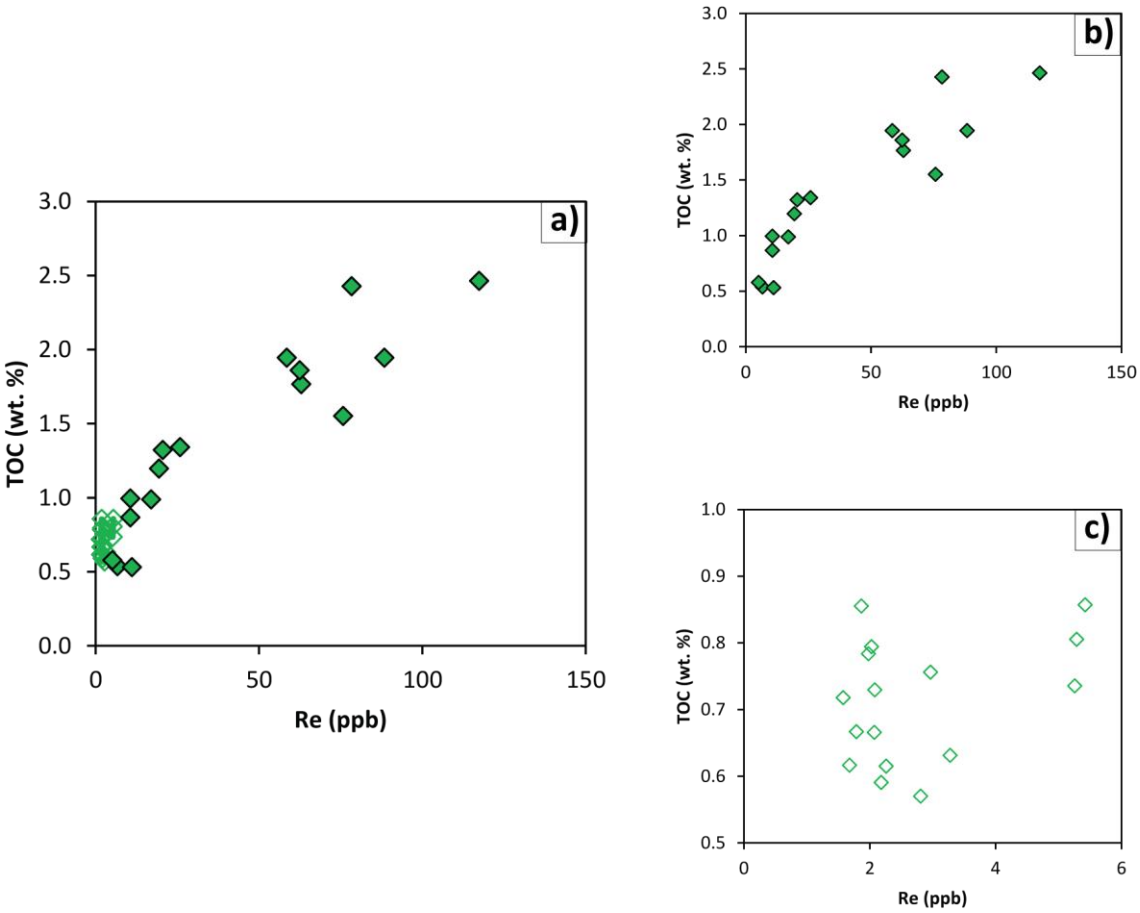

Figure 4.8: Plots showing the relationship between Re vs. TOC for: a) the whole Robin Hood's Bay section being studied; b) above the Sinemurian-Pliensbachian boundary (solid diamonds); and c) below the boundary (hollow diamonds).

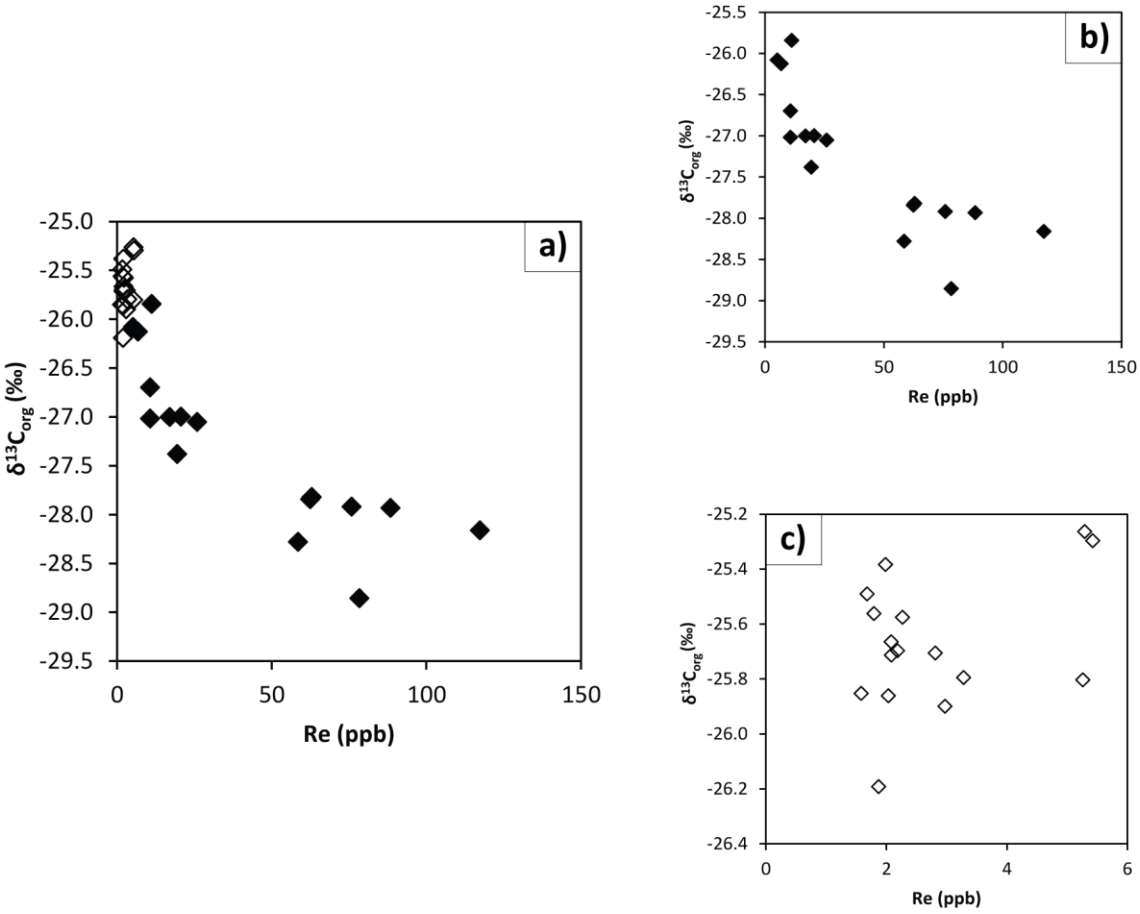

Figure 4.9: Plots showing the relationship between Re vs. $\delta^{13}C_{org}$ for: a) the whole Robin Hood's Bay section being studied; b) above the Sinemurian-Pliensbachian boundary (solid diamonds); and c) below the boundary (hollow diamonds).

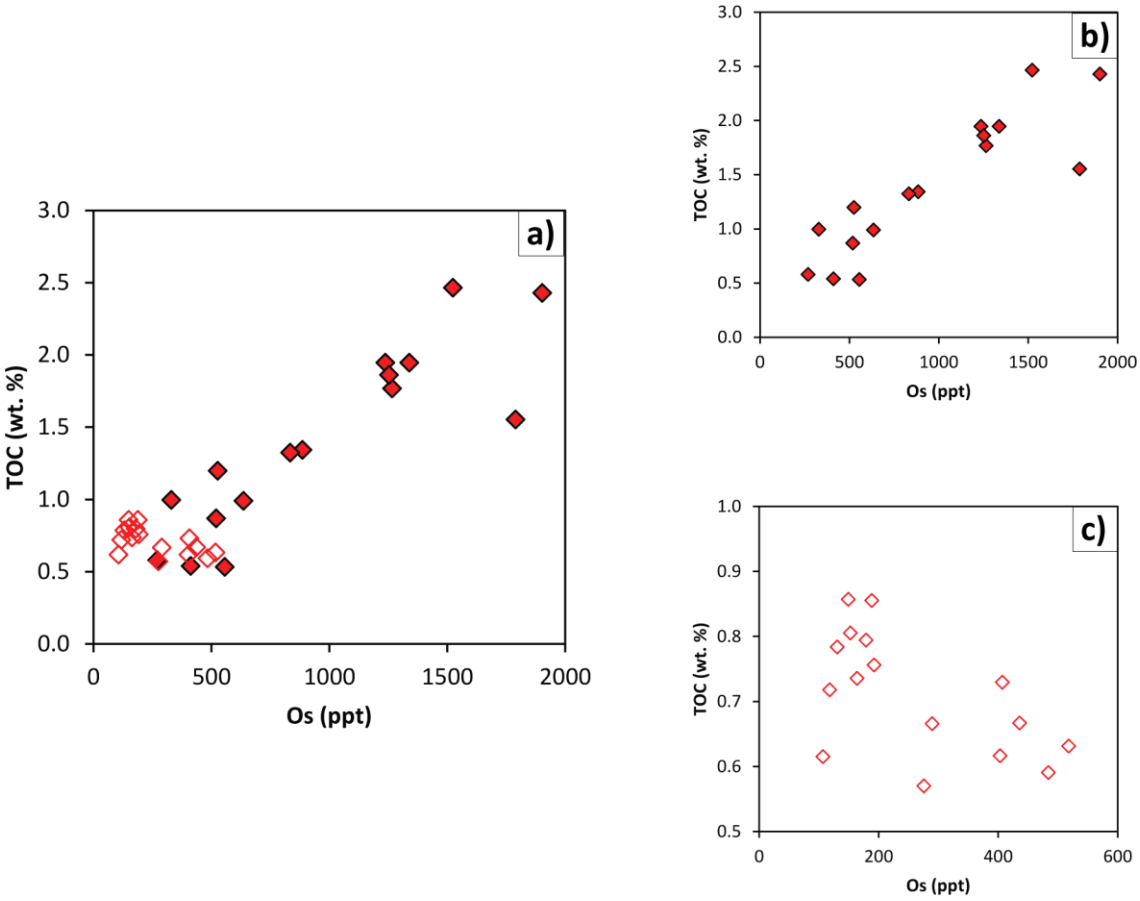

Figure 4.10: Plots showing the relationship between Os vs. TOC for: a) the whole Robin Hood's Bay section being studied; b) above the Sinemurian-Pliensbachian boundary (solid diamonds); and c) below the boundary (hollow diamonds).

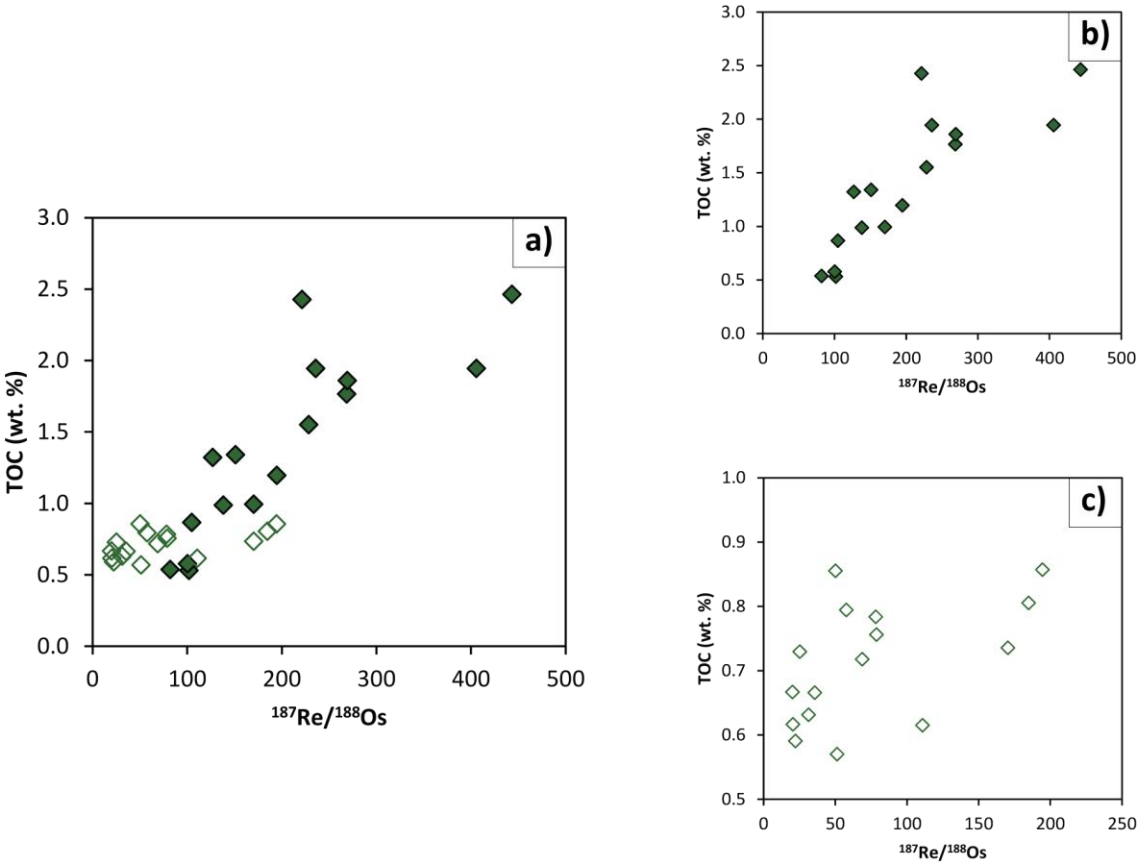

Figure 4.11: Plots showing the relationship between $^{187}Re/^{188}Os$ vs. TOC for: a) the whole Robin Hood's Bay section being studied; b) above the Sinemurian-Pliensbachian boundary (solid diamonds); and c) below the boundary (hollow diamonds).

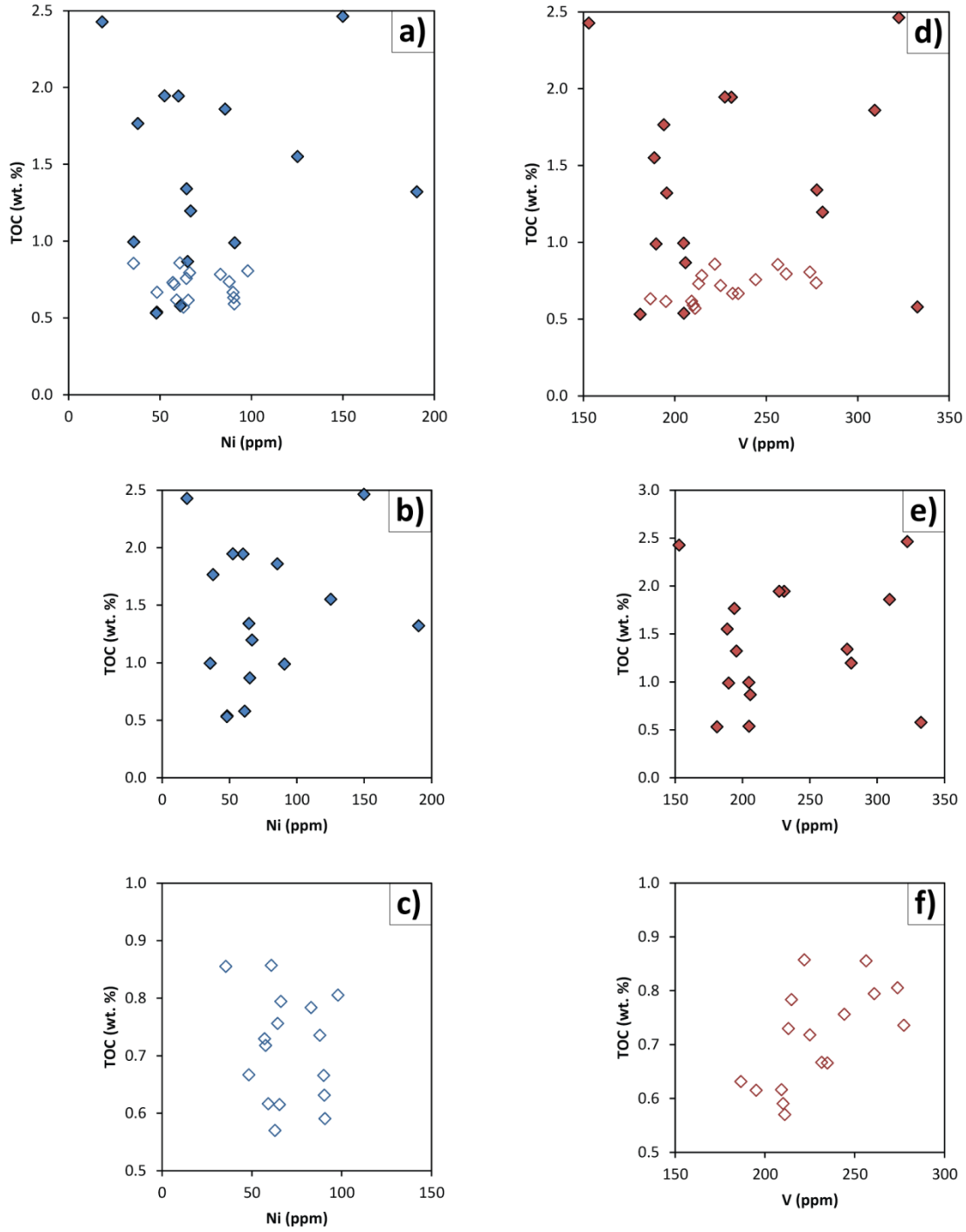

Figure 4.12: Plots showing the relationships between Ni vs. TOC (a – c; blue) and V vs. TOC (d – f; red). Boxes b) and e) show these relationships above the Sinemurian-Pliensbachian boundary (solid diamonds), and boxes c) and f) indicate these relationships below the boundary (hollow diamonds).

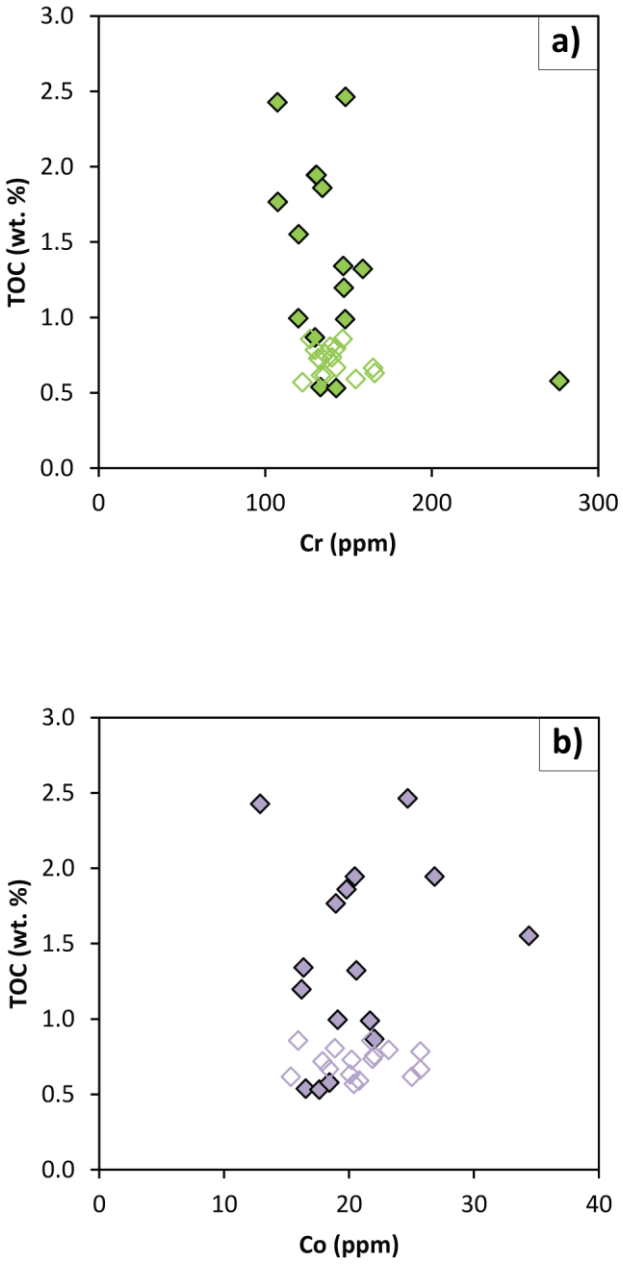

Figure 4.13: Plots showing the relationship between: a) Cr vs. TOC (green); and b) Co vs. TOC (purple). Solid diamonds indicate samples that lie above the Sinemurian-Pliensbachian boundary, and hollow diamonds represent those that lie below the boundary.

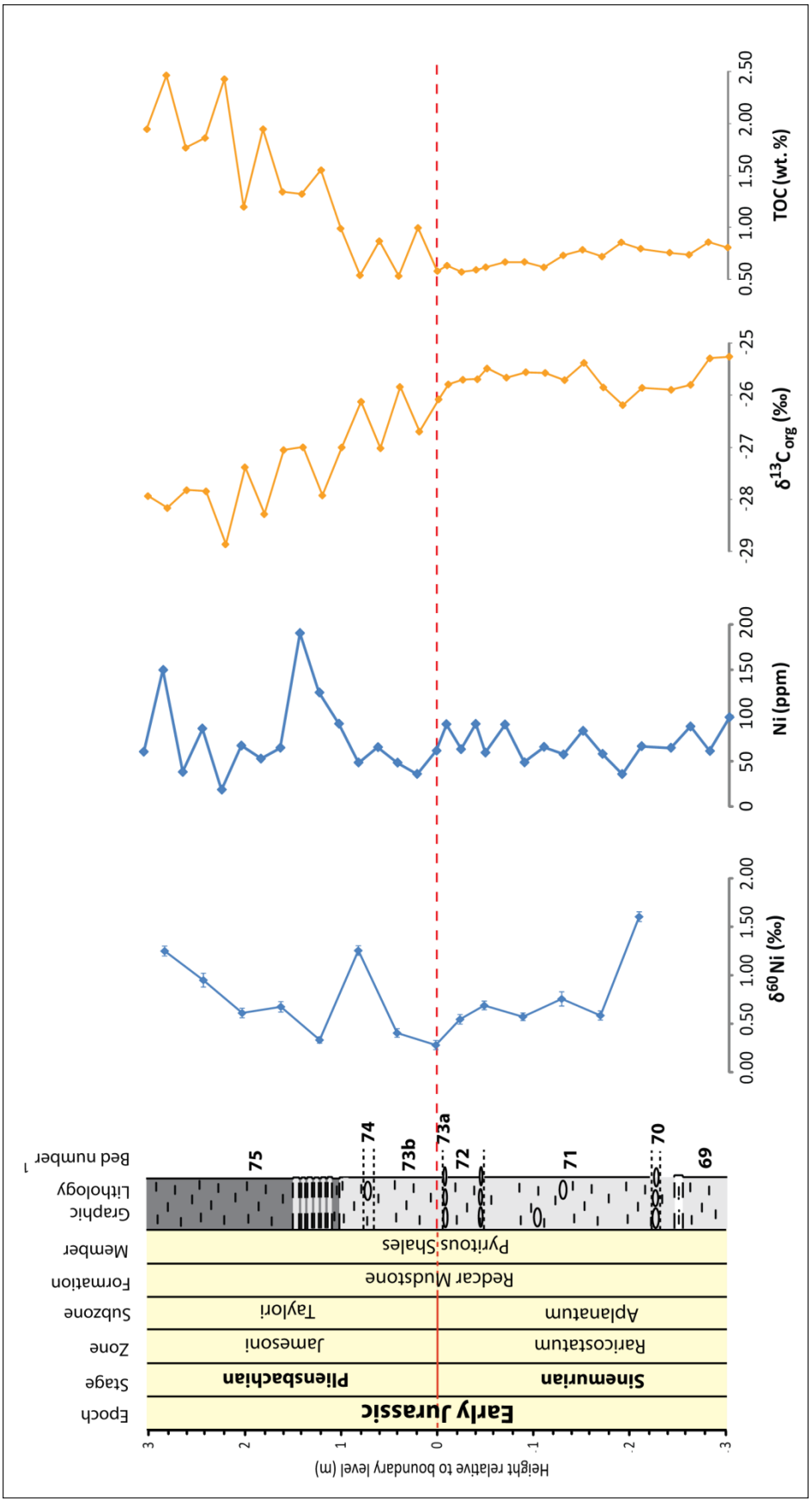

Figure 4.14: δ^{60}Ni, Ni, $\delta^{13}C_{org}$ and TOC profiles for the Robin Hood's Bay sediments, presented against a corresponding stratigraphic column and graphic log. Red dashed line indicates the position of the Sinemurian-Pliensbachian boundary. [1] Bed numbers are from Hesselbo and Jenkyns (1995).

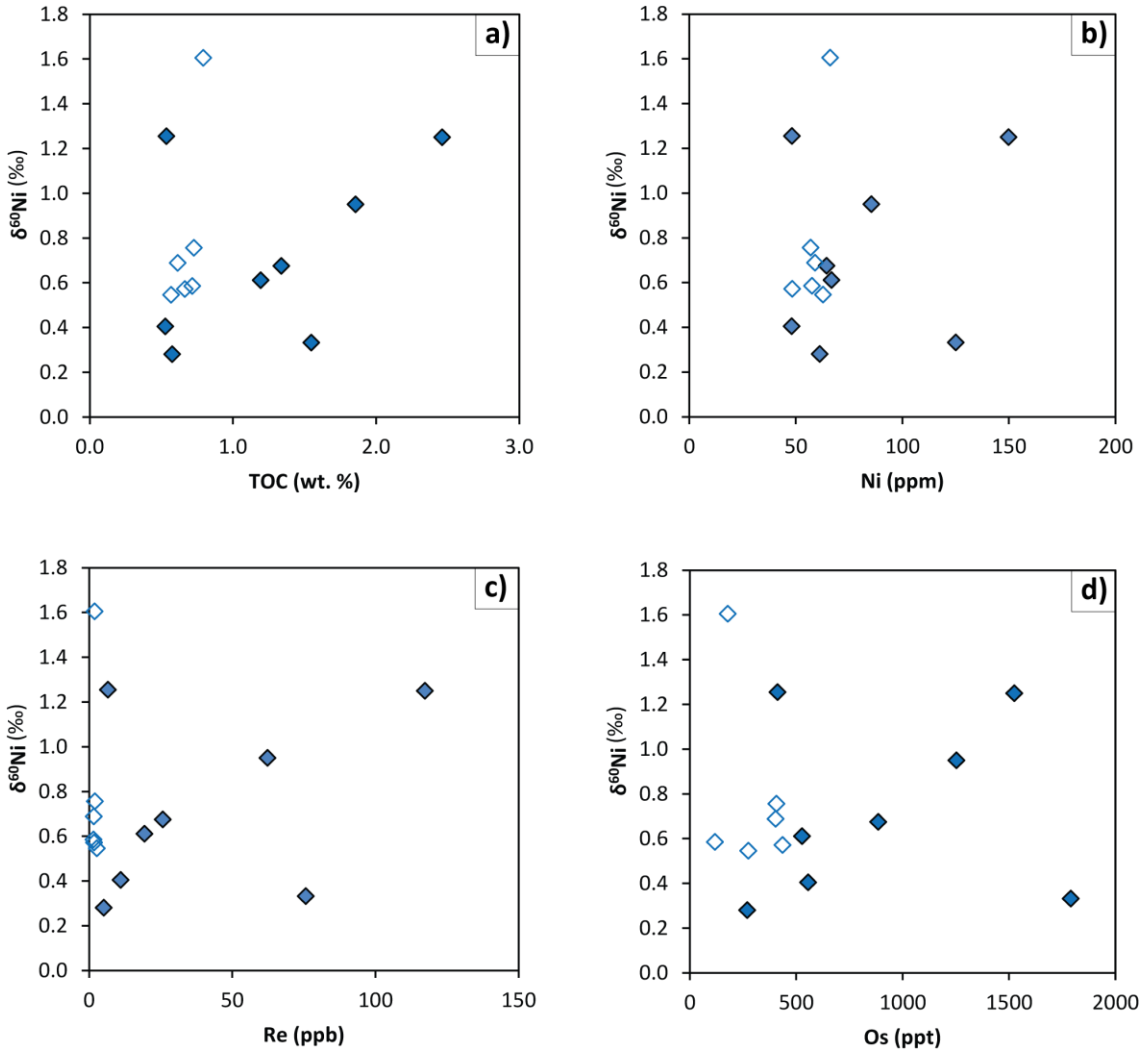

Figure 4.15: Plots showing the relationships between δ^{60}Ni and: a) TOC; b) Ni; c) Re; and d) Os. Hollow diamonds represent samples that lie below the Sinemurian-Pliensbachian boundary, and solid diamonds indicate those that lie above the boundary.

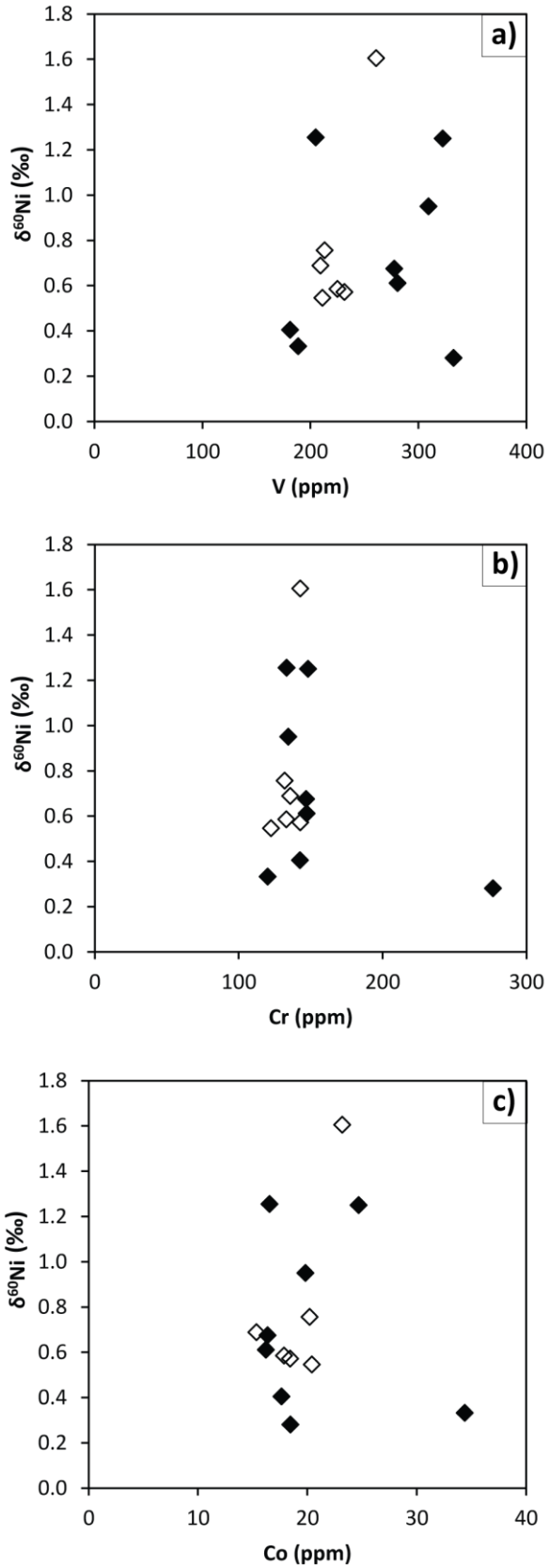

Figure 4.16: Crossplots showing the relationships between: a) δ^{60}Ni vs. V; b) δ^{60}Ni vs. Cr; and c) δ^{60}Ni vs. Co. Solid diamonds indicate samples above the Sinemurian-Pliensbachian boundary, and hollow diamonds represent samples that lie below the boundary.

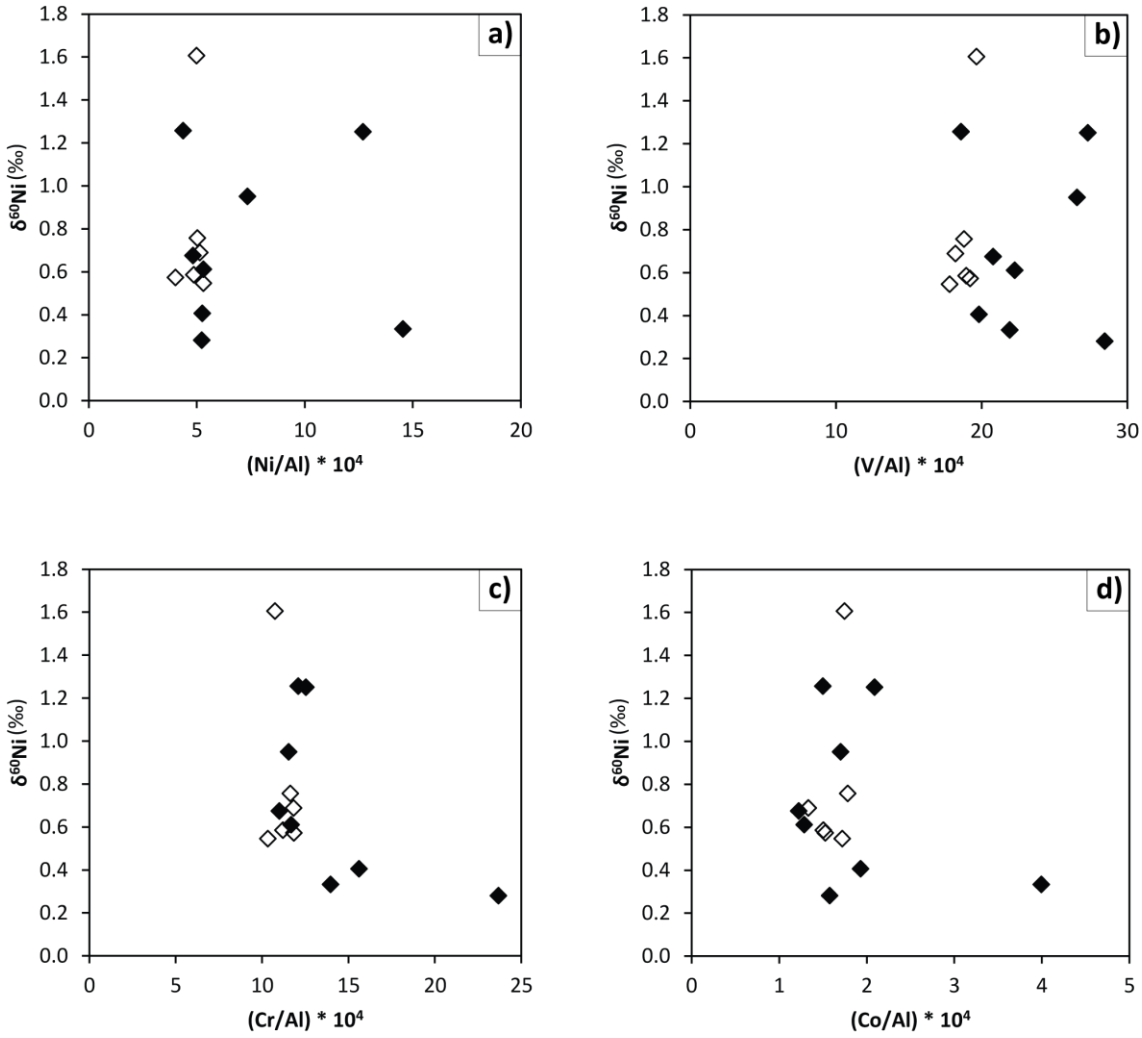

Figure 4.17: Plots showing the relationships between δ^{60}Ni and Al-normalised trace element values: a) Ni/Al; b) V/Al ; c) Cr/Al; and d) Co/Al. Hollow diamonds represent samples that lie below the Sinemurian-Pliensbachian boundary, and solid diamonds indicate those that lie above the boundary.

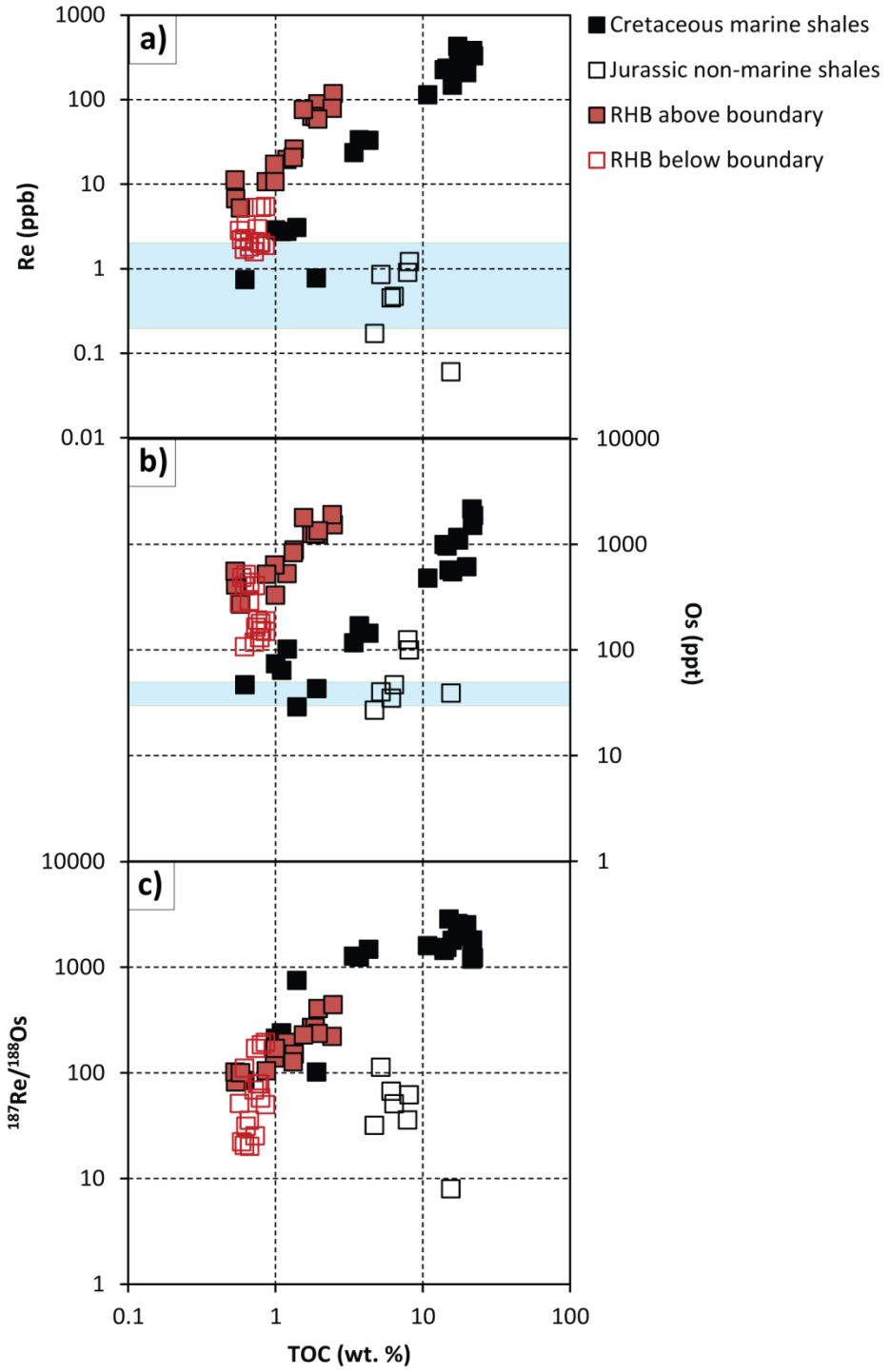

Figure 4.18: Logarithmic plot of TOC vs. a) Re; b) Os; and c) $^{187}Re/^{188}Os$. Data for Cretaceous marine shales (solid black squares) and Jurassic non-marine shales (hollow black squares) has been plotted from Baioumy *et al.* (2011). Blue boxes represent average continental crustal values for Re and Os (eg. Esser and Turekian, 1993; Peucker-Ehrenbrink and Jahn, 2001). Abbreviation "RHB" refers to Robin Hood's Bay data for above and below the Sinemurian-Pliensbachian boundary (this study).

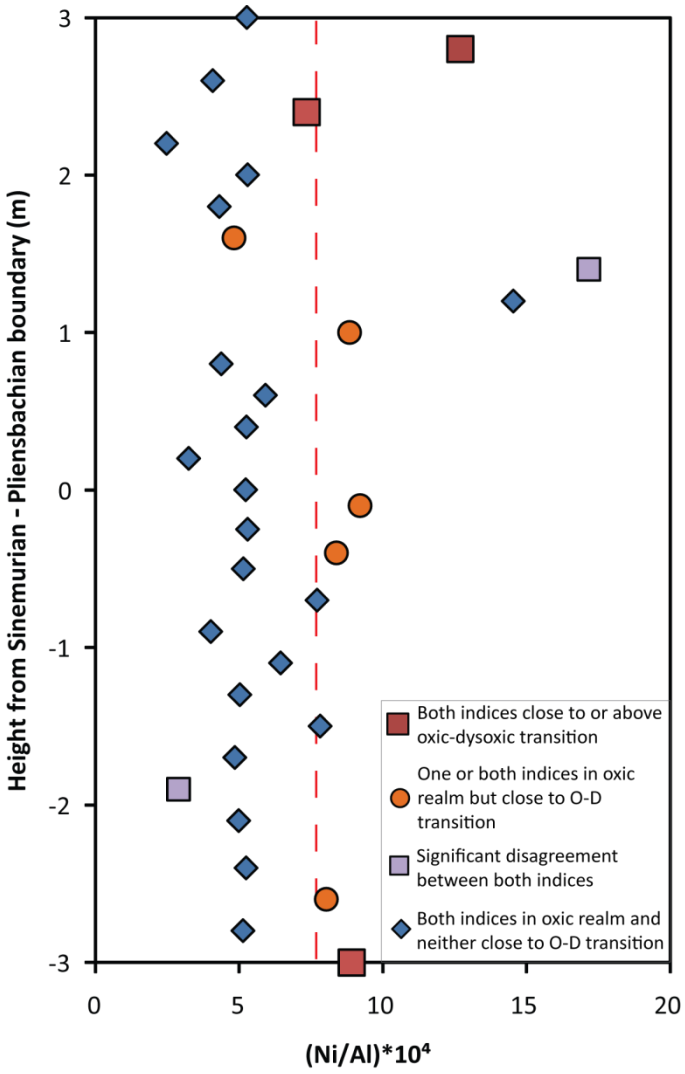

Figure 4.19: Nickel enrichment profile for the Robin Hood's Bay section relative to the Sinemurian-Pliensbachian boundary, showing the relationship between paleoredox conditions of the individual samples and enrichment. Red dashed line indicates the aluminium-normalised Ni value, $(Ni/Al)*10^4$, for average shale of ~7.7. Abbreviation "O-D" refers to oxic-dysoxic.

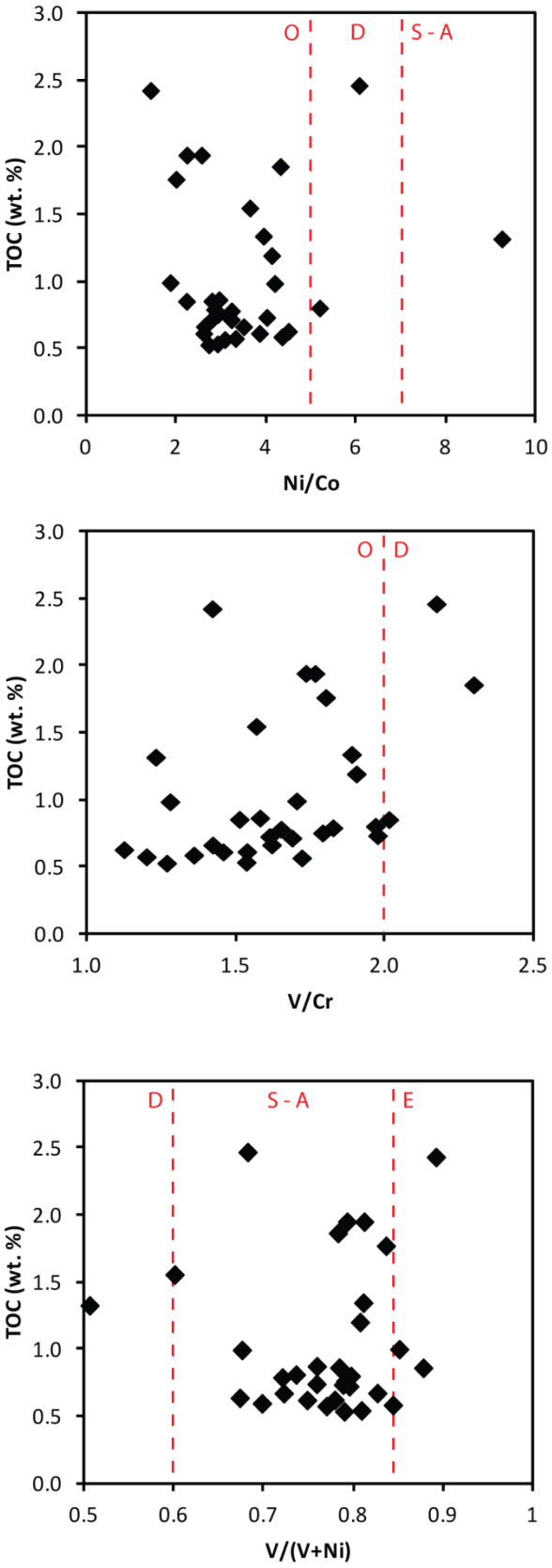

Figure 4.20: Crossplots showing the relationships between the paleoredox proxies and TOC: a) Ni/Co vs. TOC; b) V/Cr vs. TOC; and c) V/(V+Ni) vs. TOC. Red dashed lines indicate the values at which the paleoredox conditions change (Hatch and Leventhal, 1992; Jones and Manning, 1994). Abbreviations in red reflect each paleoredox environment: O, oxic; D, dysoxic; S – A, suboxic-anoxic; and E, euxinic.

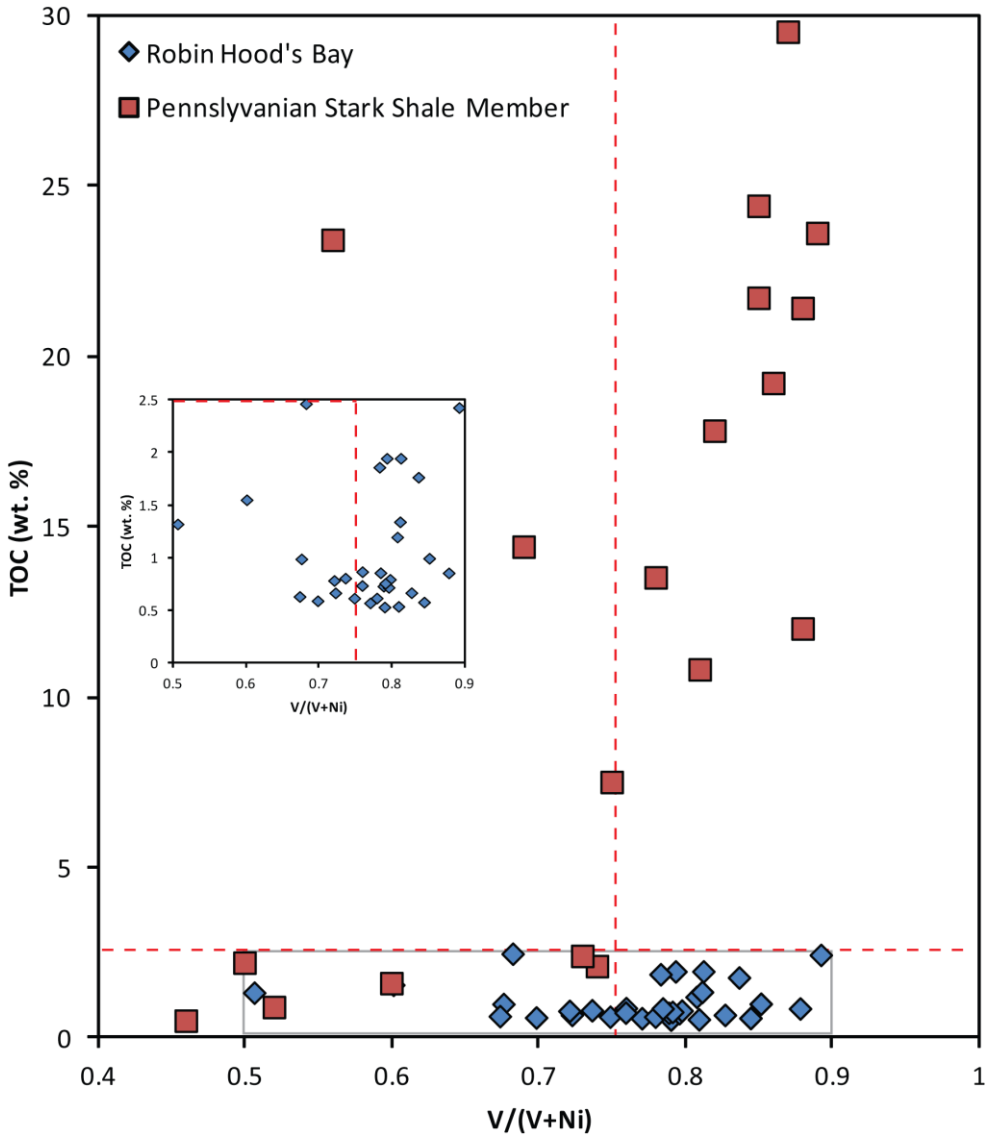

Figure 4.21: Plot showing the relationship between TOC and V/(V+Ni) for the Pennsylvanian Stark Shale Member samples (red squares) detailed in Hatch and Leventhal (1992) and for the Robin Hood's Bay sediments (blue diamonds; inset; this study). Grey box on main plot marks the extent of the inset plot. Red dashed lines mark parameters discussed in Hatch and Leventhal (1992), whereby values of > 2.5 wt. % TOC correspond to V/(V+Ni) values > 0.75 for the Pennsylvanian Stark Shale Member (see text for discussion).

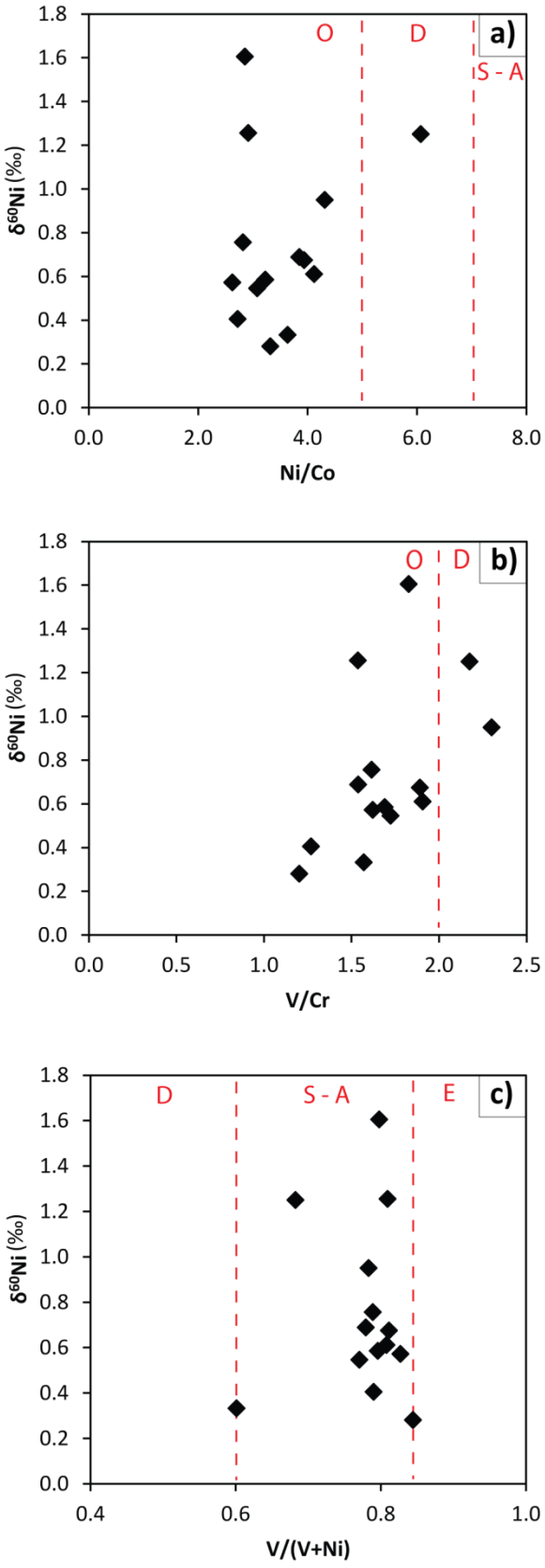

Figure 4.22: Crossplots showing the relationships between the paleoredox proxies and δ^{60}Ni: a) Ni/Co vs. δ^{60}Ni; b) V/Cr vs. δ^{60}Ni; and c) V/(V+Ni) vs. δ^{60}Ni. Red dashed lines indicate the values at which the paleoredox conditions change (Hatch and Leventhal, 1992; Jones and Manning, 1994). Abbreviations in red reflect each paleoredox environment: O, oxic; D, dysoxic; S – A, suboxic-anoxic; and E, euxinic.

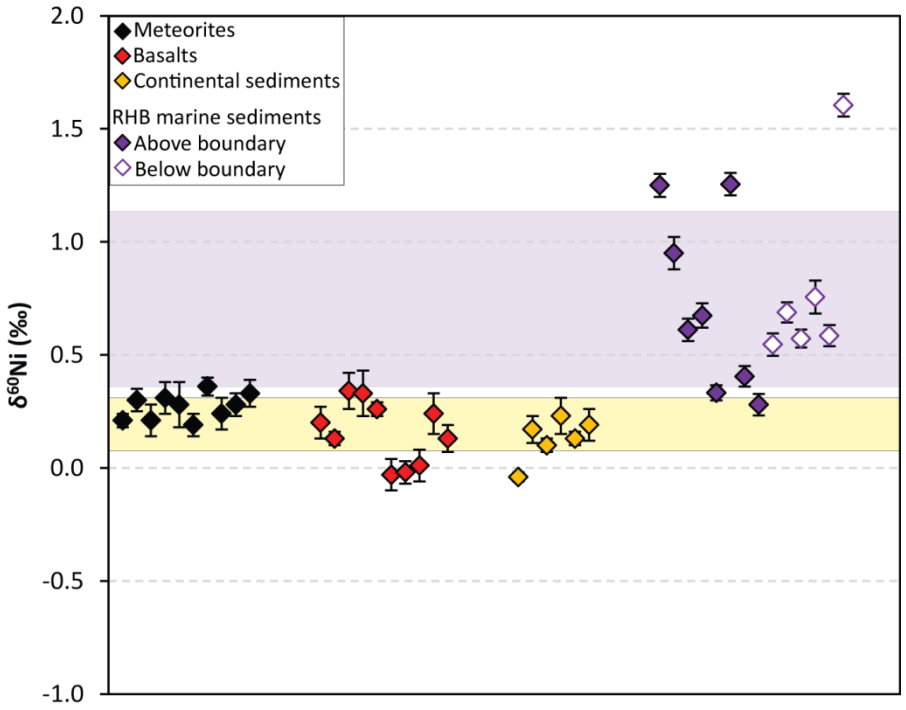

Figure 4.23: Nickel stable isotope data for extraterrestrial (meteorites), abiotic terrestrial (basalts and continental sediments) and marine organic-rich sediments. Continental sediments include river and aeolian sediments. The yellow box represents the average of the Ni isotope data for the meteorites, basalts and continental sediments (0.2 ‰ and 1 standard deviation either side of this; Cameron *et al.,* 2009). The purple box indicates the average of the Ni isotope data for the Robin Hood's Bay marine sediments (0.8 ‰ and 1 standard deviation either side of this; this study). Data for the extraterrestrial and abiotic terrestrial samples taken from Cameron *et al.* (2009). Abbreviation 'RHB' refers to Robin Hood's Bay (this study).

Table 4.1: Re-Os data for the Sinemurian-Pliensbachian boundary, Robin Hood's Bay, UK.

Sample	Distance from S-P boundary (m)	Bed number	Re (ppb)	Os (ppt)	^{192}Os (ppt)	$^{187}Re/^{188}Os$	$^{187}Os/^{188}Os$	Rho [a]	$^{187}Os/^{188}Os_{(i)}$ [b]
SP37-09	3.0	75	88.40 ± 0.39	1237.56 ± 8.93	433.22	405.93 ± 3.96	1.502 ± 0.0184	0.630	0.22
SP36-09	2.8	75	117.36 ± 0.52	1524.48 ± 11.26	526.64	443.32 ± 4.32	1.623 ± 0.0199	0.630	0.22
SP35-09	2.6	75	62.97 ± 0.28	1266.69 ± 8.25	466.35	268.63 ± 2.62	1.058 ± 0.0130	0.629	0.21
SP34-09	2.4	75	62.45 ± 0.28	1253.15 ± 8.16	461.36	269.28 ± 2.63	1.058 ± 0.0130	0.629	0.20
SP33-09	2.2	75	78.38 ± 0.35	1903.42 ± 12.26	704.34	221.37 ± 2.16	1.014 ± 0.0125	0.630	0.31
SP32-09	2.0	75	19.44 ± 0.09	527.43 ± 3.24	198.66	194.69 ± 1.90	0.864 ± 0.0106	0.630	0.25
SP31-09	1.8	75	58.51 ± 0.26	1339.44 ± 8.71	493.48	235.86 ± 2.30	1.052 ± 0.0129	0.629	0.30
SP30-09	1.6	75	25.86 ± 0.12	885.97 ± 5.15	340.30	151.16 ± 1.47	0.701 ± 0.0086	0.628	0.22
SP29-09	1.4	75	20.62 ± 0.09	833.96 ± 4.73	323.00	127.03 ± 1.24	0.633 ± 0.0078	0.629	0.23
SP28-09	1.2	75	75.81 ± 0.34	1790.13 ± 11.60	660.20	228.44 ± 2.23	1.043 ± 0.0128	0.628	0.32
SP27-09	1.0	75	17.02 ± 0.08	636.65 ± 3.68	245.05	138.20 ± 1.35	0.684 ± 0.0084	0.629	0.25
SP26-09	0.8	75	6.71 ± 0.03	412.56 ± 2.23	162.12	82.29 ± 0.81	0.515 ± 0.0063	0.628	0.25
SP25-09	0.6	73b	10.69 ± 0.05	520.99 ± 2.91	202.77	104.85 ± 1.02	0.593 ± 0.0073	0.629	0.26
SP24-09	0.4	73b	11.15 ± 0.05	556.50 ± 3.07	217.32	102.05 ± 1.00	0.566 ± 0.0070	0.629	0.24
SP23-09	0.2	73b	10.65 ± 0.05	329.82 ± 2.03	124.31	170.51 ± 1.67	0.858 ± 0.0106	0.631	0.32
SP22-09	0.0	S-P boundary	5.19 ± 0.02	270.47 ± 1.64	102.65	100.56 ± 0.99	0.801 ± 0.0099	0.629	0.48
SP38-09	-0.1	72	3.28 ± 0.04	518.25 ± 2.57	208.02	31.38 ± 0.44	0.346 ± 0.0043	0.436	0.25
SP21-09	-0.3	72	2.81 ± 0.01	275.83 ± 1.46	109.00	51.30 ± 0.52	0.470 ± 0.0058	0.616	0.31
SP39-09	-0.4	72	2.19 ± 0.01	484.32 ± 2.37	195.01	22.32 ± 0.23	0.321 ± 0.0040	0.606	0.25
SP20-09	-0.5	71	1.68 ± 0.01	403.24 ± 1.96	162.59	20.58 ± 0.21	0.310 ± 0.0038	0.590	0.25
SP19-09	-0.7	71	2.08 ± 0.01	289.80 ± 1.47	115.77	35.73 ± 0.37	0.384 ± 0.0047	0.605	0.27
SP18-09	-0.9	71	1.79 ± 0.01	436.18 ± 2.11	176.00	20.27 ± 0.21	0.305 ± 0.0037	0.595	0.24
SP17-09	-1.1	71	2.27 ± 0.01	107.09 ± 0.66	40.68	110.84 ± 1.17	0.794 ± 0.0101	0.629	0.44
SP16-09	-1.3	71	2.09 ± 0.01	407.07 ± 2.00	163.76	25.33 ± 0.26	0.328 ± 0.0040	0.601	0.25
SP15-09	-1.5	71	1.98 ± 0.01	130.77 ± 0.77	50.43	78.30 ± 0.82	0.669 ± 0.0084	0.615	0.42
SP14-09	-1.7	71	1.58 ± 0.01	118.28 ± 0.69	45.76	68.82 ± 0.75	0.642 ± 0.0081	0.595	0.42
SP13-09	-1.9	71	1.87 ± 0.01	188.64 ± 1.03	74.18	50.21 ± 0.52	0.509 ± 0.0063	0.603	0.35
SP12-09	-2.1	71	2.03 ± 0.01	179.00 ± 1.00	69.96	57.81 ± 0.60	0.560 ± 0.0070	0.609	0.38
SP8-09	-2.3	69	2.97 ± 0.01	192.49 ± 1.08	74.99	78.84 ± 0.80	0.585 ± 0.0073	0.622	0.33
SP9-09	-2.6	69	5.26 ± 0.02	164.12 ± 1.04	61.38	170.52 ± 1.71	0.923 ± 0.0115	0.636	0.38
SP10-09	-2.8	69	5.43 ± 0.02	149.32 ± 0.97	55.48	194.57 ± 1.95	0.980 ± 0.0122	0.638	0.36
SP11-09	-3.0	69	5.29 ± 0.02	152.90 ± 0.98	56.94	184.94 ± 1.86	0.960 ± 0.0120	0.637	0.37

Results presented to 2σ level of uncertainty.

[a] Rho is the associated error correlation (Ludwig, 1980)

[b] The initial $^{187}Os/^{188}Os$ isotope ratio calculated at 189.6 Ma

Ages calculated using the $\lambda\,^{187}Re = 1.666 \times 10^{-11}\,yr^{-1}$

Table 4.2: Summary of TOC, trace element data and the associated paleoredox ratios for the Robin Hood's Bay organic-rich sediments.

					Concentrations in ppm				Redox indices		
Sample	Distance from S-P boundary (m)	TOC (wt. %)	$\delta^{13}C$ (‰)	Re (ppb)	V	Cr	Ni	Co	V/Cr	Ni/Co	V/(V+Ni)
SP37-09	3.0	1.94	-27.93	88.4	230.9	130.6	60.11	26.87	1.77	2.24	0.79
SP36-09	2.8	2.46	-28.16	117.4	322.4	148.2	149.9	24.70	2.18	6.07	0.68
SP35-09	2.6	1.76	-27.82	63.0	194.0	107.6	37.86	18.95	1.80	2.00	0.84
SP34-09	2.4	1.86	-27.84	62.4	309.3	134.5	85.57	19.82	2.30	4.32	0.78
SP33-09	2.2	2.43	-28.86	78.4	152.9	107.5	18.43	12.88	1.42	1.43	0.89
SP32-09	2.0	1.20	-27.38	19.4	280.8	147.3	66.81	16.21	1.91	4.12	0.81
SP31-09	1.8	1.94	-28.28	58.5	227.3	130.9	52.47	20.46	1.74	2.56	0.81
SP30-09	1.6	1.34	-27.05	25.9	277.7	146.9	64.49	16.37	1.89	3.94	0.81
SP29-09	1.4	1.32	-27.00	20.6	195.6	158.7	190.5	20.61	1.23	9.24	0.51
SP28-09	1.2	1.55	-27.92	75.8	188.8	120.2	125.2	34.40	1.57	3.64	0.60
SP27-09	1.0	0.99	-27.00	17.0	189.8	148.2	90.83	21.69	1.28	4.19	0.68
SP26-09	0.8	0.54	-26.13	6.7	204.9	133.4	48.25	16.55	1.54	2.92	0.81
SP25-09	0.6	0.87	-27.02	10.7	205.8	130.1	65.09	22.05	1.58	2.95	0.76
SP24-09	0.4	0.53	-25.84	11.1	181.1	142.6	48.06	17.63	1.27	2.73	0.79
SP23-09	0.2	0.99	-26.70	10.7	204.8	120.1	35.70	19.10	1.71	1.87	0.85
SP22-09	0.0	0.58	-26.08	5.2	332.6	276.8	61.23	18.45	1.20	3.32	0.84
SP38-09	-0.1	0.63	-25.80	3.3	186.7	165.8	90.33	20.09	1.13	4.50	0.67
SP21-09	-0.3	0.57	-25.71	2.8	211.1	122.5	62.86	20.41	1.72	3.08	0.77
SP39-09	-0.4	0.59	-25.70	2.2	210.1	154.5	90.66	20.83	1.36	4.35	0.70
SP20-09	-0.5	0.62	-25.49	1.7	209.2	135.9	59.13	15.35	1.54	3.85	0.78
SP19-09	-0.7	0.67	-25.67	2.1	234.8	164.9	90.00	25.73	1.42	3.50	0.72
SP18-09	-0.9	0.67	-25.56	1.8	231.6	142.8	48.40	18.42	1.62	2.63	0.83
SP17-09	-1.1	0.61	-25.58	2.3	195.1	133.8	65.42	25.03	1.46	2.61	0.75
SP16-09	-1.3	0.73	-25.71	2.1	213.1	132.0	57.04	20.22	1.62	2.82	0.79
SP15-09	-1.5	0.78	-25.38	2.0	214.8	129.9	83.02	25.72	1.65	3.23	0.72
SP14-09	-1.7	0.72	-25.85	1.6	225.0	133.1	57.69	17.88	1.69	3.23	0.80
SP13-09	-1.9	0.86	-26.19	1.9	256.4	127.2	35.53	15.94	2.02	2.23	0.88
SP12-09	-2.1	0.79	-25.86	2.0	261.0	142.8	66.18	23.19	1.83	2.85	0.80
SP8-09	-2.3	0.76	-25.90	3.0	244.2	136.2	64.39	22.01	1.79	2.93	0.79
SP9-09	-2.6	0.74	-25.80	5.3	277.4	140.3	87.84	21.88	1.98	4.01	0.76
SP10-09	-2.8	0.86	-25.30	5.4	222.0	146.7	60.89	21.79	1.51	2.79	0.78
SP11-09	-3.0	0.81	-25.26	5.3	273.9	139.0	97.97	18.88	1.97	5.19	0.74

Table 4.3: Summary of aluminium-normalised trace element values and enrichment factors relative to average shale.

		Robin Hood's Bay organic-rich sediments					Enrichment factors relative to average shale			
Sample ID[a]	Distance from S-P boundary (m)	Al (ppm)	(Ni/Al)*10^4	(V/Al)*10^4	(Cr/Al)*10^4	(Co/Al)*10^4	Ni	V	Cr	Co
SP37-09	3.0	114166	5.26	20.23	11.44	2.35	0.68	1.38	1.12	1.12
SP36-09	2.8	118134	12.69	27.29	12.55	2.09	1.65	1.86	1.23	1.00
SP35-09	2.6	92550	4.09	20.96	11.62	2.05	0.53	1.43	1.14	0.98
SP34-09	2.4	116504	7.35	26.55	11.54	1.70	0.95	1.81	1.13	0.81
SP33-09	2.2	74376	2.48	20.56	14.46	1.73	0.32	1.40	1.42	0.82
SP32-09	2.0	126020	5.30	22.28	11.69	1.29	0.69	1.52	1.15	0.61
SP31-09	1.8	121564	4.32	18.70	10.77	1.68	0.56	1.27	1.06	0.80
SP30-09	1.6	133544	4.83	20.79	11.00	1.23	0.63	1.41	1.08	0.58
SP29-09	1.4	110858	17.18	17.64	14.31	1.86	2.23	1.20	1.40	0.89
SP28-09	1.2	86096	14.54	21.93	13.97	4.00	1.89	1.49	1.37	1.90
SP27-09	1.0	102580	8.85	18.50	14.45	2.11	1.15	1.26	1.42	1.01
SP26-09	0.8	110297	4.37	18.58	12.09	1.50	0.57	1.26	1.19	0.71
SP25-09	0.6	110011	5.92	18.71	11.82	2.00	0.77	1.27	1.16	0.95
SP24-09	0.4	91358	5.26	19.82	15.61	1.93	0.68	1.35	1.53	0.92
SP23-09	0.2	109950	3.25	18.63	10.92	1.74	0.42	1.27	1.07	0.83
SP22-09	0.0	116924	5.24	28.44	23.68	1.58	0.68	1.94	2.32	0.75
SP38-09	-0.1	98097	9.21	19.03	16.90	2.05	1.20	1.29	1.66	0.98
SP21-09	-0.3	118511	5.30	17.81	10.34	1.72	0.69	1.21	1.01	0.82
SP39-09	-0.4	108058	8.39	19.45	14.29	1.93	1.09	1.32	1.40	0.92
SP20-09	-0.5	114951	5.14	18.20	11.83	1.34	0.67	1.24	1.16	0.64
SP19-09	-0.7	116729	7.71	20.11	14.13	2.20	1.00	1.37	1.39	1.05
SP18-09	-0.9	120593	4.01	19.20	11.84	1.53	0.52	1.31	1.16	0.73
SP17-09	-1.1	101589	6.44	19.21	13.17	2.46	0.84	1.31	1.29	1.17
SP16-09	-1.3	113362	5.03	18.80	11.64	1.78	0.65	1.28	1.14	0.85
SP15-09	-1.5	106113	7.82	20.24	12.24	2.42	1.02	1.38	1.20	1.15
SP14-09	-1.7	118710	4.86	18.95	11.21	1.51	0.63	1.29	1.10	0.72
SP13-09	-1.9	122838	2.89	20.87	10.35	1.30	0.38	1.42	1.02	0.62
SP12-09	-2.1	132762	4.98	19.66	10.75	1.75	0.65	1.34	1.05	0.83
SP8-09	-2.3	122632	5.25	19.91	11.11	1.79	0.68	1.35	1.09	0.85
SP9-09	-2.6	109331	8.03	25.37	12.83	2.00	1.04	1.73	1.26	0.95
SP10-09	-2.8	118565	5.14	18.72	12.37	1.84	0.67	1.27	1.21	0.88
SP11-09	-3.0	109949	8.91	24.91	12.64	1.72	1.16	1.69	1.24	0.82

Table 4.4: Average enrichment factors (EF) for selected trace elements in the Robin Hood's Bay organic-rich sediments.

Element	Average shale [a, b]	Average black shale [c, d]	Robin Hood's Bay (n =32)[e]
Co (ppm)	19	10	20.54
(Co/Al) * 10^4	2.1	1.4	1.8
EF		0.7	0.9
Cr (ppm)	90	100	141
(Cr/Al) * 10^4	10.2	14.3	12.7
EF		1.4	1.2
Ni (ppm)	68	50	71.9
(Ni/Al) * 10^4	7.7	7.1	6.5
EF		0.9	0.8
V (ppm)	130	150	230.1
(V/Al) * 10^4	14.7	21.4	20.7
EF		1.5	1.4

Mean Al content for Robin Hood's Bay shales: 11.13 wt. %

[a] Average shale data from Wedepohl (1971)

[b] Mean Al content for average shale: 8.84 wt. % (Wedepohl, 1971)

[c] Mean Al content for average black shale: 7.00 wt. % (Vine and Tourtelot, 1970)

[d] Average black shale data from Vine and Tourtelot (1970)

[e] RHB enrichment factors calculated using average shale data

Table 4.5: Previously established values for the trace element ratios and their corresponding depositional paleoredox conditions.

	Oxic	Dysoxic	Suboxic-anoxic	Euxinic
V/Cr [a]	<2.00	2.00-4.25	>4.25	
Ni/Co [a]	<5.00	5.00-7.00	>7.00	
V/(V+Ni) [b]		0.46-0.60	0.54-0.82	>0.84

[a] Jones and Manning (1994)

[b] Hatch and Leventhal (1992); Schovsbo (2001)

Table 4.6: Nickel stable isotope data for the Sinemurian-Pliensbachian boundary

Height up section (m)	Distance from S-P boundary (m)	Sample ID	δ^{60}Ni (‰)		2σ	Ni (ppm)
7.1	2.8	SP36-09	1.25	±	0.05	149.92
6.7	2.4	SP34-09	0.95	±	0.07	85.57
6.3	2	SP32-09	0.61	±	0.05	66.81
5.9	1.6	SP30-09	0.67	±	0.05	64.49
5.5	1.2	SP28-09	0.33	±	0.03	125.18
5.1	0.8	SP26-09	1.26	±	0.05	48.25
4.7	0.4	SP24-09	0.40	±	0.05	48.06
4.3	0	SP22-09	0.28	±	0.05	61.23
4.05	-0.25	SP21-09	0.55	±	0.05	62.86
3.8	-0.5	SP20-09	0.69	±	0.04	59.13
3.4	-0.9	SP18-09	0.57	±	0.04	48.40
3	-1.3	SP16-09	0.76	±	0.07	57.04
2.6	-1.7	SP14-09	0.58	±	0.05	57.69
2.2	-2.1	SP12-09	1.60	±	0.05	66.18

All Ni isotope ratios expressed as per mil (‰) deviation from NIST 986 SRM isotopic Standard.

5 *Effects of thermal maturation on the Ni isotope composition of source rocks: Implications for oil-source correlation*

5.1 Introduction

The correlation of an oil to its source using geochemical techniques provides valuable data that can be used to significantly improve our understanding of subsurface petroleum systems. Determining how oil moves from its source rock to the reservoir has the potential to provide insight into oil migration pathways, basin, reservoir and trap structure, and also the ability to highlight possible new oils plays (eg. Curiale, 2008). As such, oil to source fingerprinting is an exceptionally valuable tool in petroleum exploration.

Correlation of oils to known sources also has important environmental applications. Oil spills have become a global problem, and studies have focused on oil tracing in order to settle questions regarding environmental impact and damage assessment, and legal liability (eg. Zafiriou *et al.,* 1973; Wang *et al.,* 1999). Further, changes in the chemical composition of spilled oil have a profound effect on the oil's toxicity and in turn the biological impact over time (Wang *et al.,* 1999). Therefore, being able to unambiguously trace spilled oils and petroleum products back to their original sources is essential (Wang *et al.,* 1999).

Oil to source rock correlation relies on utilising and identifying genetic parameters that are internally consistent between an oil and its source rock (Curiale, 2008). For such parameters to be useful they should be relatively insensitive to the effects of biodegradation and differences in thermal maturity levels (eg. Curiale, 2008). Geochemical parameters have been the most widely used since correlation studies began (eg. Hunt *et al.,* 1954; Welte, 1966; Williams, 1974; Dow, 1974; Alexander *et al.,* 1981; Scotchman *et al.,* 1998), as the molecular and isotopic compositions of both sample types (oil and source rock) can be measured. Traditional geochemical analyses for correlation studies focused on utilising sterane carbon number distributions and stable carbon isotope compositions (eg. Williams, 1974; Stahl, 1978; Alexander *et al.,* 1981), and gas chromatography (eg. Welte, 1966; Alexander *et al.,* 1981;

Onyema and Manilla, 2010). The use of biomarkers, ubiquitous to source rocks and oils (Moldowan *et al.,* 1992; Peters and Moldowan, 1993), has also been essential (eg. Chen *et al.,* 1996; Killops *et al.,*1997). More recently, in the quest for stable parameters that remain constant between oils and their source rocks, oil-source fingerprinting work has begun to focus on the development and application of novel isotope techniques. This has been demonstrated recently using the Re-Os isotope system (Finlay *et al.,* 2011) following pioneering work examining Re-Os geochronology of hydrocarbon deposits (Selby and Creaser, 2005; Selby *et al.,* 2005) and the Re and Os composition of oils (Selby *et al.,* 2007).

This study aims to continue to explore the potential of using novel isotope techniques by evaluating the application of the Ni stable isotope system to oil-source correlation studies. Whilst it has been demonstrated that Ni distribution has the potential to significantly improve our understanding of the genetic relationships between source rocks and oils (eg. Lewan and Maynard, 1982; Lewan, 1984; Ellrich *et al.,* 1985; Manning *et al.,* 1991; Alberdi and Lafargue, 1993; Lopez *et al.,* 1995), only one study currently exists that explores this relationship using Ni isotopes (Dewaker *et al.,* 2000). By analysing kerogens and bitumens from three geologically and geographically distinct basins, it is suggested that Ni isotope variation is basin-specific and dependent upon kerogen-type and the nature of the organic matter (Dewaker *et al.*, 2000). On a preliminary level, this suggests that Ni isotopes may be a useful oil-source correlation tool.

However, although Dewaker *et al.* (2000) present a pioneering study with regard to the application of Ni isotopes in the investigation of organic-rich samples, it is clear that their analytical protocol is oversimplified. It is known that a rigorous chemical separation technique must be utilised in order to purify Ni from organic-rich samples, and to reduce the potential of significant isobaric and sample-matrix interferences during mass spectrometry (Quitté and Oberli, 2006; Cameron *et al.,* 2009; Gall *et al.,* 2012). However, Dewaker *et al.* (2000) employ a whole-rock analytical technique and provide no mention of a chromatographic separation

procedure. Similarly, no detail is given of the monitoring of isobaric interferences during mass spectrometry. In the decade following this study there have been significant advances in Ni separation and analytical procedures (Quitté and Oberli, 2006; Cameron *et al.,* 2009; Gall *et al.,* 2012), allowing us to obtain precise and reproducible Ni isotope data for samples other than those with a meteoritic origin. However, the Ni isotope composition of organic-rich sediments still remains poorly understood.

Although the Ni isotope system has widespread potential to be applied to oil-source correlation studies, the effects of post-depositional processes such as thermal maturation on Ni isotope systematics remain poorly defined. Indeed, this factor is not discussed at any level by Dewaker *et al.* (2000). It is critical that the effects of such processes are investigated before Ni isotopes can be utilised as a petroleum tracing tool. Herein we present the first study that determines whether thermal maturation of source rocks influences the behaviour of Ni isotope systematics.

Enriched concentrations of Ni have been observed in some crude oils (eg. Hodgson, 1954; Bonham, 1965; Witherspoon and Nagashima, 1957; Ball *et al.*, 1960) and asphalts (Erickson *et al.,* 1954) that are generated from organic-rich source rocks. This indicates that at least some of the Ni migrates or is transferred from the organic-rich source rock to the generated petroleum, and as such, the hydrocarbon maturation process may indeed have a significant effect on Ni isotope systematics. However, the metallo-organic bonds formed between Ni and the organic matter have high thermal stability (Constantinides *et al.,* 1959; discussed in greater detail in Chapter 3). As such, Lewan (1980) suggests that these bonds are unlikely to be affected by generation, migration and entrapment of hydrocarbons, and as such, the enrichment of Ni in the organic matter of the source rock may be reflected in its expelled oil (Lewan and Maynard, 1982). Therefore, these processes may also prove to have little effect on Ni isotope systematics.

Vanadium is held in the same strong metallo-organic complexes in crude oils and organic-rich sediments as Ni (eg. Corbett, 1967; Dwiggins *et al.,* 1969; Filby, 1975; Lewan and Maynard, 1982; Lewan, 1984). Investigating the proportionality and concentrations of these two metals in crude oils has yielded significant information regarding the transfer of metals from source to oil during the hydrocarbon maturation process (eg. Lewan, 1984; Ellrich *et al.,*1985; Lopez *et al.,* 1995). Studies have also demonstrated that the proportionality of V to Ni has the potential to provide information about genetic relationships between crude oils, as well as genesis, migration and classification of oils (eg. Hodgson, 1959; Ball *et al.*, 1960; Tissot and Welte, 1984; Ellrich *et al.,* 1985). Further, through pyrolysis experiments, Lewan (1984) reveals that although the concentrations of these two metals may change during thermal maturation of the source, their proportionality is likely to remain constant in the expelled crude oil. This may have significant implications for the Ni isotope system, depending on whether any change in Ni concentration during thermal maturation (eg. Lewan, 1984) results in preferential loss/uptake of the lighter/heavier isotopes of Ni.

Herein we show that thermal maturation of the Exshaw Formation shales did not induce significant Ni isotope fractionation. Further, the results of this investigation demonstrate that there is potential for Ni stable isotopes to be developed as an oil to source correlation tool.

5.2 The Exshaw Formation, West Canada Sedimentary Basin (WCSB)

The West Canada Sedimentary Basin (WCSB) trends approximately NW-SE between the Canadian Shield to the East and the Western Cordillera to the West (Piggott and Lines, 1992). It is a highly significant hydrocarbon reservoir, containing approximately 1.75 billion

barrels of oil reserves (Piggott and Lines, 1992). Within the WCSB lies the Exshaw Formation, a thin but laterally continuous unit (2-12 m thick; Leenheer, 1984; Creaney and Allan, 1991) that exists in all three maturation zones (Fig. 5.1), and has thus been through the oil and gas window (eg. Piggott and Lines, 1992). As such, it has been suggested to be a prolific hydrocarbon source rock (Leenheer, 1984; Creaney and Allan, 1991).

The Exshaw Formation in south-west and western Alberta comprises a lower member of organic-rich mudrocks and black shales which rest with minor disconformity upon Upper Devonian carbonate strata (Richards *et al.,* 1999), and are abruptly to gradationally overlain by bioturbated shelf siltstones (eg. Macauley *et al.,* 1964; Macqueen and Sandberg, 1970; Richards *et al.,* 1991; Caplan and Bustin, 1999; Creaser *et al.,* 2002). The depositional interval of the lower black shale unit is well constrained biostratigraphically; between the *expansa* and *duplicata* zones of Late Famennian to Early Tournasian time (over a maximum time period of ~363 – 360 Ma; Caplan and Bustin, 1998). The Devonian-Mississippian boundary (Exshaw-type section at Jura Creek, ~80 km west of Calgary, Alberta, Canada) represents the boundary between the upper calcareous and lower non-calcareous black shale units (Richards and Higgins, 1988). Selby and Creaser (2005) provide an absolute Model 1 Re-Os age for this boundary, and thus the top of the lower black shale unit, of 361.3 ± 2.4 Ma. In addition, U-Pb monazite data from a tuff horizon close to the base of the lower black shale member constrains an absolute depositional age for this unit of 363.4 ± 0.4 Ma (Richards *et al.,* 2002). Deposition at this time represents part of a continent-wide Famennian-Tournasian black shale event, and in turn, a possible ocean anoxic event (Piggott and Lines, 1992).

The lower black shales are dark grey, bituminous, relatively thin (consistently between 3-5 m; Meijer *et al.,* 1994) and widespread (Meijer *et al.,* 1994). This member contains high TOC levels (up to ~20 wt. %; Creaser *et al.,* 2002), and enriched concentrations of Ni, V and Mo; metals that are characteristically associated with black shales (Duke, 1983). This unit is

believed to represent a euxinic shale deposit (Meijer *et al.,* 1994) with fauna such as ostracods, goniatites, languid brachiopods and Famennian conodonts of Lower *expansa* to *praesulcata* zones (Meijer and Johnston, 1993) interpreted by Raasch (1956) to be characteristic of a stagnant, shallow water coastal lagoon environment. However, the presence of goniatites and conodonts from biofacies outlined by Sandberg (1976), suggest deposition occurred in an offshore marine setting (Meijer *et al.,* 1994).

5.3 Sampling

In total, 32 samples from the Lower member of the Exshaw Formation were collected from the Alberta Energy and Utilities Board, Core Research Centre, Calgary. All samples are fine-grained black shales containing very thin parallel and undulating laminations. To avoid any potential effects of surface weathering, including loss of organic matter, as outlined by Peucker-Ehrenbrink and Hannigan (2000), drill core samples were obtained. Further, edges of the core were polished and where possible samples were taken from the central part of the core.

Over a lateral scale of ~ 150 km multiple samples were taken from 8 wells at varying depths (Fig. 5.2). This allowed analysis of a substantial depositional interval of the lower Exshaw Formation. In addition, to evaluate the effects of source rock maturation on geochemistry, the sample suite covered all three maturation zones (immature, mature and overmature). Broadly, the three maturation zones are defined by the following depth intervals: immature, ~1730-1756 m; mature, ~1756 – 2100 m; overmature, ~ 3567 – 3570 m (Fig. 5.2). Table 5.1 summarises the core features and degree of thermal maturation for each of the samples.

5.4 Analytical Protocol

5.4.1 Total Organic Carbon (TOC)

Total organic carbon was obtained as part of the carbon stable isotope analysis using an internal standard (i.e., Glutamic Acid, 40.82 % C), detailed in Chapter 4. Measurements were performed at Durham University using a Costech Elemental Analyser (ECS 4010) coupled to a ThermoFinnigan Delta V Advantage. Data accuracy is monitored through routine analyses of in-house standards, which are stringently calibrated against international standards (eg. USGS 40, USGS 24, IAEA 600, IAEA CH6): this provides a linear range in $\delta^{13}C$ between +2 ‰ and –47 ‰. Analytical uncertainty for $\delta^{13}C_{org}$ is typically ±0.1 ‰ for replicate analyses of the international standards and typically <0.2 ‰ on replicate sample analysis.

5.4.2 Trace element abundance

Samples were prepared for trace element analysis at the Northern Centre for Isotopic and Elemental Tracing (NCIET) following the method of Ottley *et al.,* (2003) outlined in detail in Chapter 4. Sample powders (~100 mg) were digested in a 4:1 solution of 29N HF (4 ml) and 16 N HNO_3 (1 ml) on a hotplate at ~150 ^{o}C for 48 hrs. Following evaporation to near dryness, 1 ml 16 N HNO_3 was added to the samples. The samples were evaporated to near dryness again, before repetition of this stage. Samples were re-dissolved in a 4 N HNO_3 solution prior to the addition of 1 ml of 1 ppm internal Re and Rh spike. Using MQ the samples were diluted to 50 ml, and further diluted 10-fold prior to analysis on the X-Series Inductively Coupled Plasma Mass Spectrometer (ICP-MS).

5.4.3 Nickel stable isotopes

All Ni isotope analyses were conducted at the University of Bristol, by Dr. Vyllinniskii Cameron. Chemical separation and purification of Ni was achieved using a 2-stage ion exchange procedure, outlined by Cameron *et al.,* (2009), and modified from Quitté and Oberli (2006). This procedure is described in detail in Chapter 4. Samples were treated multiple times with concentrated HNO_3 (15.3 N) to destroy any organic components (Cameron *et al.,* 2009) prior to digestion in a mixture of concentrated HNO_3 + HF (0.5 ml + 2 ml, respectively) at 140 ^{o}C for 48 hours.

The first-stage column is designed to separate Ni through complexation of Ni with DMG, whilst eluting matrix elements. The chemistry utilises solutions of ammonium citrate [$(NH_4)_2C_6H_6O_7$] and HNO_3 (Cameron *et al.,* 2009). The second-stage column ensures complete removal of the major atomic interferences on Ni (Fe and Zn) and purification of Ni, by utilising HCl + H_2O_2 solutions.

To correct for instrumental mass discrimination, the double spike approach (discussed in Chapter 3) was used. The spike was composed of a mixture of ^{61}Ni and ^{62}Ni, containing sub-equal portions of the two isotopes (Cameron *et al.,* 2009). All analyses were conducted using a ThermoFinnigan Neptune multi-collector (MC) ICPMS coupled to an Aridus desolvating nebuliser system (CETAC) fitted with a PFA nebuliser and spray chamber (CPI). All isotopes were measured simultaneously in static mode using a multiple Faraday collector array. Blank contributions generally accounted for <0.02 % (for ^{58}Ni) of the ion beams, and the internal error on the ^{60}Ni/^{58}Ni ratio was 0.001 – 0.002 % (2 σ) (Cameron *et al.,* 2009).

All Ni data are reported relative to NIST SRM 986, in the standard delta notation (see below) with all uncertainties reported to the 2 σ level.

5.5 Results

5.5.1 Total Organic Carbon (TOC)

Measured TOC for the Exshaw Formation is detailed in Table 5.2. The TOC content is highly variable ranging from ~1 – 22 wt. %. No correlations are observed between TOC and sample depth, or between TOC and thermal maturity (Fig. 5.3a). Further, each depth interval and therefore each maturation zone, shows a similarly broad range in TOC values (immature, ~1 – 22 wt. %; mature, ~1 – 17 wt. %; overmature, ~6 – 17 wt. %).

Covariation plots between TOC and the four trace elements used in this study (Ni, V, Cr and Co; Fig. 5.3b-e), demonstrate that overall no correlation is present between these elements and TOC. However, when the samples are ordered into maturation categories it is possible to see some trends between these parameters. For example, for the immature Exshaw samples there is a noticeable positive correlation between Ni and TOC (R^2 = ~0.69; Fig. 5.3b). However, little to no correlation can be seen between Cr, Co and V vs. TOC (R^2 = 0.29, 0.25 and 0.15, respectively; Fig. 5.3c-e). No trends are present between TOC and the trace elements in the mature Exshaw samples (R^2 in all cases between ~0.02 – 0.13). In contrast, the overmature Exshaw samples exhibit discernible positive correlations between TOC and V, Co and Cr (R^2 = 0.66, 0.64 and 0.56, respectively; Fig. 5.3c-e), with a weaker positive correlation between TOC vs. Ni (R^2 = 0.39; Fig. 5.3b).

Plotting TOC against the redox parameters (Fig.5.4a-c) does not show any overall trends in the Exshaw Formation samples. Equally, when the samples are divided into their corresponding maturation categories no correlations can be seen, with R^2 values in all cases being between ~0.00 – 0.33 (Fig. 5.4).

5.5.2 Trace elements

In this study (and similarly to Chapter 4) only the trace elements necessary to accurately evaluate the redox conditions at the time of sediment deposition have been used. These are as follows: Ni, V, Cr and Co.

5.5.2.1 Abundance

The abundances of Ni, V, Co and Cr in the Exshaw Formation shales are presented in Table 5.2. The minimum abundances for these metals all occur within a 1 m depth interval (~1753 – 1754 m) in the immature shale. Sample SP9-10 (~1753 m) contains the lowest amount of V (~40.3 ppm) and Cr (~19.5 ppm), and sample SP8-10 (~1754 m) holds the minimum concentration of Ni (~54.1 ppm). Both samples contain the equal lowest quantity of Co (~3.8 ppm). The maximum abundances of V (~859.3 ppm) and Co (~16.5 ppm) occur in mature shale at ~1756.4 m (sample SP62-10). Approximately 0.5 m below this at ~1756.8 m, also within mature shale, sample SP63-10 shows the highest concentration of Ni (~252.9 m). However, the maximum concentration of Cr (~121.6 ppm) is observed at far greater depths of ~3568.7 m, in overmature shale (sample SP26-10).

No correlation is observed between metal abundance vs. depth or thermal maturation (Fig. 5.5). Similarly, covariation plots of abundances for the individual metals (Fig. 5.6) produce only very weak positive correlations, with plots of Ni vs. V, Ni vs. Co, V vs. Cr, Co vs. Cr and Ni vs. Cr having R^2 values of < 0.39 (Figs. 5.6a-e). A slightly stronger positive correlation exists between V and Co (R^2 = 0.55; Fig. 5.6f).

5.5.2.2 Enrichment

Calculating the enrichment factor for elements in organic-rich sediments is outlined previously in Chapter 4. Determining the enrichment factor allows direct comparison of the

unit of study with both average shale (values from Wedepohl, 1971) and average black shale (values from Vine and Tourtelot, 1970).

Table 5.3 presents enrichment factors for all Exshaw Formation samples in this study. Average Co, Cr, Ni and V values for average shales (Wedepohl, 1971) and average black shales (Vine and Tourtelot, 1970), together with average metal values and associated enrichment factors are also presented in Table 5.4.

The approximate order of enrichment of Ni, V, Cr and Co in the Exshaw Formation organic-rich sediments (average value, n = 32) relative to average shale (Wedepohl, 1971) is as follows: V>Ni>Cr>Co (EF = 6.1, 4.2, 1.5 and 1.0, respectively; Table 5.4, Fig. 5.7). The order of enrichment relative to average black shale (Vine and Tourtelot, 1970) differs slightly and is as follows: Ni>V>Co>Cr (EF = 4.5, 4.2, 1.5 and 1.0, respectively; Table 5.4, Fig. 5.7). All samples (n = 32) are enriched in Ni relative to both average shale and average black shale (Fig. 5.7) with Ni enrichment factors of ~1 – 10 and ~2 – 11, respectively (Table 5.4). Most samples (n = 29) are also enriched in V relative to average shale (with $(V/Al)*10^4 > 14.7$), and ~88 % of samples (n = 28) have enrichment factors between ~1 – 11 relative to average black shale (Fig. 5.7; Table 5.4). The enrichment factors for Cr and Co show far less variation, and relative to both average shale and black shale, values only fluctuate between the range of ~0.5 – 2.8 (Table 5.4). As such, a greater proportion of samples are depleted in Cr and Co compared to the average shales. For Cr, only one sample (SP32-10; $(Cr/Al)*10^4$ = ~9.6) is depleted in comparison to average shale (EF = 0.94; Table 5.4), and 40 % of samples (n = 13) are depleted relative to average black shale (Fig. 5.7). In contrast, only two samples (SP8-10 and SP32-10) are depleted in Co relative to average black shale (with $(Co/Al)*10^4$ values of ~1.1 and ~1.3, and EF = 0.8 and 0.9, respectively), whereas 44 % of the samples (n = 14) are depleted relative to average shale values. No correlations exist between either depth and degree of metal enrichment relative to average shale and black shale, or between enrichment and thermal maturation (Fig. 5.7).

Crossplots of Al-normalised trace metal values (eg. (element X/Al)*10^4) demonstrate that no discernible correlations (R^2 < 0.19) are present between Ni/Al vs. Cr/Al, V/Al vs. Cr/Al or Co/Al vs. Cr/Al (Fig. 5.8a-c, respectively). Although showing higher R^2 values, little correlation can also be seen between Co/Al vs. V/Al (Fig. 5.8d; R^2 = ~0.34) and Ni/Al vs. V/Al (Fig. 5.8e; R^2 = ~0.29). A stronger positive correlation (R^2 = ~0.63) is observed between Ni/Al vs. Co/Al (Fig. 5.8f).

5.5.2.3 Redox indices

The trace element ratios for the Exshaw Formation shales and their inferred redox conditions are presented in Table 5.2 and Figure 5.9, respectively. The published values for these redox indices, used to determine the redox conditions at the time of deposition of the shales in this study, are shown in Table 5.5.

The Ni/Co ratio ranges from ~8 – 32, with all samples falling within the suboxic-anoxic parameter (Fig. 5.9). The V/Cr ratio (~1 – 14 units) suggests that a greater range of redox conditions were present at the time of sediment deposition (Fig. 5.9), with four samples indicating oxic conditions (V/Cr ratio of <2: SP32-10, ~1.4; SP48-10, ~1.0; SP49-10, ~1.3 and SP27-10, ~1.2) and four samples suggesting dysoxic conditions (V/Cr ratio of ~2 – 4.25: SP8-10, ~2.0; SP9-10, ~2.1; SP67-10, ~3.3 and SP29-10, ~4.1). However, most of the samples (n = 24) indicate that the depositional environment was suboxic-anoxic (Fig. 5.9). Similarly, the majority of samples have V/(V+Ni) values of ~0.60 – 0.84 (n=24), indicating suboxic-anoxic depositional conditions (Fig. 5.9), although V/(V+Ni) values of ~0.53 and ~0.59 for samples SP32-10 and SP67-10, respectively, suggest dysoxic conditions (Fig. 5.9).

For the majority of the samples (n=24, ~75 %) there is good agreement between all three of the redox indices, shown by the crossplots in Fig. 5.10 and the histograms in Fig.5.11, indicating that the depositional environment during accumulation of the Exshaw Formation

was predominantly suboxic-anoxic. This is in agreement with redox data obtained by Selby *et al.* (2009) for Exshaw Formation samples from Jura Creek. However, both the V/Cr and V/(V+Ni) ratios suggest that there were intermittent oxic and dysoxic periods during sediment deposition (Figs. 5.10 and 5.11), and in the case of the V/(V+Ni) index, that euxinic conditions may have been present (samples SP62-10, SP24-10 and SP25-10, at depths of 1756.4, 3567.7 and 3568.2 m, respectively; Figs. 5.10 and 5.11).

Figure 5.10 illustrates that there is no correlation between the values obtained for the individual redox indices and depth or maturation.

5.5.3 Nickel stable isotopes

New Ni stable isotope data for the Exshaw Formation shales is presented in Table 5.6. In total 8 samples were analysed for Ni stable isotopes, with representative samples from the immature (SP8-10, SP9-10, SP10-10 and SP13-10) and thermally mature zones (SP31-10, SP32-10, SP38-10 and SP39-10). The sampled cores and the relative positions of the samples therein are shown in Fig. 5.12.

The Ni isotope compositions (δ^{60}Ni) of these organic-rich shales are shown in Figure 5.13. The δ^{60}Ni values range from 0.46 ± 0.04 to 2.50 ± 0.04 ‰ (Table 5.6; Fig. 5.13a). Overall, there is no correlation between δ^{60}Ni and sample depth (Fig. 5.13b). However, the greatest spread in δ^{60}Ni values is observed within the immature shales (~2.04 ‰), which span the full range of δ^{60}Ni seen for the entire sample set (0.46 ± 0.04 to 2.50 ± 0.04 ‰; Fig. 5.13). Conversely, the Ni isotope composition of the mature shales is relatively consistent, ranging from 1.17 – 1.51 ‰ (a range of ~0.34 ‰; Fig. 5.13). The δ^{60}Ni values for the mature samples therefore fall well within the δ^{60}Ni range defined by the immature shales (Fig. 5.13).

The relationships between δ^{60}Ni vs. TOC and the trace elements (Ni, V, Cr and Co) are presented in Fig. 5.14a-e. The most prominent positive correlation is observed between δ^{60}Ni

vs. TOC for the thermally mature samples (R^2 = 0.90; Fig. 5.14a). Whilst at a first glance there is no correlation between the immature samples and TOC, if sample SP10-10 is disregarded, these samples show a near-perfect positive correlation (R^2 = 0.96). The trace element concentrations of the immature samples show no correlation with δ^{60}Ni (Fig. 5.14b-e). No relationships exist between Ni, V and Cr vs. δ^{60}Ni for the mature samples (R^2 = 0.35, 0.03 and 0.20, respectively; Fig. 5.14b-d), but a stronger positive correlation is noted between δ^{60}Ni and Co (R^2 = 0.76; Fig. 5.14e).

Plots of δ^{60}Ni vs. Al-normalised trace element values are given in Figure 5.15a-d. No trends are observed for any of the normalised values within either the immature or the mature shales, with R^2 values ranging between 0 and ~0.14. In addition, Figure 5.16 demonstrates that there is no relationship between δ^{60}Ni and the redox conditions at the time of sediment deposition.

5.6 Discussion

5.6.1 Correlation of trace element abundance with TOC and redox

No correlation exists between trace element (Ni, V, Cr, Co) abundance and TOC for the majority of the Exshaw Formation samples (Fig. 5.3), indicating that the degree of organic matter accumulation was not a primary control on metal uptake during sediment deposition. Although a trend between Ni vs. TOC is observed for immature samples (Fig. 5.3b), no such trend is seen in the mature or overmature shales. A possibility is that maturation has caused cleavage of the metallo-organic bonds formed by Ni, thus destroying any coupling of Ni with TOC. However, V is held in the same type of stable metallo-organic complexes (eg. Lewan, 1984) and no such trend is observed with TOC. In addition, these complexes are known to be

highly stable (Lewan and Maynard, 1982; Lewan, 1984). Instead, the lateral and vertical scale over which sampling has occurred in this study could easily facilitate significant local variations in the type of organic-matter, which may have a profound effect on the correlation of Ni with TOC.

Variation in trace element abundance is not controlled by redox and in addition there is no discernible relationship between TOC and redox conditions (Fig. 5.4). Preferential preservation of metallo-organic complexes occurs under anoxic conditions (Lewan and Maynard, 1982; Lewan, 1984), and as such, if the environmental redox conditions were the single control on the enrichment of metals in organic-rich sediments, a clear trend would be observed between these two parameters. The lack of such a trend (Fig. 5.4) suggests that the redox conditions of the bottom-waters during sediment deposition were not the sole control on metallation, and therefore did not solely control the enrichment or depletion trends observed relative to average shale and black shale (Fig. 5.7).

Although the paleoredox conditions in this Exshaw Formation study are different to those at Robin Hood's Bay (presented in Chapter 4), a similarity is observed between these two studies. The lack of strong relationships between metal abundance vs. TOC and redox in these investigations, demonstrates that factors in addition to TOC concentration and bottom-water redox conditions controlled the uptake and abundance of metals in the organic-rich sediments discussed herein. Such factors could include the type of the organic matter present, sediment accumulation rates and biogeochemical cycling of the elements in the ocean.

5.6.2 The suitability of V/(V+Ni) as a redox proxy

The suitability of V/(V+Ni) as a redox proxy was discussed previously in Chapter 4. Here the applicability of this redox proxy is also discussed in relation to the Exshaw Formation shales. In this study, and unlike for the Robin Hood's Bay sediments, there is reasonable

agreement between the Ni/Co, V/Cr and V/(V+Ni) redox proxies (Figs. 5.10 and 5.11). Although intermittent oxic-dysoxic and euxinic periods are suggested by the V/Cr and V/(V+Ni) ratios, all three of the indices indicate that the sediments examined in this study were deposited in a predominantly suboxic-anoxic environment (Fig. 5.11). However, in the case of V/(V+Ni), three samples have values lower than the minimum parameter established for this redox proxy (0.46; lowermost boundary for dysoxic conditions), which once again calls into question the validity of using this ratio as a redox proxy (see also discussion in Chapter 4).

As in Chapter 4, V/(V+Ni) vs. TOC data for the Exshaw Formation has been plotted against corresponding data for Robin Hood's Bay and the Pennsylvanian Stark Shale Member (Fig. 5.17; data from Hatch and Leventhal, 1992). Although the Exshaw samples are more similar lithologically to the Stark Shale Member samples than those from Robin Hood's Bay, once again it is observed that the relationship between TOC and V/(V+Ni) (Fig. 5.17) differs distinctly from that described by Hatch and Leventhal (1992). This reinforces the conclusion drawn in Chapter 4; that this redox index was developed for a specific geological basin, and therefore may not be applicable to other geological samples regardless of lithological similarities, particularly those with differing geochemical characteristics.

5.6.3 The effect of thermal maturation on source rock geochemistry: trace element abundances and proportionality of V and Ni

Trace elements in petroleum and source rocks have been used as a diagnostic tool to yield information about genetic relationships between oils and migration processes (eg. Hodgson *et al.,* 1959; Ball *et al.,* 1960; Tissot and Welte, 1984; Ellrich *et al.,*1985; López *et al.,* 1995). Of these trace elements the most abundant are V and Ni (López *et al.,* 1995), bound predominantly in porphyrin structures (Lewan and Maynard, 1982; Lewan, 1984) which themselves are well known as important biomarkers (eg. Triebs, 1934). The tenacious bonds

formed by both Ni and V with the metallo-organic complexes are unlikely to de-metallate until metamorphic conditions are encountered (Lewan, 1984).

As such, although thermal maturation, migration and reservoir alterations may change the absolute concentrations of V and Ni in the oil relative to its source (Lewan, 1984), their proportionality to one another should remain unchanged (Hunt, 1979; Lewan, 1984). As a result, both Ni and V, and specifically the proportionality of V to Ni, have been recognised to occupy an important role in the geochemical research of oil-source and oil-oil correlations (eg. Lewan and Maynard, 1982; Lewan, 1984; Ellrich *et al.,* 1985; López *et al.,* 1995), and in investigations of paleo-environmental conditions of sedimentation (Hitchon and Filby, 1984; Lewan, 1984; Manning *et al.,* 1991; Hatch and Leventhal, 1992; Alberdi and Lafargue, 1993; Schovsbo, 2001).

The primary focus of this study is to examine the effects of hydrocarbon maturation on the Ni isotope composition of source rocks, with a view to establishing Ni stable isotopes as an oil-source correlation tool. As a precursor to this, it is essential to also understand trace element behaviour as a result of thermal maturation. Abundances of the trace elements Ni, V, Cr and Co were determined from samples spanning a range of hydrocarbon maturity levels from immature to overmature. From Figure 5.5 it can be observed that there is significant variation in trace metal content of the shales within each depth interval (and therefore each maturation level). Further, each different depth and maturation window shows a similar range in trace element concentrations (Fig. 5.5). These plots of element concentration against depth (and level of thermal maturation) demonstrate that the degree of hydrocarbon maturation does not affect the abundance of these metals in the Exshaw Formation shales. Further, they also indicate that thermal maturation did not cleave the metallo-organic bonds formed by these metals in the organic-rich sediments.

To examine this further, trace element concentrations have been plotted against T_{max} (^{o}C) values for corresponding samples from Creaser *et al.* (2002) (Fig. 5.18). The T_{max} parameter determines sample hydrocarbon maturity level and represents the temperature of peak hydrocarbon release by kerogen cracking via Rock-Eval pyrolysis (Hunt, 1979). Figure 5.18 clearly demonstrates that certainly for V and Cr, and indeed the proportionality of these metals, there is little correlation between abundance and hydrocarbon maturation level (T_{max}). In contrast, Ni and Co show a similar trend to one another, increasing in abundance with elevated T_{max}. Examination of Ni/V and V/(V+Ni) values for the four samples presented on Fig. 5.18 shows that proportionality of these metals is consistent (~1 – 2 and ~0.67 – 0.69, respectively) for the immature and mature samples (immature: SP8-10 and SP13-10; mature: SP32-10). The overmature sample (SP24-10) exhibits greater V/Ni (~7.5) and V/(V+Ni) (~0.88) values due to heightened enrichment of V (~620 ppm) for this sample relative to Ni, rather than significant depletion of Ni. However, although T_{max} data is not available for all samples presented in this study, Table 5.2 and Figure 5.9 clearly show that V/(V+Ni) values are variable both between and within each of the maturation zones for the Exshaw Formation. This suggests that V and Ni proportionality in these source rocks is not affected by the degree of hydrocarbon maturation, but instead relates to the initial abundance following metal uptake into the organic-rich sediments. Given the substantial variability of V/(V+Ni) ratios in the source rocks studied herein, this investigation also proposes that use of this ratio to extract meaningful genetic information about source rocks may be limited.

In summary, these results indicate that hydrocarbon maturation is unlikely to be the cause of the variation in trace element concentrations seen within the Exshaw Formation. As such, this demonstrates that thermal maturation has not affected the strong metallo-organic bonds formed by Ni and V, which is a positive start for the potential development of Ni isotopes as an oil-source correlation tool. The variation in metal concentration is likely to be

controlled during initial metallation of the organic-rich sediments (Lewan, 1984), and may instead be caused by smaller-scale lateral and temporal compositional variability, particularly with respect to organic matter (eg. Tyson, 1995; Curiale, 2008). Although no correlation is observed between either metal abundance and TOC content (Fig. 5.3b-e), with the exception of TOC vs. Ni for the immature samples (Fig. 5.3b), or TOC content vs. depth and maturation (Fig. 5.3a), localised changes in the type of the organic matter accumulation, which often occur on the centimetre scale (eg. Huc *et al.,* 1992; Aplin *et al.,* 1992; Curiale, 1994; Jones *et al.,* 1997; Barker *et al.,* 2001), may be a factor (eg. Curiale, 2008). Additional factors that are likely to influence but not solely control the concentration and proportionality of V and Ni, as well as the abundance of other trace metals (eg. Cr and Co) in organic-rich sediments include, sedimentation rate and the persistence of an open sediment system (Lewan and Maynard, 1982; Lewan, 1984), biogeochemical cycling of the elements in the ocean, redox conditions, and the preservation of the tetrapyrrole complexes holding the metals (Lewan and Maynard, 1982; Lewan, 1984).

5.6.4 Nickel isotope fractionation in marine sediments: A comparison between the Exshaw Formation and the Sinemurian-Pliensbachian GSSP

To enhance our understanding of Ni isotope systematics in marine sediments, and with no other such datasets available for comparison external to this investigation, the similarities and differences between the Ni isotope signatures of the organic-rich sediments from the Exshaw Formation and the Sinemurian-Pliensbachian boundary (this thesis, Chapter 4), will be discussed.

Figure 5.19 compares Ni stable isotope data for the Exshaw Formation, Sinemurian-Pliensbachian sediments (Chapter 4), and extraterrestrial (iron and stone meteorites) and abiotic terrestrial (continental sediments: riverine and aeolian) samples from Cameron *et al.*

(2009). The meteorites, basalts and continental sediments are characterised by δ^{60}Ni values averaging 0.2 ‰ (Cameron *et al.*, 2009; yellow box, Fig. 5.19). Further, the degree of Ni isotope fractionation for these extraterrestrial and abiotic terrestrial samples is indistinguishable. As with the organic-rich sediments from Robin Hood's Bay, the Exshaw Formation shales define a realm of δ^{60}Ni values (0.46 ± 0.04 to 2.50 ± 0.04 ‰) that are distinct from the sample groups analysed by Cameron *et al.* (2009) (Fig. 5.19). This range of values also overlaps with, and is comparable to, the δ^{60}Ni data from the Sinemurian-Pliensbachian boundary (0.28 ± 0.05 to 1.60 ± 0.05 ‰). These datasets demonstrate that Ni isotope fractionation in marine sediments occurs to a much greater extent than within extraterrestrial and abiotic terrestrial samples. In agreement with the conclusion drawn in Chapter 4, Figure 5.19 may also indicate that the Ni isotopic signature of marine sediments is distinct to that of meteorites, basalts and continental sediments. However, the reasons for this distinction are poorly understood due to an extremely limited database.

In addition, following examination of Ni isotope data from organic material (microorganisms; δ^{60}Ni = ~ 0.0 – -1.6 ‰) analysed by Cameron *et al.* (2009), it is noted that the Ni isotope ratios in the organic-rich sediments herein appear to have been driven in the opposite direction to those of the microorganisms. Whilst the causes of Ni isotope fractionation in these sediments are poorly understood, it appears that there is a fractionation effect associated with the Ni isotope system that may have parallels to the carbon isotope system. Further, a comparison of the data herein and that from Cameron *et al.* (2009), suggests that the microorganisms take up isotopically lighter Ni, leaving behind an isotopically heavier Ni isotope signature in the sediments. However, to investigate the potential parallels between the carbon and Ni isotope systems, additional datasets are required and further investigation is needed.

The complexity of the sediment-seawater system may be a factor that causes such enhanced levels of Ni isotope fractionation in marine sediments relative to meteorites, basalts and continental sediments. Therefore, in order to attempt to understand this, it is important that the relationships between Ni isotope fractionation and factors ubiquitous to the marine depositional system, such as bottom-water redox conditions and TOC content, are explored.

In order to critically assess the data herein, it is necessary to ascertain whether the level of Ni isotope fractionation observed in the Exshaw Formation has resulted from variations in the depositional environment, including TOC content and the redox conditions during sedimentation, or from thermal maturation. Figure 5.13 presents δ^{60}Ni data for the Exshaw Formation and shows the range of δ^{60}Ni values obtained from the Sinemurian-Pliensbachian sediments for comparison.

No relationship exists between δ^{60}Ni and total Ni abundance in the Exshaw Formation (Fig. 5.14b), demonstrating that the level of Ni isotope fractionation in these marine sediments (both immature and mature) is not dictated by the degree of Ni enrichment. This is further supported by the lack of correlation between δ^{60}Ni and the Al-normalised Ni values (Fig. 5.15a), which indicate that isotopic fractionation is unrelated to variations in the concentration of hydrogenous Ni. This observation is also true for the organic-rich sediments across the Sinemurian-Pliensbachian boundary (Chapter 4). Although currently limited to only two datasets, these studies strongly suggest that Ni isotope fractionation in marine sediments is not controlled by the degree of uptake or enrichment of Ni during sediment accumulation.

The amount of Ni fractionation in the Exshaw Formation does not correlate with the paleoredox conditions at the time of sediment deposition (Fig. 5.16). Conversely to the sediments from the Sinemurian-Pliensbachian boundary discussed previously (this thesis, Chapter 4), the samples selected for Ni isotope analysis from the Exshaw Formation were deposited under predominantly suboxic-anoxic conditions (Fig. 5.16). Both sample suites

display significant variations in δ^{60}Ni data (Sinemurian-Pliensbachian: ~1.32 ‰, and Exshaw Formation: ~2.04 ‰) that do not correlate with the redox ratios, suggesting that the extent of Ni isotope fractionation in marine sediments is not directly determined by the paleoredox conditions during deposition. However, evidence from these datasets suggests that paleoredox conditions have the potential to significantly influence the relationship between δ^{60}Ni and TOC in marine sediments.

Although the δ^{60}Ni data and TOC contents of the Sinemurian-Pliensbachian and Exshaw Formation sediments are not correlated with redox (Chapter 4, Fig. 4.20 and this study, Fig. 5.4, respectively), the relationship between the amount of isotopic fractionation and TOC appears to strengthen significantly with the transition from oxic to suboxic-anoxic conditions. For example, the upper 5 samples from the Pliensbachian (deposited in oxic conditions) have TOC concentrations >1 wt. % and correlation with δ^{60}Ni yields an R^2 value of ~0.7. Further, the mature Exshaw Formation samples (deposited under suboxic-anoxic conditions) contain TOC levels of >6 wt. % (6.8 – 16.8 wt. %) and exhibit a stronger correlation with δ^{60}Ni (R^2 = 0.90; Fig. 5.14a). Additionally, disregarding sample SP10-10 (TOC = 11 wt. %), the immature samples, although characterised by lower TOC concentrations (1.2 – 2.9 wt. %), show a near perfect positive correlation between δ^{60}Ni and TOC (R^2 = 0.96; Fig. 5.14a). It can be observed that all samples contain TOC >1 wt. %. As discussed in Chapter 4, the Sinemurian samples (oxic) which all contain 0.6 – 0.8 wt. % TOC, show a far weaker correlation with δ^{60}Ni. These combined datasets therefore suggest, firstly, that TOC concentration in marine sediments may exert control on Ni isotope fractionation when above a potential threshold of ~1 wt. %, possibly regardless of depositional redox conditions. Secondly, the data puts forward an additional hypothesis: that correlation of δ^{60}Ni vs. TOC may be strongest in marine sediments accumulated under suboxic-anoxic conditions. If this relationship is true, the, or one of, the causal factor(s) may be related to the preferential preservation of the tetrapyrrole

complexes (binding the Ni to the organic matter) under reducing conditions (eg. Lewan and Maynard, 1982). Such preservation could significantly reduce the potential for heterogeneous break-down of these complexes prior to lithification, therefore minimising the likelihood of any associated isotopic fractionation. The observed degree of Ni isotope fractionation could therefore correspond to the preferential uptake of ^{60}Ni into sediments with elevated TOC content. However, presently the reasons for this are poorly understood, and the current dataset is limited by not including suboxic-anoxic samples containing <1 wt. % TOC. As such, the causes of the δ^{60}Ni vs. TOC relationship can only be hypothesised.

An additional complication to this relationship is noted when comparing the δ^{60}Ni vs. TOC trends for only the Exshaw Formation (Fig. 5.14a). Although the immature and mature samples both exhibit strong positive correlations between these parameters (still disregarding sample SP10-10), the level of Ni isotope fractionation is most variable in the low TOC samples (all immature, ~1.2 – 2.9 wt. % TOC, δ^{60}Ni of ~1.09 – 2.50 ‰; Fig. 5.14a). Unlike the Sinemurian-Pliensbachian boundary sediments, such variability cannot be potentially accounted for by formation under oxic depositional conditions or the poor preservation of the tetrapyrrole complexes (eg. Lewan and Maynard, 1982). Instead there must be a control that is distinct for each group (immature and mature) of Exshaw Formation samples. Aside from the degree of thermal maturation experienced by the rocks, the fundamental difference existing between these two sample groups is lithological (Fig. 5.12), therefore relating to variations in the depositional environment and type of sediment influx.

By examining the core photographs in Figure 5.12 it is immediately apparent that there are clear lithological differences between the immature and mature samples. The mature samples (Figs. 5.12c-e) all share the same characteristics, being dark brown/black, exceptionally fine-grained and containing multiple fine horizontal laminations on the millimetre scale. The immature samples (Figs. 5.12a,b) however, are far more varied. Sample

SP8-10 (Fig. 5.12a) has the closest resemblance to the mature samples, being near-black and with a very fine-grained matrix. However, samples SP9-10 (Fig. 5.12a), SP10-10 and SP13-10 (Fig. 5.12b) vary from pale to mid-grey in colour with a coarser matrix and a greater silt concentration. These paler shales more closely resemble those from the Sinemurian-Pliensbachian boundary (Chapter 4).

The mature samples (showing little compositional variability) define a relatively restricted range of δ^{60}Ni values (~1.17 – 1.51 ‰). The immature sample that is lithologically very similar to the mature samples (SP8-10, ~1.09 ± 0.04 ‰) lies just outside of uncertainty (~0.03 ‰) of the average δ^{60}Ni value for the mature shales (including 1 standard deviation from this average value, marked by the red box in Fig. 5.13a). Conversely, the immature samples that differ compositionally from these and bear a closer resemblance to the Sinemurian-Pliensbachian sediments, display a much greater range of δ^{60}Ni values (~0.46 – 2.50 ‰; Fig. 5.13a). Although the current dataset is limited to only 8 samples, the δ^{60}Ni values presented for the Exshaw Formation demonstrate that the sample lithology of marine sediments may exert a control on the degree of Ni isotope fractionation observed. Our present understanding of what may cause such a relationship is incomplete. However, differences between the type of sediment influx, amount and type of organic matter and sedimentation rate (possibly slower for the finely laminated black shales) may contribute to this relationship. Further, the immature and mature samples both show significant correlations between δ^{60}Ni vs. TOC, although with differing gradients (Fig. 5.14a). Variability between the sedimentation rates and the types of the organic matter in the accumulating sediments may have a significant influence on this.

The next step is to examine the potential effects of thermal maturation on Ni isotope systematics in the Exshaw Formation, and how this may have contributed to the isotopic fractionation patterns observed for these samples.

5.6.5 Effects of hydrocarbon maturation on Ni isotope systematics

Understanding how Ni isotope systematics in source rocks respond to thermal maturation is critical to assessing the viability of Ni stable isotopes as an oil to source correlation tool. Although Dewaker *et al.* (2000) demonstrate that Ni isotopes have the potential to yield valuable insight into oil-source correlation, their study has substantial limitations, with little understanding of the behaviour of Ni isotope systematics in marine sediments and no discussion of the possibility of maturation-induced isotope fractionation. It is therefore essential that any potential effects of hydrocarbon maturation are identified, before correlation studies can be conducted confidently.

The Ni stable isotope data (δ^{60}Ni) for Exshaw Formation samples spanning the immature and mature hydrocarbon maturity levels is presented in Table 5.6 and Fig. 5.13. The first observation is that Ni isotope fractionation occurs to a greater extent in the immature samples (~2.04 ‰), ranging from 0.46 ± 0.04 to 2.50 ± 0.04 ‰. Dissimilarly, the mature samples exhibit a far more restricted level of isotopic fractionation with δ^{60}Ni values ranging from 1.17 ± 0.03 to 1.51 ± 0.04 ‰ (a range of ~0.34 ‰). Interestingly, this range of δ^{60}Ni sits well inside that defined by the immature samples (Fig. 5.13). In addition, the average δ^{60}Ni values for the immature and mature samples are within uncertainty of one another (1.51 ± 0.91 ‰ and 1.31 ± 0.15 ‰, respectively; Fig. 5.13).

As discussed previously, the Ni isotope signatures shown by the immature and mature shales could result from variations in their respective depositional environments. We now need to assess whether the observed isotopic characteristics could have been influenced by hydrocarbon maturation. As this is the first study to record Ni isotope fractionation in organic-rich sediments that have experienced varying degrees of thermal maturation, our understanding of the effects of maturation on Ni isotope systematics are exceptionally limited. If maturation exerted control on the Ni isotope composition of the Exshaw Formation (Fig.

5.13) and is therefore responsible for the relatively consistent δ^{60}Ni values of the thermally mature samples, it would appear that it caused the Ni isotope composition to reset to a homogenous value. However, although a definitive conclusion cannot be drawn without comparison with additional datasets, studies demonstrating the stability of Ni in organic-rich sediments (Lewan, 1980; Lewan and Maynard, 1982) and that of other isotopic systems that have undergone maturation tests, suggest that such an effect on the Ni isotope system may be unlikely.

Nickel is strongly bound within high molecular weight metallo-organic complexes (Lewan and Maynard, 1982) that have a high thermal stability (Constantinides *et al.,* 1959). Such stability ensures that these bonds are unlikely to cleave under diagenetic conditions (Lewan and Maynard, 1982). Further, it suggests that these metallo-organic bonds will not be affected by generation and migration of petroleum (Lewan, 1980). As such, it seems unlikely that thermal maturation would induce isotopic homogeneity within these highly stable complexes.

Although no previous studies have characterised the behaviour of Ni isotope systematics following thermal maturation, investigations have focused on such characterisation of the stable carbon isotope and Re-Os systems. Analysis of kerogens (sedimentary organic matter) in the natural environment (Hoefs and Frey, 1976) and following hydrous pyrolysis experiments (Lewan, 1983), demonstrate that the effect of thermal maturation on δ^{13}C values is negligible. Further, Lewan (1983) shows that the δ^{13}C values of pyrolysed kerogens are relatively consistent within analytical error (± 0.3 ‰) throughout the maturation windows. As such, δ^{13}C values have been recognised as a potential oil-source correlation tool (Lewan, 1983). In addition, Re-Os geochronology of immature, mature and overmature samples from the Exshaw Formation yielded absolute ages that show little

variation (Creaser *et al.,* 2002; Selby and Creaser, 2005). This indicates that thermal maturation did not disturb Re-Os isotope systematics in the Exshaw Formation.

It is not possible to definitively state that thermal maturation does not have an effect on Ni isotope systematics based solely on the dataset presented herein. However, with our current understanding of the high stability of Ni in organic-rich sediments, and the ability of other isotope systems to withstand this process, it seems unlikely that the Ni isotope system would be an exception. Although it may be unlikely that thermal maturation fully dictates the Ni isotope signature, this study cannot rule out the possibility that it may contribute to a small degree. However, this cannot be quantified without significantly expanding the available datasets. As such, this study suggests that the observed Ni isotope signature in the Exshaw Formation cannot be attributed to the effects of thermal maturation, and is instead related to compositional and chemical variability of the samples.

5.6.6 Do Ni isotopes have the potential to be used as an oil-source correlation tool?

The high stability of Ni in organic-rich sediments (Lewan and Maynard, 1982; Lewan, 1984) makes it an ideal candidate for isotopic correlation studies. Until now, this has been impeded by difficulties in the chemical separation of Ni from organic-rich sample matrices. Further, there was little understanding of Ni isotope fractionation in organic-rich marine sediments, and no quantification of possible isotopic fractionation induced by the hydrocarbon maturation process. Without awareness of the behaviour of Ni isotope systematics in these settings, it would not be possible to draw meaningful conclusions on the potential for Ni isotopes to be used as an oil-source correlation tool.

The dataset herein demonstrates that the significant level of Ni isotope fractionation (~2.04 ‰) in the Exshaw Formation is likely to result from chemical and compositional variations in the samples, rather than from thermal maturation. Further, the thermally mature

samples, which are compositionally similar, present a relatively constricted range of δ^{60}Ni values (~0.34 ‰, averaging 1.31 ± 0.15 ‰). Such negligible variation in the Ni isotope composition of the mature samples (from which oil would be generated) is an ideal precursor for oil-source correlation studies, as it provides a distinct δ^{60}Ni signal that can be directly compared to the δ^{60}Ni value of the generated oil.

Although the process of thermal maturation may cause variations in the concentrations of Ni and V (Lewan, 1984), the high thermal stability of the metallo-organic complexes suggests that their proportionality to one another will be unaffected by oil generation and migration (Lewan, 1980). As such, this proportionality is expected to be maintained by the expelled oil (Lewan, 1984). The next step will be to assess whether potential variations in Ni concentration with thermal maturation and oil generation result in differing Ni isotope compositions between oil and source. With our current understanding of the strength of the organic-Ni complexes, it seems unlikely that maturation will result in the preferential loss of one or more Ni isotopes in either oil or source. However, the dataset needs to be expanded to include oils generated from the Exshaw Formation in order to answer this conclusively.

5.7 Conclusions

This investigation provides an increased geochemical understanding of the lower black shale member of the Exshaw Formation; a hydrocarbon-generating source rock within the Western Canada Sedimentary Basin (Leenheer, 1984; Creaney and Allan, 1991) that exists in all three thermal maturation zones (immature, mature and overmature; Piggott and Lines, 1992).

Further, the study herein examines the effect of thermal maturation on source rock geochemistry, with a view to developing Ni stable isotopes as a new oil-source correlation tool.

Trace element data indicates that the Exshaw Formation was deposited under a predominantly suboxic-anoxic environment. Although the V/Cr and V/(V+Ni) ratios suggest that there were intermittent oxic-dysoxic and euxinic bottom-water conditions, there is reasonable agreement between all three paleoredox proxies (Figs. 5.10 and 5.11).

The Al-normalised trace element values indicate that Ni and V are significantly enriched in the Exshaw Formation relative to average shale and black shale compositions. Thermal maturation does not exert control on the level of trace element enrichment in the Exshaw Formation shales. The degree of organic matter accumulation during sedimentation of the Exshaw Formation is also unlikely to have been a primary control on metal enrichment, as few correlations between trace element concentration and TOC are observed. Similarly, trace element enrichment was not dictated by the redox conditions at the time of deposition. As such, and similarly to the organic-rich sediments at Robin Hood's Bay, it is likely that factors in addition to TOC and redox controlled the level of metal enrichment in the Exshaw Formation. Such factors may include the type of organic matter being accumulated in the sediments, sedimentation rates, and biogeochemical cycling of the elements in the ocean.

This study builds upon the work of Chapter 4, by further characterising the Ni isotope composition of marine organic-rich sediments. In addition to this, the data herein is the first to quantify the impact of thermal maturation on Ni isotope fractionation in source rocks. In agreement with δ^{60}Ni data from the Sinemurian-Pliensbachian boundary (Chapter 4), the Exshaw Formation shales define a domain of δ^{60}Ni values that are isotopically distinct from extraterrestrial and abiotic terrestrial samples (Fig. 5.19). Further, these values correspond with the δ^{60}Ni trend from the Sinemurian-Pliensbachian boundary, suggesting that marine sediments may have a characteristic Ni isotope signature. The reasons for this are poorly

understood due to a currently limited sample database, however this study suggests that the enhanced degree of Ni isotope fractionation in marine sediments may be related to complexities in the sediment-seawater system that are not present in the extraterrestrial and abiotic terrestrial sample environments. In addition, comparison of δ^{60}Ni values from the organic-rich sediments herein and from microorganisms (Cameron *et al.,*2009), indicates that a parallel may exist between the Ni and carbon isotope systems. However, this requires further investigation.

In a similar manner to the Sinemurian-Pliensbachian boundary sediments, the amount of Ni isotope fractionation in the Exshaw Formation is not controlled by Ni enrichment in the sediments or by paleoredox conditions during deposition. However, the immature and mature samples are characterised by possible correlations with TOC; stronger than that observed in the Sinemurian-Pliensbachian boundary samples. This suggests that the δ^{60}Ni vs. TOC relationship may be strongest in marine sediments deposited under suboxic-anoxic conditions. This may be accounted for by considering the greater preservation of the metallo-organic tetrapyrrole complexes under these conditions. However, further work on additional datasets is required to further our understanding of the δ^{60}Ni vs. TOC relationship.

Although there is a strong relationship between δ^{60}Ni and TOC, there must be an additional control on the level of Ni isotope fractionation in the Exshaw Formation that accounts for the highly variable δ^{60}Ni values of the immature samples (ranging from ~0.46 – 2.50 ‰) and almost negligible variability of δ^{60}Ni values for the mature samples (ranging from ~1.17 – 1.51 ‰). The inconstancy of the immature δ^{60}Ni values cannot be attributed to potentially poor preservation of the tetrapyrrole complexes. Due to the highly stable nature of Ni in these complexes, it is also unlikely that thermal maturation would induce isotopic near-homogeneity in the thermally mature samples. Whilst it is possible that TOC concentrations in marine sediments may influence the δ^{60}Ni composition when above a potential threshold of ~1

wt. %, there may be additional factors to take into consideration. Herein it is suggested that the compositional variability of the samples may have a significant effect on the Ni isotope composition. Evidence from core analysis (Fig. 5.12) demonstrates that the mature samples are compositionally very similar, being very fine-grained black shales. Conversely, the immature samples display more variability, with a coarser grain size, fluctuating silt content, and mostly with lower TOC contents. Although the current dataset is limited, the observed δ^{60}Ni signal in the Exshaw Formation, considering the likely relationship between δ^{60}Ni and sample composition, may reflect varying contributions from hydrogenous and terrigenous sources. For example, from their lithological descriptions the mature samples are likely to be dominated by a hydrogenous component, whereas the immature samples clearly contain varying proportions of a terrigenous, detrital component. This may have a profound effect on the type of organic matter present in the sediments. However, the Ni isotopic composition of these sources remains undefined, as does the potential effect of varying types of organic matter on Ni isotope fractionation, and as such more work needs to be conducted to quantify the effect that these variables may have on the Ni isotope composition of marine sediments.

Finally, this study concludes that there is significant potential for Ni isotopes to be a valuable tool in oil-source correlation studies. Thermal maturation does not affect the Ni isotope composition of the Exshaw Formation source rocks, suggesting that the Ni stable isotope system within organic-rich sediments has significant thermal stability. With careful sampling to ensure that there is little compositional variability between the mature source rock samples being analysed, this study demonstrates that further investigation and development of Ni isotopes as an oil-source correlation tool is indeed worthwhile.

5.8 References

Alberdi, M., and Lafargue, E., 1993, Vertical variations of organic matter content in Guayuta Group (upper Cretaceous), Interior Mountain Belt, Eastern Venezuela: Organic Geochemistry, v. 20, no. 4, p. 425-436.

Alexander, R., Kagi, R. I., and Woodhouse, G. W., 1981, Geochemical correlation of Windalia oil and extracts of Winning Group (Cretaceous) potential source rocks, Barrow Sub-basin, Western Australia: American Association of Petroleum Geologists Bulletin, v. 65, p. 235-250.

Aplin, A. C., Bishop, A. N., Clayton, C. J., Kearsley, A. T., Mossman, J. R., Patience, R. L., Rees, A. W. G., and Rowland, S. J., 1992, A lamina-scale geochemical and sedimentological study of sediments from the Peru Margin (Site 680, ODP Leg 112), *in* Summerhays, C. P., Prell, W. L., and Emeis, K. C., eds., Upwelling Systems: Evolution since the Early Miocene, Volume 64, Geological Society Special Publication, p. 131-149.

Archer, C., and Vance, D., 2004, Mass discrimination correction in multiple-collector plasma source mass spectrometry: an example using Cu and Zn isotopes: Journal of Analytical Atomic Spectrometry, v. 19, no. 5, p. 656-665.

Ball, J. S., Wenger, W. J., Hyden, H. J., Horr, C. A., and Myers, A. T., 1960, Metal content of twenty-four petroleums: Journal of Chemical and Engineering Data, v. 5, p. 553-557.

Barker, C. E., Pawlewicz, M., and Cobabe, E. A., 2001, Deposition of sedimentary organic matter in black shale facies indicated by the geochemistry and petrography of high-resolution samples, Blake Nose, western North Atlantic, Western North Atlantic Palaeogene and Cretaceous Palaeoceanography, Volume 183, Geological Society, London, Special Publication, p. 49-72.

Bonham, L. C., 1956, Geochemical investigation of crude oils: American Association of Petroleum Geologists Bulletin, v. 40, p. 897-908.

Cameron, V., Vance, D., Archer, C., and House, C. H., 2009, A biomarker based on the stable isotopes of nickel: Proceedings of the National Academy of Sciences, v. 106, p. 10944-10948.

Caplan, M. L., and Bustin, R. M., 1998, Sedimentology and sequence stratigraphy of Devonian-Carboniferous strata, southern Alberta: Bulletin of Canadian Petroleum Geology, v. 46, p. 487-514.

Caplan, M. L., and Bustin, R. M., 1999, Palaeoceanographic controls on geochemical characteristics of organic-rich Exshaw mudrocks: role of enhanced primary production: Organic Geochemistry, v. 30, no. 2-3, p. 161-188.

Chen, J., Bi, Y., Zhang, J., and Li, S., 1996, Oil-source correlation in the Fulin basin, Shengli petroleum province, East China: Organic Geochemistry, v. 24, no. 8–9, p. 931-940.

Constantinides, G., Arich, G., and Lomi, C., 1959, Detection and behaviour of porphyrin aggregates in petroleum residues and bitumens: Proceedings of the 5th World Petroleum Congress, v. Section V, p. 131-142.

Corbett, L. W., 1967, Distribution of heavy metals in asphalt residua: American Chemical Society, Division of Petroleum Chemistry v. 12, p. A83-A87.

Creaney, S., and Allan, J., 1991, Hydrocarbon generation and migration in the Western Canada sedimentary basin: Geological Society, London, Special Publications, v. 50, no. 1, p. 189-202.

Creaser, R. A., Sannigrahi, P., Chacko, T., and Selby, D., 2002, Further evaluation of the Re-Os geochronometer in organic-rich sedimentary rocks: a test of hydrocarbon maturation effects in the Exshaw Formation, Western Canada Sedimentary Basin: Geochimica et Cosmochimica Acta, v. 66, no. 19, p. 3441-3452.

Curiale, J. A., 1994, High-resolution organic record of Bridge Creek deposition, northwest Mexico: Organic Geochemistry, v. 21, p. 489-507.

Curiale, J. A., 2008, Oil-source rock correlations - Limitations and recommendations: Organic Geochemistry, v. 39, no. 8, p. 1150-1161.

Dewaker, K. N., Chandra, K., Arunachalam, J., and Karunasagar, D., 2000, Isotopic fractionation of Ni60/Ni61 in kerogen and bitumen samples: Current Science, v. 79, no. 12, p. 1720-1723.

Dow, W. G., 1974, Application of Oil-Correlation and Source-Rock Data to Exploration in Williston Basin: American Association of Petroleum Geologists Bulletin, v. 58, no. 7, p. 1253-1262.

Duke, M. J. M., 1983, Geochemistry of the Exshaw Shale of Alberta: An application of neutron activation analysis and related techniques: M.Sc. thesis, University of Alberta.

Dwiggins, C. W. J., Willcox, K. W., Dougaty, D. A., and Heemstra, R. J., 1969, Separation and characterization of metallo-organic materials in petroleum: U.S. Bureau of Mines Report of Investigations 7273, p. 41 p.

Ellrich, J., Hirner, A., and Stärk, H., 1985, Distribution of trace elements in crude oils from southern Germany: Chemical Geology, v. 48, no. 1-4, p. 313-323.

Erickson, R. L., Myers, A. T., and Horr, C. A., 1954, Association of uranium and other metals with crude oil, asphalt, and petroliferous rocks: American Association of Petroleum Geologists Bulletin, v. 38, p. 2200-2218.

Filby, R. H., 1975, The nature of metals in petroleum, *in* Yen, ed., The Role of Trace Elements in Petroleum, Ann Arbor Science Publishers, p. 31-58.

Finlay, A. J., Selby, D., and Osborne, M. J., 2011, Re-Os geochronology and fingerprinting of United Kingdom Atlantic margin oil: Temporal implications for regional petroleum systems: Geology, v. 39, no. 5, p. 475-478.

Gall, L., Williams, H., Siebert, C., and Halliday, A., 2012, Determination of mass-dependent variations in nickel isotope compositions using double spiking and MC-ICPMS: Journal of Analytical Atomic Spectrometry, v. 27, no. 1.

Hatch, J. R., and Leventhal, J. S., 1992, Relationship between inferred redox potential of the depositional environment and geochemistry of the Upper Pennsylvanian (Missourian) Stark Shale Member of the Dennis Limestone, Wabaunsee County, Kansas, U.S.A: Chemical Geology, v. 99, no. 1-3, p. 65-82.

Hitchon, B., and Filby, R. H., 1984, Use of trace elements for classification of crude oils into families - example from Alberta, Canada: American Association of Petroleum Geologists Bulletin, v. 68, p. 838-849.

Hodgson, G. W., 1954, Vanadium, nickel, and iron trace metals in crude oils of Western Canada: American Association of Petroleum Geologists Bulletin, v. 38, p. 2537-2554.

Hodgson, G. W., Fiores, J., and Baker, B. L., 1959, Geochemical aspects of petroleum migration in Pembina, Red Water, Joffre and Lloyd-Minster oilfields of Alberta and Saskatchewan, Canada: American Association of Petroleum Geologists Bulletin, v. 43, p. 311-328.

Hoefs, J., and Frey, M., 1976, The isotopic composition of carbonaceous matter in a metamorphic profile from the Swiss Alps: Geochimica et Cosmochimica Acta, v. 40, no. 8, p. 945-951.

Huc, A. Y., Lallier-Vergès, E., Bertrand, P., Carpentier, B., and Hollander, D. J., 1992, Organic matter response to change of depositional environment in Kimmeridgian shales, Dorset, UK, Organic Matter: Productivity, Accumulation, and Preservation in Recent and Ancient Sediments: New York, Columbia University Press, p. 469-486.

Hunt, J., 1979, Petroleum Geochemistry and Geology, Freeman, San Francisco, California, 617 pp.

Hunt, J. M., Stewart, F., and Dickey, P. A., 1954, Origin of hydrocarbons of Uinta Basin, Utah: American Association of Petroleum Geologists Bulletin, v. 38, p. 1671-1698.

Issler, D. R., Willett, S. D., Beaumont, C., Donelick, R. A., and Grist, A. M., 1999, Paleotemperature history of two transects across the Western Canada Sedimentary Basin: Constraints from apatite fission track analysis: Bulletin of Canadian Petroleum Geology, v. 47, p. 475-486.

Jones, B., and Manning, D. A. C., 1994, Comparison of geochemical indices used for the interpretation of palaeoredox conditions in ancient mudstones: Chemical Geology, v. 111, no. 1-4, p. 111-129.

Jones, T. P., Fortier, S. M., Mosbrugger, V., Roessler, J., Utescher, T., and Ashraf, A. R., 1997, $^{13}C/^{12}C$ ratio double cyclicity in a Miocene browncoal: isotopic signals and orbital forcing: Terra Nova, v. 9, p. 19-23.

Killops, S. D., Cook, R. A., Sykes, R., and Boudou, J. P., 1997, Petroleum potential and oil-source correlation in the Great South and Canterbury Basins: New Zealand Journal of Geology and Geophysics, v. 40, no. 4, p. 405-423.

Leenheer, M. J., 1984, Mississippian Bakken and other equivalent formations as source rocks in the Western Canada basin: Organic Geochemistry, v. 6, p. 521-533.

Lewan, M. D., 1980, Geochemistry of vanadium and nickel in organic matter of sedimentary rocks: Ph.D. dissertation, Univ. of Cincinnati.

Lewan, M. D., 1983, Effects of thermal maturation on stable organic carbon isotopes as determined by hydrous pyrolysis of Woodford Shale: Geochimica et Cosmochimica Acta, v. 47, no. 8, p. 1471-1479.

Lewan, M. D., 1984, Factors controlling the proportionality of vanadium to nickel in crude oils: Geochimica et Cosmochimica Acta, v. 48, no. 11, p. 2231-2238.

Lewan, M. D., and Maynard, J. B., 1982, Factors controlling enrichment of vanadium and nickel in the bitumen of organic sedimentary rocks: Geochimica et Cosmochimica Acta, v. 46, no. 12, p. 2547-2560.

López, L., Lo Mónaco, S., Galarraga, F., Lira, A., and Cruz, C., 1995, VNi ratio in maltene and asphaltene fractions of crude oils from the west Venezuelan basin: correlation studies: Chemical Geology, v. 119, no. 1-4, p. 255-262.

Manning, L. K., Frost, C. D., and Branthaver, J. F., 1991, A neodymium isotopic study of crude oils and source rocks: potential applications for petroleum exploration: Chemical Geology, v. 91, no. 2, p. 125-138.

Maréchal, C. N., Télouk, P., and Albarède, F., 1999, Precise analysis of copper and zinc isotopic compositions by plasma-source mass spectrometry: Chemical Geology, v. 156, no. 1–4, p. 251-273.

Meijer, N. C., and Johnston, D. I., 1993, Geology of the Devonian-Carboniferous boundary beds in Alberta: Karvonen, R.

Meijer, N. C., Johnston, D. I., and Fullmer, E. G., 1994, Devonian stratigraphy and depositional history across Peace River Highland, west central Alberta and nearby British Columbia: Geological Survey of Canada Open File 2851, p. 40 pp.

Moldowan, J. M., Albrecht, P., and Philip, R. P., 1992, Biological Markers in Sediments and Petroleum, Prentice Hall, Englewood Cliffs, NJ, 410 pp. p.:

Onyema, M. O., and Manilla, P. N., 2010, Light Hydrocarbon Correlation of Niger Delta Crude Oils: Journal of American Science, v. 6, no. 6, p. 82-88.

Peters, K. E., 1986, Guidelines for evaluating petroleum source rock using programmed pyrolysis: American Association of Petroleum Geologists Bulletin, v. 70, no. 3, p. 318-329.

Peters, K. E., and Moldowan, J. M., 1993, The Biomarker Guide, Prentice Hall, Englewood Cliffs, NJ.

Peucker-Ehrenbrink, B., and Hannigan, R. E., 2000, Effects of black shale weathering on the mobility of rhenium and platinum group elements: Geology, v. 28, no. 5, p. 475-478.

Piggott, N., and Lines, M. D., 1992, A case study of migration from the West Canada Basin, *in* England, W. A., and Fleet, A. J., eds., Petroleum Migration, Volume 59, Geological Society Special Publication, p. 207-225.

Quitté, G., and Oberli, F., 2006, Quantitative extraction and high precision isotope measurements of nickel by MC-ICPMS: Journal of Analytical Atomic Spectrometry, v. 21, p. 1249-1255.

Richards, B. C., and Higgins, A. C., 1988, Devonian-Carboniferous beds of the Palliser and Exshaw formations at Jura Creekm Rocky Mountains, southwestern Alberta, *in* McMillan, N. J., ed., Devonian of the world, Canadian Society of Petroleum Geologists Memoir, Volume 14, p. 399-412.

Richards, B. C., Mamet, B. L., and Bamber, E. W., 1999, Uppermost Devonian and Carboniferous sequence stratigraphy, biostratigraphy and basin development, Banff region, southwestern Alberta, XIV International Congress on the Carboniferous and Permian, Field Trip, 4-7 and 4-17 Guidebook: Calgary, Alberta.

Richards, C., Ross, G. M., and Utting, J., 2002, U-Pb geochronology, lithostratigraphy and biostratigraphy of tuff in the Upper Famennian to Tournaisian Exshaw Formation: Evidence for a mid-Paleozoic magmatic arc on the northwestern margin of North America, *in* Hills, L. V., Henderson, C. M., and Bamber, E. W., eds., Carboniferous and Permian of the World: XIV ICCP Proceedings, Volume 19, Can Soc Petrol Geol Mem, p. 158-207.

Schovsbo, N. H., 2001, Why barren intervals? A taphonomic case study of the Scandinavian Alum Shale and its faunas: Lethaia, v. 34, no. 4, p. 271-285.

Scotchman, I. C., Griffith, C. E., Holmes, A. J., and Jones, D. M., 1998, The Jurassic petroleum system north and west of Britain: a geochemical oil-source correlation study: Organic Geochemistry, v. 29, no. 1–3, p. 671-700.

Selby, D., and Creaser, R. A., 2005, Direct radiometric dating of the Devonian-Mississippian time-scale boundary using the Re-Os black shale geochronometer: Geology, v. 33, p. 545-548.

Selby, D., and Creaser, R. A., 2005, Direct Radiometric Dating of Hydrocarbon Deposits Using Rhenium-Osmium Isotopes: Science, v. 308, p. 1293.

Selby, D., Creaser, R. A., Dewing, K., and Fowler, M., 2005, Evaluation of bitumen as a ^{187}Re–^{187}Os geochronometer for hydrocarbon maturation and migration: A test case from the Polaris MVT deposit, Canada: Earth and Planetary Science Letters, v. 235, no. 1–2, p. 1-15.

Selby, D., Creaser, R. A., and Fowler, M. G., 2007, Re–Os elemental and isotopic systematics in crude oils: Geochimica et Cosmochimica Acta, v. 71, no. 2, p. 378-386.

Stahl, W. J., 1978, Source rock-crude oil correlation by isotopic type-curves: Geochimica et Cosmochimica Acta, v. 42, no. 10, p. 1573-1577.

Tissot, B. P., and Welte, D. H., 1984, Petroleum Formation and Occurrence, Springer, Berlin.

Treibs, A., 1934, Chlorophyll- und Häminderivate in bituminösen Gesteinen, Erdölen, Erdwachsen und Asphalten: Ann. Chem., v. 510, p. 42-62.

Tyson, R. V., 1995, Sedimentary organic matter, organic facies and palynofacies, London, Chapman & Hall.

Vine, J. D., and Tourtelot, E. B., 1970, Geochemistry of black shale deposits - A summary report: Economic Geology, v. 65, p. 253-272.

Wang, Z., Fingas, M., and Page, D. S., 1999, Oil spill identification: Journal of Chromatography A, v. 843, no. 1–2, p. 369-411.

Wedepohl, K. H., 1971, Environmental influences on the chemical composition of shales and clays: Physics and Chemistry of The Earth, v. 8, p. 305-333.

Welte, D. H., 1966, Correlation problems among crude oils, *in* Hobson, G. D., and Speers, G. C., eds., Advances in organic geochemistry: London, Pergamon Press, p. 111-127.

Williams, J. A., 1974, Characterization of Oil Types in Williston Basin: American Association of Petroleum Geologists Bulletin, v. 58, no. 7, p. 1243-1252.

Witherspoon, P. A., and Nagashima, K., 1957, Use of trace metals to identify Illinois crude oils: Illinois State Geological Survey, Circular, v. 239, p. 15.

Zafiriou, O. C., Myers, J., Bourbonniere, R., and Freestone, F. J., 1973, Oil Spill-Source Correlation by Gas Chromatography: An Experimental Evaluation og System Performance, Prevention and Control of Oil Spills, Proceedings of Joint Conference: Washington, DC, p. 153-159.

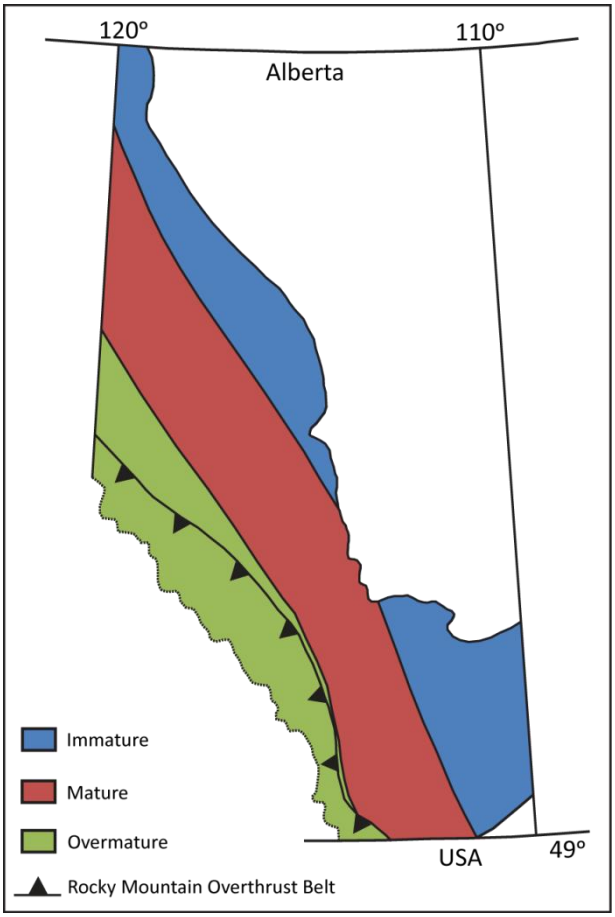

Figure 5.1: Present-day maturity map of the Exshaw Formation within Alberta, Canada (modified from Creaney and Allan, 1991). Map shows the location of the thermally immature, mature and overmature zones parallel to the Rocky Mountain Front.

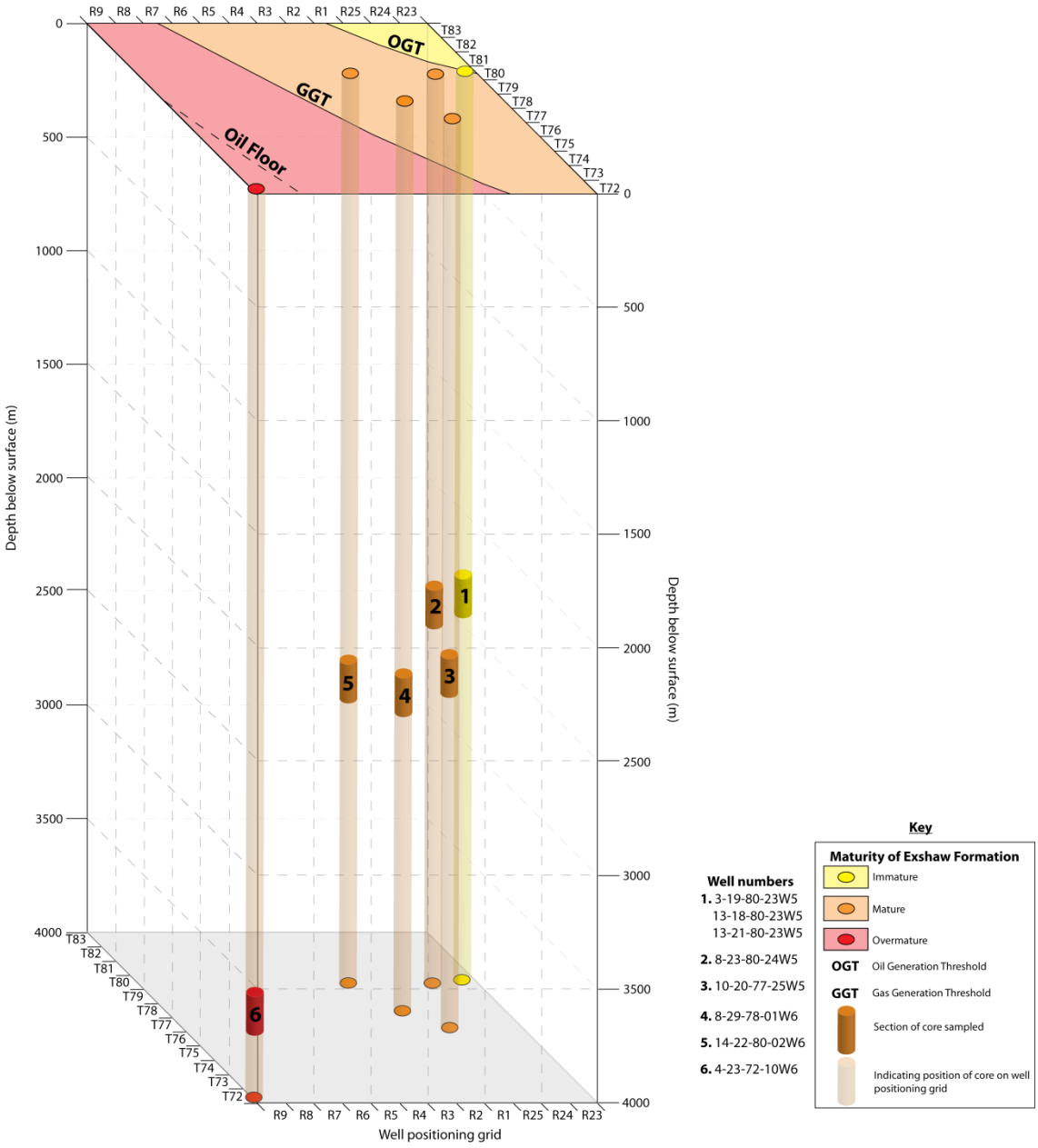

Figure 5.2: Block diagram illustrating the location of the Exshaw Formation sample cores within the Well Positioning Grid, and relative to the Oil Floor, Oil Generation Threshold and Gas Generation Threshold. Diagram shows the relative depths of the cores sampled, and their relative thermal maturity. Well Positioning Grid modified from Piggott and Lines (1992).

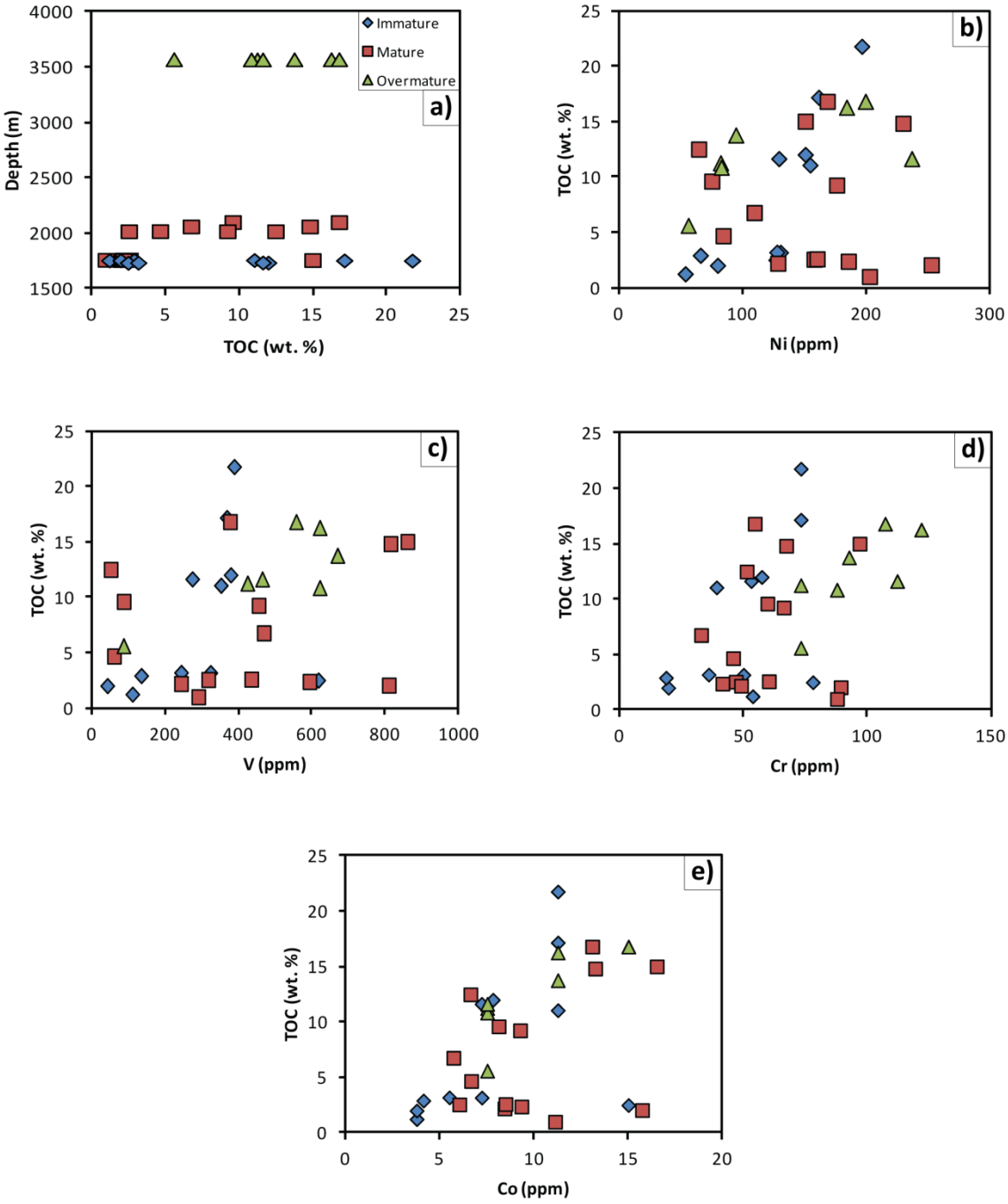

Figure 5.3: Plots showing the relationships between TOC, the trace elements, and depth and degree of thermal maturation: a) Depth vs. TOC; b) TOC vs. Ni; c) TOC vs. V; d) TOC vs. Cr; and e) TOC vs. Co.

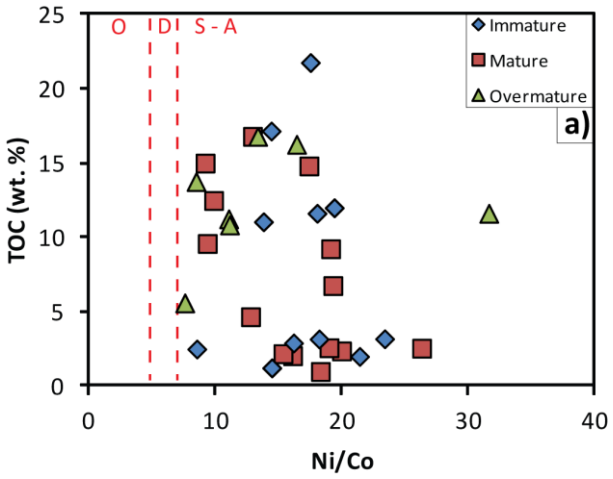

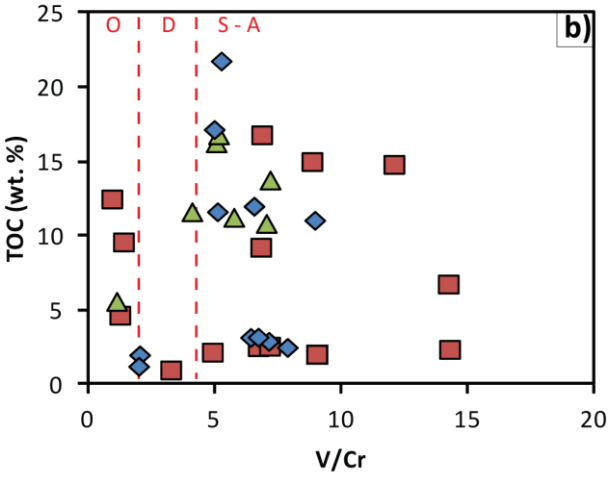

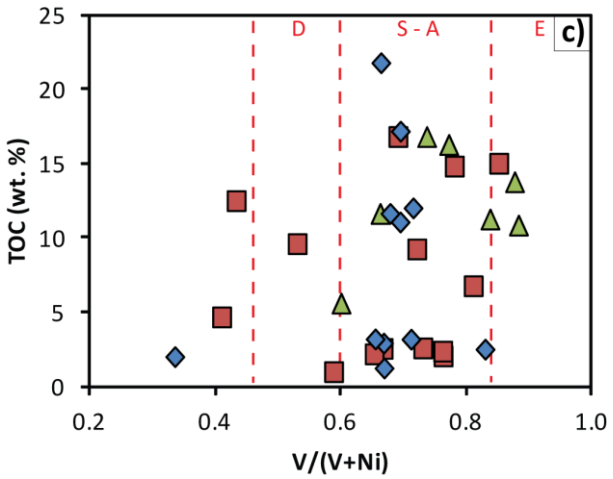

Figure 5.4: Plots illustrating the relationships between TOC, the trace element ratios used as paleoredox proxies, and the level of thermal maturation within the Exshaw Formation: a) TOC vs. Ni/Co; b) TOC vs. V/Cr; and c) TOC vs. V/(V+Ni). Values for Ni/Co and V/Cr are taken from Jones and Manning (1994), and the ranges for V/(V+Ni) are from Hatch and Leventhal (1992).

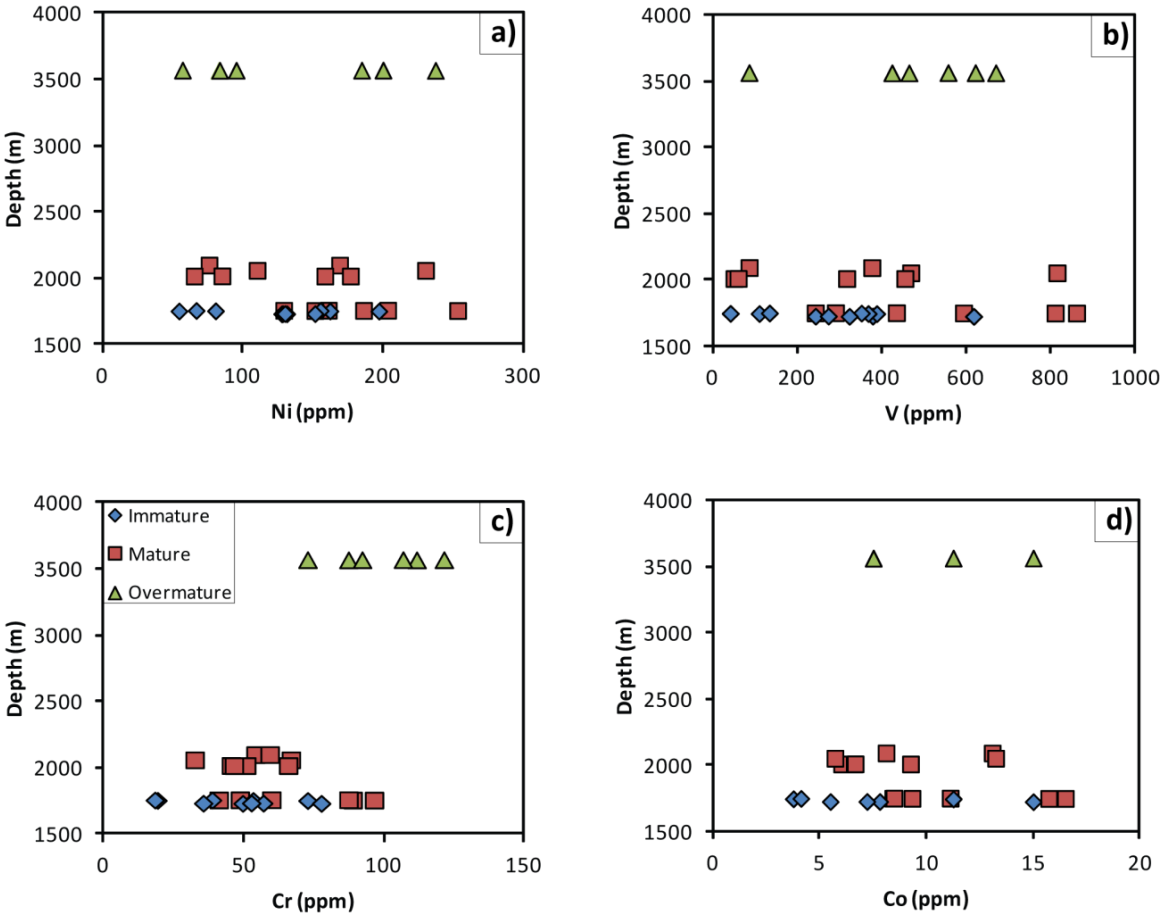

Figure 5.5: Plots showing the relationships between the trace elements, and depth and degree of thermal maturation: a) Depth vs. Ni; b) Depth vs. V; c) Depth vs. Cr; and d) Depth vs. Co.

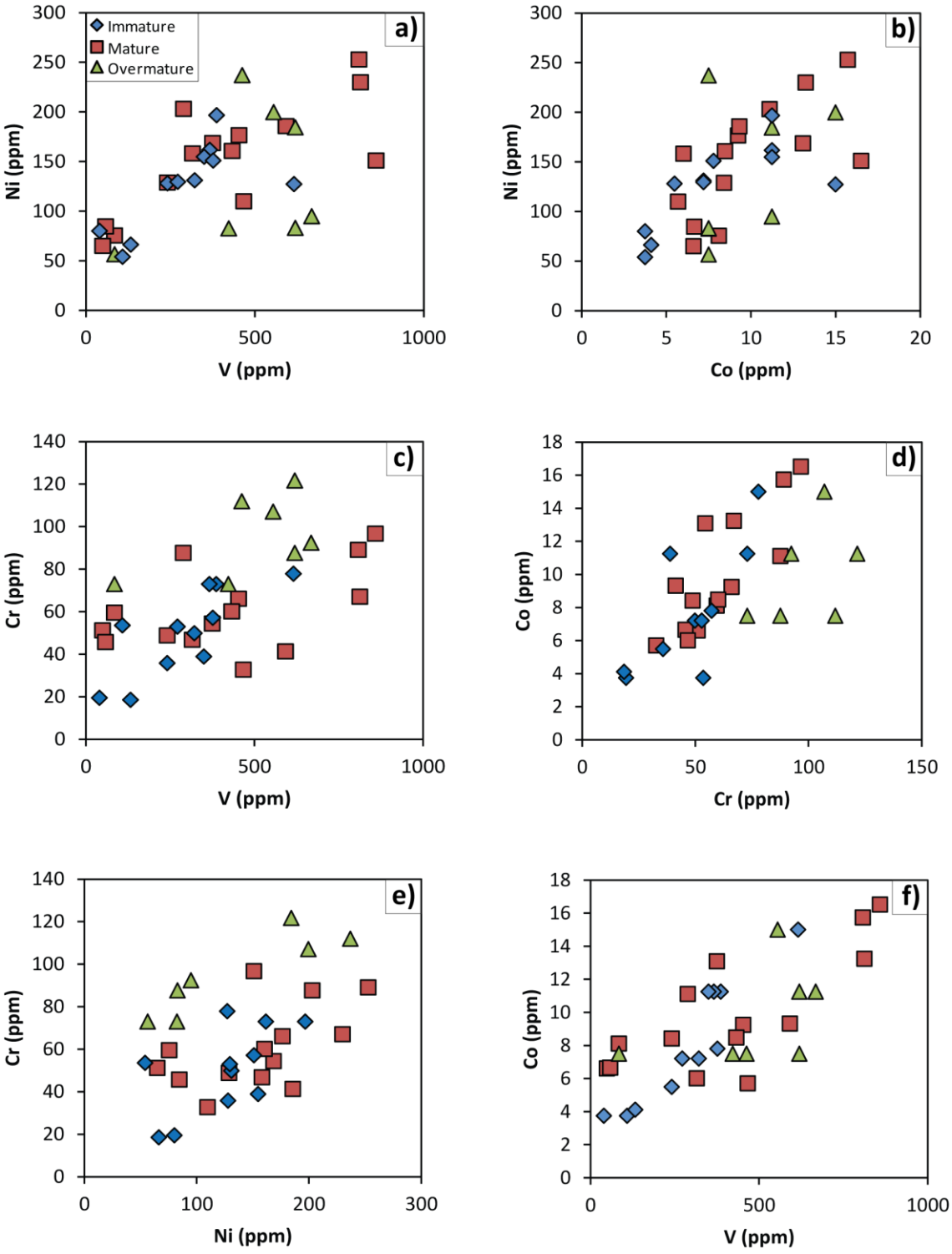

Figure 5.6: Crossplots of trace element abundances for the Exshaw Formation: a) Ni vs. V; b) Ni vs. Co; c) Cr vs. V; d) Cr vs. Co; e) Cr vs. Ni; and f) Co vs. V.

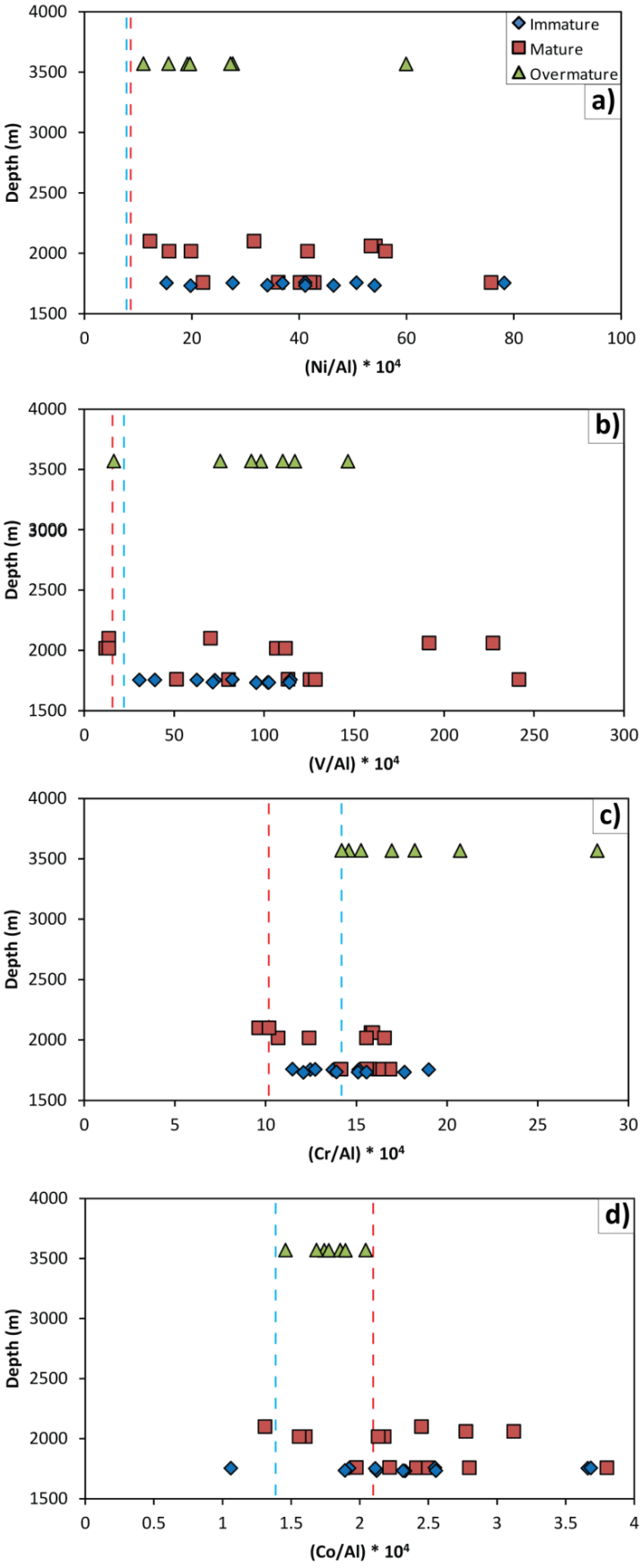

Figure 5.7: Plots showing the aluminium-normalised trace element values for the Exshaw Formation shales and their degree of enrichment relative to average shale values (red dashed line; from Wedepohl, 1971) and average black shale values (blue dashed line; from Vine and Tourelot, 1970): a) Ni/Al; b) V/Al; c) Cr/Al; and d) Co/Al.

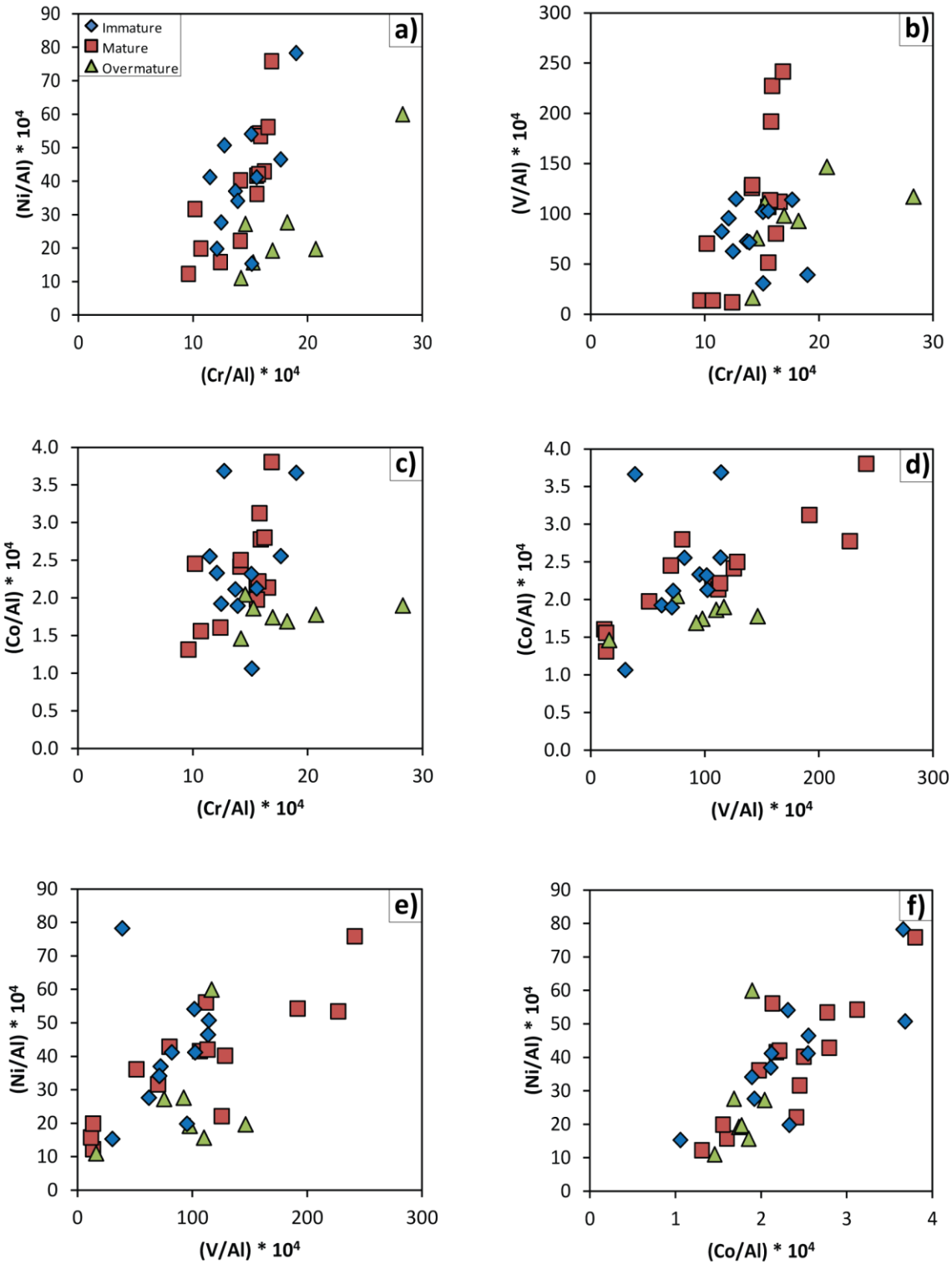

Figure 5.8: Crossplots of aluminium-normalised trace element values: a) Ni/Al vs. Cr/Al; b) V/Al vs. Cr/Al; c) Co/Al vs. Cr/Al; d) Co/Al vs. V/Al; e) Ni/Al vs. V/Al; and f) Ni/Al vs. Co/Al.

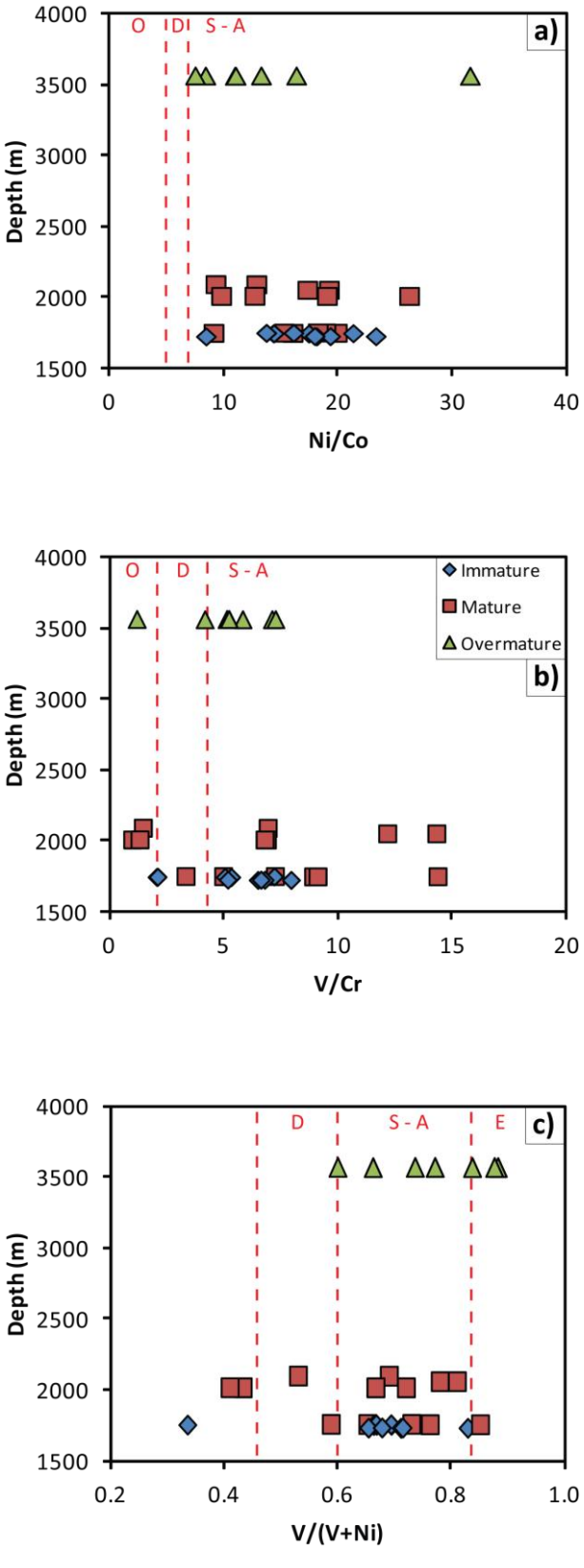

Figure 5.9: Plots showing the relationships between the paleoredox proxies and depth and degree of thermal maturation in the Exshaw Formation: a) Ni/Co; b) V/Cr; and c) V/(V+Ni). Red dashed lines indicate the ranges for Ni/Co and V/Cr (Jones and Manning, 1994) and V/(V+Ni) (Hatch and Leventhal, 1992).

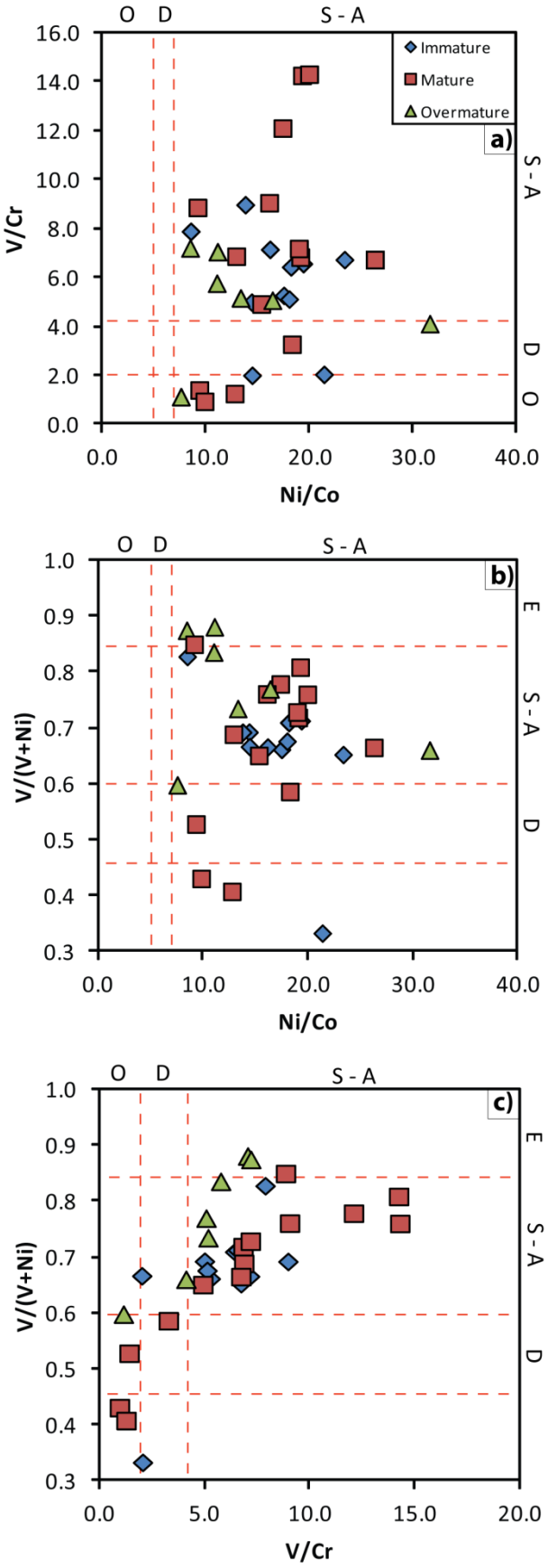

Figure 5.10: Crossplots of the trace element ratios used as paleoredox proxies: a) V/Cr vs. Ni/Co; b) V/(V+Ni) vs. Ni/Co; and c) V/(V+Ni) vs. V/Cr. Red dashed lines indicate the ranges for Ni/Co and V/Cr (Jones and Manning, 1994) and V/(V+Ni) (Hatch and Leventhal, 1992).

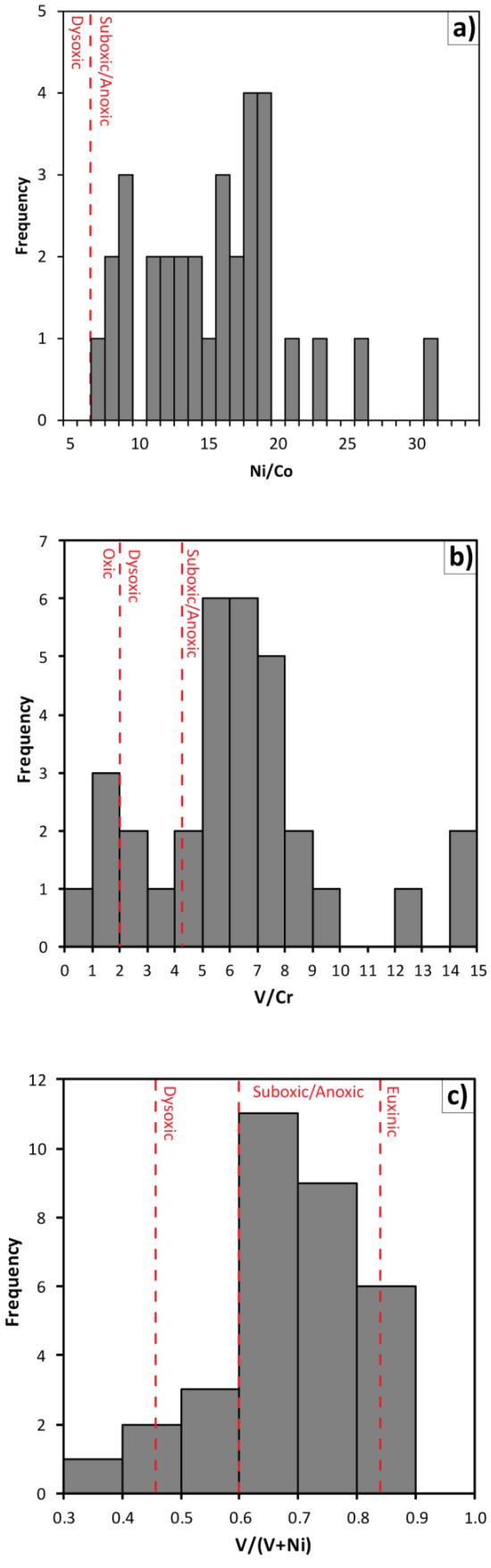

Figure 5.11: Histograms for the paleoredox proxies: a) Ni/Co; b) V/Cr; and c) V/(V+Ni). Values defining the redox conditions for V/Cr and Ni/Co are from Jones and Manning (1994) and ranges for V/(V+Ni) are taken from Hatch and Leventhal (1992) (red dashed lines).

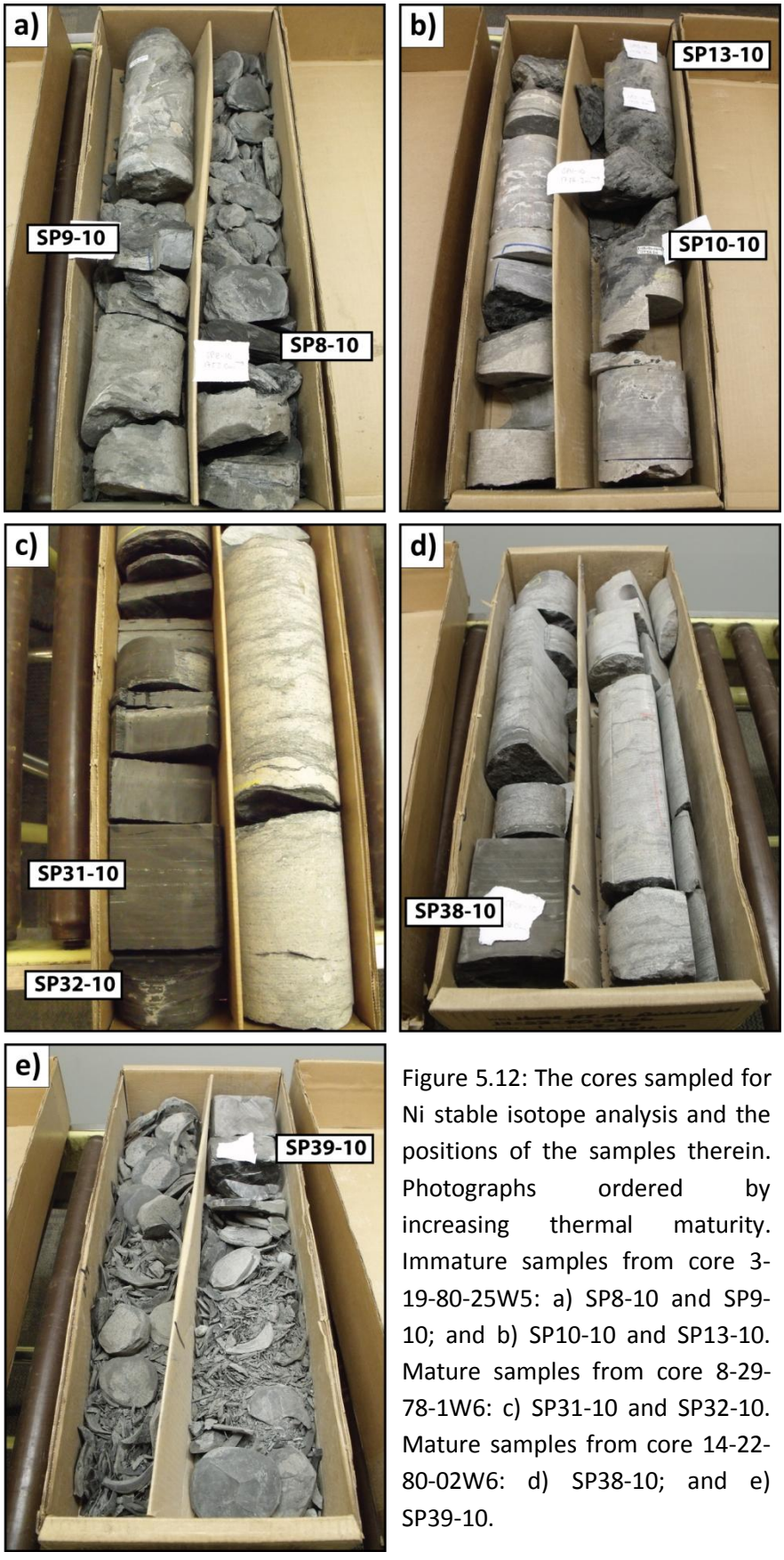

Figure 5.12: The cores sampled for Ni stable isotope analysis and the positions of the samples therein. Photographs ordered by increasing thermal maturity. Immature samples from core 3-19-80-25W5: a) SP8-10 and SP9-10; and b) SP10-10 and SP13-10. Mature samples from core 8-29-78-1W6: c) SP31-10 and SP32-10. Mature samples from core 14-22-80-02W6: d) SP38-10; and e) SP39-10.

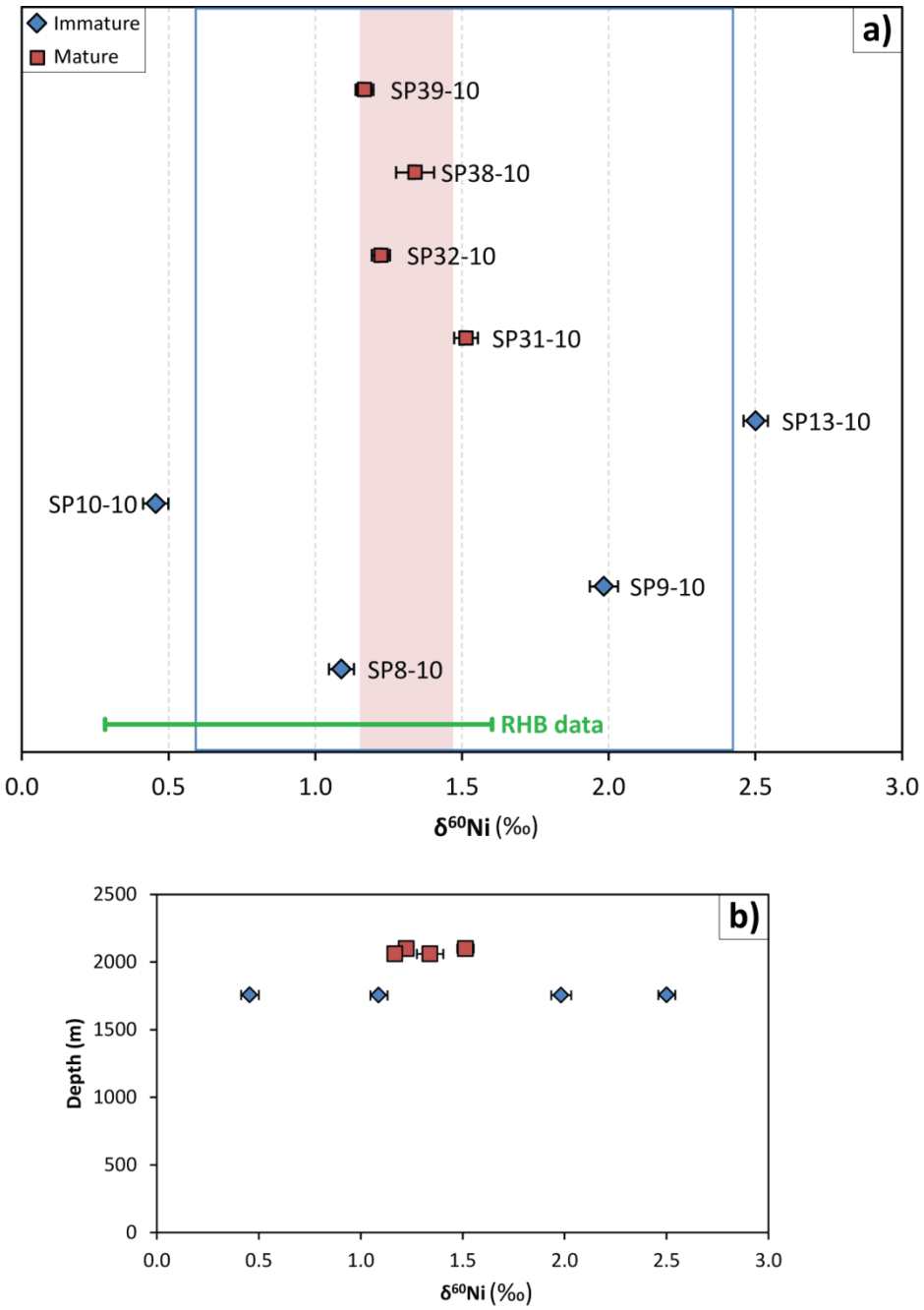

Figure 5.13: New Ni stable isotope data for the Exshaw Formation: a) Samples ordered by thermal maturity. The red box indicates the average of the δ^{60}Ni values for the mature shales (~1.31 ‰ and 1 standard deviation either side of this), and the blue box outlines the average δ^{60}Ni value for the immature shales (~1.51 ‰ and 1 standard deviation either side of this). The green error bar marks the range of δ^{60}Ni values for the Robin Hood's Bay (RHB) samples (this thesis, Chapter 4); b) samples ordered by depth.

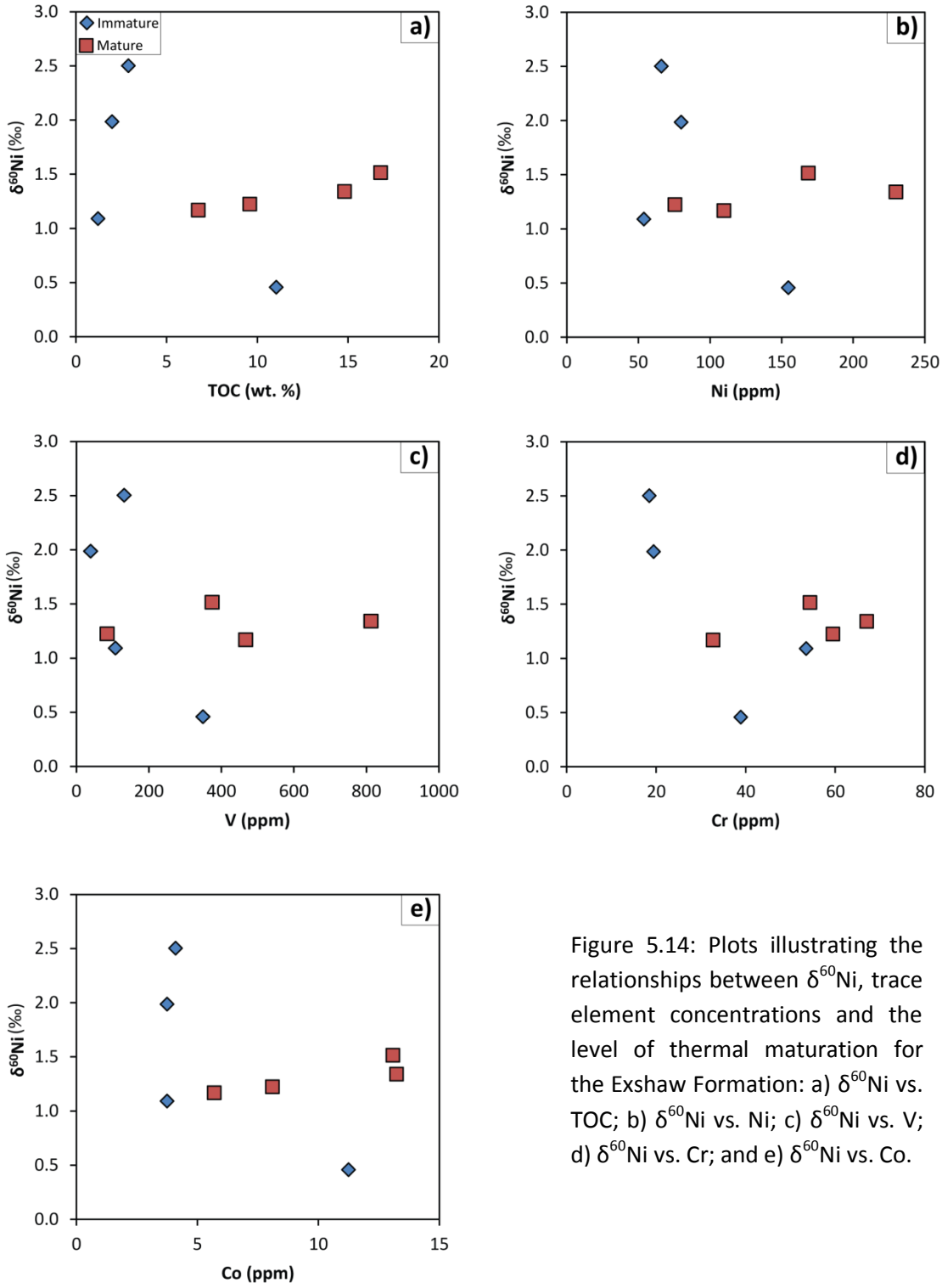

Figure 5.14: Plots illustrating the relationships between δ^{60}Ni, trace element concentrations and the level of thermal maturation for the Exshaw Formation: a) δ^{60}Ni vs. TOC; b) δ^{60}Ni vs. Ni; c) δ^{60}Ni vs. V; d) δ^{60}Ni vs. Cr; and e) δ^{60}Ni vs. Co.

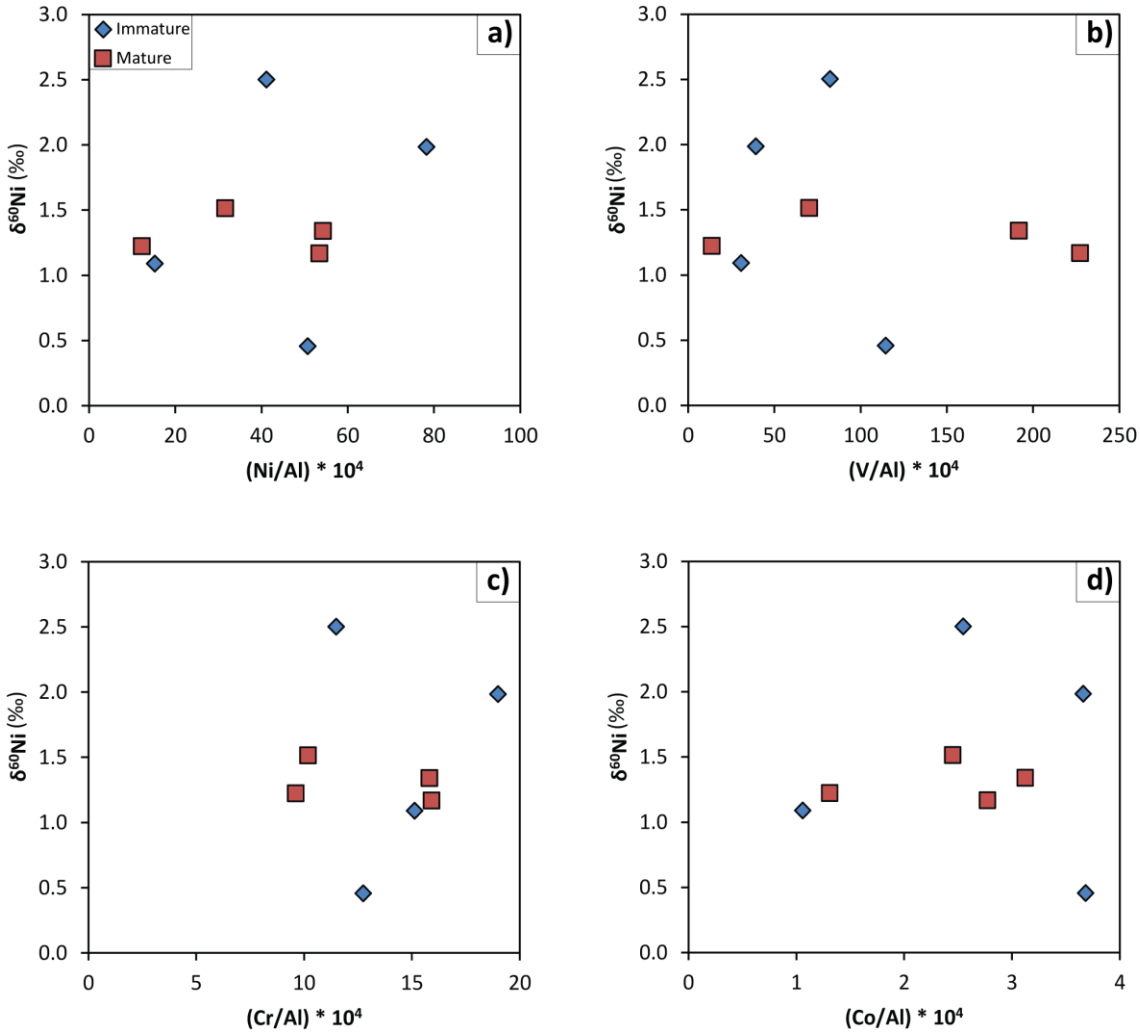

Figure 5.15: Plots illustrating the relationships between δ^{60}Ni, Al-normalised trace element values and the level of thermal maturation for the Exshaw Formation: a) δ^{60}Ni vs. Ni/Al; b) δ^{60}Ni vs. V/Al; c) δ^{60}Ni vs. Cr/Al; and d) δ^{60}Ni vs. Co/Al.

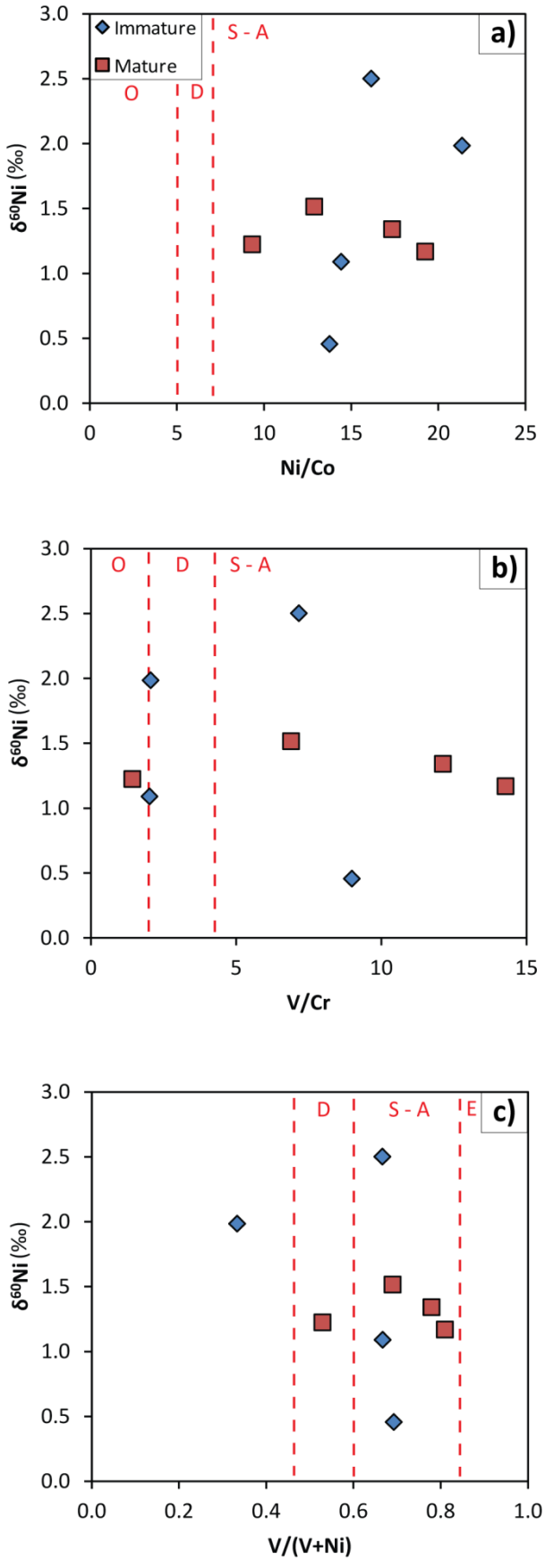

Figure 5.16: Plots showing the relationship between δ^{60}Ni, the paleoredox proxies and the degree of thermal maturation for the Exshaw Formation: a) δ^{60}Ni vs. Ni/Co; b) δ^{60}Ni vs. V/Cr; and c) δ^{60}Ni vs. V/(V+Ni). Ranges for Ni/Co and V/Cr are taken from Jones and Manning (1994), and values for V/(V+Ni) are from Hatch and Leventhal (1992) (red dashed lines). Abbreviations in red reflect each paleoredox environment: O, oxic; D, dysoxic; S – A, suboxic-anoxic; and E, euxinic.

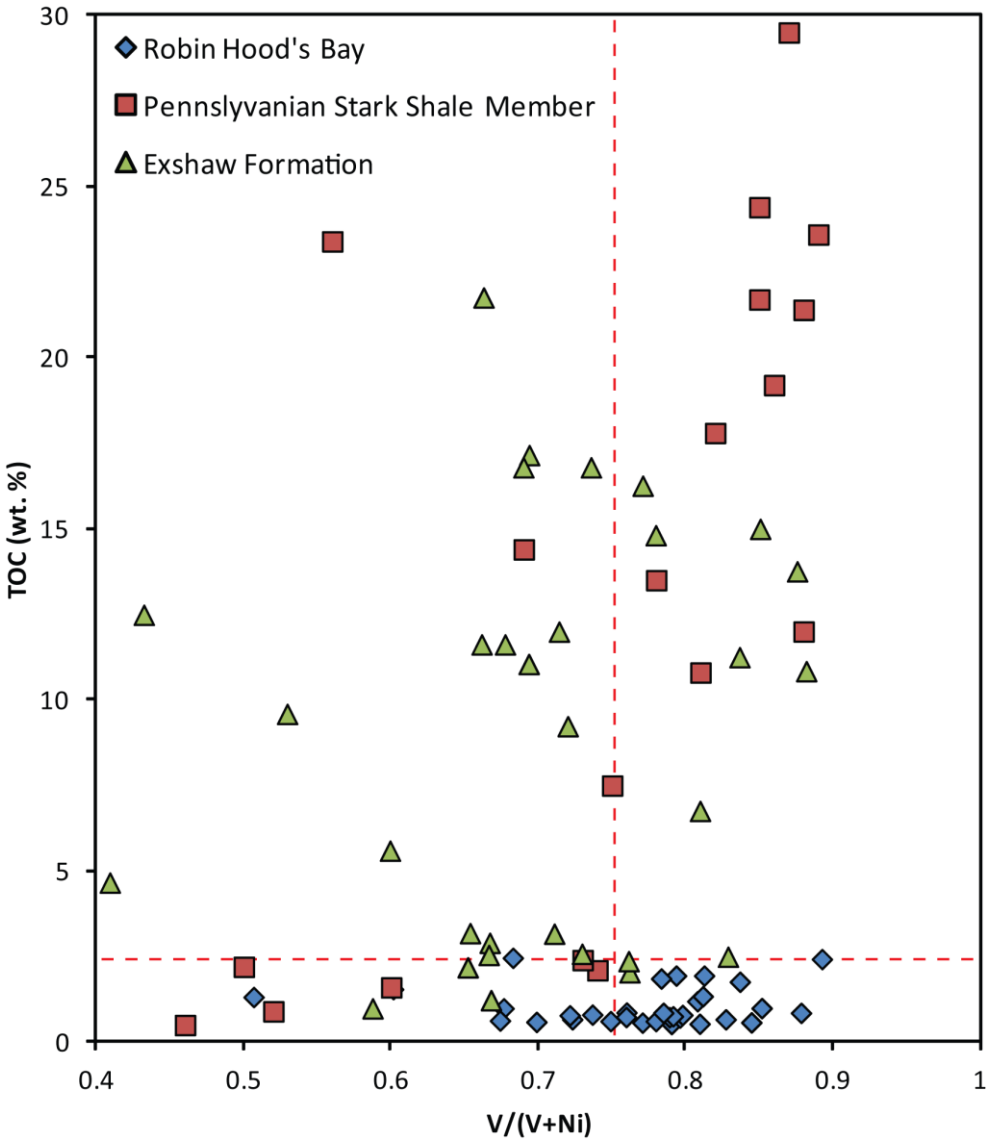

Figure 5.17: Plot showing the relationship between TOC and V/(V+Ni) for the Pennsylvanian Stark Shale Member samples (red squares) detailed in Hatch and Leventhal (1992), Robin Hood's Bay sediments (blue diamonds; Chapter 4) and the Exshaw Formation shales (green triangles; this study). Red dashed lines mark parameters discussed in Hatch and Leventhal (1992), whereby values of > 2.5 wt. % TOC correspond to V/(V+Ni) values > 0.75 for the Pennsylvanian Stark Shale Member (see text for discussion).

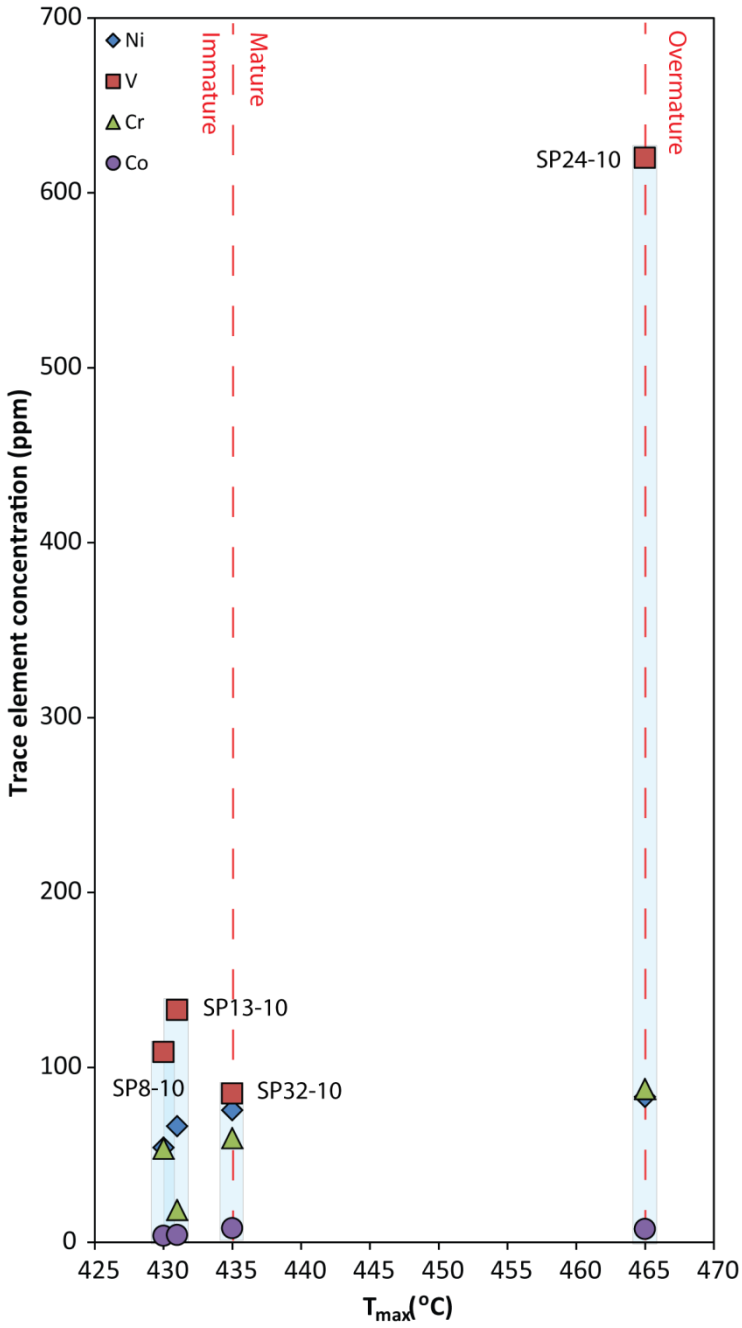

Figure 5.18: Plots showing the relationship between hydrocarbon maturity level (defined by T_{max} values) and trace element concentrations (Ni, blue diamonds; V, red squares; Cr, green triangles; and Co, purple circles) for the Exshaw Formation. The four samples used in this study (SP8-10, SP13-10, SP24-10 and SP32-10) are from the same cores and depths as those analysed by Creaser *et al.* (2002) (PEx 8, PEx 10, PEx 21 and PEx 14), and as such the corresponding T_{max} values determined by that study have been used here. The red dashed lines define the T_{max} values representing the transition between the different levels of thermal maturity (immature, <435 °C; mature, 435 – 465 °C; and overmature, > 465 °C; Peters, 1986). The transparent blue boxes group together the trace element data for each individual sample.

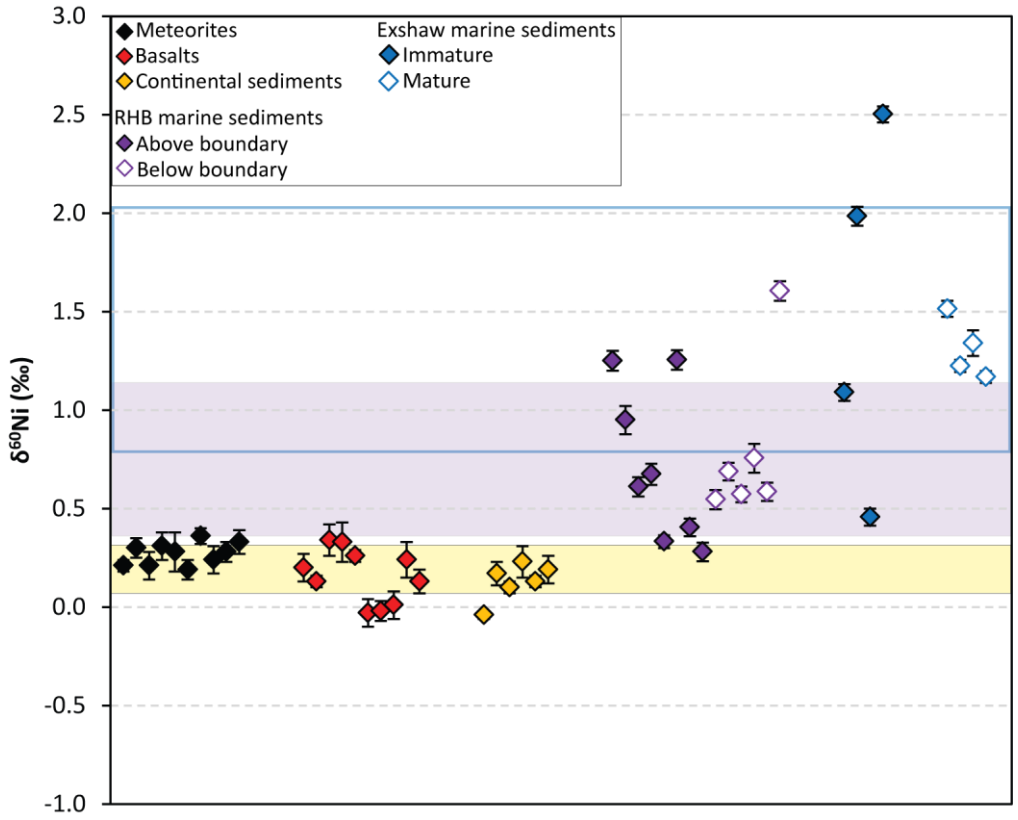

Figure 5.19: Nickel stable isotope data for extraterrestrial samples (meteorites), abiotic terrestrial samples (basalts and continental sediments) and marine organic-rich sediments. Continental sediments include river and aeolian sediments. The yellow box represents the average of the Ni isotope data for the meteorites, basalts and continental sediments (0.2 ‰ and 1 standard deviation either side of this; Cameron *et al.,* 2009). The purple box indicates the average of the Ni isotope data for the Robin Hood's Bay marine sediments (0.8 ‰ and 1 standard deviation either side of this; this study). The blue outline shows the average of the Ni isotope data for the Exshaw Formation shales (1.5 ‰ and 1 standard deviation either side of this; this study). Data for the extraterrestrial and abiotic terrestrial samples taken from Cameron *et al.* (2009). Abbreviation 'RHB' refers to Robin Hood's Bay (this study).

Table 5.1: Exshaw Formation sample identification, together with sample depth (m), degree of thermal maturation, and the number of the core from which the samples were taken.

Sample ID[a]	Depth (m)	Core	Maturity
SP1-10	1751.8	**3-19-80-23W5**	Immature
SP7-10	1752.9		
SP8-10	1753		
SP9-10	1754		
SP10-10	1756.2		
SP13-10	1756.5		
SP15-10	1731.5	**13-18-80-23W5**	Immature
SP52-10	1731.8	**13-21-80-23W5**	Immature
SP53-10	1732.8		
SP54-10	1733.15		
SP55-10	1733.85		
SP31-10	2099.1	**8-29-78-01W6**	Mature
SP32-10	2099.2		
SP38-10	2060	**14-22-80-02W6**	Mature
SP39-10	2059.8		
SP47-10	2016.4	**10-20-77-25W5**	Mature
SP48-10	2016.7		
SP49-10	2017		
SP50-10	2016.2		
SP62-10	1756.35	**8-23-80-24W5**	Mature
SP63-10	1756.8		
SP64-10	1757.4		
SP65-10	1757.75		
SP66-10	1758.65		
SP67-10	1759.35		
SP23-10	3567.5	**4-23-72-10W6**	Overmature
SP24-10	3567.7		
SP25-10	3568.2		
SP26-10	3568.7		
SP27-10	3569.45		
SP29-10	3567.2		
SP30-10	3569.1		

[a] Samples listed in order of increasing thermal maturity

Table 5.2: Summary of trace element data and the associated ratios used for paleoredox proxies, and TOC data for the Exshaw Formation.

			Trace elements (ppm)				Redox ratios			TOC
Sample ID[a]	Depth (m)	Maturity[b]	V	Cr	Co	Ni	V/Cr	Ni/Co	V/(V+Ni)	(wt.%)
SP1-10	1751.8	I	386.4	73.0	11.3	196.7	5.3	17.5	0.66	21.8
SP7-10	1752.9	I	366.3	73.0	11.3	161.8	5.0	14.4	0.69	17.2
SP8-10	1753	I	108.7	53.5	3.8	54.1	2.0	14.4	0.67	1.2
SP9-10	1754	I	40.3	19.5	3.8	80.1	2.1	21.4	0.33	2.0
SP10-10	1756.2	I	350.2	38.9	11.3	154.9	9.0	13.8	0.69	11.0
SP13-10	1756.5	I	132.8	18.5	4.1	66.3	7.2	16.1	0.67	2.9
SP15-10	1731.5	I	615.9	77.8	15.0	127.3	7.9	8.5	0.83	2.5
SP52-10	1731.8	I	321.7	49.8	7.2	131.0	6.5	18.2	0.71	3.2
SP53-10	1732.8	I	241.6	35.8	5.5	128.1	6.8	23.4	0.65	3.2
SP54-10	1733.15	I	376.9	57.2	7.8	151.0	6.6	19.4	0.71	12.0
SP55-10	1733.85	I	272.1	52.9	7.2	129.7	5.1	18.0	0.68	11.6
SP31-10	2099.1	M	375.1	54.4	13.1	168.7	6.9	12.9	0.69	16.8
SP32-10	2099.2	M	85.0	59.5	8.1	75.6	1.4	9.3	0.53	9.6
SP38-10	2060	M	813.2	67.1	13.2	229.9	12.1	17.4	0.78	14.8
SP39-10	2059.8	M	467.1	32.7	5.7	109.8	14.3	19.3	0.81	6.8
SP47-10	2016.4	M	453.3	66.1	9.2	176.4	6.9	19.1	0.72	9.2
SP48-10	2016.7	M	49.4	51.1	6.6	64.9	1.0	9.8	0.43	12.5
SP49-10	2017	M	58.6	45.6	6.7	84.7	1.3	12.7	0.41	4.7
SP50-10	2016.2	M	315.7	46.7	6.0	158.2	6.8	26.3	0.67	2.5
SP62-10	1756.35	M	859.3	96.7	16.5	151.0	8.9	9.1	0.85	15.0
SP63-10	1756.8	M	808.7	89.1	15.7	252.9	9.1	16.1	0.76	2.0
SP64-10	1757.4	M	592.1	41.3	9.3	185.8	14.3	19.9	0.76	2.4
SP65-10	1757.75	M	241.4	48.8	8.4	128.8	4.9	15.3	0.65	2.2
SP66-10	1758.65	M	433.1	60.1	8.5	160.6	7.2	19.0	0.73	2.6
SP67-10	1759.35	M	288.9	87.6	11.1	203.0	3.3	18.3	0.59	1.0
SP23-10	3567.5	O	422.7	73.0	7.5	82.6	5.8	11.0	0.84	11.2
SP24-10	3567.7	O	619.9	87.6	7.5	83.1	7.1	11.1	0.88	10.8
SP25-10	3568.2	O	668.2	92.4	11.3	94.9	7.2	8.4	0.88	13.8
SP26-10	3568.7	O	619.9	121.6	11.3	184.4	5.1	16.4	0.77	16.3
SP27-10	3569.45	O	84.5	73.0	7.5	56.5	1.2	7.5	0.60	5.6
SP29-10	3567.2	O	462.9	111.9	7.5	237.0	4.1	31.6	0.66	11.6
SP30-10	3569.1	O	555.5	107.0	15.0	199.6	5.2	13.3	0.74	16.8

[a] Samples listed in order of increasing thermal maturity

[b] Thermal maturity abbreviations: I = Immature, M = Mature, O = Overmature. Hydrocarbon maturity expected based on location of the well, from Piggott and Lines (1992)

Table 5.3: Summary of aluminium-normalised trace element values, and enrichment factors relative to average shale and average black shale, for the Exshaw Formation.

		Exshaw Formation shales					Enrichment factors relative to average shale				Enrichment factors relative to average black shale			
Sample ID[a]	Depth (m)	Al (ppm)	(Ni/Al)*10^4	(V/Al)*10^4	(Cr/Al)*10^4	(Co/Al)*10^4	Ni	V	Cr	Co	Ni	V	Cr	Co
SP1-10	1751.8	53235.469	36.94	72.59	13.71	2.11	4.80	4.94	1.34	1.01	5.20	3.39	0.96	1.51
SP7-10	1752.9	58524.614	27.64	62.59	12.47	1.92	3.59	4.26	1.22	0.92	3.89	2.92	0.87	1.37
SP8-10	1753	35359.875	15.30	30.74	15.13	1.06	1.99	2.09	1.48	0.51	2.15	1.44	1.06	0.76
SP9-10	1754	10242.883	78.24	39.30	19.00	3.66	10.16	2.67	1.86	1.74	11.02	1.84	1.33	2.62
SP10-10	1756.2	30539.442	50.71	114.67	12.74	3.68	6.59	7.80	1.25	1.75	7.14	5.36	0.89	2.63
SP13-10	1756.5	16116.857	41.16	82.40	11.48	2.55	5.34	5.61	1.13	1.21	5.80	3.85	0.80	1.82
SP15-10	1731.5	64372.776	19.78	95.67	12.09	2.33	2.57	6.51	1.19	1.11	2.79	4.47	0.85	1.66
SP52-10	1731.8	28203.83	46.44	114.08	17.66	2.56	6.03	7.76	1.73	1.22	6.54	5.33	1.24	1.83
SP53-10	1732.8	23685.669	54.08	102.00	15.10	2.32	7.02	6.94	1.48	1.10	7.62	4.77	1.06	1.65
SP54-10	1733.15	36715.411	41.13	102.66	15.57	2.12	5.34	6.98	1.53	1.01	5.79	4.80	1.09	1.52
SP55-10	1733.85	38029.609	34.09	71.55	13.91	1.89	4.43	4.87	1.36	0.90	4.80	3.34	0.97	1.35
SP31-10	2099.1	53370.575	31.61	70.28	10.19	2.45	4.11	4.78	1.00	1.17	4.45	3.28	0.71	1.75
SP32-10	2099.2	61825.319	12.22	13.75	9.62	1.31	1.59	0.94	0.94	0.62	1.72	0.64	0.67	0.94
SP38-10	2060	42400.544	54.22	191.79	15.81	3.12	7.04	13.05	1.55	1.49	7.64	8.96	1.11	2.23
SP39-10	2059.8	20555.598	53.42	227.24	15.91	2.77	6.94	15.46	1.56	1.32	7.52	10.62	1.11	1.98
SP47-10	2016.4	42440.267	41.56	106.80	15.57	2.18	5.40	7.27	1.53	1.04	5.85	4.99	1.09	1.56
SP48-10	2016.7	41222.443	15.76	11.99	12.40	1.60	2.05	0.82	1.22	0.76	2.22	0.56	0.87	1.15
SP49-10	2017	42679.833	19.85	13.73	10.69	1.56	2.58	0.93	1.05	0.74	2.80	0.64	0.75	1.11
SP50-10	2016.2	28200.138	56.09	111.95	16.56	2.13	7.28	7.62	1.62	1.02	7.90	5.23	1.16	1.52
SP62-10	1756.35	68388.83	22.08	125.65	14.14	2.41	2.87	8.55	1.39	1.15	3.11	5.87	0.99	1.72
SP63-10	1756.8	62901.995	40.20	128.56	14.16	2.50	5.22	8.75	1.39	1.19	5.66	6.01	0.99	1.79
SP64-10	1757.4	24506.257	75.80	241.62	16.86	3.80	9.84	16.44	1.65	1.81	10.68	11.29	1.18	2.72
SP65-10	1757.75	30074.278	42.84	80.25	16.24	2.80	5.56	5.46	1.59	1.33	6.03	3.75	1.14	2.00
SP66-10	1758.65	38206.773	42.03	113.36	15.72	2.22	5.46	7.71	1.54	1.06	5.92	5.30	1.10	1.58
SP67-10	1759.35	56219.48	36.10	51.39	15.58	1.98	4.69	3.50	1.53	0.94	5.09	2.40	1.09	1.41
SP23-10	3567.5	43044.187	19.19	98.19	16.95	1.74	2.49	6.68	1.66	0.83	2.70	4.59	1.19	1.24
SP24-10	3567.7	42257.266	19.66	146.70	20.72	1.77	2.55	9.98	2.03	0.85	2.77	6.85	1.45	1.27
SP25-10	3568.2	60545.67	15.67	110.36	15.27	1.86	2.04	7.51	1.50	0.88	2.21	5.16	1.07	1.33
SP26-10	3568.7	66737.841	27.63	92.89	18.22	1.69	3.59	6.32	1.79	0.80	3.89	4.34	1.27	1.20
SP27-10	3569.45	51386.418	11.00	16.45	14.20	1.46	1.43	1.12	1.39	0.70	1.55	0.77	0.99	1.04
SP29-10	3567.2	39548.191	59.92	117.05	28.29	1.90	7.78	7.96	2.77	0.90	8.44	5.47	1.98	1.35
SP30-10	3569.1	73403.025	27.19	75.68	14.58	2.04	3.53	5.15	1.43	0.97	3.83	3.54	1.02	1.46

Table 5.4: Average enrichment factors (EF) for selected trace elements in the Exshaw Formation.

			Exshaw Formation		
Element	Average shale [a, b]	Average black shale [c, d]	Average data (n=32)[e]	EF relative to average shale	EF relative to average black shale
Co (ppm)	19	10	9.2		
(Co/Al) * 10^4	2.1	1.4	2.1		
EF		**0.7**		**1.0**	**1.5**
Cr (ppm)	90	100	64.5		
(Cr/Al) * 10^4	10.2	14.3	14.9		
EF		**1.4**		**1.5**	**1.0**
Ni (ppm)	68	50	139.7		
(Ni/Al) * 10^4	7.7	7.1	32.3		
EF		**0.9**		**4.2**	**4.5**
V (ppm)	130	150	390.2		
(V/Al) * 10^4	14.7	21.4	90.2		
EF		**1.5**		**6.1**	**4.2**

Mean Al content for Exshaw Formation shales: 4.33 wt. %

EF abbreviation refers to Enrichment Factor

[a] Average shale data from Wedepohl (1971)

[b] Mean Al content for average shale: 8.84 wt. % (Wedepohl, 1971)

[c] Mean Al content for average black shale: 7.00 wt. % (Vine and Tourtelot, 1970)

[d] Average black shale data from Vine and Tourtelot (1970)

[e] Exshaw Formation enrichment factors calculated using average shale data

Table 5.5: Previously established values for the trace element ratios and their corresponding depositional paleoredox conditions.

	Oxic	Dysoxic	Suboxic-anoxic	Euxinic
V/Cr [a]	<2.00	2.00-4.25	>4.25	
Ni/Co [a]	<5.00	5.00-7.00	>7.00	
V/(V+Ni) [b]		0.46-0.60	0.54-0.82	>0.84

[a] Jones and Manning (1994)

[b] Hatch and Leventhal (1992); Schovsbo (2001)

Table 5.6: New nickel stable isotope data for a selection of thermally immature and mature samples from the Exshaw Formation.

Sample ID[a]	Depth (m)	Maturity[b]	δ^{60}Ni (‰)		2σ	Ni (ppm)
SP8-10	1753	I	**1.09**	±	0.04	54.1
SP9-10	1754	I	**1.98**	±	0.05	80.1
SP10-10	1756.2	I	**0.46**	±	0.04	154.9
SP13-10	1756.5	I	**2.50**	±	0.04	66.3
SP31-10	2099.1	M	**1.51**	±	0.04	168.7
SP32-10	2099.2	M	**1.22**	±	0.03	75.6
SP38-10	2060	M	**1.34**	±	0.06	229.9
SP39-10	2059.8	M	**1.17**	±	0.03	109.8

[a] Samples listed in order of increasing thermal maturity

[b] Thermal maturity abbreviations: I = Immature, M = Mature. Hydrocarbon maturity expected based on location of the well, from Piggott and Lines (1992)

6 *Conclusions and future research*

6.1 Conclusions

This study is the first to apply Ni stable isotopes to organic-rich marine sediments. The application of Ni isotopes to marine sediments in two geologically distinct settings has allowed thorough evaluation of the chemical composition of these sediments from a new geochemical perspective. Further, analysis of trace element enrichment, paleoredox ratios and TOC concentrations enabled us to better constrain influences on the behaviour of Ni isotope systematics in these settings. Additionally, the effects of thermal maturation on Ni stable isotope systematics are shown to be minimal, thereby advocating the use of Ni stable isotopes as a tool for yielding valuable spatial information for petroleum systems.

Through achieving the aims of this project, the research herein presents a number of important scientific outcomes:

1. Osmium isotopes across the Sinemurian-Pliensbachian boundary show an increased contribution of unradiogenic Os to the oceans in the Early Jurassic, possibly reflecting the opening of the trans-Pangean Hispanic Corridor
2. Significant Ni isotope fractionation occurs across the Sinemurian-Pliensbachian boundary section
3. No relationship exists between Ni isotope fractionation and Ni enrichment or redox conditions in the marine sediments analysed herein
4. There is a potential linear relationship between TOC content and Ni isotope fractionation when TOC levels are > ~1 wt. %. Further, paleoredox conditions may exert some control on this relationship for the samples herein
5. Nickel isotope fractionation in the Exshaw Formation may be controlled by compositional variability of the samples

6. The Ni isotope composition of marine sediments is distinct to that of extraterrestrial and abiotic terrestrial samples
7. Thermal maturation has a minimal effect on the trace element and Ni isotope composition of source rocks
8. Significant potential exists for Ni stable isotopes to be developed as an oil-source correlation tool

Chapter 2: Osmium isotopes across the Sinemurian-Pliensbachian boundary

Osmium isotope profiling across the Sinemurian-Pliensbachian boundary GSSP at Robin Hood's Bay, UK, demonstrates that seawater at this time became dominated by an unradiogenic $^{187}Os/^{188}Os$ signal that is not resolvable by influxes from continental weathering or meteorite impact. Although there is some fluctuation in the calculated seawater initial $^{187}Os/^{188}Os$ ratios, these values can be broadly separated into three groups that become progressively unradiogenic up-section ($^{187}Os/^{188}Os_{(i)}$ = ~0.38, 0.28 and 0.21).

The Robin Hood's Bay section is not ideally suited to Re-Os geochronology due to the highly variable $^{187}Os/^{188}Os_{(i)}$ values. However, the positive correlation of $^{187}Re/^{188}Os$ with present-day $^{187}Os/^{188}Os$ yields a date in agreement with the Geological Time Scale 2004 (189.6 ± 1.5 Ma; Gradstein *et al.,* 2004) of 179 ± 16 Ma, indicating that Re-Os systematics here are undisturbed. This emphasises the validity of the $^{187}Os/^{188}Os_{(i)}$ values in representing Early Jurassic ocean chemistry.

This unradiogenic signal is attributed to hydrothermal activity during the development of the Hispanic Corridor in the Early Pliensbachian, which was associated with rifting of the Pangean supercontinent and formation of the Central Atlantic Ocean. Emplacement of the Central Atlantic Magmatic Province during the Late Triassic – Early Jurassic, driven by continental segregation at this time, and its subsequent weathering, cannot reconcile the

observed Os isotope signal at the Sinemurian-Pliensbachian boundary. The increasing contribution of unradiogenic Os to the oceans across the boundary is coincident with flooding of the Hispanic Corridor, evident from sudden levels of faunal exchange between the eastern Pacific and western Tethyan oceans in the earliest Pliensbachian (Damborenea and Manceñido, 1979; Smith and Tipper, 1986; Smith *et al.,* 1990). As such, the unradiogenic $^{187}Os/^{188}Os_{(i)}$ signal across the Sinemurian-Pliensbachian boundary is hypothesised to mark the onset of hydrothermal activity associated with formation and flooding of the Hispanic Corridor.

Chapter 3: Chemical separation of nickel at Durham University

Our chemical separation procedure for Ni in organic-rich sample matrices at Durham University, requires the addition of the double-spike approach to correct for mass discrimination during mass spectrometry, and to resolve the effects of column-induced isotopic fractionation during chromatography. This chapter demonstrates that although Ni isotope fractionation for Ni standard NIST 986 SRM is not resolvable when the entire Ni elution is collected, fractionation does occur during the final stages of the second column. Further, analysis of shale standard USGS SDO-1 SRM demonstrates that variable and inconsistent yields are captured when processing samples with a more complex matrix than that of the Ni standard. Again, this advocates the use of the double-spike approach in allowing full development of our analytical procedure.

Chapter 4: Nickel isotope stratigraphy at the Sinemurian-Pliensbachian boundary

The data herein provides an increased understanding of the chemical composition of the organic-rich marine sediments across the Sinemurian-Pliensbachian boundary, by enhancing a geochemical dataset previously limited to TOC, oxygen, strontium, carbon and osmium isotopes. Further, in order to assess the potential for Ni stable isotopes to be used as

an oil-source correlation tool, it is important that we have a good understanding of Ni isotope systematics in stratigraphy and are able to recognise any potential controls on Ni isotope fractionation.

This study is the first to characterise the behaviour of Ni isotopes in marine sediments and presents a Ni isotope (δ^{60}Ni) profile across the boundary. The δ^{60}Ni values range from 0.28 ± 0.05 to 1.60 ± 0.05 ‰ producing a stratigraphic profile that closely resembles that of the trace elements, and shows an overall trend to heavier δ^{60}Ni values up-section. Trace element data indicates that the sediments across this boundary were deposited under predominantly oxic conditions. No linear relationships are observed between δ^{60}Ni vs. Ni enrichment or δ^{60}Ni vs. paleoredox ratios, demonstrating that Ni isotope fractionation in these marine sediments is not controlled by these factors. However, there is a clear relationship between δ^{60}Ni and TOC when TOC exceeds ~1 wt. % above the Sinemurian-Pliensbachian boundary, indicating that Ni isotope fractionation is partly controlled by the concentration and possibly type of organic matter accumulating in the sediment.

When compared to δ^{60}Ni data for extraterrestrial and abiotic terrestrial samples (from Cameron *et al.,* 2009), the δ^{60}Ni values from the Sinemurian-Pliensbachian boundary demonstrate that marine sediments yield a Ni isotope signature that is distinct from meteorites, basalts and continental sediments. Despite the much greater degrees of Ni fractionation observed in the marine sediments (total fractionation of ~1.32 ‰) relative to these samples (fractionation totals of ~0.17 – 0.37 ‰), there is minimal overlap between their δ^{60}Ni signals, emphasising this distinction. Although difficult to conclude definitively without additional marine sediment datasets, the greater amount of Ni isotope fractionation in these samples may be controlled by complexities in the seawater-sediment environment that are not otherwise relevant to meteorites, basalts or continental sediments.

Chapter 5: The effects of thermal maturation on the Ni isotope composition of source rocks

This chapter enhances our geochemical understanding of the lower black shale member of the Exshaw Formation, as well as building upon our current knowledge of the behaviour of Ni isotope systematics in marine organic-rich sediments. Further, this study focuses on quantifying the effect of thermal maturation on the Ni isotope composition of the Exshaw Formation, with a view to assessing the viability of developing Ni isotopes as an oil-source correlation tool. As such, thermally immature and mature samples were utilised for Ni isotope analysis.

The Ni isotope composition of the immature Exshaw Formation samples is highly variable, with δ^{60}Ni values ranging from 0.46 ± 0.04 to 2.50 ± 0.04 ‰. Conversely, there is almost negligible variability between the δ^{60}Ni values for the mature samples (1.17 ± 0.03 to 1.51 ± 0.04 ‰).

Trace element ratios suggest that the Exshaw Formation was deposited under predominantly suboxic-anoxic conditions. Similarly to the Sinemurian-Pliensbachian sediments, the Ni isotope composition of the Exshaw Formation is not controlled by Ni enrichment in the sediments or by the paleoredox conditions during deposition. The level of Ni isotope fractionation in the Exshaw Formation is strongly correlated with TOC for both the immature and mature samples, although the gradients of these linear correlations are distinct. Whilst it is apparent that TOC concentrations >1 wt. % influence the level of Ni isotope fractionation in the Exshaw Formation, this study also demonstrates that the compositional variability between the samples may in part account for the observed δ^{60}Ni values. It is unclear at present exactly what fraction of the sample composition is responsible for this relationship, however this study suggests that the type of organic matter present in the samples may be a key factor.

When combined with the δ^{60}Ni data from the Sinemurian-Pliensbachian boundary and compared to the extraterrestrial and abiotic terrestrial data from Cameron *et al.* (2009), the Exshaw Formation clearly supports the hypotheses presented in Chapter 4: that marine sediments contain a Ni isotopic signature that is distinct to meteorites, basalts and continental sediments, and that the degree of Ni isotope fractionation in marine sediments is far greater than that within these other sample groups. Again, although the Ni isotope record for marine sediments is limited, this study suggests that the observed range in δ^{60}Ni values in these sediments may be related to complexities in the seawater-sediment environment.

The final part of this study indicates that thermal maturation of the Exshaw Formation has had a minimal effect on the Ni isotope composition of the sediments therein. As such, ensuring careful sampling so as to capture as little sample variation as is possible visually, this chapter concludes that there is significant potential for Ni isotopes to be applied to oil-source correlation studies and further development of Ni isotopes as a correlation tool is worthwhile.

6.2 Future research

Chapter 2 demonstrates that an unradiogenic $^{187}Os/^{188}Os$ signal dominated the Early Jurassic ocean as a result of the formation of the Hispanic Corridor. Although studies of seawater composition across the Triassic-Jurassic boundary have utilised several global successions for correlation (eg. Cohen and Coe, 2007; Kuroda *et al.,* 2010), the current study regarding Hispanic Corridor formation is at present limited to only one succession. As such, it is necessary to expand this dataset to include $^{187}Os/^{188}Os_{(i)}$ data from other global successions for comparison. Further, more detailed correlation of the geochemistry and biostratigraphy associated with opening of the Hispanic Corridor would increase our understanding of ocean

circulation and seaway formation. Determination of Rare Earth Element (REE) concentrations in seawater at this time would also yield insight into the release of hydrothermal fluids into the oceans (eg. Michard and Albarède, 1986). In summary, the following suggestions for future research are made to further investigate formation of the Hispanic Corridor at the Sinemurian-Pliensbachian boundary:

1. **Correlation of seawater $^{187}Os/^{188}Os_{(i)}$ data from global successions**
2. **Greater correlation of geochemistry and biostratigraphy**
3. **Determine Rare Earth Element (REE) concentrations to further identify evidence of hydrothermal activity**

Application of the Ni stable isotope system to marine organic-rich sediments is still at an exceptionally early phase. As such, available datasets are currently limited and our understanding of the behaviour of Ni isotope systematics in the marine setting needs to be furthered. The data herein demonstrates that Ni isotopes have the potential to yield valuable information about the marine depositional environment, which emphasises the need to further explore the relationship observed between $\delta^{60}Ni$ and TOC and how this may relate to the type of organic matter present in the sediments. Similarly, the lack of any discernible maturation-induced disturbance to the Ni isotope composition of the Exshaw Formation source rocks, demonstrates that Ni isotopes may be a valuable tool for improving our spatial understanding of petroleum systems through oil to source correlation. Further research and development of the Ni stable isotope system as an oil-source correlation tool is therefore encouraged.

In order to increase our understanding of Ni isotope systematics in marine organic-rich sediments, and to optimise the scientific gain from utilising Ni isotopes in geological research, the following suggestions are made for future research:

1. **Apply the double-spike method to the Ni separation protocol at Durham University:** Chapter 3 outlines the necessity for the double-spike approach (described in detail by Gall *et al.,* 2012) to be applied to our new Ni separation procedure at Durham University, in order to overcome the effects of inconsistent Ni yields and column-induced Ni fractionation.

2. **Increase sample resolution:** Due to time constraints and uncertainty of the viability of Ni isotopes in yielding meaningful geological information, only select samples from the Sinemurian-Pliensbachian and Exshaw Formation sample suites were utilised for Ni isotope analysis. Conducting Ni isotope analysis on all samples from these suites would allow further evaluation of the relationship between δ^{60}Ni and TOC. Further, expanding the δ^{60}Ni dataset for the Exshaw Formation would enable a more thorough understanding of the effect of sample composition and thermal maturation on Ni isotope fractionation.

3. **Quantify thermal maturity levels:** Rock-Eval pyrolysis allows determination of the sample hydrocarbon maturity level through the T_{max} parameter (temperature of peak hydrocarbon release by lab-based kerogen cracking). The T_{max} values for 4 Exshaw Formation samples herein are already determined (taken from Creaser *et al.* (2002) due to identical sampling). However, to fully quantify and therefore better understand the relationship (or lack

thereof) between Ni isotope fractionation and hydrocarbon maturation, obtaining T_{max} values for all Exshaw Formation samples used for Ni isotope analysis is recommended.

4. **Characterise the type of organic matter present:** In order to fully understand the apparent relationship between TOC content and Ni isotope fractionation, it is necessary to gain an understanding of whether the type of organic matter in the sediments can influence the degree of Ni isotope fractionation. Further, understanding the effect of sedimentary organic variability on Ni isotope systematics is key to developing a precise and reliable oil-source correlation tool (eg. Curiale, 2008). Whole-rock Rock-Eval pyrolysis can be utilised to characterise the type of organic matter present in the organic-rich sediments.

5. **Analyse a selection of Exshaw Formation oils:** This thesis has determined that thermal maturation of the Exshaw Formation may have had a minimal effect on the Ni isotope composition of the source rocks. This is a positive start for the development of Ni isotopes as an oil-source correlation tool. The next step will be to conduct Ni isotope analysis on oils from the Exshaw Formation, to see if their Ni isotope signature matches that of the mature shales (~1.31 ± 0.15 ‰).

6. **Directly compare Ni stable isotopes to PGEs for oil-source correlation:** If analysis of oils from the Exshaw Formation indicates that Ni isotopes are likely to be a successful oil-source correlation tool, the next step will be to apply this tool to a petroleum system where both the source and expelled oil are known, and one that has already been subjected to successful isotopic correlation for comparison. Finlay *et al.* (2010) demonstrate that the Lower Jurassic Gordondale Formation is the major source of the oils within the West Canadian Tar Sands, through utilising a combination of $^{187}Os/^{188}Os_{(i)}$ values and other PGEs

(Pt/Pd). Nickel isotope analyses could be conducted on this same suite of source rocks and oils in order to conclusively determine whether the Ni stable isotope system can be used as an oil-source correlation tool.

6.3 References

Cameron, V., Vance, D., Archer, C., and House, C. H., 2009, A biomarker based on the stable isotopes of nickel: Proceedings of the National Academy of Sciences, v. 106, p. 10944-10948.

Cohen, A. S., and Coe, A. L., 2002, New geochemical evidence for the onset of volcanism in the central Atlantic magmatic province and environmental change at the Triassic-Jurassic boundary: Geology, v. 30, no. 3, p. 267-270.

Cohen, A. S., and Coe, A. L., 2007, The impact of the Central Atlantic Magmatic Province on climate and on the Sr- and Os-isotope evolution of seawater: Palaeogeography, Palaeoclimatology, Palaeoecology, v. 244, p. 374 – 390.

Creaser, R. A., Sannigrahi, P., Chacko, T., and Selby, D., 2002, Further evaluation of the Re-Os geochronometer in organic-rich sedimentary rocks: a test of hydrocarbon maturation effects in the Exshaw Formation, Western Canada Sedimentary Basin: Geochimica et Cosmochimica Acta, v. 66, no. 19, p. 3441-3452.

Curiale, J. A., 2008, Oil-source rock correlations - Limitations and recommendations: Organic Geochemistry, v. 39, no. 8, p. 1150-1161.

Damborenea, S. E., and Manceñido, M. O., 1979, On the palaeogeographical distribution of the pectinid genus weyla (bivalvia, lower jurassic): Palaeogeography, Palaeoclimatology, Palaeoecology, v. 27, p. 85-102.

Finlay, A. J., 2010, Re-Os and PGE geochemistry of organic-rich sedimentary rocks and petroleum: PhD thesis (Department of Earth Sciences, Durham University).

Gall, L., Williams, H., Siebert, C., and Halliday, A., 2012, Determination of mass-dependent variations in nickel isotope compositions using double spiking and MC-ICPMS: Journal of Analytical Atomic Spectrometry, v. 27, no. 1.

Gradstein, F. M., Ogg, J. G., Smith, A. G., Bleeker, W., and Lourens, L. J., 2004, A new Geologic Time Scale, with special reference to Precambrian and Neogene: Episodes, v. 27, no. 2, p. 83-100.

Kuroda, J., Hori, R. S., Suzuki, K., Gröcke, D. R., and Ohkouchi, N., 2010, Marine osmium isotope record across the Triassic-Jurassic boundary from a Pacific pelagic site: Geology, v. 38, no. 12, p. 1095-1098.

Michard, A., and Albarède, F., 1986, The REE content of some hydrothermal fluids: Chemical Geology, v. 55, no. 1–2, p. 51-60.

Smith, P. L., and Tipper, H. W., 1986, Plate Tectonics and Paleobiogeography: Early Jurassic (Pliensbachian) Endemism and Diversity: PALAIOS, v. 1, no. 4, p. 399-412.

Smith, P. L., Westermann, G. E. G., Stanley, G. D., Jr., Yancey, T. E., and Newton, C. R., 1990, Paleobiogeography of the Ancient Pacific: Science, v. 249, no. 4969, p. 680-683.